Liquidus Tracking:

a promising vitrification technique for large scale encapsulated 3-D cell culture preservation

A thesis submitted for the degree of Doctor of Philosophy (PhD)

Eva Puschmann

2015

UCL Division of Surgery & Interventional Science
Royal Free Campus
Department of Surgery

(in collaboration with)

UCL Institute for Liver and Digestive Health
Royal free Campus
Devision of Medicine

Declaration

I, Eva Puschmann confirm that the work presented in this thesis is my own. Where information has been derived from other sources, I confirm that this has been indicated in this thesis.

Abstract

Liver organ shortage is an increasing problem worldwide and many die each year waiting for a new liver. In case of acute liver failure a bioartificial liver (BAL) device could “buy” time until a donor liver is available or until the liver has spontaneously undergone self-repair.

For the clinical application of a BAL large quantities of cells should be available immediately necessitating cryo-banking. However, cryopreservation of large volumes results in increased ice formation and increased cell death. Ice formation can be prevented by vitrification, but the high cryoprotectant agent (CPA) concentrations needed are normally toxic to mammalian cells. Short exposure time minimizes toxicity but can only be achieved in small samples where fast cooling rates can be reached. To reduce CPA toxicity a vitrification machine (Liquidus Tracker) designed by Planer plc was used, which provides the lowest toxic effect that can be established for a given CPA concentration by decreasing the sample temperature to just above the melting point of that particular mix. The CPA concentration is then gradually increased as temperature is decreased along the liquidus curve.

The first aspect of this thesis was to standardise a rapid and reliable method to describe post-stress viability. A digital imaging system was used to evaluate membrane integrity and enzyme activity by quantifying the fluorescence signal of fluorescein and propidium iodide.

To understand the Liquidus Tracking (LT) process but also to pre-test conditions for automatic LT, different methods to carry out manual LT were established, evaluated and improved. To further increase cell viability a low-toxicity CPA solution was developed with the requirement of low viscosity so that it may be used within the Liquidus Tracker. Finally improvements were applied to automatic Liquidus Tracking. The development of a new stirring system substantially increased post-warming viability.

In conclusion, an optimised large scale slow cooling vitrification protocol was developed for alginate encapsulated liver cells which may be used in a BAL.

List of Contents

COVER PAGE ---- 1
DECLARATION ---- 2
ABSTRACT ---- 3
LIST OF CONTENTS ---- 4
LIST OF FIGURES ---- 11
LIST OF TABLES ---- 14
ABBREVIATION ---- 15
ACKNOWLEDGMENTS ---- 18

CHAPTER 1: GENERAL INTRODUCTION ---- 19

1.1 THE LIVER ---- 19
1.1.1 Liver functions ---- 20
1.1.1.1 Metabolic functions ---- 20
1.1.1.2 Detoxification ---- 20
1.1.2 Liver regeneration ---- 21
1.2 LIVER FAILURE ---- 22
1.2.1 Acute Liver Failure ---- 22
1.2.2 Acute on-chronic Liver Failure ---- 23
1.3 LIVER DONOR SHORTAGE ---- 23
1.4 EXTRACORPOREAL LIVER DEVICES ---- 24
1.4.1 Artificial Liver Devices ---- 24
1.4.2 Bioartificial Liver Devices ---- 25
1.5 LIVER GROUP BAL ---- 26
1.5.1 HepG 2 cell line ---- 27
1.5.2 Alginate encapsulation ---- 27
1.5.2.1 HepG2 cell growth in alginate beads ---- 29
1.5.3 The fluidized bed bioreactor system ---- 30
1.6 BIOARTIFICIAL LIVER PRESERVATION ---- 30
1.6.1 Short-term preservation ---- 31
1.6.2 Short-term Bioartificial Liver preservation ---- 32
1.7 CRYOPRESERVATION: LONG-TERM PRESERVATION ---- 32
1.7.1 Extracellular ice formation ---- 33
1.7.2 Intracellular ice formation ---- 33
1.7.3 Intercellular ice formation ---- 34
1.7.4 Osmotic effects and dehydration ---- 34
1.7.5 The Equilibrium Melting temperature of aqueous solutions ---- 35
1.7.6 Cryoprotectant agents ---- 36
1.7.6.1 Penetrating CPAs ---- 36

1.7.6.2 Non-penetrating CPAs ---- 37
1.7.7 Slow cooling protocols ---- 37
1.7.7.1 Supercooling and Ice Nucleation ---- 38
1.7.7.2 Warming process ---- 39
1.7.8 Vitrification ---- 39
1.7.9 Cooling and warming of bulky samples ---- 40
1.7.10 Liquidus Tracking ---- 41
1.8 AIM OF THE PROJECT ---- 44

CHAPTER 2: GENERAL METHODS AND MATERIALS ---- 46

2.1 CELL CULTURE ---- 46
2.1.1 Preparation of complete media for monolayer cell culture ---- 46
2.1.2 Trypsinising monolayer cells ---- 47
2.1.3 Cell Count and viability using Trypan blue exclusion test ---- 48
2.1.4 Culture of Encapsulated HepG2s ---- 48
2.2 ENCAPSULATION OF HEPG2 CELLS INTO ALGINATE ---- 49
2.3 CELL COUNT USING THE CHEMOMETECT NUCLEO COUNTER ---- 52
2.4 FLUORESCIN DIACETATE/PROPIDIUM IODIDE STAINING ---- 54
2.4.1 Viability assessment in beads – Image analysis ---- 54
2.5 METHYLTHIAZOLYLDIPHENYL-TETRAZOLIUM BROMIDE (MTT) ASSAY ---- 55
2.6 QUANTIFICATION OF HEPATO-SPECIFIC PROTEINS SYNTHESISED AND SECRETED IN CULTURE ---- 56
2.7 USE OF CONTROLLED RATE FREEZERS ---- 58
2.8 STORAGE OF CRYOPRESERVED SAMPLES ---- 59
2.8.1 Temperature measurements during cryopreservation ---- 59
2.9 STATISTICAL ANALYSIS ---- 60

CHAPTER 3: VALIDATION OF IMAGE ANALYSIS FOR CELL VIABILITY QUANTIFICATION ---- 61

3.1 INTRODUCTION ---- 61
3.1.1 Membrane integrity test for single cells ---- 61
3.1.2 Membrane integrity test for encapsulated cells and cell spheroids ---- 62
3.1.3 Viability test for encapsulated cells and cell spheroids ---- 63
3.1.4 Fluorescein diacetate staining ---- 64
3.1.5 Digital imaging system ---- 64
3.1.6 Dynamic range ---- 65
3.2 AIMS ---- 66
3.3 METHODS AND MATERIALS ---- 67
3.3.1 Microscope viability quantification ---- 67
3.3.1.1 FDA threshold setting ---- 68

3.3.1.2 Reduction of background pixels ---- 69
3.3.1.3 PI threshold setting ---- 69
3.3.1.4 Signal to noise ratio ---- 70
3.3.2 Plate reader viability quantification ---- 70
3.3.2.1 Volume of beads per well determination ---- 70
3.3.2.2 Omega plate reader sample preparation ---- 70
3.3.2.3 Staining samples with FDA and PI ---- 72
3.3.2.4 Omega plate reader settings ---- 72
3.3.2.5 Calculating the equalization factor X ---- 73
3.4 RESULTS ---- 76
3.4.1 Results for microscope viability quantification ---- 76
3.4.1.1 Background reduction ---- 76
3.4.1.2 Minimum FDA exposure time ---- 77
3.4.1.3 FDA exposure time evaluation ---- 77
3.4.1.4 PI exposure time evaluation ---- 78
3.4.1.5 Final set-up: day 3 to 13 after encapsulation ---- 79
3.4.1.6 FDA and PI threshold setting evaluation ---- 80
3.4.1.7 Cell density impacts cell viability ---- 80
3.4.1.8 Threshold setting for low cell density beads ---- 81
3.4.1.9 Viability data compared to cell count, ELISA and MTT data ---- 81
3.4.2 Results for plate reader viability quantification ---- 86
3.4.2.1 Volume of beads per well ---- 86
3.4.2.2 Plate reader gain ---- 86
3.4.2.3 Equalization factor X ---- 86
3.4.2.4 Evaluating plate reader viability test set-up ---- 86
3.4.2.5 Final equation for Omega plate reader viability measurements ---- 88
3.5 DISCUSSION ---- 90
3.6 CONCLUSION ---- 95

CHAPTER 4: MANUAL LIQUIDUS TRACKING ---- 96

4.1 INTRODUCTION ---- 96
4.1.1 Manual Liquidus Tracking ---- 96
4.1.2 Improved laboratory translation for manual Liquidus Tracking ---- 97
4.1.3 The Refractive Index ---- 97
4.2 AIMS ---- 99
4.3 METHODS AND MATERIALS ---- 100
4.3.1 Dimethyl sulfoxide toxicity at different temperatures and concentrations ---- 100
4.3.1.1 Dimethyl sulfoxide toxicity at temperatures below zero ---- 100
4.3.2 Determination of osmotic effects ---- 101

4.3.3 Manual Liquidus Tracking ---- 101
4.3.3.1 Manual Liquidus Tracking set-up 1 ---- 102
4.3.3.2 Manual Liquidus Tracking set-up 2 ---- 104
4.3.3.3 Manual Liquidus Tracking set-up 3 ---- 105
4.3.3.4 Manaual Liquidus Tracking warming procedure ---- 106
4.3.4 Manual Liquidus Tracking step by step ---- 107
4.3.5 Temperature recordings ---- 109
4.3.6 Approximate freezing point detection for dimethyl sulfoxide ……109
4.3.7 Refractive index of dimethyl sulfoxide ---- 110
4.3.7.1 Improved manual Liquidus Tracking ---- 111
4.4 RESULTS ---- 113
4.4.1 Can CPA toxicity be reduced by decreasing the temperature? ---- 113
4.4.1.1 Me_2SO toxicity at different temperatures and incubation times ---- 113
4.4.1.2 Me_2SO toxicity at different temperatures below zero ---- 114
4.4.1.3 Dimethyl sulfoxide toxicity over time ---- 115
4.4.2 Determination of osmotic effects ---- 116
4.4.3 Thermocouple defined approximate freezing point (TdAFP) for dimethyl sulfoxide - 117
4.4.4 Liquidus Tracking step-by-step (set-up 1) ---- 119
4.4.5 Liquidus Tracking step-by-step (set-up 1, 2 and 3) ---- 120
4.4.6 Liquidus Tracking step-by-step at 0.5°C. ---- 121
4.4.7 Liquidus Tracking temperature profile ---- 122
4.4.8 Improved manual Liquidus Tracking ---- 124
4.5 DISCUSSION ---- 127
4.6 CONCLUSION ---- 138

CHAPTER 5: CRYOPROTECTANT AGENT DEVELOPMENT ---- 139

5.1 INTRODUCTION ---- 139
5.1.1 Cryoprotectant agent (CPA) toxicity ---- 139
5.1.2 Viscosity; the limiting factor for a CPA solution for Liquidus Tracking ---- 140
5.1.3 CPA concentration for Liquidus Tracking ---- 140
5.2 AIMS ---- 142
5.3 METHODS AND MATERIALS ---- 143
5.3.1 CPA toxicity test ---- 143
5.3.2 Viscosity rating of new CPA solutions ---- 144
5.3.3 Viscosity measurement ---- 144
5.3.4 Standard vitrification protocol ---- 145
5.3.5 Equilibrium melting point measurements by Differential Scanning Calorimetry ---- 145
5.3.6 Improved manual LiquidusTracking ---- 146
5.3.7 Most commonly used CPAs for vitrification ---- 147

5.3.8 Viscosity of commonly used Cryoprotectant agents ---- 148
5.3.9 CPAs for Liquidus Tracking ---- 150
5.4 RESULTS ---- 151
5.4.1 Methanol vs. ethanol as penetrating low viscosity CPAs ---- 151
5.4.2 Testing different sugars and sugar combinations ---- 151
5.4.3 Viscosity rating of candidate CPA combinations ---- 153
5.4.4 CPA mixtures of low viscosity ---- 154
5.4.5 Toxicity test of low viscous CPA solutions ---- 155
5.4.5.1 Solutions with higher predicted toxicity than reference solution No.27 ---- 156
5.4.5.2 Solutions with lower predicted toxicity than reference solution No.27 ---- 157
5.4.6 Optimal CPA solutions ---- 158
5.4.7 Viscosity of optimal CPA solutions ---- 161
5.4.8 Toxicity of dimethyl sulfoxide and ethylene glycol ---- 161
5.4.9 Vitrification properties of low toxic CPA solutions ---- 163
5.4.10 Vitrification and devitrification properties of low toxic CPA solutions ---- 163
5.4.11 Liquidus curve of optimized CPA solution No.18 ---- 164
5.4.12 Liquidus curve of CPA solution No.18 in comparison to dimethyl sulfoxide ---- 166
5.4.13 Manual Liquidus Tracking with CPA solution No.18 and dimethyl sulfoxide ---- 167
5.5 DISCUSSION ---- 169
5.6 CONCLUSION ---- 176

CHAPTER 6: THE AUTOMATIC LIQUIDUS TRACKER ---- 177

6.1 INTRODUCTION ---- 177
6.1.1 The dual solution mode ---- 177
6.1.2 The single solution mode ---- 178
6.1.3 The Liquidus Tracker ---- 179
6.1.4 The stirrer ---- 182
6.1.5 Heat transfer ---- 183
6.2 AIMS ---- 184
6.3 METHODS AND MATERIALS ---- 185
6.3.1 Liquidus Tracker set-up ---- 185
6.3.1.1 The CfgPid profile ---- 185
6.3.1.2 Delta T ---- 186
6.3.1.3 Pump calibration ---- 186
6.3.1.4 Freezer connection ---- 187
6.3.1.5 Filling the sample carrier ---- 187
6.3.1.6 The CPA concentration/temperature curve ---- 187
6.3.2 Changes made to the original Liquidus Tracker set-up ---- 188
6.3.2.1 Temperature control ---- 188

6.3.2.2 Outlet filter *system* ---- 189
6.3.2.3 Increasing inlet tube lengths ---- 190
6.3.3 Automatic Liquidus Tracking cooling ---- 191
6.3.3.1 Standard Planer Liquidus Tracking procedure ---- 191
6.3.3.2 Combined manual/automatic Liquidus Tracking ---- 192
6.4 RESULTS ---- 193
6.4.1 The temperature-concentration curve ---- 193
6.4.2 Devitrification ---- 194
6.4.3 Liquidus Tracking temperature measure ---- 195
6.4.4 Reducing the temperature difference between liquidus curve and temperature/concentration curve ---- 196
6.4.5 The combined manual/automatic Liquidus Tracking approach ---- 198
6.4.6 Combined manual/automatic Liquidus Tracking temperature profile ---- 199
6.4.7 First runs with dimethyl sulfoxide and CPA solution No.18 ---- 201
6.5 DISCUSSION ---- 202
6.6 CONCLUSION ---- 206

CHAPTER 7: AUTOMATIC LIQUIDUS TRACKING ---- 207

7.1 INTRODUCTION ---- 207
7.2 AIMS ---- 208
7.3 METHODS AND MATERIALS ---- 209
7.3.1 The 50-60-66% CPA inlet ---- 209
7.3.2 Automatic Liquidus Tracking warming ---- 209
7.3.2.1 The single solution reverse mode ---- 209
7.3.2.2 The four step reverse mode ---- 211
7.3.3 The complete Liquidus Tracking procedure ---- 212
7.3.4 Manual two-step Liquids Tracking ---- 213
7.4 RESULTS ---- 215
7.4.1 Pre-testing conditions with manual Liquidus Tracking ---- 215
7.4.2 Minimum CPA addition and inlet temperature ---- 218
7.4.3 Impact of sample volume on cell viability ---- 220
7.4.4 Inhomogeneous “cell per bead” survival ---- 220
7.4.5 High concentrated CPA inlet solution ---- 221
7.4.6 Reduced outlet port height ---- 224
7.4.6.1 Short outlet port-diminishes viability ---- 224
7.4.6.2 Inhomogeneous CPA extraction ---- 225
7.4.7 The Liquidus Tracking stirrer ---- 227
7.4.8 Manual Liquidus Tracking warming process ---- 228
7.4.9 Automatic Liquidus Tracking warming process ---- 229

7.4.9.1 The one solution reverse mode ---- 230
7.4.9.2 The four-step reverse mode ---- 231
7.4.10 CPA toxicity over time ---- 232
7.4.11 Cell density impacts cell survival ---- 233
7.4.12 Complete automatic Liquidus Tracking procedure ---- 235
7.5 DISCUSSION ---- 237
7.6 CONCLUSION ---- 246

CHAPTER 8: GENERAL DISCUSSION ---- 247

8.1 VIABILITY ASSESSMENT ---- 247
8.2 CRYOPROTECTANT AGENTS FOR LIQUIDUS TRACKING ---- 248
8.3 LIQUIDUS TRACKING ---- 249
8.4 MANUAL LIQUIDUS TRACKING ---- 250
8.5 AUTOMATIC LIQUIDUS TRACKING ---- 250
8.6 IMPROVING THE LIQUIDUS TRACKING PROCEDURE ---- 251
8.7 FURTHER METHODS TO INCREASE CELL RECOVERY ---- 253
8.8 FURTHER APPLICATIONS FOR LIQUIDUS TRACKING ---- 254

REFERENCES ---- 256

APPENDICES ---- 276

List of Figures

Figure 1.1 The bioartificial liver device ---- 27
Figure 1.2 Alginate bead size and cell spheroid formation ---- 27
Figure 1.3 HepG2 cell proliferation in alginate beads ---- 30
Figure 1.4 Equilibrium melting curve (liquidus curve) for Me_2SO ---- 43
Figure 2.1 JetCutter set up ---- 52
Figure 3.1 A histogram showing the pixel intensity distribution ---- 68
Figure 3.2 Low threshold setting for FDA ---- 69
Figure 3.3 Viability-RLU correlation ---- 73
Figure 3.4 FDA-PI equalization factor X ---- 75
Figure 3.5 Clean and smooth function ---- 76
Figure 3.6 Determining the minimum FDA exposure time ---- 77
Figure 3.7 Signal to noise ratio for FDA stained AELC ---- 78
Figure 3.8 Threshold setting for PI fluorescence ---- 79
Figure 3.9 Viability determined by image analysis compared to cell count and MTT data ---- 83
Figure 3.10 AELC protein production ---- 84
Figure 3.11 Microscope images of AELC with decreasing viabilities ---- 87
Figure 3.12 Viability standard deviation comparison for equalization factor and gain combination evaluation ---- 89
Figure 4.1 Osmotic stress ---- 101
Figure 4.2 A schematic of manual LT set-up 1. ---- 103
Figure 4.3 A schematic of manual LT set-up 2. ---- 104
Figure 4.4 A schematic of manual LT set-up 3. ---- 105
Figure 4.5 LT warming-step by step. ---- 106
Figure 4.6 Step-by-step manual LT ---- 108
Figure 4.7 Supercooling and release of latent heat ---- 110
Figure 4.8 Refractive index of Me2SO ---- 111
Figure 4.9 Improved manual LT ---- 112
Figure 4.10 AELC viability at increasing Me_2SO concentrations, incubation temperatures and time ---- 114
Figure 4.11 Temperature impact on Me_2SO toxicity ---- 115
Figure 4.12 Me_2SO toxicity over time at 4˚C ---- 116
Figure 4.13 Effect of temperature on osmotic injury ---- 117
Figure 4.14 Equilibrium melting point detection for increasing concentrations of Me_2SO ---- 118
Figure 4.15 Me_2SO Liquidus curve: TdAFP vs. literature data ---- 119
Figure 4.16 LT step-by-step (set-up 1) ---- 120
Figure 4.17 LT step-by-step (set-up 1, 2 and 3) ---- 121
Figure 4.18 LT step-by-step at 0.5°C ---- 122
Figure 4.19 LT temperature profile set-up 1 ---- 123

Figure 4.20 LT temperature profile set-up 2 and 3 ---- 123
Figure 4.21 LT insolation system ---- 125
Figure 4.22 Manual LT stirring device. ---- 126
Figure 5.1 Toxicity test methanol vs. ethanol ---- 151
Figure 5.2 Sugars and sugar combination as non-penetrating CPA ---- 152
Figure 5.3 Toxicity comparison of low toxic CPA solutions ---- 159
Figure 5.4 Fluorescent microscope images of CPA solutions exhibiting lowest toxicity to AELC ---- 160
Figure 5.5 Viscosity of the nine best CPA solutions ---- 161
Figure 5.6 CPA toxicity Me_2SO versus EG ---- 162
Figure 5.7 CPA solutions of low toxicity used to vitrify AELC ---- 163
Figure 5.8 Vitrification properties of low toxic CPA solutions ---- 164
Figure 5.9 Determination of equilibrium melting point using differential scanning calorimetry (DSC). 165
Figure 5.10 TdAFP and equilibrium melting point determination using “release of latent heat” and “DSC”. ---- 166
Figure 5.11 Liquidus curve of CPA No.18 in comparison to the liquidus curve of Me_2SO ---- 167
Figure 5.12 Manual LT with CPA solution No.18 vs. Me_2SO ---- 168
Figure 6.1 The dual solution mode ---- 178
Figure 6.2 The single solution mode ---- 179
Figure 6.3 The Liquidus Tracker ---- 181
Figure 6.4 Sample holder and stirrer ---- 182
Figure 6.5 The CfgPid software ---- 186
Figure 6.6 Filling the sample carrier ---- 187
Figure 6.7 Monitoring inlet, outlet and sample temperature ---- 189
Figure 6.8 Outlet port filter system ---- 190
Figure 6.9 The temperature/concentration curve ---- 193
Figure 6.10 Devitrification during the warming process ---- 194
Figure 6.11 CfgPid curve and sample T/C curve temperature difference ---- 195
Figure 6.12 LT temperature/CPA concentration profiles ---- 197
Figure 6.13 Temperature/concentration curve achieved with LT CfgPid profile A-1 and B-3 ---- 198
Figure 6.14 Combined manual and automatic LT ---- 199
Figure 6.15 Combined manual/automatic LT temperature profile ---- 200
Figure 6.16 Automatic Liquidus Tracking-Me_2SO vs. CPA No.18 ---- 201
Figure 7.1 Complete LT process ---- 213
Figure 7.2 Decreased Me_2SO and increased glucose concentration ---- 215
Figure 7.3 Automatic LT-decreased Me_2SO and increased glucose concentration ---- 216
Figure 7.4 Pre-test of CPA No.18 variations, sample carrier solutions, pre-incubation additives ---- 217
Figure 7.5 Final CPA addition temperature – manual LT ---- 219
Figure 7.6 Final CPA addition temperature – automatic LT ---- 219
Figure 7.7 Impact of sample volume on cell viability ---- 220

Figure 7.8 Inhomogeneous “cell per bead” survival ---------- 221
Figure 7.9 CPA inlet reduced from 80% to 50% (w/v) ---------- 222
Figure 7.10 Reduced inlet CPA concentration ---------- 223
Figure 7.11 Long versus short LT outlet port design ---------- 224
Figure 7.12 Long versus short LT outlet port: impact on cell viability ---------- 225
Figure 7.13 Inhomogeneous LT extraction ---------- 226
Figure 7.14 Planer stirrer versus propeller stirrer ---------- 227
Figure 7.15 Propeller stirrer- increased cell viability ---------- 228
Figure 7.16 Manual LT warming sequence ---------- 229
Figure 7.17 PBS inlet into subzero CPA solution ---------- 231
Figure 7.18 LT warming protocols ---------- 232
Figure 7.19 Toxicity over time using automatic LT ---------- 233
Figure 7.20 High vs. low cell density beads for LT ---------- 234
Figure 7.21 Impact of low and high cell densities on post-LT viability ---------- 234
Figure 7.22 Impact of low and high cell densities on cell recovery ---------- 236

List of Tables

Table 2.1 Cell count dilution scheme ---- 53
Table 2.2 Hepato-specific protein ELISA methodology ---- 58
Table 3.1 Omega Plate reader sample preparation scheme ---- 71
Table 3.2 Example for FDA RLU values and corresponding viability ---- 73
Table 3.3 Low FDA threshold ---- 276
Table 3.4 Low PI threshold ---- 277
Table 3.5 FDA/PI ratio ---- 80
Table 3.6 FDA and PI threshold setting ---- 278
Table 3.7 Percentage of positive control for viability, cell count and ELISA data ---- 85
Table 3.8 Equalization factor X ---- 86
Table 3.9 Gain and equalization factor evaluation ---- 279
Table 4.1 LT transfer temperatures for Me_2SO ---- 103
Table 4.2 Amount of CPA to be added to increase sample CPA concentration by 10% ---- 105
Table 5.1 CPA toxicity pipetting scheme ---- 143
Table 5.2 Amount of 80% CPA required to increase the sample CPA concentration by 10% ---- 146
Table 5.3 Me_2SO and mixed CPA transfer temperatures ---- 147
Table 5.4 Summary of vitrification protocols ---- 148
Table 5.5 Specifications of penetrating CPAs ---- 149
Table 5.6 Viscosity of sugars at different concentrations and temperatures ---- 150
Table 5.7 Viscosity rating part 1: The viscosity of 21 CPA combinations ---- 154
Table 5.8 Viscosity rating part 2: CPA solutions of reduced viscosity ---- 155
Table 5.9 Solutions predicted to have higher toxicity effects than reference solution No.27 ---- 157
Table 5.10 Solutions with lower or similar toxicity than reference solution No.27 ---- 158
Table 6. 1 CfgPid table (standard program) one-solution mode using 80% (w/v) Me_2SO ---- 191
Table 6. 2 CfgPid profile for automatic LT ---- 280
Table 7.1 One solution mode warming protocol ---- 211

Abbreviation

3-D	3-dimensional
Ab	Antibody
ACLF	Acute-on-chronic liver failure
ADC	Analogue and digital converter
AELC	Alginate encapsulated liver cell
AFP	Alpha-fetoprotein
AFP	Antifreeze proteins
AGP	Alpha acid glycoprotein
ALF	Acute liver failure
alpha-MEM	Alpha minimum essential media
AO	Antioxidants
ATP	Adenosinetriphosphate
BAL	Bioartificial liver device
BSA	Bovine serum albumin
CCD	Charge-coupled device
CIDOCD	Cryopreservation-induced-delayed-onset-cell-death
CPA	Cryoprotectants agents
CRF	Controlled rate freezer
CT	Computed tomography
DMEM	Dubelco's modified eagle medium
DNA	Deoxyribonucleic acid
DSC	Differential scanning calorimetry
DMSO	Dimethylsulfoxide
EDTA	Ethylenedinitrilotetraacetic acid
EG	Ethylene glycol
ELAD	Extra-corporeal liver assist device
ELISA	Enzyme-linked immunosorbent assay
FBB	Fluidised bed-based bioreactor
FCS	Fetal calf serum
FDA	Fluorescein diacetate

FTIR	Fourier transform infrared spectroscopy
GAGs	Glycosaminoglycans
HBSS	Hanks balanced salt solution
HE	Encephalopathy
HEPES	4-(2-hydroxyethyl)-1piperazineethanesulfonic acid
HG	High glucose
HGF	Hepatocyte growth factor
HSPs	Heat shock proteins
HTK	Histidine-tryptophan-ketoglutarate
LN	Liquid Nitrogen
LT	Liquidus Tracking
MARS	Molecular adsorbents recirculating system
mDSC	Modulated DSC
MEM	Minimum Essential Medium
Me_2SO	Dimethyl sulfoxide
MTT	Methylthiazol tetrazolium assay
NAFLD	Non-alcoholic fatty liver disease
NIBSC	National Institute for Biological Standards and Controls
NMR	Magnetic resonance spectroscopy
PBS	Phosphate buffered saline
PFC	Perfluorodecalins
PG	Propylene glycol
PI	Propidium iodide
PMT	Photomultiplier tube
ROS	Reactive oxygen species
RT	Room temperature
RT-qPCR	Quantitative real-time PCR
SIB	Ice-blockers
SNR	Signal-to-noise ratio
TB	Thermal buffer
T/C curve	Temperature/concentration curve
TdAFP	Thermocouple defined approximate freezing point

T_g	Glass transition temperature
T_h	Homogeneous nucleation temperature
UW	University of Wisconsin

Acknowledgements

Firstly, I would like to express my special appreciation and thanks to my supervisors Dr Clare Selden and Professor Barry Fuller for their guidance and support and for encouraging my research.

This thesis was co-funded by the Liver Group Charity and Planer plc and I would like to thank both organisations for their generous support. At Planer, I would like to thank Geoffrey Planer, Steven Butler and David Wingate for their help and interesting discussions.

To all my dear colleagues from the Liver group, thank you for your support and kindness. Special thanks to Eloy Erro, who I could always talk to and rely on and to Kathrine Lintern for being my friend and for correcting my thesis.

A special thanks to my parents who always supported me in all my pursuits, for their love and faith in me. To my brothers for their support and down-to-earth attitude that often helped me to calm down. To my beloved husband Jorge for always being there for me, for his love, his patience and constant encouragements. This thesis would have never been possible without you.

And last, but not least, to my daughter Nora, who was a toddler when I first started and who has now grown into a beautiful school girl. You are all a mother could wish for and I want to dedicate this work to you.

CHAPTER 1
General Introduction

Liver failure is a life threatening illness with increasing mortality worldwide. Although the liver has an unique ability for natural regeneration, a liver transplant is usually inevitable. However, due to an increasing shortage of donor organs many patients die while waiting for a liver transplant. Mortality could be reduced by temporarily substituting healthy liver function by using a bioartificial liver (BAL) device, until either a transplant becomes available or until the liver has spontaneously undergone self-repair. Treatment must be available almost immediately for unpredictable emergency use, which points out the necessity for a suitable BAL storage method. For liver cells, which are the main component of a BAL device, cryopreservation is the only measure to maintain cell function over a longer period of time.

1.1 The Liver

The liver is the biggest internal organ and the largest gland of the human body with a weight of about 1.5kg (Moore et al., 2007). It is incredibly complex and is responsible for more than 500 known different functions. In humans, the liver is mostly located in the right upper abdomen directly below the diaphragm. The human liver is divided into two large lobes. At the bottom of the liver is the so called hilum (porta hepatis), at which the portal vein and the hepatic artery enter and bile ducts leave the liver. The hepatic artery provides the liver with oxygen-rich blood from the heart and the portal vein carries nutrients from stomach and intestines, degradation products from the spleen and hormones from the pancreas to the liver. The liver lobes again divided into tiny lobules which are of hexagonal formation and consist mainly of hepatocytes which are arranged in strings ("liver cell columns"). Capillaries (liver sinusoids) are arranged between the liver cells allowing them to be perfused with blood. These sinusoids are lined up with a discontinuous endothelium and contain specific macrophages, the Kupffer cells, which are mainly responsible for phagocytosis and cytokine production (Tacke et al., 2009). The space (Space of Disse) between the liver cells and the endothelial cells of liver sinusoids, is where the actual exchange of substances between

blood and hepatocytes occurs. Within this space the satellite cells are found which store fat droplets and retinoic acid (Kordes et al., 2009).

1.1.1 Liver functions

Hepatocytes (parenchymal cells) are responsible for the majority of liver metabolic functions and make up 70% to 80% of the liver's cytoplasmic mass. Morphologically, they appear cuboidal with a large, central nucleus, which can be diploid or polyploid. Hepatocytes are about 20 to 30µm in diameter, and are metabolically very active. Signs of the high metabolic activity are the highly developed endoplasmic reticulum and Golgi apparatus and a high concentration of mitochondria. They also contain lysosomes, peroxisomes, and secretory vesicles. Another characteristic of hepatocytes is intracellular glycogen deposits which function as energy sources.

1.1.1.1 Metabolic functions

The liver fulfils a large variety of metabolic tasks that are crucial for the rest of the body. This includes the formation of clotting factors and the processing of intestinal nutrients to endogenous substances, which are then used by other organs. Hepatocytes produce a variety of proteins of which albumin is one of the most important. Albumin ensures that blood fluids remain in the bloodstream and that poorly soluble substances in the blood can be transported by binding to albumin. Additionally, hepatocytes synthesise carbohydrates, cholesterol, bile salts, fatty acids, triglycerides, phospholipids, glycoproteins, lipoproteins and lipoproteins. Moreover the liver is responsible for transamination (amino acid conversion) to produce non-essential amino acids.

1.1.1.2 Detoxification

The liver plays an important role in the detoxification of harmful substances for example by transforming toxic ammonia into non-toxic urea, which is then excreted in urine by the kidneys. Dehydrogenases convert alcohol into acetic acid, which is ultimately changed into fat. One of the important enzymes for the removal of toxins and drugs is cytochrome P450, which catalyze the oxidation of organic substances. The liver also filters hormones and cell debris from the blood. Bacteria and viruses may be removed through phagocytic Kupffer cells. Water-insoluble pollutants are emitted via bile into the intestine. Water-soluble pollutants are released into the blood stream which

carries it to the kidneys where they can be excreted in the urine from the body (Moore et al., 2007).

1.1.2 Liver regeneration

The liver is the only inner organ that has the capacity to naturally regenerate. The physiological size is normally adjusted to match the host for example after transplantation or to regain its former size (e.g. size before hepatectomy), which in turn depends on complex variables such as normalisation of the body's blood circulation and metabolism. Liver regeneration reportedly occurs mostly during the first two weeks after the damaging insult. Under normal conditions hepatocytes of an adult liver barely proliferate, but when the liver functional mass is reduced for example by surgical removal or following chemical or viral insult, a process of cell hypertrophy, rapid proliferation and restoration of functional mass is initiated. Mature, highly differentiated hepatocytes re-enter the cell cycle and proliferate for a limited number of divisions. This rather unique process of adult cells re-entering the cell cycle is a result of extracellular stimuli and intracellular signalling pathways and profound modifications of gene expression (Michalopoulos, 2013). Another type of cell that is phenotypically similar to hepatoblasts, is also thought to play a role in liver regeneration. The so called "oval cells" are found in close proximity to bile ducts (Bird et al., 2008). Although there is still some doubt regarding the exact properties of these cells, it is generally accepted that oval cells are bipotential liver stem cells, with the potential to differentiate into either hepatocytes or cholangiocytes (bile duct epithelial cells). It is believed that they are activated in response to growth factors released following disease or injury when mitosis of hepatocytes cannot occur.

Liver regeneration is limited and injury to the liver can be of too long duration or too severe to allow full recovery. As a result, the liver creates scar tissue, also called fibrosis, which can still be treated with medication in some cases and at early stages. However, the continuous build-up of scar tissue leads to cirrhosis, a condition in which the liver slowly deteriorates and is unable to function normally. At this point the disease is not curable and a liver transplantation is inevitable.

1.2 Liver Failure

Liver failure is the inability of the liver to perform its normal synthetic and metabolic function and can be classed into acute and chronic liver failure.

1.2.1 Acute Liver Failure

Acute liver failure (ALF) is defined as a rapid loss (80% to 90%) of hepatocellular function in a patient without known prior liver disease. ALF can be classified into hyperacute (1 week), acute (8-28 days) and subacute (8 weeks) liver failure, describing the time from first symptoms until an onset of coagulopathy and encephalopathy (O'Grady et al., 1993). Common early symptoms are fatigue, nausea, poor appetite, dark urine and jaundice, which is caused by an accumulation of unconjugated bilirubin in the blood. Coagulopathy (abnormal blood clotting) occurs as clotting proteins are not being synthesised; encephalopathy is a brain dysfunction caused by toxin and ammonia build up in the brain. Liver failure can also lead to haemodynamic and cardio-respiratory compromise, metabolic derangements, inflammation and infection, renal failure, cerebral edema, and finally multi-organ failure. Patients with acute and hyperacute liver failure are at greater risk of developing cerebral oedema and encephalopathy, which is thought to be a consequence of a longer buildup of toxic substances in the brain (Hazell & Butterworth, 1999; O'Grady, 2005). There are many causes such as viral hepatitis, drug intolerance, paracetamol overdose, alcoholic excess, toxins and acute fatty liver of pregnancy. Wilson's disease which is hereditary copper accumulation has also been linked to ALF. Despite a number of treatments available, liver transplantation, which has a reported 1-year survival rate of more than 83%, is oftentimes inevitable (Adam & Hoti, 2009). Without transplantation the fatality rate for ALF has been estimated to be greater than 80% (O'Grady et al., 1993). In the United States, as in other countries, patients with ALF have the highest priority for donor organs (Belle et al., 1995). However, there are not sufficient donor organs available to meet this urgent clinical need. A BAL device could provide time until a donor liver is available or until the liver has spontaneously undergone self-repair.

1.2.2 Acute on-chronic Liver Failure

Acute-on-chronic liver failure (ACLF) is an acute deterioration of liver functions in patients with cirrhosis. Symptoms are similar to those of ALF, but treatment and prognosis may vary (Jalan et al., 2012). Predominate causes for liver cirrhosis, especially in Europe and the US, are excessive alcohol abuse, hepatitis B and hepatitis C, which is mostly caused by illegal drug injection. This unhealthy lifestyle is regarded as unfavorable for the qualification for a liver transplant. There are also other life-style related liver pathologies such as non-alcoholic fatty liver disease (NAFLD). Although reversible in some cases, depending on the severity and nature of the acute and chronic insult (Sarin et al., 2009), the necessity for transplantation as a result of progressed cirrhosis is most likely.

1.3 Liver donor shortage

Liver organ shortage is an increasing problem worldwide. In the US more than 15,000 people were listed for a liver transplant in 2013 (Organ Procurement and Transplantation Network Data). About 9,000 new cases are reported each year, but only 5,000 livers from deceased donors are available for liver transplantation and approximately 1,400 people die each year waiting for a new liver. In the UK a total of 726 liver transplants were carried out between 2011 and 2012. However, the number of people who need a liver transplant is much higher and an estimated 12% die while being on the waiting list. In Germany 1191 liver transplantations were carried out in 2001, but 1792 new patients were put on the waiting list (Manns, 2013). It is expected that donor liver shortage will increase substantially over the next decades. In order to determine whose need is most critical, the United Network for Organ Sharing has developed a rating system. Patients with ALF, with a life expectancy fewer than seven days without transplant have been defined as the most urgent group. People with active alcohol or substance abuse problems might not qualify for a transplant as there is a high risk that patients will continue with their unhealthy lifestyle, leading the newly transplanted liver to fail. Patients with additional severe diseases (cancer other than liver cancer, multi-organ failure) also don’t qualify for a transplant as the mortality risk is extremely high. Living donation has been developed by surgeons to help overcome the organ donor shortage by removing a portion of liver from a live donor and

transplanting it into a recipient. However this bears a risk for the live donor with a predicted mortality rate of 1:200 (Neuberger et al., 2003).

1.4 Extracorporeal Liver Devices

Extracorporeal liver devices are used outside of the body and are supposed to support liver functions. There are two types of support systems: Artificial Liver devices and Bioartificial Liver devices.

1.4.1 Artificial Liver Devices

There are currently two artificial liver devices for toxin removal by chemical and physical means which are available including the molecular adsorbents recirculating system (MARS) and Prometheus.

MARS (Gambro Hospal GmbH) is an albumin-based dialysis system that removes both water-soluble and fat-soluble toxins. A specific membrane enables the selective transport of albumin bound metabolites to the albumin containing dialysate compartment, where the loaded transport albumin is cleared by adsorption and returned to the patient (Klammt et al., 2002). MARS is the best studied artificial liver device with data from about 15,000 patients from 150 centers (Leise et al., 2014). It was approved by the Federal Drug Administration (FDA (USA)) for treating drug overdose and hepatic encephalopathy (HE) caused by chronic liver disease (Al Sibae & McGuire, 2009; O'Grady, 2006). The MARS system was demonstrated to be effective in removing albumin-bound toxins, such as fatty acids, bile acids and bilirubin (Stange et al., 2002). However, there was no beneficial effect on survival in patients with ACLF (Bañares et al., 2013).

The Prometheus device (Fresenius Medical Care, Sweden) is a combination of albumin adsorption with high-flux haemodialysis. In a first step endogenous albumin is separated from the patient's blood with the help of a filter. The albumin then passes via two absorbers which retain toxic molecules and the purified albumin is returned to the patient. Water soluble toxins are removed via dialysis. Studies suggest improved serum levels of conjugated bilirubin, urea, bile acids, ammonia, cholinesterase, creatinine, and blood pH (Rifai et al., 2003). Both systems rely solely on filtration; many vital liver

functions are not carried out, resulting in them being inapplicable for long-term supportive treatment with no extension to survival shown.

1.4.2 Bioartificial Liver Devices

The bioartificial liver (BAL) device is a system that mimics the functions of a liver by perfusing an extracorporeal hepatocyte-containing bioreactor with patient plasma. There are several different BAL applications that are under development of which some have undergone clinical trials. However until now none of the BAL devices is commercially available. Systems differ in reactor and cell types, of which the following have been used: primary porcine hepatocytes, immortalized hepatocytes and primary human hepatocytes (Allent et al., 2001).

The HepatAssist or Hepamate (Circe Medical, US) is a porcine hepatocytes based hollow fibre bioreactor. The patients' blood is first separated into plasma and cellular components in a plasmapheresis device. The plasma first goes through two charcoal filters, which filter out plasma bacteria and particulates. Subsequently plasma is flushed through the hepatocyte-lined hollow fiber column. The purified plasma is then reunited with the plasma component, and the whole blood is reinfused into the patient. Although promising results were gained with ALF patients during clinical phase I and II, insufficient efficacy for market approval was reported for phase III studies (Demetriou et al., 2004). At the moment a new phase III is being planned.

Another system is the AMC BAL developed by Chamuleau at the Academic Medical Centre of Amsterdam. This system uses nonwoven hydrophilic polyester matrix for cell attachment, hollow fibres for the oxygen supply and porcine derived liver cells. The system has undergone clinical trial phase I in 2002 with promising results. Six of the seven ALF patients were successfully bridged to orthotopic liver transplantation and one patient showed improved liver function after two treatments. However no second trial phase has been carried out within the last 12 years (van de Kerkhove et al., 2002).

The Extra-corporeal liver assist device (ELAD) (Vital Therapies, US) uses the immortalized human hepatoma cell line C3A, a subclone of the HepG2 cell line. Cells are housed within a hollow-fibre cartridge. Although the ELAD system was proven to

be safe, no significant differences between standard medical and ELAD treatment were observed during a pilot trial including 24 patients (Ellis et al., 1996).

1.5 Liver group BAL

The UCL liver group BAL consists of a fluidised bed-based bioreactor (FBB) that contains alginate-encapsulated liver (HepG2) cells (AELC) which mimic many functions of adult hepatocytes. A large number of hepatocytes are required to treat ALF. It has been estimated that for a clinical setting more than $2x10^{11}$ cells may be required to support a patients' liver function. The system described here has been used with a numbers of cells in the region of $7x10^{10}$, for clinical usage by increasing the volume of alginate beads and by adjusting the geometry of the biomass chamber. In order to treat ALF, several stages must be completed. In a first step single cells are encapsulated within the alginate matrix. After a culturing period of at least 11-12 days within the FBB, cell numbers will have increased to several thousand cells per bead. Once sufficient biomass has been produced, the BAL device can be connected to the patients' circulation via a plasmapheresis machine. Plasma, which is separated from the remainder of the blood, is perfused through AELC housed within the BAL. HepG2 cells simultaneously detoxify plasma and secrete liver-specific proteins into the patient's plasma. The treated plasma undergoes a filtration process to hold back DNA, endotoxins, cell debris and alginate particulates before the plasma is finally reinfused into the patient to meet regulatory requirements (Figure 1.1).

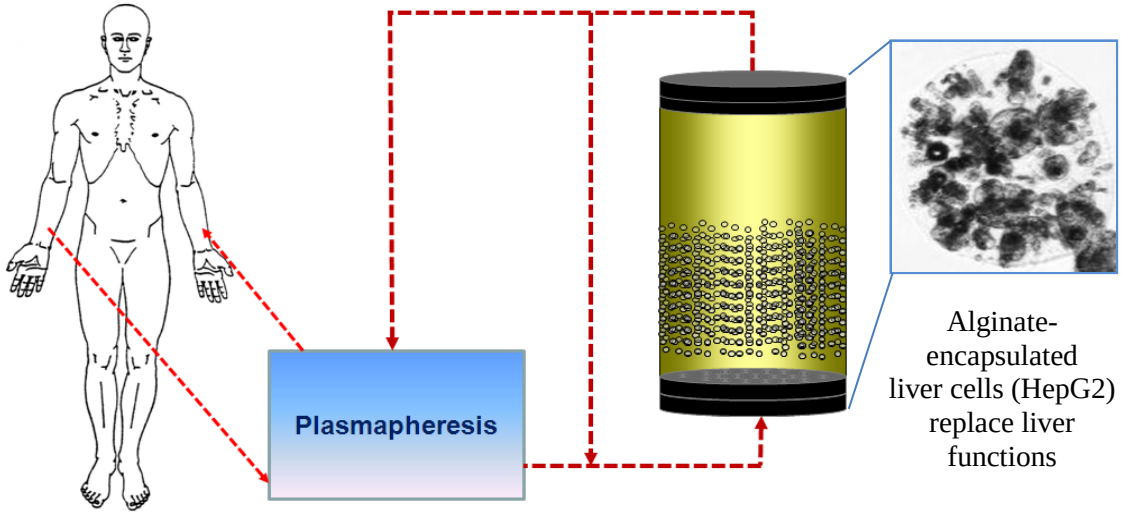

Figure 1.1. The bioartificial liver device

The extracorporeal bioartificial liver (BAL) device sustains the patient's liver functions. The patient's plasma is perfused against alginate encapsulated liver cells housed within the fluidized bioreactor. HepG2 cells detoxify the plasma and secrete liver-specific proteins. The treated plasma undergoes a filtration process to eliminate unwanted bi-products.

1.5.1 HepG 2 cell line

The immortal human hepatoblastoma HepG2 cell line was derived from a 15 year old Caucasian male. HepG2 cells which are epithelial in morphology, are well characterised and perform many of the liver functions (Slany et al., 2010). However they do not possess comparable detoxification function of ammonia (Mavri-Damelin et al., 2007) or xenobiotics (Hart et al., 2010) compared to adult hepatocytes. The advantage of utilising a cell line is that availability is sufficient and that cells are allogeneic. In contrast, primary human hepatocytes have the disadvantage that they are not readily available, as good-quality explant livers are usually used for transplantation. Primary porcine hepatocytes which are available in sufficient numbers bear the risk of zoonosis transmission and potential species incompatibility in protein/protein receptor interaction (Roussel et al., 2008). Any source of primary liver cells also requires enzymatic digestion of the liver, a process which is expensive and not easily standardized.

1.5.2 Alginate encapsulation

Alginate (a salt of alginic acid) is a biocompatible anionic polysaccharide that is found in the cell walls of brown algae. The raw material after extraction and processing,

commonly sold as a dry powder, is known as sodium alginate. Alginate has been used in a variety of very different applications due to its ability to reversibly form a hydrogel by quickly absorbing water (up to 200-300 times of its own weight) whilst undergoing cross-linking induced by calcium ions, and it is innocuous to the human body. It has been used in the manufacture of paper and textiles, in the food industry and in various pharmaceutical preparations. Alginates from different species of brown seaweed can vary in their chemical structure, for example in the ratio of mannuronic and guluronic acids. This can have an impact on the hydrogel rigidity and permeability which are important factors for the encapsulation and culturing process of AELC. The alginate hydrogel for cell encapsulation normally consists of approximately 99% water to allow for sufficient diffusion of nutrients and oxygen, and to provide enough space for the cells to grow unhindered. Alginate beads are of approximately 450µm +/- 31 (average +/- SD, n=100) and contain a few hundred cells over the first few days. HepG2 cells proliferate rapidly within the alginate scaffold forming tissue like spheroids within 2-3 days of culture (Figure 1.2). Cell mass and cell functions are significantly increased in comparison to the same cells in monolayer cell cultures (Bokhari et al., 2007; Coward et al., 2009; Selden et al., 1999). In three dimensional HepG2 cultures, cell-cell contacts such as gap junctions and desmosomes but also large amounts of extracellular matrix have been observed, indicating that 3D alginate encapsulation provides an environment for HepG2 cells that is similar to that found *in situ*. The in-vivo like environment and the tissue like growth of AELC is thought to be responsible for the markedly upregulated cell function.

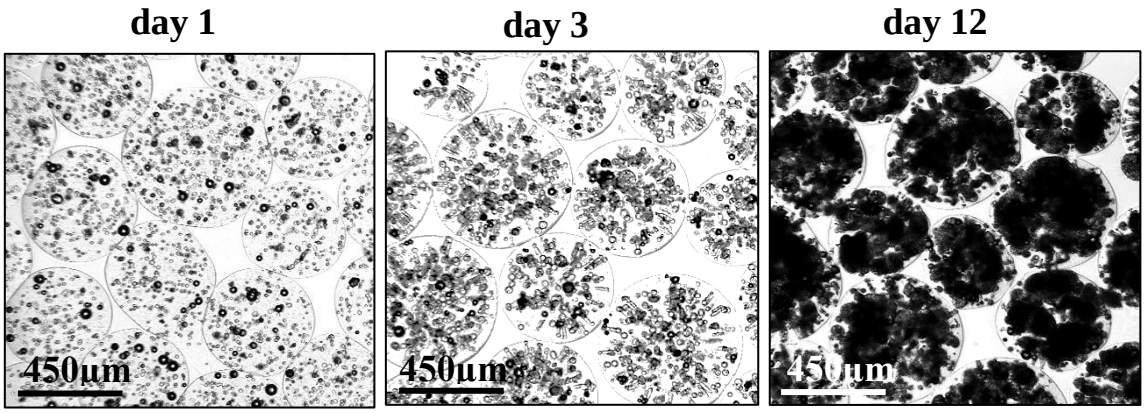

Figure 1.2. Alginate bead size and cell spheroid formation

A single cell suspension is used for the alginate encapsulation process. The average bead size is 450µm +/- 31 (average +/- SD, n= 100). One day after encapsulation cells still exist as single cells, with a hundred cells per bead. After 2-3 days cell spehroids start to form. After 12 days most of the alginate bead is filled with cells with a few thousand cells per bead.

1.5.2.1 HepG2 cell growth in alginate beads

A concentration of 1.75 million cells per ml of alginate-media mixture and an average bead size of 450µm has shown to be most suitable for rapid cell growth, providing sufficient mass transport and cell density. With initially about a hundred cells per bead, cell density is increased to several thousand cells per bead after 12 days of growth. The initial linear growth rate (day 0 to day 7) of approximately one million/cells per 24 hours increases to more than three million cells per 24 hours between day 8 and 11. After 11 days cell growth slows down and after 12 days the stability of the alginate matrix is strongly diminished, leading beads to break and cells to grow outside the scaffold.

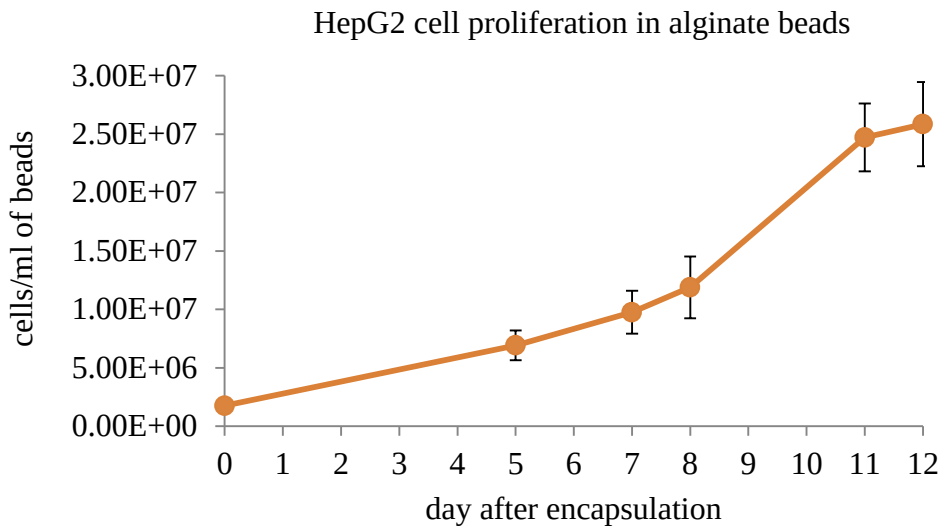

Figure 1.3. HepG2 cell proliferation in alginate beads

The graph shows HepG2 cell proloferation in alginate beads over 12 days. Cell numbers were measured by nucleocount. The data presents the average of 6 indiviual experiments (n=6 +/-SD). Cell density increases from initially 1.75 million cells/ml of beads on day zero to 26 million cells/ml of beads on day 12.

1.5.3 The fluidized bed bioreactor system

Two main criteria are of special importance when designing a BAL system: the availability of sufficient biomass and a high transfer of toxic metabolites from the blood to the cells for detoxification, and molecules synthesised by AELC to the patient. Inside the fluidized bed bioreactor (FBB) an upward flow of media and downward force of gravity are keeping cells in continuous motion. The FBB imposes no physical filtration barrier between the biomass and the patient's plasma circulation. That means that the patient's plasma is in direct access to the alginate hydrogel beads, providing high mass transfer. Culturing cells in a FBB provides optimized homogenous distribution of nutrition and oxygen, while shear forces are kept to a minimum. Also temperature and pH are controlled. All these properties help to increase proliferation rates and maintain high viabilities (Coward et al., 2005; David et al., 2004; Erro et al., 2013).

1.6 Bioartificial Liver preservation

In many cases the BAL device must be ready for use within a few hours to effectively treat ALF. A large number of cells are required to treat an adult patient and even in

optimal conditions it takes up to 11 days to obtain sufficient cell mass and to condition them in the AELC format to effectively support the patient's liver functions. In order to be applicable for rapidly available routine clinical therapy and for transportation purposes to the treating hospital, some sort of preservation technology is needed.

1.6.1 Short-term preservation

Storage on ice or at 4°C (fridge) can be used to maintain cell viability and function over a short period of time and during transportation. Cold storage or hypothermic storage is often used for tissues and organs for which cryopreservation is not suitable, but is also applied to preserve single cells, for example for transportation purposes. A reduction in temperature slows down the cell metabolism and therefore helps to reduce the oxygen and glucose demand, both needed to maintain the mitochondrial adenosinetriphosphate (ATP) production. Loss or decreased ATP synthesis can result in membrane ion pump failure and a loss of membrane integrity which consequently results in cellular swelling, membrane leakage and a cascade of degenerative processes. Cells can overcome a lack of oxygen by switching over to an anaerobic metabolism whereby lactate is produced (Fuller, 1987; Fuller et al., 2013). However, this process can only provide 5% of the normal ATP production. A strategy to minimize oxygen depletion is the addition of perfluorodecalins (PFC) to the incubation solution. PFC has shown to dissolve large amounts of oxygen and therefore can provide an additional supply of oxygen during storage (Baertschiger et al., 2008).

Organs, such as kidneys, pancreas and liver, and also tissues for transplantation are especially prone to ischaemia, which is caused by a restriction in blood supply and a resulting shortage of oxygen and glucose. Reperfusion injury which include oxidative stress, and inflammatory responses occur as the organ is returned to 37°C and oxygen delivery is restored (de Rougemont et al., 2009). Special preservation solutions such as the University of Wisconsin (UW) solution have been developed to reduce ischaemia and reperfusion injury and PFC is used to sandwich organs between a layer of PFC and organ preservation solution to minimize oxygen depletion (Liu et al., 2007).

1.6.2 Short-term Bioartificial Liver preservation

A considerable advantage for hypothermic storage is that there are no special requirements for the transport at 4°C and logistics are comparably easy and cost effective, thus, making it an attractive option to maintain the cold-chain until delivery. A disadvantage is that the storage time is limited, at most to a few days (Massie et al., 2013). This has several consequences for the BAL production. The estimated cost to manufacture a BAL (until use) is in the range of 10000 pounds. This means an enormous economic loss for each BAL that is not being used. On the other hand availability cannot be assured as quality and sterility problems during the production process can lead to the loss of a BAL device. Long-term storage is therefore preferable over short-term preservation. It also allows producing AELC on a very large scale, which reduces manufacturing costs. Moreover, the amount of AELC needed can be adjusted depending on the length of treatment and the patient's needs. For example, children might need less biomass to support their liver functions than an adult male patient. As adequate cell mass and cell function are crucial, an appropriate freezing method for high volume applications (1-2 litres) must be developed which retains all the necessary liver functions during the early post-thaw period.

1.7 Cryopreservation: long-term preservation

Cryopreservation is a process whereby cells or tissues are cooled below the temperature of their biological activity and down to ultra-low temperatures (below the glass transition ~-120°C) which in theory could provide infinite shelf life. For example, sperm have been successfully stored for more than 20 years (Yogev et al., 2010). Cryopreservation is routinely used to preserve semen, blood, stem cells, oocytes, embryos and plant cells, but attempts to freeze larger tissues or even whole organs have failed. However, cell suspensions such as red blood cells have been cryopreserved at intermediate volumes (Sputtek et al., 2011). Normally samples are cooled to -180°C and are stored at -196°C (77K), the boiling point of liquid nitrogen. In practice, cryopreservation is a complicated procedure that has to overcome several obstacles during the freezing and thawing process. However, if the cells can reach ultra-low temperature without injury, cells are relatively safe from further damage during prolonged holding in that biopreserved state. There are several additive stresses which

result from the freezing and thawing or cooling and warming process and they include solution effects, osmotic effects, dehydration, oxidative stress, extracellular and intercellular ice formation and particularly intracellular ice crystals, which can all be individually or collectively responsible for cell damage.

1.7.1 Extracellular ice formation

Extracellular ice formation is a normal event for a slow cooling process and is well tolerated for a variety of cells in suspension. On the other hand, intracellular ice formation which is in most cases cell damaging has been suggested to be a direct consequence of extracellular ice formation. Several theories suggest that extracellular ice initiates intracellular ice growth. For example, Mazur hypothesized that external ice could grow through aqueous membrane pores and seed the supercooled cytoplasm, but that this could only happen if the tip radius of the ice lattice is comparable to the radius of the membrane pore (Mazur, 1965). Proteinaceous membrane pores were also suggested to serve as ice propagation tunnels (Acker et al., 2001; Acker & McGann, 1989). As an alternative mechanism, observed in plants, it has been proposed that extracellular ice expands through damaged membrane sections (Dowgert & Steponkus, 1984). It was also suggested that extracellular ice alters the cell membrane so that it acts as a nucleation side for intracellular ice formation (Toner et al., 1990).

1.7.2 Intracellular ice formation

It has been commonly accepted that intracellular ice formation is a lethal insult to cells. This conclusion was based on the observation that fast cooling, which leads to excessive intracellular ice formation, results in low cell viability (Mazur, 1960). Furthermore it was shown that cell-cell contact is a mediator for ice propagation which partially explains lower viability for connected cells such as spheroids and confluent monolayer cells (Acker & McGann, 1989). A further aspect is that dehydration of multicellular components is more complex, as water must exit cells sequentially from centre to periphery (Balasubramanian et al., 2006; Ehrhart et al., 2009). Nevertheless, more recent observations have shown that intracellular ice formation can be tolerated to some extent and that small fractions of intracellular ice might even provide some

cryoprotection by preventing cell dehydration during slow cooling (Acker & McGann, 2000).

1.7.3 Intercellular ice formation

Especially problematic is intercellular ice formation in tissues or multi-component cell spheroids where ice crystals can disrupt the tissue structure that is required for maintenance of function (Liu & McGrath, 2005; Pegg et al., 2006). Another mechanism by which intercellular ice can be damaging in tissues is the formation of ice lenses. More and more water is drawn to the ice lenses via capillary action and cells that are in close proximity might become dehydrated and suffer from osmotic stress. Also as the ice lenses grow they can produce mechanical stress (Muldrew et al., 2000). It has also been reported that cell concentration has an effect during freezing as higher hemolysis levels were observed for closely packed erythrocytes. Cell-cell contacts, reduced dehydration and mechanical forces were suggested as potential causes for an increase in cell injury (Nei, 1981; Pegg, 1981).

1.7.4 Osmotic effects and dehydration

Osmosis is a process that occurs when two aqueous solutions are separated by a semi-permeable membrane which allows only water and selected molecules to diffuse through. Cell membranes are semi-permeable. When cells are placed in hypertonic solutions, water molecules are osmotically drawn from the cell interior to the extracellular environment to maintain a chemical potential equilibrium. This is shown by the volume shrinkage of the cell and dehydration of intracellular compartments. Extreme dehydration is normally seen during slow cooling procedures with increasing salt concentrations outside the cell. During this process cell water can decrease to less than 10% of the initial content, which is a lethal irreversible insult for most mammalian cells. Cell membranes can continue to permit water flux from the cells even at very low temperatures during the slow cooling process. If the cooling is faster, (for example between five to ten minutes to below -100°C), the cell cannot dehydrate to balance the external increase in osmotic concentrates, and a higher residual cell water is left inside the cell, potentially causing ice formation. A reverse osmotic stress occurs especially after the thawing and warming process when mobile water molecules become released

from the ice - solute matrix or the freezing or vitrification media is exchanged too quickly with fresh media and the cells, now loaded with cryoprotectants (CPA – see section 1.7.6), may undergo extreme swelling as water molecules will re-enter the cell, which can lead to membrane rupture (Acker & McGann, 2000; Farrant & Woolgar, 1972; Lovelock, 1953). Step-wise addition and removal of CPAs have been shown to significantly improve survival of various cell types including oocytes (Isachenko et al., 2004; Wang et al., 2010) and Islets of Langerhans (de Freitas et al., 1998). To minimize osmotic stress non-penetrating CPAs like sugars are oftentimes added to the cryoprotectant mix and/or the thawing medium (Terry et al., 2010).

1.7.5 The Equilibrium Melting temperature of aqueous solutions

Ice nucleation requires an appropriate temperature and a nucleating centre to achieve organisation of water molecules to form an ice nucleus. As ice nucleation is a stochastic event within a certain temperature range, an exact freezing temperature cannot be consistently determined. The temperature at which a solution freezes is therefore not considered as a characteristic property of that particular aqueous mixture, and instead the melting point, defined as the temperature at which the last ice crystal disappears, is used to indicate the temperature at which ice formation would theoretically be possible. It is possible to objectively define this using calorimetric methods. The process of aqueous solutions being cooled below their equilibrium melting temperature without ice formation is termed supercooling and is a critical event during slow cooling cryopreservation (Diller, 1975). As an example: water normally freezes at just below 0°C, but pure water which has been specifically treated to be free of nucleation sites can be "supercooled" at standard pressure to well below 0˚C, and may even approach the homogeneous nucleation temperature of -48°C. There are different ways to measure the melting point of a solution. When ice forms, energy is released as a result of the phase change from liquid to solid. The exothermic event of ice formation causes the temperature of the mixture to rise close to the equilibrium melting point, although this is restricted in accuracy by sample volume and the surrounding temperature. Another method to determine the melting temperature is to visually inspect at which temperature the last ice crystal melts, but for exact measurements sensitive differential scanning calorimetry has to be used. The melting (freezing) temperature of water and aqueous

solutions can be depressed by adding compounds that interact with water molecules. The efficacy depends on the ability of the compound to interrupt the formation of organized water patterns (i.e. the ice lattices). As the concentration of the introduced compound is increased, the more the freezing point temperature is depressed. These compounds are also called cryoprotectants in the case where they exhibit cellular protective functions against freezing damage, and the process is known as colligative action.

1.7.6 Cryoprotectant agents

Cryoprotectants agents (CPA) are molecules that protect cells from any sort of cryo-damage. In nature in extreme environments, there are several animal species like frogs, fishes, reptiles and insects which have adapted to sub-zero temperatures. They use natural CPAs like sugars or polyols (e.g. glycerol, glucose) to lower the melting (freezing) temperature of intracellular water and function as a water substitute for vital hydrogen bonding, e.g. to DNA and proteins. Cryoprotectants can be broadly classed into two groups: penetrating CPAs and non-penetrating CPAs.

1.7.6.1 Penetrating CPAs

Penetrating CPAs are small, non-ionic molecules that can pass relatively quickly through the cell membrane. Penetrating CPAs have several functions, but one main action is the depression of the freezing point, when they are used in sufficient concentrations, usually in terms of 10 to 15% weight per volume, or 1 to 2 mol per litre for a slow cooling approach. Me_2SO (DMSO or CH_32SO), one of the most commonly used penetrating CPAs is often used in combination with fetal calf serum (FCS) which is an extracellular protein with some cryoprotectant properties. Inside the cell, penetrating CPAs may interact with the remaining water molecules and so ice crystal formation is minimized or ideally avoided. As CPAs reduce the freezing point inside and outside the cells, longer dehydration times can be provided. Additionally, solute concentrations which are potentially toxic are reached at lower temperatures at which they are supposedly less toxic (Lovelock & Bishop, 1959). Some CPAs such as glycerol also stabilise membrane components and macromolecules such as proteins during dehydration (Meryman, 2007).

The efficacy of penetrating CPAs depends on membrane permeability as firstly the CPA must be present intracellular to be effective. To ensure sufficient CPA permeation is a comparatively simple process for single cell, but is more complicated for tissues and organs as the intracellular CPA concentration will differ between cells located at the tissue surface and deep inside the core. Perfusion, longer incubation times or at higher incubation temperatures will rectify this; however sustained exposure to CPA at temperatures required for permeation may in itself result in cell death (Karlsson et al., 1993; Mukherjee et al., 2007). Methods to determine the CPA concentration within a tissue can give important information of how to improve incubation parameters. For example, attempts have been made to determine CPA penetration in cartilage by measuring the remaining water using Fisher's titration (Pegg et al., 2006).

1.7.6.2 Non-penetrating CPAs

Non-penetrating CPAs are water-soluble molecules that are too large to pass the cell membrane barrier. They typically include sugars such as sucrose, glucose or ficoll or carbohydrates such as hydroxyl ethyl starch. They are generally less toxic than penetrating CPAs and may be primarily used to reduce the risk of lethal intracellular ice formation by decreasing the volume of intracellular mobile water by osmotic dehydration (Fuller et al., 2004). The use of non-penetrating CPAs alone is normally not sufficient to protect cells during cryopreservation but may be used to reduce the required concentration of more toxic penetrating CPAs. This approach has been utilised for slow cooling cryopreservation of stem cells where Me_2SO was partially substituted with sucrose (Petrenko et al., 2008) and is commonly applied in vitrification procedures for which high concentrations of toxic penetrating CPAs are needed to prevent any ice formation. Additionally some sugars have been shown to have good membrane stabilizing effects (Crowe et al., 1987) and can help to reduce osmotic pressure during the cooling and warming process.

1.7.7 Slow cooling protocols

Controlled-rate or slow freezing has been used over the last 40 years and since then many well established protocols to freeze e.g. oocytes, blood products, embryo, sperm and stem cells have been developed. Intracellular ice formation is avoided by cell dehydration and penetrating CPAs hold non-freezable water fractions within the cell. As

pure water molecules are drawn out of solution to form ice lattices, the external solute concentration increases, leading to higher osmotic cell pressure. To equilibrate the extracellular and intracellular osmotically-active solute concentrations, water molecules are drawn to the extracellular environment. With increasing solute concentrations outside the cell (as more ice is formed at lower temperatures), the amount of water inside the cell decreases and therefore less residual cell water remains to freeze inside the cell. Intracellular CPAs interact with remaining water molecules, preventing the formation of ice lattices. A slow cooling rate has to be applied to provide cells with sufficient time to dehydrate. The optimal cooling rate is dependent on the cell type (e.g. cells with membranes that allow fast diffusion of water molecules outside the cells can tolerate accelerated cooling rates as they can dehydrate faster). A typical cooling rate for many mammalian cells is about -1˚C/minute and can be achieved either by using a benchtop portable freezing container or a controlled-rate freezer which can normally support cooling rates between -0.1°C and -10°C/minute. As a result of dehydration the electrolyte concentration within the cell increases. High electrolyte and CPA concentrations inside and outside the cell are cell damaging. It has been suggested that these solution effects are the main reasons for cell damage during the slow cooling process and exposure time to these hypertonic solutions should be minimised. Hence, the optimal cooling rate for a specific cell type will be an intermediate rate, which allows dehydration (to avoid intracellular ice formation) but also minimizes exposure to toxic solute concentrations (Lovelock & Bishop, 1959; Mazur et al., 1972).

1.7.7.1 Supercooling and Ice Nucleation

Another obstacle that has to be overcome during the slow cooling process is the event of supercooling. If nucleation is initiated in a supercooled extracellular solution, ice will form abruptly leaving less time for cell dehydration. Due to the exothermic reaction of ice formation, the temperature will increase to approximately the melting point of the solution; however the temperature of the freezer will, if not changed, remain low. Thus the cooling rate will differ from the optimal cooling rate as there will be a higher difference between sample and freezer temperature. Supercooling can be prevented or reduced by adding nucleators such as cholesterol (Massie et al., 2011) or by ice seeding which is a method to initiate the formation of ice once the solution has supercooled by introducing a nucleation point in form of an ice crystal or cryogen-cooled forceps.

"Seeding" is commonly and effectively used for the cryopreservation of small samples such as oocytes (Stachecki & Cohen, 2004) and spermatozoa (Songsasen & Leibo, 1997), but is difficult to apply to larger sample volumes due to strong temperature deviations throughout the sample.

1.7.7.2 Warming process

Even more problematic than the cooling process can be the warming process. Dehydrated cells can be damaged by osmotic injury when the water flux inside the cell happens abruptly, leading to cell swelling. On the other hand ice re-crystallization might occur during warming as small intracellular ice crystals, (if those have formed during the cooling process) will melt first. The now freely mobile water molecules will, if the temperature is too low, connect with larger ice crystals to form longer detrimental ice lattices. Nevertheless, if the warming rate is high enough, re-crystallization can be reduced, but rapid thawing might cause higher osmotic pressure and CPA toxicity (Mazur, 1984).

1.7.8 Vitrification

A second method to prevent intracellular ice formation is by vitrification. First approaches to vitrify small living organisms without CPAs but at very high cooling rates go back as far as 1937 (Luyet & Gehenio, 1940; Luyet, 1937). Later, with the discovery of glycerol by Polge, post-warming viabilities were substantially increased (Polge et al., 1949).

Vitrification is a process at which a solution is cooled below its glass transition temperature without ice crystal formation leading to an amorphous matrix that could also be defined as an extremely cold viscous liquid. The glass transition temperature is solution specific and determines the point at which all molecular motion is being stopped. In cryobiology, vitrification can only be achieved by adding high amounts of CPAs (in excess of 40% weight/volume) which interact with the remaining water molecules in the whole sample and prevent the formation of necessary organised patterns of interacting water molecules (so-called nucleation centres), which initiate the ice crystal lattices. Thus, no ice can form, however deep the subzero temperature is. However, high CPA concentrations are normally toxic to mammalian cells, and

therefore the exposure time should be minimised. This can be achieved in small samples such as a few tens of microliters where high but non-vitrifying concentrations of CPA can be tolerated and fast cooling (in the order of -500˚C/minute) kinetically outruns the potential for ice crystals to nucleate and grow to damaging sizes. Even though high cooling rates could be achieved, enough time must be given for CPAs to penetrate into the cells. For larger tissues and organs, and also for cell spheroids, this time can be too long to avoid CPA toxicity.

1.7.9 Cooling and warming of bulky samples

A well-controlled slow freezing cryopreservation protocol normally fails when it comes to any kind of bulky sample. A sample volume that exceeds the typical laboratory scale of a few micro to millilitres prevents uniform and homogenous thermal transfer throughout the whole sample, which is necessary to obtain the optimal cooling rate for successful dehydrative cryopreservation and the high warming rates to prevent ice re-crystallisation for all cells within a sample. In essence, if the cooling profile of a bulky object is set to be the optimal measured with cells in small volumes, the surface cells within a radius of a few millimetres will cool appropriately; however, deeper in the core of the sample, the cooling rate will be lower because the heat transfer properties of the sample will not match those of the cooling chamber. This difference will be smaller for lower cooling rates but the time in which cells are exposed to high solute concentration can be problematic. For cell suspensions, but not for organs or tissues, a more homogeneous cooling rate could possibly be established by mixing the suspension. The slow cooling process is further complicated by the release of latent heat of ice crystal formation. In bulky samples this heat cannot be conducted out of the samples as easily and it can be assumed that smaller intracellular ice crystals might melt to then form larger, damaging ice lattices.

Similar difficulties arise for the vitrification of large volumes. There are specific requirements for sample volume and cooling rates, which must be imposed to avoid non-equilibrium glass transitions (Edgar & Gook, 2012), which are likely to favour devitrification (formation of lager ice crystals) during the warming process. Ultra-rapid sample manipulation (of a few tens of seconds) and cooling rates normally in excess of -500°C/minute, are in general required to avoid toxic effects from high CPA

concentrations, and kinetically favour the glass transition. Cooling rates for volumes of several hundred millilitres are substantially lower than for volumes of a few hundred microliters - the normal volume for vitrification. Consequently CPA toxicity will be detrimental. An additional problem of ultra-fast cooling is the instability of the amorphous state, which can lead to the formation of cracks during the vitrification process (Pegg et al., 1997; Wassenaar et al., 1997). Cracking or fracturing is caused by mechanical stresses such as thermal expansion or contraction, leading to pressure and tension. Single cells are not thought to be affected, but tissues and organs for which the functionality of the entire unit is important can detrimentally be damaged. It has also been reported that fractures might initiate ice nucleation that can lead to devitrification (Williams, 1989). Similar mechanical stresses might affect the container material. Materials have been developed for cryovials of up to 5ml, but larger containers are more problematic as they are more susceptible to mechanical stress. Plunging the container into liquid nitrogen bears the risk of not withstand the rapid temperature change.

1.7.10 Liquidus Tracking

Liquidus Tracking (LT) is a method of achieving vitrification in an aqueous mixture by using incrementally increasing concentrations of penetrating CPAs (up to 70%) at decreasing temperatures. It also provides the lowest toxic effect that can be established for a given CPA concentration by decreasing the sample temperature to just above the melting point of that particular mix. At low temperatures CPA toxicity is reduced due to decreased cell activity and reduced CPA permeation. This approach was first carried out some 40 years ago by Farrant (Farrant, 1965b) who originally intended to avoid solution effects and to maintain a constant electrolyte concentration during the cooling process. Later the benefits of avoiding ice per se became more evident. The technique has been revived and more clearly defined in recent years by Pegg's group, and has become known as Liquidus Tracking (Pegg et al., 2006; Wang et al., 2007). The main advantage of this method is the diminution of CPA toxicity. The liquidus curve defines the equilibrium melting point temperature for a given CPA mixture (i.e. the highest sub-zero temperature at which ice crystals and liquid can co-exist), and this knowledge allows prediction of the lowest subzero temperature which can be reached for that given CPA mix without ice nucleating. Cryoprotectants are less toxic at lower temperatures

(Matheny et al., 1969; Weihe, 1973) and lower concentration. By adding smaller amounts of CPA at each step and subsequently cooling the sample to just above its freezing point, toxicity is minimized when attempting to achieve the very high CPA concentrations required for vitrification. The more increments used, the closer the sample can be kept to the liquidus curve of its carrier CPA solution. Due to reduced CPA toxicity, and avoidance of ice nucleation, samples can be vitrified without the necessity of fast cooling rates, preferable for cooling large volumes, or when longer exposure times are required to allow for sufficient CPA penetration - for example for organ and tissue vitrification.

Of equal importance for these larger volumes is the warming process, which must be reversed in a controlled (stepwise) fashion to dilute the high CPA concentration whilst avoiding any propensity for ice to nucleate. Elford and Walter used the LT approach to study the role of anionic composition and pH of the carrier solution needed to deliver the increasing concentrations of CPA (Elford & Walter, 1972). Isolated strips of taenia coli muscle were progressively cooled to -79°C with a final concentration of 60% (w/v) Me_2SO to prevent freezing. Muscles showed slow recovery and were severely damaged both functionally and structurally when the incubation media had a similar composition to that of Krebs solution, but showed better recovery after rewarming when potassium-rich media containing Na^+, K^+, and Cl^- were used. The degree of recovery was dependent on the size of the anion, showing better contractility of the muscles for glycerophosphate, TES or PIPES (*N*-tris-(hydroxymethyl)-methly-2 amino- or piperazine-*NN′*-bis-2-ethanesulfonates) than for sulfate or ethylsulfate derived anions. When using potassium-rich PIPES media, recovery was lower when the pH was reduced.

The technique lay dormant for many years until it was revived by David Pegg and colleagues (Pegg et al., 2006; Wang et al., 2007). Pegg used the same protocol as Elford and Walter (but with different incubation times) for LT vitrification of articular cartilage and found that damage was predominantly associated with the formation of ice during standard cryopreservation, which supported the use of a vitrification protocol, but CPA toxicity and the need for rapid warming resulted in inadequate recovery. By using the LT (equilibrium vitrification) approach, cartilage was successfully recovered with good

metabolic activity (based on an incorporation of sulphate into newly synthesized glycosaminoglycans (GAGs) at 70% of that of fresh control cartilage). The first experiments were carried out using a Dow Corning oil bath for step-wise cooling, and manual transfer of the samples to increase CPA sufficiently to suppress ice formation at the set temperatures; thereafter a controlled rate Planer freezer was used to achieve continuously lowering temperatures which could be held at selected low temperature points. For optimisation, David Pegg in collaboration with Planer (a company specialising in cryogenic engineering), established an automatic pump and stirring system which constantly increases the CPA concentration whilst temperature is decreased. For the warming process normally the reverse protocol is used by constantly increasing the temperature whilst the CPA concentration is reduced (Figure 1.).

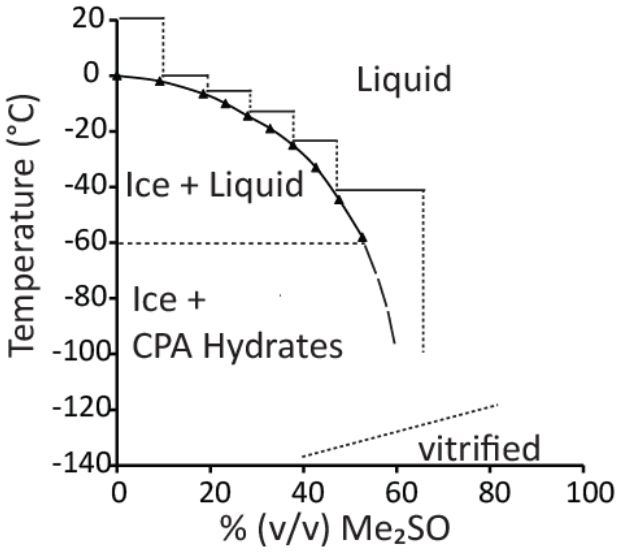

Figure 1.4 Equilibrium melting curve (liquidus curve) for Me_2SO

A schematic showing the Tm equilibrium melting curve (liquidus curve) for Me_2SO (modified from Elford, 1970 and Farrant, 1965). Arrows indicate a scheme for incremental addition of CPA to obtain the lowest toxicity for a given CPA concentration. This is achieved by decreasing the sample temperature to just above the freezing point (dashed vertical line above the liquidus curve) before adding more CPA (solid horizontal line) to prevent freezing at lower temperatures.

1.8 Aim of the project

The overall aim of this project was to develop a cryopreservation protocol which allows us to cryo-bank and warm high volumes of alginate-encapsulated liver cells for use in the BAL in order to provide a rapid treatment for acute liver failure. To cool a whole bioreactor with sufficient AELC to treat an adult patient would be the optimal solution for clinical applications. This approach would provide a rapid, easy to apply and more sterile product for clinical end-users than a situation in which cells from different small containers would be thawed and then mixed together. As cell mass and functional activities are crucial for the performance of the BAL, very high viability has to be obtained using a cryopreservation process. For rapid treatment high recovery should be optioned two days after re-warming. Due to slow thermal transfer and inhomogeneous temperatures in large volumes, neither the slow cooling protocol nor the fast vitrification procedure seems to be feasible for large scale cryopreservation (1-2 litres).
A slow cooling process to freeze a biochamper resulted in almost complete cell death after 48 hours of re-warming (Massie, 2011). No information currently exists for the use of the LT method for multicellular entities such as alginate encapsulated cell spheroids, but from theoretical considerations it may be an appropriate approach. LT is in many ways advantageous:

- It reduces or prevents osmotic injury, as CPA addition and reductions occurs continuously.
- If the chosen CPA concentration is high enough intracellular ice formation during cooling and re-crystallisation during the warming process will be suppressed.
- Solution effects, such as uncontrolled high CPA concentrations changing electrolyte concentration, will be prevented, and toxicity of controlled CPA concentrations is decreased by utilising low temperatures.
- However it can be assumed that chilling injuries like oxidative stress and changes in the cell membrane will still occur which could be problematic as both cooling and warming are slow processes.

Thus my aims were:

Chapter 3: To develop a fast and reliable method to assess cell recovery after the preservation process without the need to dissolve the alginate matrix. Viability can be determined by measuring the fluorescence of fluorescein diacetate and propidium iodide, dyes that stain viable cells green and dead cells red. Two methods to measure florescence intensity, a fluorescent microscope for which image analysis is used and a fluorescent plate reader will be evaluated.

Chapter 4: To develop a low toxic but also low viscous CPA solution so it can be used in a liquidus tracking procedure. Vitrification properties of the new CPA solution will be tested and the liquidus curve of the new CPA solutions will be determined.

Chapter 5: To evaluate whether Liquidus Tracking is a feasable method to cryopreserve AELC. For this it will be investigated whether CPA toxicity is reduced at lower temperatures. Different methods to carry out small scale manual liquidus tracking will be evaluated. To distinguish between osmotic injury and cytotoxicity the impact of osmotic pressure on cell viability will be assessed.

Chapter 6: To set up the automatic Liquidus Tracker and develop a filter system to maintain AELC inside the sample carrier. To increase the cooling rate by reducing the controlled rate freezer temperature.

Chapter 7: To optimize post-warming recovery. A simplified manual LT set-up will be used to pre-screen conditions which could be beneficial for automatic LT. Further stirring effect and CPA toxicity over time will be investigated.

CHAPTER 2
General Methods and Materials

The following protocols were developed previously to this work either as part of the alginate encapsulation process or as a means of quality control of HepG2 cell growth and function or for cryopreservation purposes and were implemented as standard operation procedures (SOPs) in the UCL Liver Group. The viability imaging analysis was developed as part of this thesis (Chapter 3).

2.1 Cell Culture

Cell culture was carried out under sterile conditions using a class II cabinet. The cells were grown in an incubator at 37°C in a humidified atmosphere of 95% air and 5% CO_2.

2.1.1 Preparation of complete media for monolayer cell culture

Materials

MEM-Alpha Minimum Essential Medium *(PAA, Cat. No. T1059, 2500)*

FCS 10% *(Hyclone, Cat. No. SV3016003)*

Insulin Acreacip 9.5 μg/ml *(Novo Nordisc, Cat. No. 8-0201-01-203-3)*

Penicillin and Streptomycin 100U/ml and 0.1mg/ml *(Gibco, Cat. No. 15070-063)*

BSA/Linoleic Acid 50μg/ml *(Sigma, Cat. No. L9530-5ml)*

Sodium Selenite 0.002μg/ml *(Sigma,Cat. No. S5261)*

Hydrocortisone 0.04μg/ml *(Sigma, Cat. No. HO888)*

Thyrotropin Release Hormone (TRH) 0.04μg/ml *(Sigma, Cat. No. P1319)*

Fungizone 1.25μg/ml *(Gibco, Cat. No. 15290-26)*

Filter Minisart *(Sartorius Stedim, Cat. No. 16534)*

Method

The previous components were added to a 500ml bottle of Alpha MEM using aseptic techniques. Before addition to the bottle supplements were filtered through 0.2μm Minisart filter (UCL/Liver Group SOP75).

2.1.2 Trypsinising monolayer cells

Materials

Trypsin solution pH 7.8, aliquots stored at -20°C:

Trypsin 0.25g/L, EDTA 0.1g/L *(Invitrogen, Cat. No. 15400-054)*

Trisodium citrate $2H_20$ 4.4g/L *(VWR, Cat. No. BDH102427X)*

KCl 10g/L *(VWR, Cat. No. BDH101983X)*

Hanks BSS Media *(PAA, Cat. No. H15-010)*

0.2µm filter *(Sartorius Stedim, Cat. No. 16534)*

Complete medium *(see 2.1.1)*

37°C warming oven

Syringes

21G needle

Nunc tubes and microfuge tube

Method

Trypsin is a serine protease that cleaves proteins mainly at the arginine residues and lyses the carboxyl side chains. It is used to cut the adhesion proteins in cell-cell and cell-matrix interactions. Calcium ions are essential for adhesion protein interaction, which is why EDTA is added as a calcium chelator. By reducing the calcium ion concentration protein binding can be further reduced. Cells were trypsinised at 70-80% confluency. In a first step cells were washed 3 times with 25ml HBSS media (RT) to remove any unattached dead cells. Then 50ml trypsin was added, covering all layers of the Triple Layer flask. Before use, trypsin was filtered (0.2µm Minisart) and pre-warmed in a warming oven (37°C). Trypsin was kept as aliquots in a -20°C freezer and was only stored for up to 1 week after thawing at 4°C to avoid post-thaw inactivation. After addition, the flask was stored in the incubator for a maximum of 5 minutes as trypsin is cytotoxic. Once the cells were detached (slight tapping of the flask might be required), 50ml of complete medium was added to stop the reaction and the mixture was split into two 50ml centrifuge tubes. Tubes were centrifuged at 300g for 4 minutes at room temperature and the cell pellet was re-suspended in 10ml of pre-warmed (37°C) complete medium. In order to disaggregate the cells, the mixture was passed 3 times through a 21G needle. After measuring cell counts and viability, $5x10^6$ cells and 100ml complete medium were added to a new triple layer flask which was kept in the

incubator at 37°C. Culture media were exchanged the following day after trypsinisation and then every 48 hours (UCL/Liver Group SOP18).

2.1.3 Cell Count and viability using Trypan blue exclusion test

Materials

Hemocytometer: *Neubauer Zählkammer*

Trypan blue *(Sigma, Cat. No. T-6146)*

Hanks BSS Media *(PAA, Cat. No. H15-010)*

Nikon TMS Microscope

Method

Trypan blue is a diazo dye that has its name from its ability to kill the parasite trypanosome. It traverses the membrane of dead cells and stains them blue, whereas living cells maintain their natural translucent colour. To perform cell counts and viability, 160µl HBSS, 20µl trypan blue and 20µl cell suspension were mixed in a microfuge tube and 9µl of this mixture was loaded into each side of a haemocytometer. A Nikon TMS light microscope was used to perform two cell counts using a 10x eyepiece and a 10x objective magnification (UCL/Liver Group SOP22).

Evaluation:

Cell number: (average living cells) x 10^5 cells/ml

Viability: 100*(number of living cell /total number of cells (living + dead)

2.1.4 Culture of Encapsulated HepG2s

Materials

High glucose medium (complete Medium with 25mM D-glucose):

0.2 µm filter Minisart *(Sartorius Stedim, Cat. No. 16534)*

45% D-glucose solution *(Sigma, Cat No. G8769)*

Method

Encapsulated cells were grown in complete media with additional glucose which was filtered before addition. Cells were grown in T175 flasks and the bead to media ratio was kept at 1:32 with a maximum of 6ml of beads per flask. For experiments cells were

grown in 6 well plates with 8ml media per well and 0.25ml beads (UCL/Liver Group SOP18).

2.2 Encapsulation of HepG2 cells into alginate

Materials

Alginic acid *(Sigma, Cat. No. A2033)*

Pluronic acid *(Sigma, Cat. No. P1300)*

DMEM *(PAA, Cat. No. 15883)*

High glucose media (see 2.1.4)

0.2µm hydrophilic filter *(Sartorius Stedim, Cat. No. 16534)*

0.2µm hydrophobic filter *(Sartorius Stedim, Cat. No. 16596)*

Sodium chloride-HEPES buffer (pH 7.4):

Sodium chloride 0.15M *(VWR, Cat. No. 27810,364)*

HEPES 15mM *(Gibco, Cat. No. 15630)*

Polymerisation Buffer (pH 7.4):

Sodium chloride 0.15M *(VWR, Cat. No. 27810,364)*

HEPES 15mM *(Gibco, Cat. No. 15630)*

Calcium chloride 0.204M *(Sigma, Cat. No.12022)*

Material baked at 180°C for 3 hours:

Glass Beads 10-50µm *(G. Kisker, Steinfurt, Germany)*

0.5-1L glass beakers

Material autoclaved at 121°C:

Bottomless beaker

JetCutter cutting tool

JetCutter cutting cover

JetCutter nozzle holder

JetCutter inlet filter

JetCutter tubing

JetCutter 300ml pressure vessel

Stainless steel forceps

Stainless steel spatula

Magnetic flea

Materials sterilized using 70% ethanol:

Elastic band

Nylon mesh *(Clarcor, Cat. No. NY/MO/2001/37/1020)*

JetCutter 350µm nozzle

JetCutter cutting disc (number of wires = 60, wire diameter = 100)

JetCutter system (*Genialab, Braunschweig, Germany*)

Method

To make a 2% (w/v) alginate solution, the adequate amount of alginic acid powder was slowly added to sodium chloride-HEPES buffer while being stirred and left for further stirring overnight. Alginate solution was autoclaved in the small Prestige Medical autoclave at 121°C for 10 minutes and left on ice to cool down before use. Cells were trypsinized and cell number determined according to 2.1.2 and 2.1.3, respectively. For encapsulation a 1:1 mixture of high glucose media and alginate solution (final alginate concentration 1% w/v) with a final density of $1.75x10^6$cells/ml and 1.75% (w/v) glass beads was prepared. Glass beads were filtered using a 200µm nylon mesh before use. The 1% alginate mixture was then aseptically added to the 300ml pressure vessel. One litre of polymerization buffer was autoclaved using a Prestige Medical autoclave (20 minutes, reaching 121°C) and was left to cool down at 4°C. Pluronic acid (0.2g) was dissolved in 5ml of the polymerization buffer and filter-sterilized using a 0.2µm hydrophilic filter. The filtered solution was returned to the polymerization buffer. 450ml were added to a 1L glass beaker for bead collection.

The JetCutter system was set up as follows: the nozzle holder was connected to the inline filter, which in turn had to be connected to the pressure vessel outlet. A nozzle (ethanol sterilized) was then screwed into the nozzle holder (Figure 2.1). The compressed air line was attached to a sterile hydrophobic filter which was connected to tubing attached to the pressure vessel inlet. The filled pressure vessel was attached to the overhead stirrer (stirs the alginate-media mixture inside the pressure vessel) and the motor was set to 1000rpm for 10 seconds, then to 150rpm. The compressed air line was opened as well as the pressure vessel outlet to start the flow through the encapsulator

(start pressure at around 0.25bar). For calibrating the system, 7.5ml alginate solution was collected in a 15ml centrifuge tube and the time was measured. The pressure was adjusted until the flow rate was approximately 20ml/minute. On the JetCutter control panel set-up run parameters for a standard run was set to: flow rate = 0.33-0.34ml/sec, nozzle size = 350µm, number of wires = 60, wire diameter = 100µm and motor speed = 3300rpm. The JetCutter software calculated the optimal angle of inclination, which was manually set on the JetCutter itself. Subsequently the cutting disc was placed onto the cutting tool which was then screwed to the JetCutter, followed by the collection cover. The beaker containing the polymerisation buffer and a magnetic flea (lowest stirring speed) was placed on a magnetic stirrer below the opening of the JetCutter collection disc. After adjust the opening on the collection cover the stream was collected. The beads were left for further 10 minutes in polymerization buffer while being stirred. Beads were collected in bottomless beaker with a mesh (hold by a rubber band) and transferred to a new beaker containing DMEM media (~150ml). Beads were washed twice for 10 minutes and processed as described before (UCL/Liver Group SOP142).

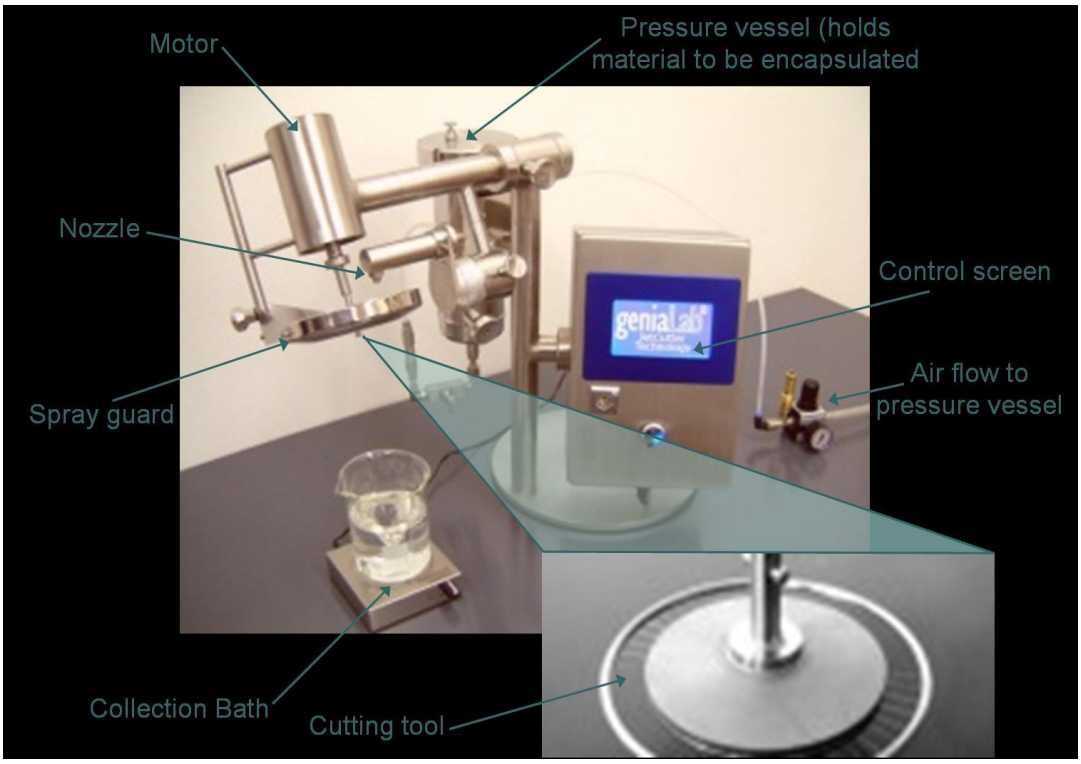

Figure 2.1 JetCutter set up (modified from geniaLab®)

The alginate solution within the pressure vessel is stirred by an overhead stirrer. A compressed air line is connected to the pressure vessel to create the flow. The alginate, then coming from the pressure vessel, goes through the JetCutter filter, the nozzle holder and finally the nozzle, resulting in a fine alginate stream which is cut in little beads by the spinning cutting discs. Beads are collected in a beaker containing polymerization buffer which is slowly stirred by a magnetic flea.

2.3 Cell count using the Chemometect Nucleo Counter

Materials

EDTA solution (pH 7.4):

16mM EDTA *(Sigma, Cat. No. ED4SS)* and 0.15M NaCl *(VWR, Cat. No. 27810,364)*

PBS (without Ca^{2+} and Mg^{2+})

Reagent A100 *(Chemometec, Cat. No. 910-0003)*

Reagent B *(Chemometec, Cat. No. 910-0002)*

Nucleocassettes *(Chemometec, Cat. No. 941-0002)*

Nucleocounter (*Chemometec)*

Method

The nucleocounter from Chemometec determines the cell number by staining cell nuclei from lysed cells with propidium iodide. The fluorescent dye is immobilized in the flow channels of a nucleocassette. The cassette takes up approximately 10µl of lysed cell suspension. After a few seconds the fluorescent signal can be measured by the Chemometect fluorescent reader. For appropriate counts cells have to be removed from the alginate matrix. Therefore beads were washed with HBSS in a ratio of 1/32 (beads/PBS). Beads were then dissolved by adding 16mM ethylenedinitrilotetraacetic acid (EDTA) (pH 7.4) at a ratio of 1/8. EDTA chelates calcium ions which are necessary to keep alginate chains polymerized. The dissolved alginate and cell mixture was centrifuged at 13000rcf (g) for 5 minutes and the cell pellet was resuspended in an adequate amount of 1xPBS (Table 2.1) by passing the solution through a 21G needle.

Table 2.1 Cell count dilution scheme

Day after encapsulation	Volume of 1xPBS (µl)
0-1	100
2-3	200
4-5	300
6 onwards	500

Chemometec reagent A100 which is a cell lysis buffer was added to the cell suspension and the mixture was vortexed for 10 seconds. Then Chemometec reagent B, a stabilising buffer was added and the mixture was vortexed for 10 additional seconds. To make up the reaction mixture the same volume of cell suspension, reagent A and reagent B was used. The nucleocassette was introduced in the cell mixture for 10 seconds before fluorescent reading. The reading was then multiplied by the appropriate multiplication factor (MF) to obtain the final cell concentration (UCL/Liver Group SOP173):

$MF = V_B^{-1} * V_{final}$

where V_B *= volume of alginate beads (in ml)*

and V_{final} *= final volume: PBS+ReagentA+ReagentB*

2.4 Fluorescin diacetate/propidium iodide staining

Fluorescein diacetate (FDA) is cell membrane-permeable and when hydrolysed by esterases present in metabolically active cell cytoplasm, emits a green fluorescence. PI is cell membrane-impermeable and emits a red fluorescence when bound to DNA. Therefore, PI staining will occur only when cell membranes are compromised, representing non-viable cells, whilst FDA staining diminishes in dying cells.

Materials

1mg/ml FDA (*Sigma, Cat. No. F7378-5G)* in Me_2SO

1mg/ml PI *(Sigma, Cat. No. 70335-5ML-F)* in water

1x PBS containing calcium and magnesium

Microscope slides

Tissue

Coverslips

Method

Approximately 250µl alginate beads were transferred to a 1.5ml microfuge tube, allowed to settle and medium aspirated. Beads were washed with 1ml PBS, then 500µl PBS and resuspended in 500µl of PBS. Then 20µl PI and 10µl FDA were added, gently mixed and incubated for 90 seconds. PBS was aspirated and beads washed a further 2 times as before. Beads were resuspended in 500µl of PBS and transferred to a microscope slide. Excess liquid was removed using tissue if required and a coverslip was placed over the beads. The beads were then visualised using a fluorescence microscope (UCL/Liver Group SOP03).

2.4.1 Viability assessment in beads – Image analysis

Materials

Microscope: Nikon TE200

Camera: Nikon DS-Fi1c with an 0.67x adapter *(means 67% of the Microscope picture will be captured with the camera)* and a DS-U2 PC control unit

Software: NIS-Elements AR 4.00.03

PI excitation filter of 510-560nm and emission filter of 590nm

FDA excitation filter of 465-495nm and an emission filter of 515-555nm

Alginate encapsulated liver cells

Method

Cell viability was quantified from captured images using image analysis. Phase contrast, live and dead images were captured using a Nikon DS-Filc camera and NIS imaging software. FDA and PI images were captured at x4 magnification at exposures of 150 and 1000ms respectively. For each sample (slide) 5 images for phase, FDA and PI were taken. For both PI and FDA the upper threshold was 256 and the lower threshold 41 for AELC cultured for at least 4 days after encapsulation. For AELC 0-3 days after encapsulation a lower threshold of 20 was used (see Chaper 3). Viability was calculated as below and expressed as the percentage of live cells within the total field.

$$viability(\%) = \frac{sumIntensityFDA}{sumIntensityFDA + sumIntensityPI} x100$$

2.5 Methylthiazolyldiphenyl-tetrazolium bromide (MTT) assay

The MTT assay is a colorimetric assay to assess cell viability. Tetrazolium salts such as MTT are reduced to formazan by mitochondrial and microsomal reductases which are present in metabolically active cells. The amount of purple formazan can be quantified using absorbance readings and be directly related to cell activity. Methylthiazolyldiphenyl-tetrazolium bromide (MTT) was used here.

Materials

Methylthiazolyldiphenyl-tetrazolium bromide (MTT) (*Sigma, Cat. No. M5655*)
Sterile PBS
4mM HCl in isopropanol
16mM EDTA in 0.15M NaCl
Small spatula
21G needle
2ml microfuge tubes
Orbital plate shaker
Spectrophotometer at 570nm

Method

MTT aliquots of 0.75mg/ml were prepared and stored at -20˚C until use. Per sample 150µl settled beads were used which were washed twice with sterile PBS and transferred to 2ml microfuge tubes. Then 1.5ml 16mM EDTA was added to dissolve the alginate matrix. Cells were microfuged at maximum speed for 5 minutes and the supernatant was discarded. To each tube 0.25ml of pre-warmed MTT was added. Tubes lids were pierced and samples were incubated at 37°C for 3 hours until blue/purple crystals had formed. MTT was aspirated and 350µl acidified isopropanol was added to each tube. Tubes were left on an orbital plate shaker for 30 minutes until all crystals had dissolved. 100µl were transferred to a 96-well plate and absorbance at 570nm was measured using a fluorescence plate reader. Each sample was measured in duplicates (UCL/Liver Group SOP44).

2.6 Quantification of hepato-specific proteins synthesised and secreted in culture

Enzyme-linked immunosorbent assays (ELISA) were used to assess cell function by quantifying hepato-specific protein synthesis. ELISA assays are antibody-based detection methods (assay) which result in enzymatic color reaction, which can be measured with spectrophotometer. Antigens (here hepato-specific proteins) are captured by a first antibody (Ab) which are coated to a microtiter plate. A second antibody is added to detected and quantify the antigen. Typical detection systems include alkaline phosphatase and horseradish peroxidise (HRP), as here. The substrate for HRP is hydrogen peroxide which is cleaved and coupled to the oxidation of o-phenylenediamine (OPD) to form an orange product that can be quantified using a spectrophotometer.

Materials

96 well Maxisorp plate

200ml coating buffer containing 0.318g Na_2CO_3, 0.596g $NaHCO_3$ (pH 9.6)

Capture antibodies (Table 2.2, all purchased from Abcam unless otherwise stated)

Clingfilm

Plate washer

Wash buffer: 1x PBS containing 0.05% Tween 20

Blocking buffer: 5% protein in wash buffer (Table 2.2)

Standards (Table 2.2)

Detection antibodies (Table 2.2, all purchased from Abcam unless otherwise stated)

12ml OPD solution: 2 OPD tablets, 6µl hydrogen peroxide

Aluminium foil

1M sulphuric acid

Spectrophotometer at 492nm

Method

The capture Ab was diluted in coating buffer and 100µl was added into each well of the 96-well plate. The plate was covered with clingfilm and incubated at 37˚C for one hour or overnight at 4˚C depending on the assay (see). Plates were aspirated and washed 3 times with 200µl washing buffer using the plate washer. Then 100µl blocking buffer was added, plate covered with clingfilm and incubated for one hour a 37˚C (Table 2.2). Samples were diluted as necessary and a standard curve which was run on each plate was prepared for each protein using serial dilution (200-6.25ng/ml). A standard curve was run on each plate. Samples that did not fell within the range of the standard curve were diluted. Then 100µl standard and sample was added into the blocking buffer. As before the plate was covered with clingfilm and incubated for 90 minutes at 37°C. The plate was washed as described above and detection Ab diluted in blocking buffer and 100µl added to each well (see). The plate was covered in clingfilm and incubated for 1 hour at 37°C. Detection Ab was aspirated and plate washed 5 times as described above. 100µl OPD solution was added to each well at timed intervals, plate covered in foil and incubated until orange colour developed. The reaction was stopped by addition of 50µl acid to each well at timed intervals. The absorbance was measured at a wavelength of 492nm using the plate reader (UCL/Liver Group SOP 37 to 42).

Table 2.2 Hepato-specific protein ELISA methodology

		Albumin	Alpha-1-fetoprotein	Alpha-1-antitrypsin	Alpha-1-acid glycoprotein	Fibrinogen
Capture Antibody	Cat. #	Dako A0001	Ab10071	Dako A0012	Dako A0011	ab6666
	Dilution	1/1000	1/1000	1/790	1/1000	1/1000
	Incubation	1h at RT	Overnight at 4°C	Overnight at 4°C	Overnight at 4°C	Overnight at 4°C
Blocking buffer		5% non-fat milk	5% non-fat milk	5% non-fat milk	5% non-fat milk	5% non-fat milk (removed)
	Incubation	1h at RT	1h at RT	2h at RT	1h at RT	1h at RT
Detection Antibody	Cat. #	ab24458-200	Ab10072	ab7635-s	Ab34720-10	ab7539
	Dilution	1/4444	1/3500	1/2000	1/4000	1/1000
	Incubation	1h at 37˚C	1h at 37˚C	1h at 37˚C	1h at 37˚C	1h at 37˚C
Standard		Dako X0908	Abcam ab38189	Citrated plasma	Dako X0908	Citrated plasma

2.7 Use of controlled rate freezers

A controlled rate freezer (CRFs) was used to carry out manual and automatic liquidus tracking experiments.

Materials

Liquid nitrogen supply (for storage in vapour phase)

CRF nitrogen Dewar 35L

Kryo10 and baskets (Planer)

Method

A Planer Kryo10 CRF with the following specifications was used: cooling rate from -0.01 to -50˚C/minute, warming rate from 0.01 to 10˚C/minute and working temperature from -180 to 50˚C. The CRFs relies on a nitrogen vapour supply via solenoid valve in a feedback loop for cooling. Prior to a cooling run, the CRF nitrogen Dewar was filled with liquid nitrogen. Programmes were entered as per the manufacturers' instructions for each CRF. This was done by either using the controller

or a personal computer and the Delta T software. The decant valve on CRF Dewar was opened and pressure adjusted to between 0.3 and 0.5 bar using the pressure raising coil if required. The cooling profile was started once the desired start temperature was reached and samples loaded into the CRF chamber. The freezer chamber temperature was measured by the integrated freezer thermometer and by using additional thermocouples to measure the freezer and sample temperatures (UCL/Liver Group SOP20).

2.8 Storage of cryopreserved samples

Materials

Liquid nitrogen supply

Biostor 5 (*Statebourne*)

Method

Upon completion of the cooling run, samples were normally stored at nitrogen storage within a Biostor 5. The Biostor 5 was topped up with liquid nitrogen every 2-3 days to ensure that cryogenic storage temperatures were maintained.

2.8.1 Temperature measurements during cryopreservation

A Pico Logger for data collection and thermocouples were used to measure the temperature of both chamber, samples and CPA solutions.

Materials

Type K thermocouple (*Pico Technology*)

TC-08 data logger (*Pico Technology*)

Laptop

PicoLog recorder software (*Pico Technology*)

Specially adapted cryovials

Method

Thermocouples were connected to the data logger which was connected via USB port to a laptop. Log settings were applied, typically 10 readings per second for the duration of the cooling profile. Data was logged using PicoLog software and exported into Excel for analysis.

2.9 *Statistical analysis*

For statistical analysis Microsoft Excel (MS Office (2007) Student's t test (two-tailed) was used. Values in text, tables and figures were expressed as the mean ± standard deviation (SD). The *n* numbers were given in the accompanying text. A p-value of <0.05, expressed as "*"was considered as statistically significant.

A p-value of <0.01 was expressed as "**" and was considered highly significant.

CHAPTER 3

Image analysis validation for cell viability quantification

3.1 Introduction

To evaluate the success of a cryopreservation method it is important to have a reliable test system in place to assess cell recovery after the preservation process. Viability often refers to membrane integrity tests, which are valuable techniques to give an estimation of cell recovery. A variety of more complex assays, such as specific metabolic assays, protein production and cell attachment tests can offer more realistic estimations of cell survival. However, in order to develop a complicated and time consuming test system such as the Liquidus Tracking (LT) vitrification system for alginate encapsulated liver cell (AELC) cryopreservation, a simple and rapid method to test cell recovery was needed. Others have demonstrated that the fluorescence intensity of the vital stain Fluorescein diacetate (FDA) is dependent on cellular metabolic activity and in particular esterase activity (Karmazsin et., 1979; Saruyama et al., 2013). A membrane integrity test that uses a fluorescent dye to stain dead cells in combination with FDA to obtain additional information about cell function seemed to provide a reasonable compromise.

3.1.1 Membrane integrity test for single cells

One possible method to measure membrane integrity is the use of the trypan blue exclusion. Another common method to distinguish between viable and dead cells is the nucleocounter system. Cell nuclei from dead cells are stained with propidium iodide (PI). The fluorescent dye is then immobilized in the flow channels of a nucleocassette and is read by a fluorescent reader. From the starting material two samples are taken, supposedly containing the same number of cells. The first sample will be lysed, so that all cells are dead, giving information about the total cell number. The second non-lysed sample accounts for the number of dead cells found in the starting material. The number of viable cells is then given by the difference in cell number between sample one and two. Viability can then be calculated using the common formula:

%Viability = signal PI of sample 2 (lysed)-signal PI of sample 1 (non-lysed)/

*signal PI of sample 2 (lysed)*100*

Trypan blue exclusion and nucleocounter tests are simple to carry out and are efficient techniques for day-to-day laboratory use. Flow cytometry is also a common method to assess the viability of a cell population and has been shown to have, like the nucleocounter approach, very good accuracy (Pan et al., 1996; Shah et al., 2006). However, these systems only work for single cell suspensions or small aggregates, and cannot be used for larger spheroids. Counting cells, as required for the trypan blue exclusion test, cannot be done for a 3D format such as AELC, as only the first layer of cells is visible to the viewer. Cell sorting is also not possible as this system is based on two distinct signals, either dead or alive, which is not given for spheroids which contain both type of cells in an unknown proportion. When measuring cell aggregates with the nucleocounter system, fewer cells will be taken up into the flow channel from the non-lysed sample than for the lysed sample, as it will be more difficult or even impossible for aggregates to be drawn into the channel. This leads to deviations when calculating cell viability. The error increases for larger aggregates such as AELC, which might block the inlet.

3.1.2 Membrane integrity test for encapsulated cells and cell spheroids

Cell spheroids can be disaggregated using pipetting, syringing or vortexing but this would likely result in a loss of viability due to intensive shear stress. An enzymatic digest (e.g. with trypsin) to obtain single cells might be possible, but can be assumed to be even more harmful. Either way is time consuming and will temper the true viability of the sample. For encapsulated cells and cell spheroids, an additional problem arises, as they first have to be released from the alginate matrix. This can be achieved by using EDTA to chelate divalent cations, used to crosslink alginate chains. Once depolymerised, cells can be separated from alginate via centrifugation. Viaspan, an organ preservation solution, has been shown to dissolve alginate beads and could provide a more gentle way to release the cells from the alginate scaffold. The Viaspan components lactobionic acid and Allupurinol presumably act as calcium binding chelators (Isaacson et al., 1989; Malkiel et al., 1993). If cell death can be avoided during alginate depolymerisation and subsequent spheroid disaggregation accurate membrane

integrity tests for single cell suspension might be possible, however the tight cell-cell contact makes this approach difficult.

Membrane integrity of encapsulated cells and cell spheroids may also be assessed without the need to disaggregate spheroids or dissolve the alginate capsule. This can, for example, be done by using a fluorescence microscope connected to a camera. The signal captured by the camera is transferred into an image with 256 potential intensities. By summarizing the intensities of all pixels and by using a standardized method the viability can be assessed. Similar to this method a fluorescent plate reader can be used. The requirements for any system are the capability to measure the wave lengths of at least one dye (normally PI, which can be correlated to dead cells), the ability to quantify the signal, and this without the need to disrupt the alginate bead or the spheroids. As for the nucleocounter system, an "untreated" sample and a sample with only dead cells have to be measured. Viability is then calculated according to the formula for the nucleocounter system as described above.

3.1.3 Viability test for encapsulated cells and cell spheroids

A vital dye such as FDA might be used to assess the vitality of a cell population without the need to dissolve the alginate bead or disaggregate the cell spheroids. For this test system either a vital dye that measures cell activity, or a vital dye in combination with a dye to stain dead cells can be used. As described in 3.1.2, fluorescence can be measured either with a microscope connected to a camera or a plate reader. If only the vital dye is used, two samples have to be measured: the positive control and the sample. Viability should then be given as a fraction of the positive control and not as absolute viability, as the positive control is likely to include some dead cells. The method is only feasible when a positive control is available for each test day. When two dyes are used, only one sample has to be measured. This has the advantage that cells and the cell number, which both alter the sum intensity, are the same for both signals (dead and viable). As before, the total intensity of FDA and PI are measured and the viability can be calculated following the formula:

$$\%Viability = signal\ FDA / (signal\ FDA + signal\ PI)*100$$

3.1.4 Fluorescein diacetate staining

Fluorescein diacetate (FDA) is a non-fluorescent substance that permeates cells freely. Inside the cell the FDA molecule is broken into two acetates and one strongly fluorescent fluorescein molecule by nonspecific esterases, such as lipase and acylase (Gilbert et al., 1992). It was first proposed that the intensity of fluorescence is dependent on cellular metabolic activity by Bentley-Mowat back in 1982 (Bentley-Mowat, 1982). FDA staining has also been used to estimate the activity of microbes (Koester et al., 1991; Schnürer & Rosswall, 1982) microalgae (Gilbert et al., 1992) and phytoplankton (Jochem, 1999) and (Saruyama et al., 2013). A close correlation between cell viability and cell function has also been reported for cultured hepatocytes. Both albumin production and lidocaine metabolism (P-450 activity) were significantly increased in the high fluorescence group compared to the low fluorescence group (Nyberg et al., 1993).

3.1.5 Digital imaging system

The digital imaging system is a combination of a microscope, a charge-coupled device (CCD) camera, a computer and an imaging software program. The microscope magnifies the sample specimen and depending on the microscope will also transfer the sample into a visible phase or a fluorescent image which is then captured by the CCD camera. The camera sends the information to the computer where it can be stored and analysed by the imaging software.

Photons coming from the sample are captured by the charge-coupled device (CCD) of the camera. The CCD chip is composed of a silicon surface that is covered with a network of strips defining millions of tiny squares or pixels, which function as light sensitive photodiodes. These photodiodes store photoelectrons, derived from incident photons. Depending on the size of the pixel (4-25μm) thousands of electrons can be stored. The more electrons captured, as a result of higher fluorescence or exposure time (time the camera shutter is open), the higher is the signal. The signal is then amplified and transmitted as variable voltage to the analogue and digital converter (ADC), which converts it into a zero and one binary code. An 8-bit camera (2^8) gives 256 different steps which are converted into a grey-level output between 0-255, with 0 normally

being black and 255 being white (Sluder & Wolf, 2007). Higher bit cameras will have a higher output range, but the display of a typical computer monitor only ranges from 0-255. This makes it necessary to split the higher output range into 256 groups, each representing one grey-level on the monitor. However, the "real" intensity of each pixel is not lost and it will be used by the imaging software for data analysis purposes. Data can be stored in different file formats such as TIF or JPEG. TIF files can store more data than JPEG files, which means that a higher number of grey levels is recorded. Even if the difference might not be visible on the monitor, it will have an effect when using the imaging software for data analysis. Images can normally be captured in colour or monochrome mode by a colour camera. Colour mode means that the wavelength of red, blue and green light is captured by the camera's photodiodes. This corresponds to the red, blue and green receptors of the human eye. Wavelengths are added together in various ways to reproduce a broad range of colours. The monochromatic mode has been optimized for use with fluorescence specimens where oftentimes only a single colour or two colours are being captured.

3.1.6 Dynamic range

The dynamic range of a fluorescence instrument indicates the range of fluorescence intensity that is detectable and is determined by the minimum and maximum detection limits of an instrument. For the microscope images analysis system the dynamic range is given by the number of photonelectrons that have to be collected to surpass the background signal and the maximum number of photonelectrons the CCD chip is able to collect. The exposure time is used to maintain fluorescent intensity within those limits. The fluorescence plate reader uses a photomultiplier tube (PMT) as a detector. Instead of the exposure time, gain adjustment is used to regulate the signal. The gain controls the amount of voltage that crosses the PMT and thereby making the PMT more or less responsive to the intensity of the measured signal. This means that the original fluorescent signal can be more or less intensified.

3.2 Aims

The aim of this chapter was to develop and evaluate different quantitative methods to determine the viability of alginate encapsulated liver cells and spheroids. The test system was intended to be simple, fast and inexpensive but also reliable and without the necessity to disaggregate the alginate matrix or cell spheroids, to be suitable for developing the Liquidus Tracking (LT) method and to monitor the growth process of alginate encapsulated liver cells (AELC). Hence, a standard method to use a fluorescence microscope and plate reader to measure the viability of AELC was developed and results were compared to enzyme-linked immunosorbent assay (ELISA), methylthiazol tetrazolium (MTT) and cell count data.

3.3 Methods and Materials

3.3.1 Microscope viability quantification

Materials

Microscope: Nikon TE200

Camera: Nikon DS-Fi1c with an 0.67x adapter *(means 67% of the Microscope picture will be captured with the camera)* and a DS-U2 PC control unit

Software: NIS-Elements AR 4.00.03

PI excitation filter of 510-560nm and emission filter of 590nm

FDA excitation filter of 465-495nm and an emission filter of 515-555nm

Alginate encapsulated liver cells

Method

The fluorescent signal coming from the fluorescent microscope was captured by a CCD camera and analysed using imaging software tools to distinguish between viable and dead cells stained with fluorescent dyes. Fluorescein diacetate (FDA) and propidium iodide (PI) were used for this purpose. The sum intensity of either green or red fluorescence is given by the sum of intensity of each pixel of a chosen area. In theory the signal of a population of 100% viable cells has to be equal to the same number of 100% dead cells of the same population. Fluorescein gives a higher fluorescent signal than PI for the same number of stained cells if measured with the same exposure time. To obtain approximately the same signal, the exposure time has to be adjusted with longer exposure for PI than for FDA. However, the Nikon camera software only allows the exposure time to be set in steps (e.g 50, 100, 200). For this reason a fine adjustment is not possible. This can be overcome by setting different thresholds for PI and FDA.

To determine which exposure time to use, a population of AELC was divided in half; one half was incubated in 80% (w/v) Me_2SO for 20 minutes at room temperature to kill all cells. Afterwards beads were washed several times with an excess 1xPBS ($+Mg^{2+}$, Ca^{2+}). AELC were stained with FDA and PI and images were taken with the fluorescent microscope to ensure all cells were dead. The other half remained untreated and was

directly stained with FDA and PI. Again, images were taken and AELC were only used to set up the standard method when the PI signal was less than 1% of the FDA signal.

3.3.1.1 FDA threshold setting

Signal intensities are given in 256 levels of grey-shades and can be set between 0 and 255 using the threshold tool of the imaging software. Signals captured by the camera will predominantly be from fluorescein, apart from some background signals of mostly low intensity (100ms), when the filter for green fluorescence is set at the microscope. To obtain all available information from the incoming signal, the higher threshold has to be set to the maximum of 255. In contrast, when setting the lower threshold at zero, all pixels will be selected. The large number of background pixels, although of low intensity, will substantially increase the sum intensity in an undefined manner. Consequently a lower threshold had to be defined. This was done by taking images of FDA stained AELC (viability >=99%) and by capturing all visible cells (Figure 3.1).

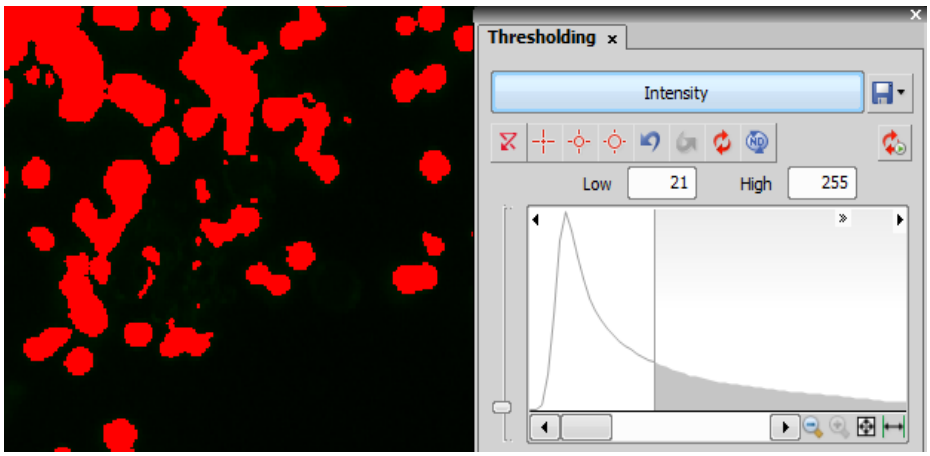

Figure 3.1 A histogram showing the pixel intensity distribution

The histogram shows background and signal pixels in the thresholding tool box. The x-axis represents the pixel intensity (0-255) and the y-axis the number of pixels. Peak in white demonstrates the number of background pixels (corresponding to black pixels in the image); peak tail in grey demonstrates the number of signal pixels (corresponds to red "overlay" pixels in the image). For this image the lower threshold was set to 21, to grasp all visible cells (overlaid in red), but not background signals of lower intensity.

When setting the lower threshold only cells or cell aggregates should be included in the sum intensity. For this reason an image magnification of 400x was chosen to select all green spots, by decreasing the lower threshold as much as necessary. Finally a

magnification of 100x was used to view the whole image. The threshold value was increased when necessary to prevent too much background being picked up (merging overlay), although as a consequence some of the "true" signal was left out (Figure 3.2).

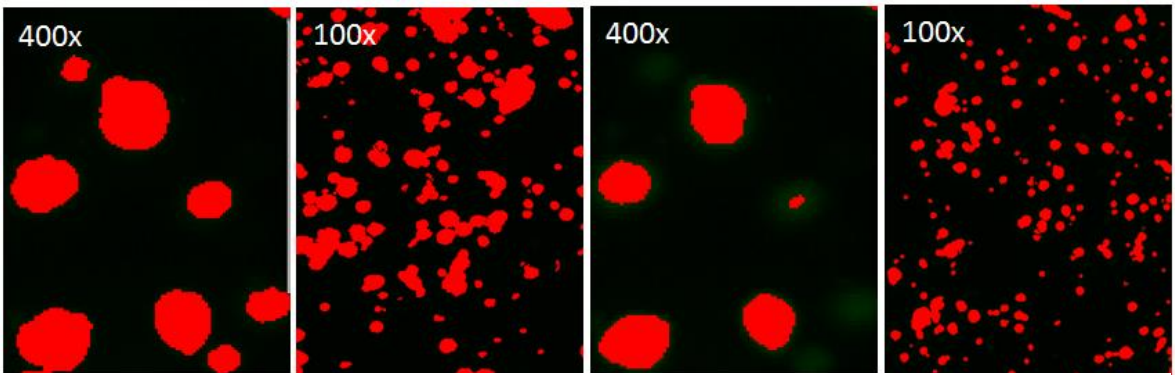

low threshold set to 24 **low threshold set to 40**

Figure 3.2 Low threshold setting for FDA

First an image magnification of 400x was chosen to distinguish between cells and background. Finally a magnification of 100x was set to see the whole image. The threshold was increased (here from 24 to 40) when necessary to minimise background signals, shown in the image by large parts of red overlay that merge with each other (threshold 24, 100x).

3.3.1.2 Reduction of background pixels

The background of empty beads was negligible if a lower threshold of more than 10 was used. To further reduce background signals the "smooth" and "clean" functions of the NIS imaging software were used. The clean function removes single pixels or very small objects that are unlikely to result from stained cells. The smooth function is a binary function that smoothens the edges of an object, making it easier to distinguish between the true signal and background.

3.3.1.3 PI threshold setting

For the same reason as described in 3.3.1.1 the higher threshold for PI was set to the maximum value of 255. The lower threshold was dependent on the fluorescein signal and was used to equalize the sum intensity of fluorescein and PI. AELC, taken from the same bead population as used for the FDA threshold setting but with dead cells, were stained with PI. Images were taken at different PI exposure times. The low PI threshold value was set in a way that the sum intensity was approximately the same as for fluorescein. The lower threshold was noted and then used as the high threshold to calculate the signal to noise ratio.

3.3.1.4 Signal to noise ratio

The signal-to-noise ratio (SNR) is a means to compare the level of a desired signal to the level of background (noise). A ratio close to zero indicates a very low signal and a high background. A ratio higher than one indicates more signal than noise. The optimal threshold is obtained when the highest possible SNR ratio is given. To obtain the sum intensity of the target signal, all visible cells have to be picked up. This is done by setting the lower threshold to an optimal value and the higher threshold to 255. The lower threshold of the target signal was then used as the higher threshold to calculate the sum intensity of the background signal while for this purpose the lower threshold was set to zero. The sum intensity of signal and background given by the NIS element software was used to calculate the SNR ratio.

3.3.2 Plate reader viability quantification

3.3.2.1 Volume of beads per well determination

Materials

Transparent 96-well plate

Alginate encapsulated liver cells (grown in FCS for one to 16 days at 37˚C after encapsulation)

Method

The volume of settled beads necessary to cover the whole well surface of a 96-well plate without forming double layers was determined. Therefore 0.75ml of PBS (+Mg, +Ca) buffer was added to 0.25ml of settled beads. From this mixture 25ul, 50ul, 75ul, 100ul and 125ul were added to a transparent 96-well plate. This was repeated six times. Images were taken using the Nikon microscope camera.

3.3.2.2 Omega plate reader sample preparation

A population of AELC was split in two; one half was incubated in 80% Me_2SO for 20 minutes at room temperature to kill all cells, and the other half remained untreated. Me_2SO treated beads were washed several times with an excessive of 1xPBS ($+Mg^{2+}$, Ca^{2+}). Untreated beads were washed with at least 5ml of 1xPBS ($+Mg^{2+}$, Ca^{2+}). To 1ml of settled beads 1ml of 1xPBS ($+Mg^{2+}$, Ca^{2+}) was added. This was done for both Me_2SO-treated and untreated beads. To the Me_2SO-treated beads 80µl of PI and to the

untreated beads 40µl of FDA were added, keeping the same ratio as for standard FDA/PI staining. After 90 seconds beads were washed three times with 2ml of 1xPBS (+Mg^{2+}, Ca^{2+}). Finally 3ml of 1xPBS (+Mg^{2+}, Ca^{2+}) were added resulting in a final volume of 4ml. This mix was used to prepare the following solutions. Both populations were combined as described in Table 3.1 to obtain the fluorescent intensity that corresponds to 5-95% viability.

Table 3.1 Omega Plate reader sample preparation scheme

%Viability	all dead	all alive	Final volume
95	50µl	950µl	1000µl
80	200µl	800µl	1000µl
65	350µl	650µl	1000µl
50	500µl	500µl	1000µl
35	650µl	350µl	1000µl
20	800µl	200µl	1000µl
5	950µl	50µl	1000µl

Of each solution, 100µl of well-mixed bead suspension (comprising12.5µl of settled beads) was added into each well (5mm diameter). For each condition five replicates were tested. Supernatant was tested in triplicates (100µl/well). The whole procedure was repeated four times in order to overcome pipetting and staining (PI, FDA) variability. The experiment was carried out with beads one day, four days, 10 days and 16 days after encapsulation as it was assumed that cell density could have an influence on the equalization factor. In order to obtain the same number of dead and viable cells for the same volume of beads the following had to be considered:

- After Me_2SO treatment all cells had to be dead: therefore 0.25ml of Me_2SO treated AELC were stained with PI and FDA and microscope images were taken. The rest of the unstained beads were only used when no green fluorescence was detected.
- Untreated cells had to be virtually 100% alive: therefore 0.25ml of untreated AELC were stained with PI and FDA and microscope images were taken. AELC were only used for the plate reader set-up when cell viability was >97%, which was measured using the microscope imaging method.

3.3.2.3 Staining samples with FDA and PI

Materials

Fluorescein diacetate 1mg/ml in Me_2SO *(Sigma, Cat. No. 31545)*

Propidium Iodide 1mg/ml in water *(Sigma, Cat. No. P4864)*

Method

For sample preparation the same protocol was used as for viability testing using the microscope set-up (2.4). After being incubated for 90 seconds in FDA and PI, beads were washed twice with 2ml of 1xPBS (+Mg^{2+}, Ca^{2+}). Then finally 1ml 1xPBS (+Mg^{2+}, Ca^{2+}) was added and 100µl of well-mixed bead suspension was added to each well.

3.3.2.4 Omega plate reader settings

Materials

BMG FLUOstar Omega Plate Reader

PBS with Mg^{2+} and Ca^{2+} *(Sigma, Cat. No. D8662)*

Black 96 well plate *(Costar, Cat. No. 3915)*

Method

The following settings were used to measure the fluorescence of PI and FDA:

Measuring mode: *Endpoint*

Positioning delay: *0.5 seconds*

Flying measurement: *off (for plate mode)*

Measurement start time: *0 seconds (no shaking or injection used)*

Number of flashes per well: *10*

Optic: *Top optic (black Nunc)*

Wavelength Settings:

FDA: excitation filter: 465-49ηm emission filter: 515-55ηm

PI: Excitation filter: 510-56ηm emission filter of 59ηm

Gain: *600 to 1200 for FDA and PI*

Path Length Correction: *off*

Pause before plate reading: *5 seconds*

Reading direction: *From left to right*

Replicate: *1 X*

Concentration/Volume/Shaking: *Default setting*

3.3.2.5 Calculating the equalization factor X

As fluorescein gives a higher fluorescent signal than PI for the same number of stained cells, an equalization factor **X** was determined ($FDA_{signal}=PI_{signal}*\mathbf{X}$). This was done by making up samples with different ratios of beads containing exclusively dead or viable cells to obtain the fluorescent intensity that corresponds to 5-95% viability. Linear regression (Excel 2007) was used to determine the equalization factor.

Step 1: Each sample was measured in five replicates. The signal (fluorescein and PI), given in relative light units (RLU), of the supernatant was subtracted from the sample RLU value (Table 3.2). Then the average (n=5) was calculated. The average value was plotted in a graph using the y-axis for either FDA or PI RLUs (Figure 3.3) and the x-axis for the corresponding viability (5-95%). A linear trendline was selected and its equation (gradient and y-intercept) was used for further calculations (step 2).

Table 3.2 Example for FDA RLU values and corresponding viability

Viability *%*	**100**	**95**	**80**	**65**	**50**	**35**	**20**	**5**
RLU sample	49900	71683	51698	45339	29215	23518	11866	2788
RLU supernatant	17344	9922	10203	7083	5415	3872	1707	231
RLU final	32556	61761	41495	38256	23800	19646	10159	2557

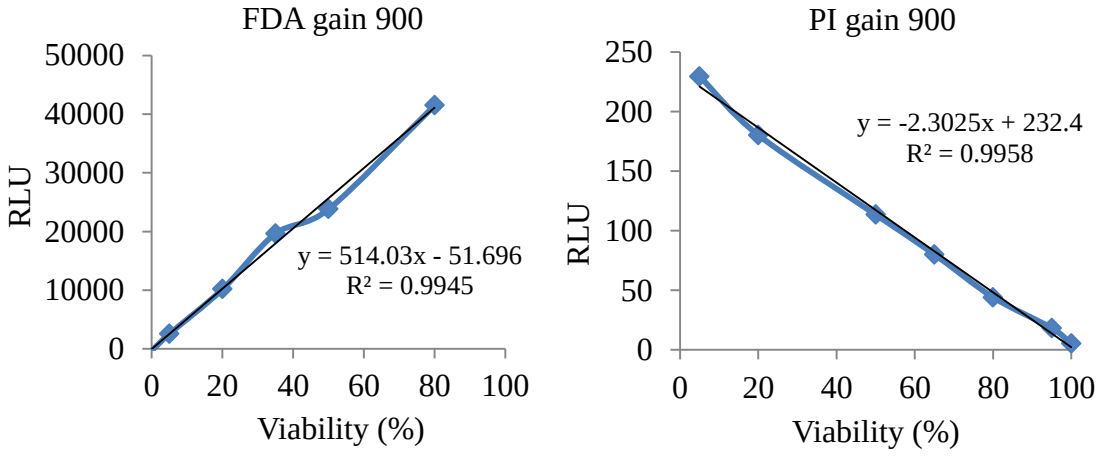

Figure 3.3 Viability-RLU correlation

Example for target viability (%) and measured FDA and PI RLU values. A linear trendline was selected and the gradient and y-intercept were used for further calculations (Step 2).

Step 2: On each test day the experiment was repeated four times. The average value of the gradient and y-intercept (step1) was calculated.

Step 3: By using the average gradient and y-intercept, corrected FDA and PI RLU values were calculated as follows:

$$\mathbf{FDA_{RLU}\text{-}corrected = x * gradient_{(FDA)} + y\text{-}intercept_{(FDA)}}$$

$$\mathbf{PI_{RLU}\text{-}corrected = x * gradient_{(PI)} + y\text{-}intercept_{(PI)}}$$

with x representing any viability value between 0 and 100.

As an example: the corrected FDA signal with a theoretical viability of 50% *(50% beads with exclusively dead cells and 50% beads with exclusively viable cells)* was calculated as:

FDA corrected *(50% viability)* **= 50 *514.03 - 51.696 = 25648**

'data used from Figure 3.3

Step 4: To determine the equalization factor **X,** a theoretical PI value had to be calculated. Viability can be determined as for the trypan blue exclusion test (2.1.3) by using cell numbers to calculate viability as follows:

*Viability (%) = number of viable cells/ (number of viable cells + number of dead cell)*100*

Similarly, viability can be determined when using fluorescence with signal intensity corresponding to cell numbers:

*Viability (%) = signal FDA / (signal FDA + signal PI)*100*

By using the corrected FDA value from Step 3 and the corresponding target viability (in %), the theoretical PI value was calculated as follows:

$$\mathbf{PI_{theoretical} = FDA_{corrected}/Viability*100-FDA_{corrected}}$$

Step 5: The theoretical PI RLU value (Step 4) was plotted against the corrected PI RLU value calculated in Step 3. A y-intercept of zero was chosen to compensate for test variations. The obtained gradient represents the equalization factor X (Figure 3.4).

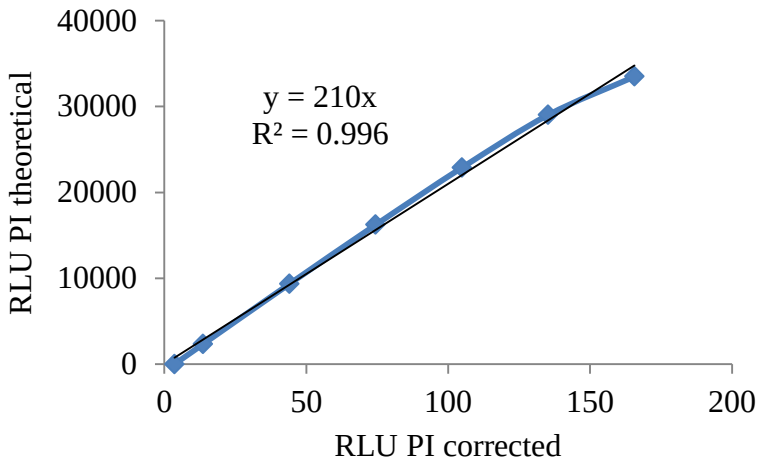

Figure 3.4 FDA-PI equalization factor X

Example for a linear trendline of PI theoretical and PI corrected (day one after encapsulation, gain 900). The theoretical PI value, which corresponds to the FDA value of equal viability, was plotted against the corrected value of the measured PI signal. A y-intercept of zero was chosen. The gradient denotes the equalization factor X.

Step 6: The viability of an independent sample was then calculated as follows:

Viability (%) = signal FDA / (signal FDA + signal PI *X)*100,

with X = equalization factor.

3.4 Results

3.4.1 Results for microscope viability quantification

3.4.1.1 Background reduction

With the smooth function set to "1", visually clearer edges were obtained, which made it easier to distinguish between cells or cell aggregates and background. The sum intensity was reduced by less than 0.1%. No further improvement was noted when the function was set to "2" or "3".When the clean function was set to "1-3", the number of small background pixels was still slightly reduced. When the clean function was set to "4" some of the cells were omitted. A clean function of "2" was selected as a suitable compromise, with a reduction in sum intensity of less than 0.5% (Figure 3.5).

Smooth:

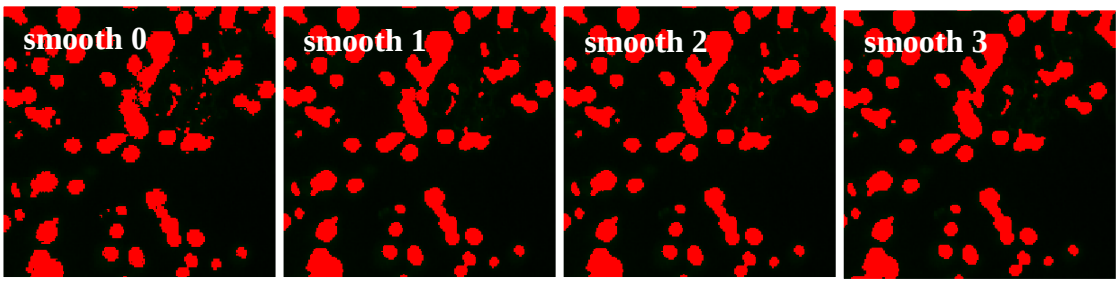

Clean:

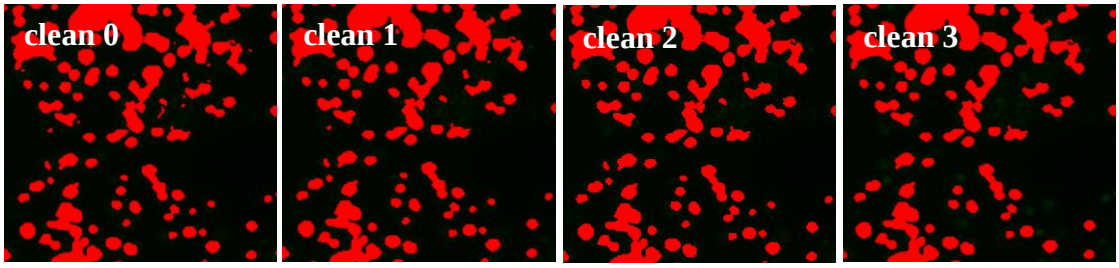

Figure 3.5 Clean and smooth function

With the smooth function set to "1", visually clearer edges were obtained and small background pixels were reduced. Higher levels than "1" did not show much further improvement. By using the clean function small background pixels were reduced. Higher levels than "2" resulted in signal loss.

3.4.1.2 Minimum FDA exposure time

Increasing exposure times were used to take images of AELC directly after the encapsulation process (day zero). To obtain enough fluorescent intensity to distinguish between cells and background an exposure time of at least 150ms had to be used (Figure 3.6).

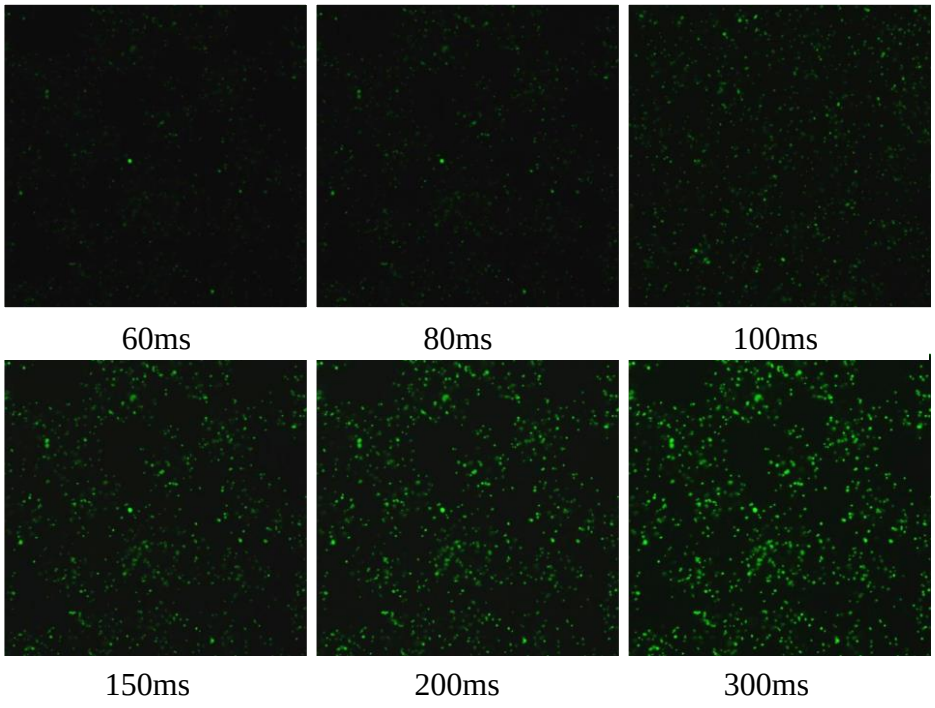

Figure 3.6 Determining the minimum FDA exposure time

Images show green fluorescent AELC taken with increasing exposure times given in milliseconds (ms). Images were taken directly after the encapsulation process (day zero). To clearly distinguish between cells and background an exposure time of at least 150ms was required.

3.4.1.3 FDA exposure time evaluation

Images of FDA stained AELC were taken at exposure times of 100, 150, 200, 300 and 400ms. The highest signal-to-noise ratio was obtained with an exposure time of 150ms. Higher exposure times showed a constant decrease in the signal-to-noise ratio. A lower exposure time (100ms) also decreased the signal to noise ratio (Figure 3.7).

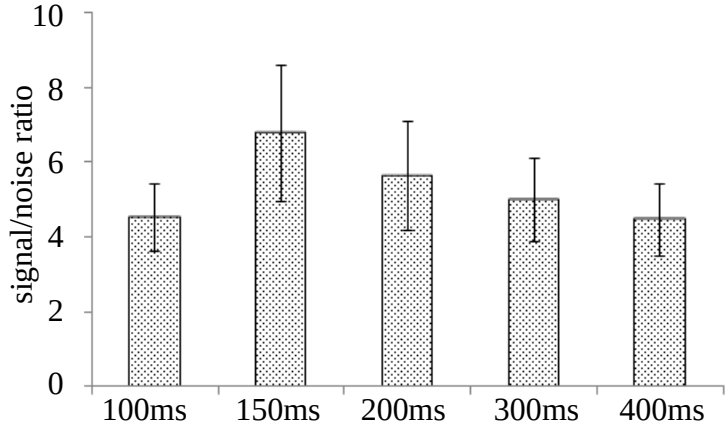

Figure 3.7 Signal to noise ratio for FDA stained AELC

Images of FDA stained AELC were taken at exposure times of 100, 150, 200, 300 and 400ms and the signal-to-noise ratio was determined as described in 3.3.1.4. Highest signal-to-noise ratio was obtained with an exposure time of 150ms. Data was n=5 +/-SD.

3.4.1.4 PI exposure time evaluation

PI fluorescent images were taken at an exposure time of 600ms, 800ms and 1000ms (one second). An exposure time of 600ms was too short to generate a signal similar to that of FDA without including a high percentage of background pixels. There was visually and in sum intensity little difference between an exposure time of 800ms and 1000ms when all cells were detected, but the signal-to-noise ratio for an exposure time of 800ms was lower (SNR = 75) than for one second (SNR= 115). The next highest exposure time possible to be set with the NIS imaging software is two seconds. As a result of the high pixel intensity only a few cells had to be included (and many omitted) to generate a signal comparable to the FDA signal. An exposure time of one second was therefore used for PI (Figure 3.8).

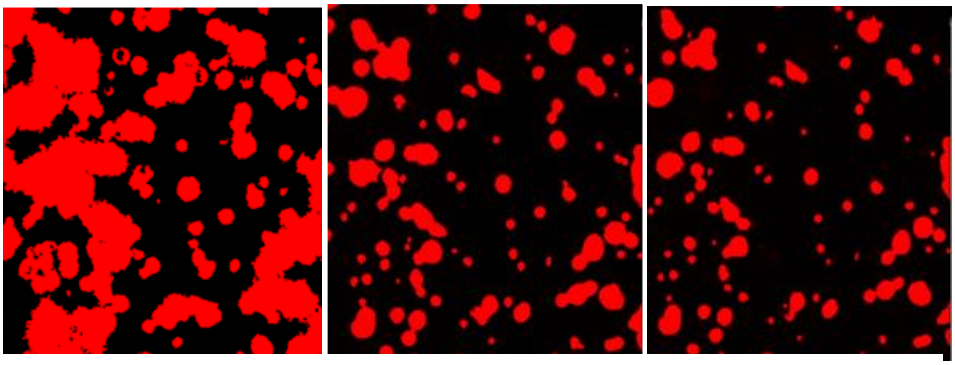

Figure 3.8 Threshold setting for PI fluorescence

Images of PI stained AELC were taken at an exposure time of 600ms, 800ms and 1000ms, (2000ms not shown). A merging red overlay indicates that background pixels are "picked up" and included in the sum intensity. Little difference was noted between an exposure time of 800ms and 1000ms.

3.4.1.5 Final set-up: day 3 to 13 after encapsulation

FDA threshold setting was carried out with AELC of increasing cell density. The low threshold had to be set to an increasingly higher number in order to include signal pixels but not background pixels as shown in the Table (Appendix). Most important are viability measurements directly after the encapsulation process and at the end of the AELC growth process, normally reached after 11-13 days and with cell densities between 20 and 30 million cells per ml of beads. For this reason the average of the low FDA threshold was calculated using images taken from AELC with a cell density of >20 million cells/ ml of beads. The same AELC population was used to define the low threshold for PI (Appendix Table 3.4). The low FDA threshold was comparable between the four samples taken from two different AELC populations (20.22 and 26.31 $*10^6$ cell/ ml beads), but varied between the two populations for the corresponding PI values (Appendix Table 3.3). The average lower threshold for FDA was 41 (SD+/- 3.2) and for PI 41 (SD+/- 16.1).

3.4.1.6 FDA and PI threshold setting evaluation

Threshold settings (value of 41 for FDA and PI) that were obtained from high cell density beads (>20*10^6 cells/ml beads) were evaluated using images taken of beads with varying cell densities (Table 3.3). The ratio of FDA to PI was supposed to be close to one, as a population of 100% viable cells should result in the same pixel sum intensity as a population of 100% dead cells when exposure times and thresholds are set correctly. The FDA/PI ratio increased with increasing cell densities as shown in Table 3.3. This indicates that the sum intensity for PI is stronger than the FDA signal for low cell densities beads. With growing cell numbers the sum intensity of both dyes become more balanced.

Table 3.3 FDA/PI ratio

cell number	FDA sum Intensity	PI sum Intensity	FDA/PI ratio
3.42*106	5444029	9319880	0.58
7.51*106	4377027	5277172	0.83
10.03*106	10756429	9574538	1.12
11.53*106	11463651	11144068	1.03
14.88*106	11946256	12077144	0.99
17.89*106	23729955	20577971	1.15
20.22*106	31748525	30125468	1.02
26.36*106	40272173	41124657	0.99

3.4.1.7 Cell density impacts cell viability

As shown in 3.4.1.6 cell density has an impact on the target FDA/PI ratio of "one" (for a equal number of dead and viable cells). A FDA/PI ratio of 0.83 obtained for a cell density of 7.51 million cells per millilitre of beads and with the threshold setting for cell densities of >20*10^6 cell/beads was still considered as acceptable. The highest impact for any deviation will be seen when the viability is at 50%. As an example: if the true FDA signal is the same as the PI signal, a FDA/PI ratio of 0.83 would then result in a viability of 54% instead of 50%, demonstrated in the following calculation:

Viability=50*/(50*0.83+50)*100=54%.

The deviation from the "true" viability value decreases as either the FDA or PI signal approaches 100% of the total signal:

Viability=100*0.83/(100*0.83+0)*100=100 or

Viability=0*0.83/(0*0.83+100)*100=0.

For viabilities above 80%, a deviation of 2% and for viabilities above 90% a deviation of 1% can be expected, considering a FDA/PI ratio of 0.83. This is less than the expected intra-sample deviation of 4% and 2% for samples with viabilities between 80% and 90% and viabilities above 90%, respectively. For viabilities close to 50% an intra-sample variation of 7% can be expected. Intra sample deviation given here is the maximum average deviation from four independent samples to the viability mean calculated from five single measurements (5xPI+5xFDA images).

3.4.1.8 Threshold setting for low cell density beads

For the cell growth process of a bioartificial liver device, day zero and day one after encapsulation are important days for quality control as viability data will indicate whether the encapsulation process was successful and if AELC are suitable to be FBB cultivation. The FDA/PI ratio decreased strongly for low cell density beads as shown in Table 3.3. Therefore a separate lower threshold was defined using AELC one day after encapsulation. The lower FDA and PI threshold of four distinct encapsulations resulted in an average value of 21 +/- 1.3 (n=4) for FDA and 20 +/- 1.0 (n=4) for PI with little difference between the samples (Appendix Table 3.6).

3.4.1.9 Viability data compared to cell count, ELISA and MTT data

In order to investigate whether changes in viability are also reflected in protein production, cell count and methylthiazol tetrazolium (MTT) production, AELC of decreasing viability had to be tested. To obtain decreasing viability levels (sample 1-3), AELC were incubating in Me_2SO. Sample viability, cell number and MTT were measured 24 hours and 48 hours after treatment. A media change was carried out 24 hours post-treatment. Media was collected 24 hours after the media change to measure the average protein production over the last 24 hours. Viability, cell count and MTT measurements refer to a specific time point while protein production is a cumulative value. In order to compare the data of the different test systems, viability, cell count and MTT measurements had to be conducted at the moment of media change and media collection. As seen in Figure 3.9 below, there was no significant difference in cell recovery 24 and 48 hours post-treatment. The only exception was the MTT data of sample 3. The ranking of the samples (sample 1=high recovery, sample 2=good

recovery, sample 2= low recovery) for viability, cell count and protein production (alpha acid glycoprotein (AGP), alpha-fetoprotein (AFP), Albumin, Anti-Trypsin and Fibrinogen), was the same for all assays (Figure 3.10). The percentage of the positive control was calculated for sample 1-3, in order to compare the recovery levels reached for the different assays. Viability data mostly correlated to values gained for cell number, AFP, Albumin and Anti-Trypsin. Fibrinogen and AGP production of sample 1-3 in respect to the positive control was more reduced than the remaining parameters. MTT results did not correlate with any other test system; clearly lower values for sample one in comparison to the control were acquired, and there was no difference between sample 1 and 2. Also the difference between sample two and three was less pronounced than seen for the remaining methods (Table 3.4).

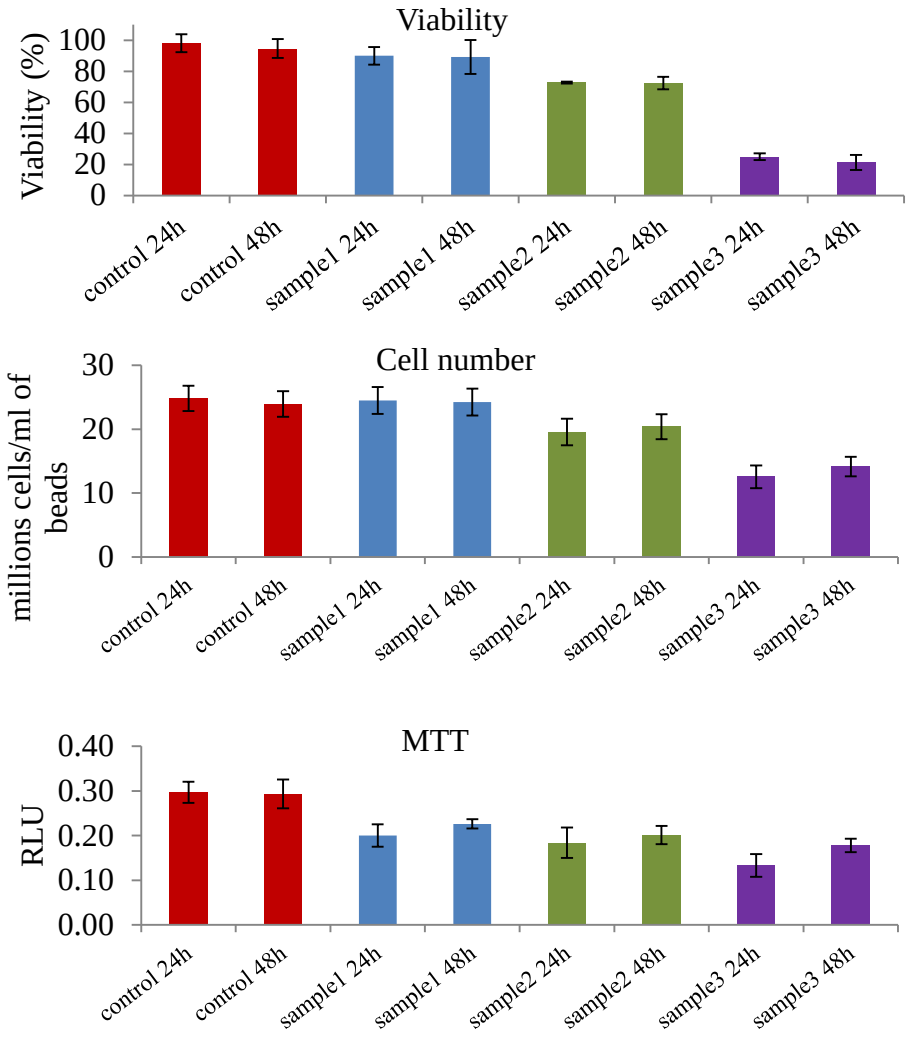

Figure 3.9 Viability determined by image analysis compared to cell count and MTT data

Samples, treated with Me_2SO to reduce viability, were tested 24 and 48 hours after treatment. Viability, cell number and MTT data was acquired. There was no significant difference between samples tested after 24 and 48 hours. Viability, cell number and MTT production decreased for samples in the order one to three. Data was n=5, +/- SD.

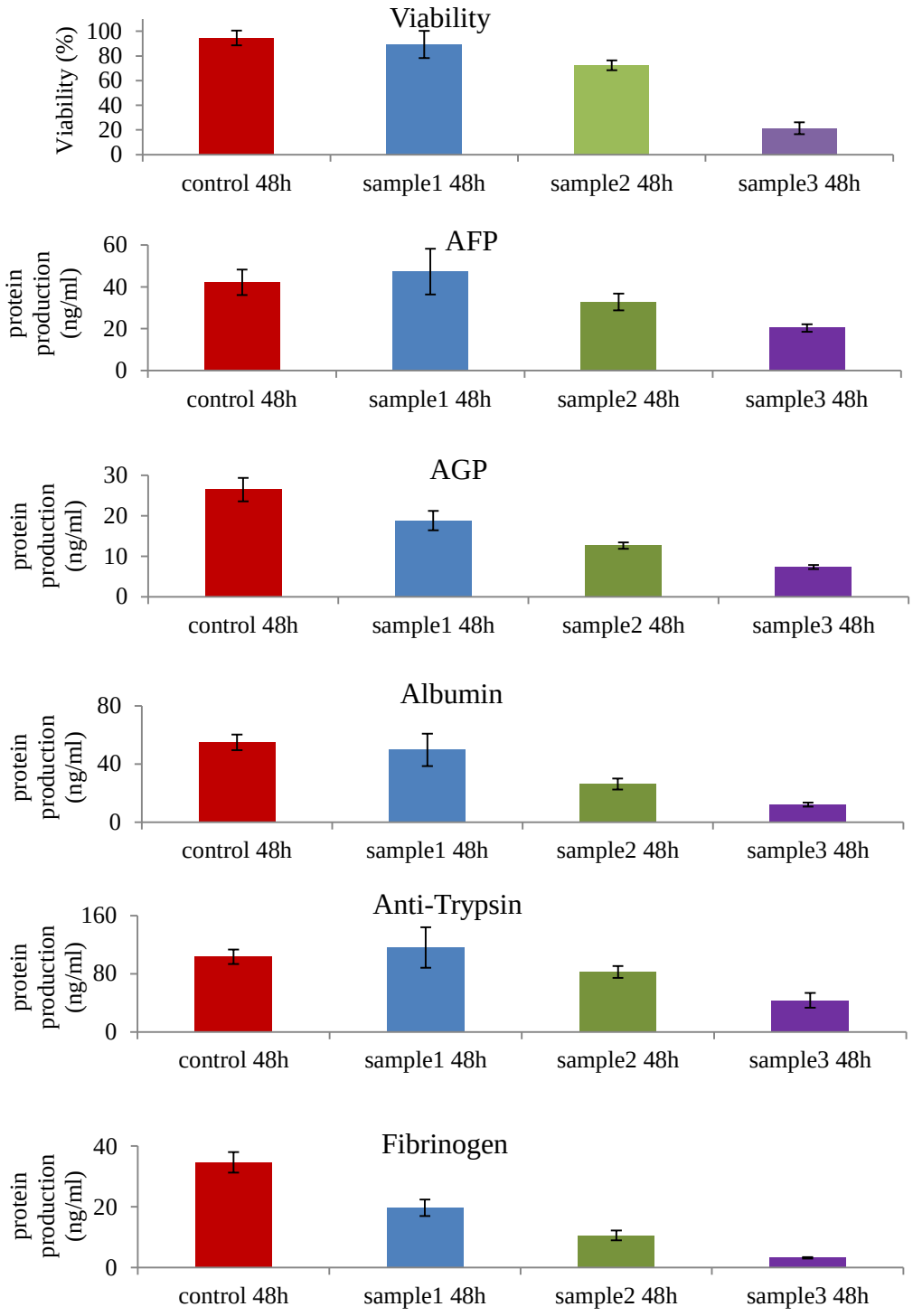

Figure 3.10 AELC protein production

Samples (0.25ml of settled beads), treated with Me_2SO to reduce viability, were incubated in 8ml of complete media and protein secretion was tested 48 hours after treatment and 24 hours after the first media change. Protein production was decreased for each sample in the order of sample one to three. Data was n=5, +/- SD.

Table 3.4 Percentage of positive control for viability, cell count and ELISA data

	Viability	cell number	MTT	AFP	AGP	Albumin	Anti Trypsin	Fibrinogen
sample 1	94	101	77	112	71	90	112	57
sample 2	76	85	69	78	48	48	80	30
sample 3	23	59	61	48	28	22	42	9

3.4.2 Results for plate reader viability quantification

3.4.2.1 Volume of beads per well

The microscope pictures that were taken to determine the volume of settled beads to be used per well showed that a volume of 12.5µl of settled beads was sufficient to cover the whole surface of one well (96 well plate) without double layer formation.

3.4.2.2 Plate reader gain

Plate reader measurements were carried out as described in section 3.3.2.4 using a gain of 300, 600, 900 and 1200 for both PI and FDA. A gain of 300 for PI resulted in underexposure and a gain of 1200 for FDA in overexposure and was therefore not used for further calculations. Otherwise the equalization factor X was calculated for all possible PI/FDA gain combinations.

3.4.2.3 Equalization factor X

As FDA, or specifically fluorescein, gives a higher fluorescent signal than PI for the same number of stained cells, an equalization factor X was determined ($FDA_{signal}=PI_{signal}*X$). AELC were tested on day 1, 5, 10 and 16 after encapsulation with cell numbers of 2.2, 4.3, 12.3 and 19.5 million cells per millilitre of beads.

Table 3.5 Equalization factor X for day 1,5,10 and 16 after encapsulation

Day 1		Day 5		Day 10		Day 16	
Gain (PI/FDA)	Equalization factor X (gradient)	Gain (PI/FDA)	Equalization factor X (gradient)	Gain (PI/FDA)	Equalization factor X (gradient)	Gain (PI/FDA)	Equalization factor X (gradient)
600/300	4.6	600/300	6.1	600/300	5.4	600/300	6.6
600/600	194	600/600	236	600/600	211	600/600	251
600/900	2370	600/900	2931	600/900	2765	600/900	3509
900/300	0.40	900/300	0.48	900/300	0.45	900/300	0.55
900/600	17	900/600	19	900/600	18	900/600	20
900/900	210	900/900	232	900/900	229	900/900	284
1200/300	0.07	1200/300	0.08	1200/300	0.07	1200/300	0.09
1200/600	2.9	1200/600	3.1	1200/600	2.9	1200/600	3.4
1200/900	35	1200/900	38	1200/900	37	1200/900	47

3.4.2.4 Evaluating plate reader viability test set-up

To evaluate the plate reader viability test set-up, samples with decreasing cell viability were made by incubating AELC (cultured for nine days) for 10 minutes in different Me_2SO concentrations. Beads used for the set-up contained either dead or viable cell,

which could influence the results. Beads used in this experiment contained both: dead and viable cells. Samples were stained and pictures were taken using the Nikon microscope (Figure 3.11).

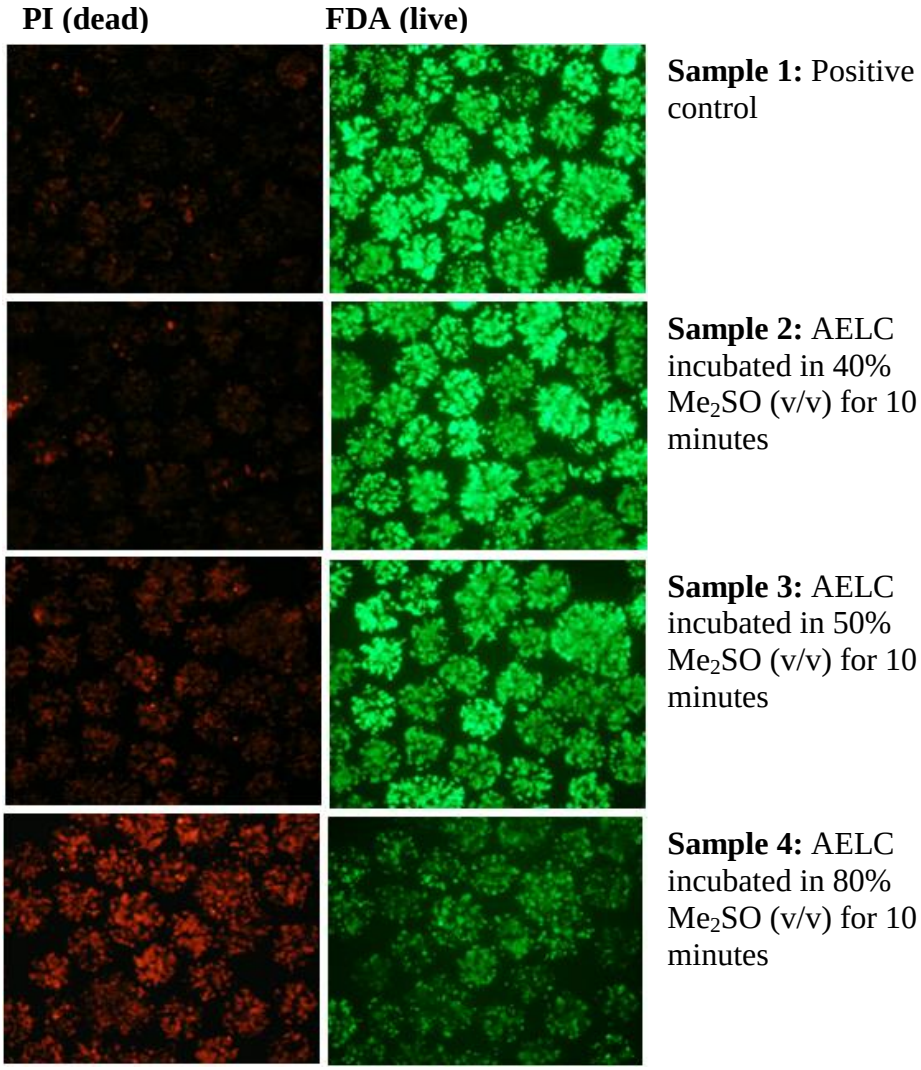

Figure 3.11 Microscope images of AELC with decreasing viabilities

Images of AELC incubated in increasing concentrations of Me_2SO to decrease cell viability. Individual beads used in this experiment contained both dead and viable cells. AELC were used to evaluate the equations listed in Table 3.5.

Samples were measured using the Omega plate reader by using gains of 600, 900 and 1200 for PI and 300, 600 and 900 for FDA. Each sample (1-4) was measured in four repeats (four wells), and the average RLU value of PI and FDA and the equalization factor given in (Table 3.5) were used to calculate the viability. The viability level was highest for low cell density beads (day 1) and lowest for high cell density beads (day

16), regardless of the PI/FDA combination. Differences in viability were more pronounced between cell densities (up to 10%) then between PI/FDA gain combinations, for which the variation in viability was less than 3%.

3.4.2.5 Final equation for Omega plate reader viability measurements

Viability data obtained from the same PI/FDA gain combination but calculated with one of the four different equalization factors for varying cell densities (day one, five, 10 and 16) (Appendix Table), were averaged and the standard deviation was calculated (Figure 3.12). This was done to determine the PI/FDA gain combination and corresponding equalization factor that would provide the lowest deviation in viability across varying cell densities, so that the same gain settings and formula could be used to determine AELC viability. The PI/FDA gain combination 900/600 and 1200/600 showed the lowest standard deviation. However the 900/600 combination was assumed to be the better choice for samples with high PI signals as the risk of overexposure is lower. The average gradient of data from day 1, 5, 10 and 16 with a gain of 900 for PI and 600 for FDA was calculated (18.48 +/- 1.42) giving the final formula:

%Viability = signal FDA / (signal FDA + signal PI *18.48)*100

Viabilities calculated with the equalization factors for distinct cell densities (day 1, 5, 10 and 16) differed from the viability calculated with the average equalization factor by less than 2% (total viability). This was equal to an intra-sample deviation of 2%. For high viability samples (viability >90%) the deviation was below 1% and comparable to an intra-sample deviation of 1.3%. Intra sample deviation given here is the maximum average deviation from three independent samples to the viability mean, calculated from five single measurements.

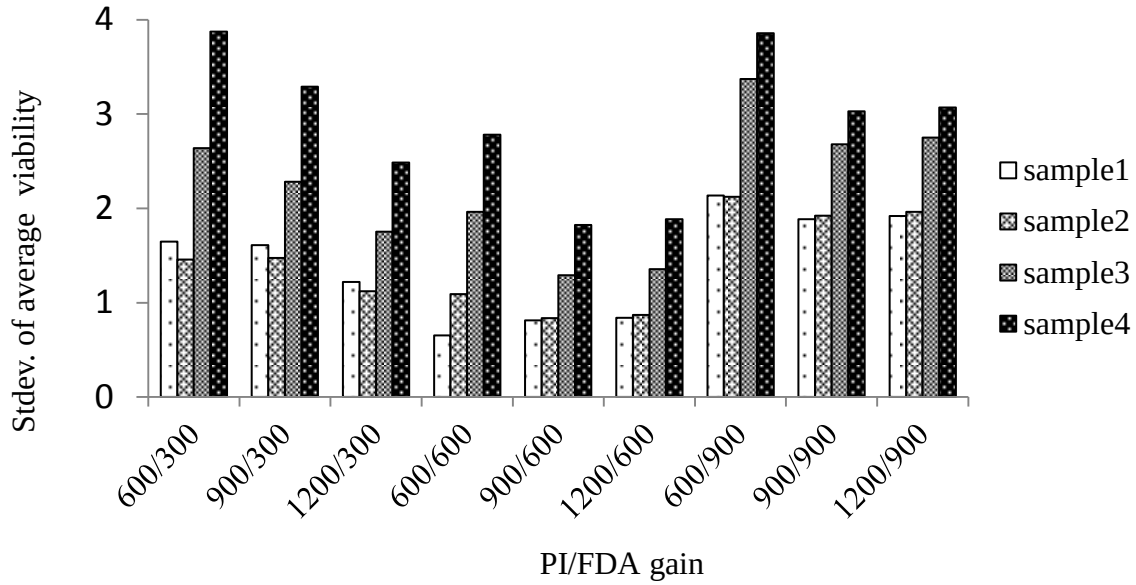

Figure 3.12 Viability standard deviation comparison for equalization factor and gain combination evaluation

Standard deviation of average viability obtained from the same PI/FDA gain combination but calculated with the four different equalization factors for varying cell densities (day 1, 5, 10 and 16) (Table 3.5). The lowest SD was obtained for a gain combination of 900/600 and 1200/600 (PI/FDA).

3.5 Discussion

In this chapter a method was established to assess cell viability of alginate encapsulated liver cells (AELC) by analysing fluorescent microscope images. Automated and semi-automated image analysis to quantify features of interest and separate the background by using differences in size, shape, density, brightness, or colour has been previously used by others (King et al., 2002; Ruifrok, 1997). The criteria or combination of criteria to choose depends on the complexity of the specimen and on the capability of the imaging software. For AELC viability measurements two different wavelengths were chosen to distinguish between viable and dead cells. The camera was set to monochrome instead to colour mode, as just the wavelength of either fluorescein or propidium iodide (PI) was intended to be captured after passing the corresponding filter. No signal was detected for samples of exclusively viable cells when the red filter was used nor for exclusively dead cells when the green filter was used. Brightness was selected to assess the intensity of both fluorescein and PI. Criteria of size, shape and density were not adequate for cell spheroids as these characteristics are subject to change during cell growth. The lowest magnification (4x) was selected to obtain the highest possible number of AELC per image to obtain a representative number of cells.

The method was based on the assumption that the fluorescence sum intensity of either PI or fluorescein would result in a linear response to an increasing cell number given, providing under and overexposure was avoided. The increase in sum intensity would therefore simply be given by the multiplication of pixel number and pixel intensity (given as a grey scale level from 0-255). The FDA exposure time was chosen regarding the following considerations. First, the conclusion was drawn that, regardless of AELC cell density, only one exposure time for FDA and one for PI should be used in order to minimize potential errors for users. Lowest fluorescence was observed directly after the encapsulation process, which is a stressful insult to the cells that leads to reduced cell activity. Consequently, AELC on the day of encapsulation were used to define the FDA exposure time. The shortest exposure at which cells could easily be identified by visual inspection ranged from 150ms to 200ms. A low exposure time had to be chosen to avoid overexposure and signal bleeding when images of beads of much higher cell

density are taken. Overexposure is indicated by white pixels and was never observed in the data presented in this thesis when the established exposure times were used. The signal-to-noise (S/N) ratio calculated for a small range of slightly lower and higher exposure times, indicated that an exposure time of 150ms was most suitable. PI exposure was defined according to the FDA signal, with the best S/N result for 1000ms.

It became evident that cell density was relevant for viability measurements. The higher the cell density, the higher the lower threshold had to be set in order to separate the background from the signal. The reason for this can be explained with the 3D format of AELC. Pixel intensity increases as more cells lie behind each other in the 3-dimensional matrix, adding to the total signal. An increment in cell density also increases the total amount of light scattering, which consequently results in a higher background signal, exceeding the lower threshold value of low cell density beads. Light scattering can be assumed to increase the background in a likewise manner for FDA and PI and therefore if the lower threshold for PI and FDA is equally increased, viability should remain unaffected. However, the FDA/PI ratio increased with cell density, which means that the sum intensity for FDA incremented more than the PI signal over the period of cell growth. This can be explained with the observation that HepG2 cells are more metabolically active when grown in a 3D format than monolayer or single cells (Selden et al., 1999). PI intercalates into DNA and is not subject to this deviation. In this respect PI might be more accurate when testing AELC of different cell densities when the same threshold settings are being used. However, this would be essentially more time consuming as two sample have to be tested, of which one has to be treated with a toxic reagent to kill all cells. Values that were obtained for the lower threshold when AELC images were taken one day after the encapsulation process were highly consistent including samples from four distinct encapsulation processes. This was similar for densities above 20 million cells/ml beads, although showed less consistency for the lower PI threshold. These findings suggest that the method is reliable for beads of similar cell density. The average lower threshold value was equivalent for FDA and PI, which means that the exposure times had been selected accurately to equalize the difference in FDA and PI fluorescent intensity. Calculations demonstrate that deviations from the true viability value will be strongest for viabilities close to 50% and negligible

for viabilities close to 100% and 0%. It was also estimated that the deviation to true value is less than the expected intra-sample deviation.

Image analysis to measure AELC viability is a simple tool that holds several advantages. First of all AELC viability can be assessed without the need to disrupt either the alginate matrix nor cell spheroids. These procedures are time consuming and also have the potential to alter the final viability result. The process is rapid; one sample can be stained, images taken (5-6 images/sample) and analysed within seven minutes, which means that results are available almost immediately. This capacity makes it especially interesting for quality control purposes but also in general when fast decisions are needed. Furthermore, the method is very economical (100 samples can be tested for less than £1) and is therefore ideal for high through-put testing. Additionally, there is little scope for variability between operators when using the established protocol and exposure times. When taking TIF images, the exposure time is recorded, and established threshold settings mean that fluorescent intensity is objectively quantified, and the translation of the threshold settings into a macro prevents the operator from changing the settings. This is in strong contrast to the trypan blue exclusion test, when a dead/viable cell count is highly subjective and dependent on the operator's interpretation.

AELC were stained simultaneously with FDA and PI. This is advantageous because the quantity of beads used per image is irrelevant, as the same sample is used to calculate the sum intensity of PI and FDA. In contrast, when only one dye is used, images of two samples have to be taken. Consequently an unequal number of beads would have a strong impact on fluorescence sum intensity, and therefore on the viability value generated. The fact that the number of beads is irrelevant allows calculating the viability of a single bead. In summary it can be stated that fluorescent microscope image analysis is a highly controllable and, apart from the simple staining process, an operator independent tool to measure cell viability. Good controllability is an important aspect for quality control.

There have been some discussions about the use of membrane integrity tests to measure the success of cryopreservation, as viability might not reflect whether cells are optimally functional (Pegg, 2010a). For this reason image analysis results were

compared to cell counts, enzyme-linked immunosorbent assay (ELISA) and methylthiazol tetrazolium (MTT) data. Samples of different viability levels (high-middle-low) followed the same ranking for cell counts, ELISA and MTT, however deviations from the positive result varied strongly between test systems. For example: the percentage of the positive control reached for alpha-fetoprotein (AFP), Anti-Trypsin and albumin production was comparable to the viability data but strongly differed to fibrinogen and alpha acid glycoprotein (AGP) production. This might be accounted for by the different pathways that were affected after the stressful insult, but also demonstrates that none of the test systems, nor a combination, is able to describe cell viability (vitality) fully.

The plate reader set-up followed the same principle as the microscope set-up with the same advantage of being simple, fast and economical. Again FDA and PI signal had to be equalized. This was done by measuring the same sample with different gains for FDA and PI and by selecting the optimal combination. The gain, which intensifies the signal, was chosen according to the dynamic range of the instrument. In this respect a gain of 1200 for FDA was too high and a gain of 300 for PI was too low, as no linear correlation was given for those gain values. An equalization factor X was calculated to further equalize the FDA and PI signal. At each test day different ratios of beads with exclusively dead and viable cells were prepared to obtain viabilities between 5% and 95%. Cells were stained and fluorescence was measured. Measured RLU levels were subsequently plotted against the target viability value. A similar approach has been patented for the viability determination of parasitic and non-parasitic worms (Peak, 2012). The gradient and the y-intercept of the linear regression of four experiments performed on the same day were determined and the average calculated, instead of calculating the mean of each viability level (n=4) and subsequently plotting the averaged RLU value against the target viability. This had the advantage that outliers were easily identified and high R-values were reached. Outliers were assumed to have occurred from pipetting errors, when different ratios of viable and dead beads were prepared. As for image analysis, the aim was to identify settings that could be used over the whole range of cell densities seen during the preparation of cells for use within the bioartifical liver assist device (BAL). For this reason an independent equalization factor was determined for AELC one, five 10 and 16 days after encapsulation. The PI/FDA

gain combination of 1200/600 and 900/600 gave the lowest viability deviation between samples measured with the same gain combination but calculated with the equalization factors established for the four cell densities. This was because of the low equalization factor deviation between cell densities, and because equalization factors were close to one, therefore having less impact on the final PI sum intensity. It was estimated that the intra-sample deviation is closely similar to the error that can be expected when the same equalization factor is used for varying cell densities with a deviation of less than 1% for viabilities exceeding 80%, and a deviation of 2% for samples of viabilities below 80%.

The main disadvantage of the plate reader set up is that fluorescein "leaching" will not be recognized. Fluorescein leaks or "leaches" out of cells with damaged cell membranes which are still enzymatically active. "Leaching" leads to falsely high FDA readings and has especially been noticed for samples with viabilities lower than 40% that were measured within the first hours after the exposure to a harming insult such as freezing or solution toxicity. This intermediate state is followed by progressive loss of cell viability with lowest viability after 24 hours, as described for AELC cryopreserved by slow cooling (Massie et al., 2011). Progressive cell death after cryopreservation has also been observed in kidney cells and has been termed cryopreservation-induced-delayed-onset-cell-death (CIDOCD). Additionally, a process of repair has been described in AELC and rat hepatocytes during which sub-lethally damaged cells regain their membrane integrity approximately between 24 and 48 hours post-warming (Massie et al., 2011; Watts & Grant, 1996). The best time to test AELC viability was therefore assumed to be 24 hours post-stress when fluorescein leaching is strongly reduced as damaged cells either have stopped enzymatic activity or undergone repair. Also, differences between conditions were expected to be most pronounced after CIDOCD and before the beginning of cell recovery and cell growth.

3.6 Conclusion

In the process of this thesis about 20000 images were taken, corresponding to about 3300 measured samples. This demonstrates the necessity for a fast and inexpensive test method, given by both approaches; image analysis and plate reader analysis. To describe the culture process of a bioartifical liver (BAL) assist device it is reasonable to measure several parameters, especially as the final protein production is crucial for the effectiveness of the BAL application. However, as setting up a complicated method, such as the Liquidus Tracking (LT) cryopreservation process implies inevitably many technical improvements, it was considered that viability measurements were sufficiently powerful to describe post-stress viability in a way to allow comparison of experimental conditions. This assumption was reinforced by enzyme-linked immunosorbent assay (ELISA), cell count and methylthiazol tetrazolium (MTT) measurements, which followed the same order as the viability data, measured by using the image analysis system. Alginate encapsulated liver cells (AELC) for LT were always taken from the same starting material, and therefore deviations regarding the cell number were not expected. Based on the observation of fluorescein cell leaching, and the general advantage of visual inspection, the microscope set up was used for viability measurements throughout the work of this thesis. Therefore samples were tested 24 hours post-stress when fluorescein leaching was reduced and differences between conditions were expected to be most pronounced.

CHAPTER 4
Manual Liquidus Tracking

4.1 Introduction

The fundamental basis of the Liquidus Tracking (LT) theory encompasses the concept that cryoprotectant agent (CPA) toxicity can be reduced if the temperature is decreased, such that concentrations high enough to lead to vitrification can be achieved step-by-step at lower temperatures. Reduced toxicity and decreased drug efficiency can be explained by decreased enzyme activity which for mammalian cells is highest at ~37°C, but is also a result of decreased reaction kinetics in general, which includes reduced chemical and/or osmotic stresses. Slower molecular motion also increases the time a substance needs to penetrate the cell, which delays its potential effect. Reduced toxicity at lower temperatures has been shown in previous work by Matheny in 1968 (Matheny et al., 1969), who incubated rabbit atria in different dimethyl sulfoxide (Me_2SO) concentrations at increasing temperatures. The effect is also reflected by reduced drug efficiency at lower body temperature, which has been widely studied by Weihe in 1973 (Weihe, 1973).

4.1.1 Manual Liquidus Tracking

Manual Liquidus Tracking holds some logistical advantages since it does not require complex equipment. It can allow small batch vitrification for samples of moderate volumes (in the region of 2 – 10ml), and can help in testing various LT conditions in parallel within one experiment (e.g. buffers, antioxidants, CPAs). This was necessary to optimize the automatic LT procedure, which is a time and material consuming process. In general three test set-ups have been defined which can be used to perform manual LT. Set-up 1 corresponds to the manual LT approach used by Farrant (Farrant, 1965b) and Pegg (Pegg et al., 2006). The sample to be vitrified is transferred from one sample container to the next, each with a higher CPA concentration whilst the temperature is decreased. Set-up 2 reflects the dual solution mode that can be used with the automatic Planer Liquidus Tracker. The sample remains within the same sample container throughout the vitrification procedure and the CPA concentration is increased by the

addition of a slightly higher concentrated CPA solution (e.g. 20% for manual LT). After mixing, the sample volume has to be reduced as a result of limited container volume and to minimize the amount of CPA needed to increase the CPA concentration in the next step. Set-up 3 reflects the Liquidus Tracker single solution mode as it uses highly concentrated CPA solutions (60-80%) to increase the CPA concentration within the sample. In contrast to the automatic approach, it is unnecessary to reduce the sample volume of the manual set-up before the next CPA addition. In general a final volume of 5ml was reached for which 15ml centrifuge tubes could be used.

4.1.2 Improved laboratory translation for manual Liquidus Tracking

Maintaining the sample temperature close to its equilibrium melting point during CPA changes, providing effective mixing and reaching the target CPA concentration is problematic for manual LT for several reasons. As the temperature gets colder over the LT process, the CPA solution becomes more viscous with the consequence that homogenisation will take more time. Thus, the freezer lid has to be open for longer and more heat fluctuation occurs. Also the addition and reduction of CPA becomes more inaccurate due to increased viscosity.

4.1.3 The Refractive Index

One of the most important measurements to control the LT procedure is to determine the CPA concentration after its increase or decrease. This information is needed to establish an effective pipetting and mixing process and to estimate the expected error, which is especially important to prevent the sample from freezing in case insufficient CPA was added. If the concentration is known during the process necessary adjustments can be carried out. A simple way to determine the CPA concentration is by measuring the refractive index of a respective solution (Umlas & O'Neill, 1980). The refractive index describes how light propagates through an optical medium and is defined as the ratio of the speed of light in a vacuum and the speed of light in a substance. To determine the refractive index a refractometer can be used, which measures the degree to which the light changes direction (angle of refraction) when crossing the interface between two media and correlates it to the refractive index of the sample. This is normally based on Snell's law with: n1*sinØ1 =n2*sinØ2, where Ø1and Ø2 are the

angles of incidence and refraction, and n1 and n2 are the refractive indices of the prism material and the sample. As the refractive index of the refractometer's prism material and the angle of incidence are known, the refractive index of the sample can be calculated. The main factors that affect refractive index measurements are concentration of the dissolved substance and the temperature of the solution.

4.2 Aims

The first aim of this chapter was to prove the principles of Liquidus Tracking (LT) by showing that Cryoprotectant agent (CPA) toxicity is reduced at lower temperatures. To estimate the impact of temperature on CPA toxicty, alginate encapsulated liver cells (AELC) were incubated in different dimethyl sulfoxide (Me_2SO) concentrations at different temperatures, including low subzero temperatures. Secondly, different methods to carry out small scale manual liquidus tracking were tested and evaluated with respect to practicablity. The most practical method was improved in terms of sample homogenisation and heat fluctuation to maintain the sample close its melting point. Parameters that could affect automatic LT approach were also investigated. To distinguish between osmotic injury and cytotoxicity the impact of osmotic pressure on cell viability was assessed.

4.3 Methods and Materials

Materials

Me_2SO *(Sigma, Cat. No.154938)*

1xPBS with Mg^{2+} and Ca^{2+} *(Sigma, Cat. No. D8662)*

Controlled Rate Freezer (*Planer, Kryo 10, Series II*)

Alginate encapsulated liver cells

4.3.1 Dimethyl sulfoxide toxicity at different temperatures and concentrations

Method

PBS was used as a cryoprotectant agent (CPA) carrier solution with a concentration of 1x for all dimethyl sulfoxide (Me_2SO) solutions. Samples were incubated at 37°C (incubator) and 4°C (fridge) at increasing concentrations of Me_2SO (10-70% (v/v)). Unless noted differently alginate encapsulated liver cells (AELC) cultured for 8-11 days were used. After the incubation beads were washed with an excess of ice cold PBS. Then after being incubated for 24 hours in complete media to allow full expression of any damage, beads were stained with FDA/PI and viability was measured. Each test day the viability of an unfrozen sample was measured as a positive control.

4.3.1.1 Dimethyl sulfoxide toxicity at temperatures below zero

AELC, cultured for 4-5 days were incubated at 37°C (incubator), 20°C (room temperature), 4°C (fridge) and -10°C, -20°C, -30°C, -40°C, -50°C (Planer Kryo 10 freezer) for 40 minutes in increasing concentrations of Me_2SO (20% to 60% (v/v)). Beads incubated at subzero temperatures were pre-incubated in the following solutions for one minute at 0.5°C (ice-water) to prevent immediate freezing before the addition to the final Me_2SO solution:

- beads incubated at -10°C: 20% (v/v) Me_2SO
- beads incubated at -20°C: 30% (v/v) Me_2SO
- beads incubated at -30°C: 40% (v/v) Me_2SO
- beads incubated at -40°C: 50% (v/v) Me_2SO
- beads incubated at -50°C: 60% (v/v) Me_2SO

Then after being incubated for 24 hours in complete media, beads were stained with FDA/PI and viability measured. Each test day the viability of an unfrozen sample was measured as a positive control.

4.3.2 Determination of osmotic effects

AELC were incubated at 0.5°C for five minutes in 20% (v/v) Me_2SO and were then transferred to 40% (v/v) Me_2SO for 15 and 40 minutes at 0.5°C (tubes on ice). Beads from the same flask were immediately incubated in 40% (v/v) Me_2SO for 15 and 40 minutes (Figure 4.1). The experiment was repeated at 37°C. Pre-incubation at 20% (v/v) Me_2SO at 37°C was reduced to two minutes as Me_2SO diffusion is increased at higher temperatures. After the incubation half the volume was removed and replaced with PBS. After two minutes half the volume was removed once again and replaced with PBS. After two further minutes all supernatant was removed and beads were washed twice with 1ml PBS. Then after being incubated for 24 hours in complete media to allow full expression of any damage, beads were stained with FDA/PI and viability was measured.

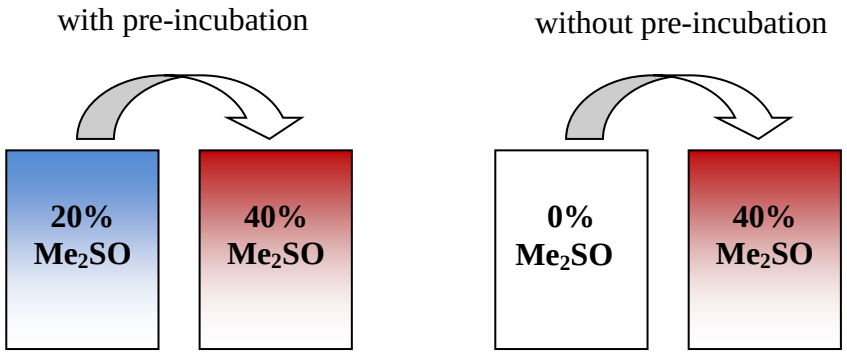

Figure 4.1 Osmotic stress

AELC were pre-incubated in 20% (v/v) Me_2SO at 0.5°C (37°C) before adding AELC to the final Me_2SO solution of 40% (v/v) Me_2SO at 0.5°C (37°C). Simultaneously AELC were incubated directly in the final 40% (v/v) Me_2SO solution at 0.5°C (37°C). AELC viability was assessed 24 hours after the incubation in complete media at 37˚C.

4.3.3 Manual Liquidus Tracking

Materials

Me_2SO *(Sigma, Cat. No154938)*

1xPBS with Mg^{2+} and Ca^{2+} *(Sigma, Cat. No. D8662)*

6-well plate

100 um cell strainers *(BD Bioscience, Cat. No. 352360)*

Controlled Rate Freezer (*Planer, Kryo 10, Series II*)

Method

AELC (0.25ml of settled beads, 9-11 days after encapsulation; unless otherwise noted) were added to **A:** cell strainer (set-up 1), **B:** 2ml microfuge tube (set-up 2) or **C:** 15ml centrifuge tube (set-up 3). Beads within the freezing solutions were maintained for approximately 30 minutes before use at 0.5°C and all further preparation was undertaken on ice. Prior to cooling, the Planer freezer was pre-cooled to 0°C. All solutions needed to increase the Me_2SO concentration were placed into the freezer at the beginning of the run. That way the sample temperature and the temperature of the new solution were kept approximately the same. The temperature was monitored by anchoring a thermocouple submerged in liquid inside. As a positive control the viability of unprocessed AELC was measured on the same day as the cooling procedure was carried out. After the warming procedure (4.3.3.4), AELC were transferred to a new 6-well plate with fresh medium and were maintained at 37°C for 24 hours before viability was measured. For all cryopreservation experiments, a programmed cooling rate of -2°C/minute was used.

4.3.3.1 Manual Liquidus Tracking set-up 1

LT experiments were carried out as follows: AELC were added to a cell strainer as described and were then placed in a 6-well plate containing 8ml of freezing solution per well. All plates were placed into the freezer at the beginning of the run into the pre-cooled freezer. At fixed temperatures, the cooling chamber was opened quickly and cell strainers transferred from one 6-well plate to the next, each subsequent one with a higher Me_2SO concentration (Figure 4.2). Melting point of the Me_2SO solutions were determined using the release of latent heat (Massie et al., 2011a) and were then compared with the literature values (Elford, 1970; Farrant, 1965b). Temperatures at which the Me_2SO change can be carried out was -5°C (from 20% to 30% Me_2SO), -10°C (from 30% to 40% Me_2SO), -20°C (from 40% to 50% Me_2SO), -30°C (from 50% to 60% Me_2SO), -40°C (from 60% to 70% Me_2SO) (Table 4.1). The transfer

temperature included an offset of approximately +30% from the equilibrium melting point of the sample to avoid any sample freezing. The lowest temperature that could be chosen for the transfer was determined by the CPA concentration of the starting plate as it contained the lower CPA concentration. The freezer temperature was set 10°C below the transfer temperature to provide sufficient cooling (8ml per well for a 6-well plate) with a holding time of 10 minutes and a freezer cooling rate of -2°C/minute). Transfer temperatures for solutions containing 50-70% (v/v) CPA were determined empirically, as viscosities at lower temperatures were too high to allow effective mixing.

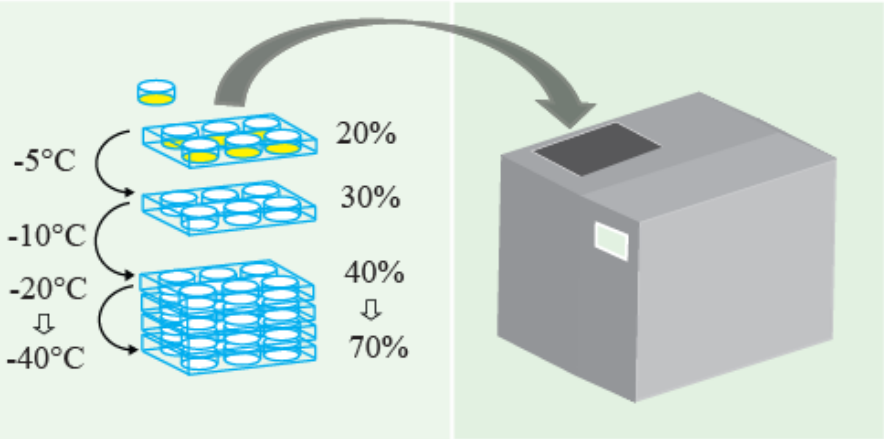

Figure 4.2 A schematic of manual LT set-up 1.

A schematic showing samples (in cell strainers) being transferred between 6-well plates with increasing CPA concentration (e.g. 20% 30%, 40%, 50%, 60% and 70% CPA) as the cooling proceeds. All plates were placed into the freezer at the beginning of the run. Temperatures at which the CPA transfer was carried out when Me_2SO was used were: -5°C (from 20% to 30% Me_2SO), -10°C (from 30% to 40% Me_2SO), -20°C (from 40% to 50% Me_2SO), -30°C (from 50% to 60% Me_2SO) and -40°C (from 60% to 70% Me_2SO).

Table 4.1 LT transfer temperatures for Me_2SO

% (v/v) Me_2SO from:	transfer at:	melting point of Me_2SO at:	freezer holding temperature
20 to 30	-5°C	20%: -8°C	-15°C
30 to 40	-10°C	30%: -15°C	-20°C
40 to 50	-20°C	40%: -30°C	-30°C
50 to 60	-30°C*	50%: -50°C	-40°C
60 to 70	-40°C*	N/A	-50°C

*transfer temperatures were determined empirically, as viscosities at colder temperatures were difficult to handle. N/A, non-applicable.

4.3.3.2 Manual Liquidus Tracking set-up 2

In this set-up 2ml microfuge tubes with a starting volume of 1.5ml were used (Figure 4.3). At each Me_2SO change 750µl of Me_2SO solution was taken out and 750µl of a 20% higher Me_2SO concentration was added, then the solution was mixed with a pasteur pipette. This procedure allowed an increase of 10% Me_2SO at each step. As 2ml microfuge tubes have a different heat transfer rate to 6-well plates, the freezer holding time and temperature had to be modified to achieve a 20 minute incubation time between each Me_2SO change. Therefore the holding time was first set to 15 minutes at the median temperature between the starting temperature and the next transfer temperature. Then the holding temperature was set 5˚C below the transfer temperature until the required temperature was reached. As for set-up 1 a cooling rate of -2°C/minute was chosen and the same transfer temperatures were used. At the beginning of the run enough CPA solution of e.g. 40% 50%, 60%, 70% and 80% Me_2SO was stored in the freezer to be cooled. To assure corresponding cooling rates, the volume of each solution was similar to the sample volume of 1-2ml.

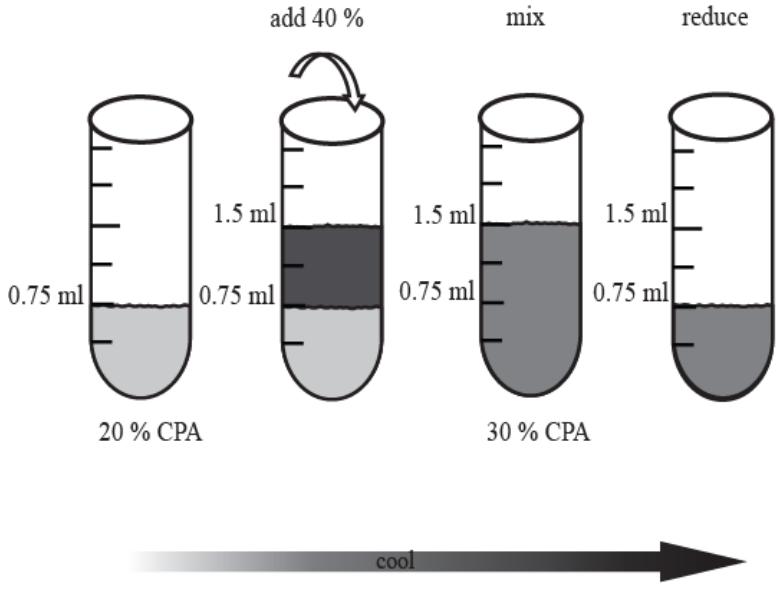

Figure 4.3 A schematic of manual LT set-up 2.

When using set-up 2 the sample remained in the same sample container throughout the vitrification procedure. To increase the CPA concentration by increments of 10% an equal amount of a 20% higher concentrated CPA solution was added. Samples were mixed pippeting up and down for at least five times before the volume was reduced. The same transfer temperatures as for set-up 1 (Table 4.1) were used.

4.3.3.3 Manual Liquidus Tracking set-up 3

In this test set-up 15ml centrifuge tubes were used. The Me_2SO concentration was increased by adding small amounts of highly concentrated Me_2SO (Table 4.2). The volume was not reduced during the cooling procedure, as in general a starting volume of 750µl was used, resulting in a final volume of 4.5ml (Figure 4.4).The cooling protocol was kept as for LT set-up 2.

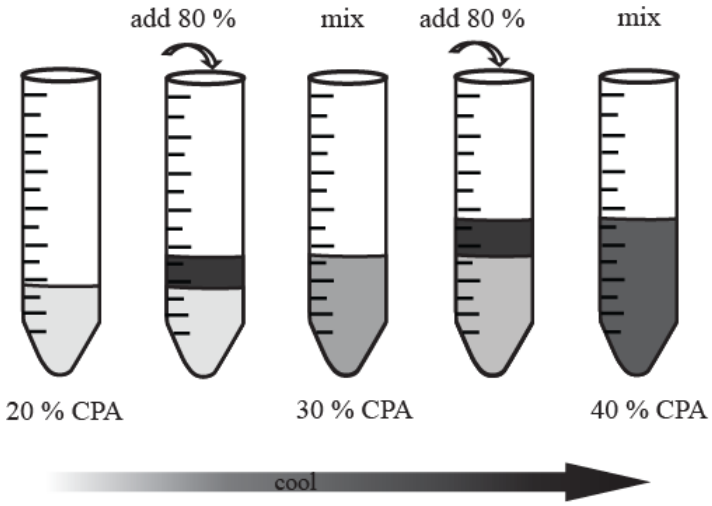

Figure 4.4 A schematic of manual LT set-up 3.

For set-up 3 two highly concentrated CPA solutions 60% and 80% were used to increase the CPA concentration of the sample. Smaller volumes were necessary to increase the sample CPA concentration so that the sample volume did not have to be reduced after each addition as for set-up 2.

Table 4.2 Amount of CPA to be added to increase sample CPA concentration by increments of 10%

Initial CPA (%)	Initial Vol. (µl)	Vol. (µl) of 60% (80%)* CPA to add	Target CPA (%)
20	750	200	30
30	900	400	40
40	1125	400*	50
50	1500	800*	60
60	2250	2400*	70
final vol.	4500		

Formula to determine the amount of 60% (80%) CPA to be added: B=(A*c-A*a)/(b-c) with B=volume of 80% CPA to add, A=start vol., c= final CPA concentration, a=start CPA concentration, b=80% CPA

4.3.3.4 Manaual Liquidus Tracking warming procedure

To avoid osmotic injury the Me_2SO decrease per step was reduced to 20% (v/v), except for step one, which decreased from 70% to 40% (v/v) Me_2SO. Temperatures were chosen according to freezers that were available in the laboratory. A -80°C and -20°C freezer were required as some samples were warmed at the same time others were cooled with the controlled rate freezer, of which only one was available. Samples with a Me_2SO concentration of 20-30% (v/v) were placed directly (**A**) into ice-cold PBS for 10 minutes, then washed several times with an excess of PBS and were then transferred to complete media and incubated at 37°C for 24 hours. Samples containing 40-50% (v/v) Me_2SO were placed into (**B**) ice-cold 20% (v/v) Me_2SO for 10 minutes and were then processed as described for **A**. Samples at 60% (v/v) Me_2SO and samples at 70% (w/w) Me_2SO at -60°C were placed into (**C**) 40% (v/v) Me_2SO at -20°C for 15 minutes and then processed following step **B** and **A**. Vitrified samples were kept at -80°C for 20 minutes and then processed following step **C**, **B** and **A** (Figure 4.5).

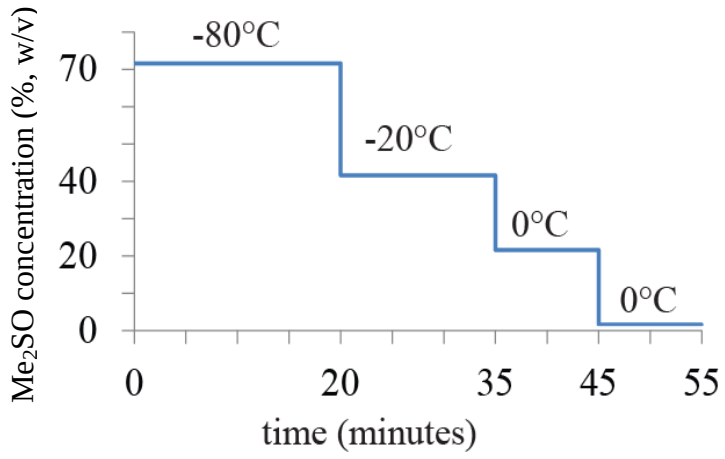

Figure 4.5 LT warming-step by step.

Samples were kept in a -80˚C freezer for 20 minutes, then CPA concentration was reduced to 40% (v/v) and samples were incubated in a -20˚C freezer for 15 minutes. CPA concentration was reduced to 20% and then 0% (v/v). In both concentrations AELC were incubated for 10 minutes while being kept on ice (0.5˚C).

4.3.4 Manual Liquidus Tracking step by step

For each experiment seven samples were used. One sample was taken out of the Planer freezer before the Me_2SO concentration was increased and temperature further reduced for the remaining samples. Beads incubated in 70% (v/v) Me_2SO were cooled either down to -60°C and warmed directly or cooled to -160°C (vitrified) and stored for 3-7 days in liquid nitrogen until use (Figure 4.6). For the complete LT pathway, the time taken to achieve the vitrified state was about 10 minutes.

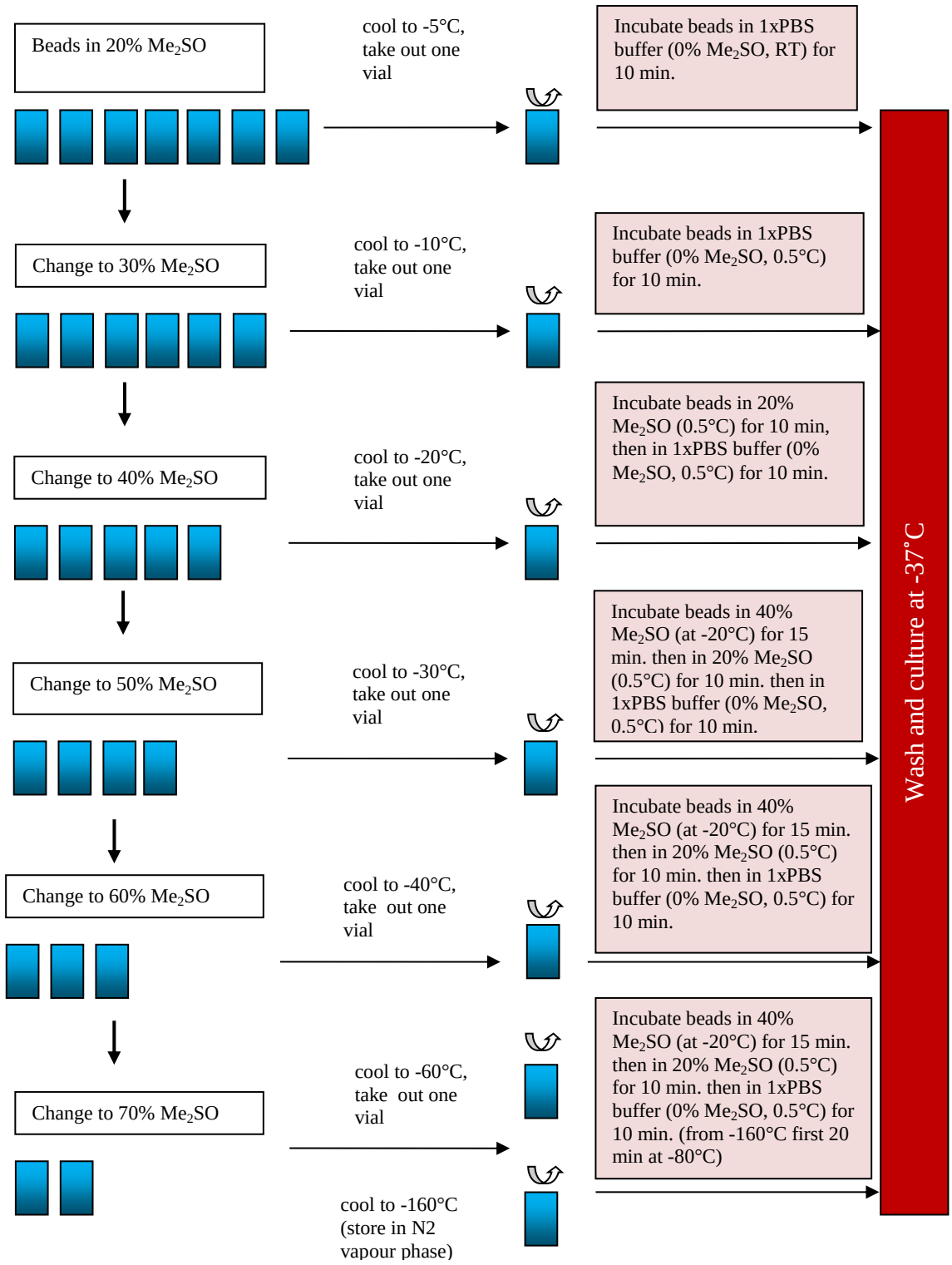

Figure 4.6 Step-by-step manual LT

One sample was taken out of the freezer before the Me_2SO concentration was increased and temperature reduced. Samples were processed following a warming protocol (4.3.3.4). AELC were cultured for 24 hours in complete media at 37˚C before measuring viability.

4.3.5 Temperature recordings

Sample temperatures were measured using a Type K thermocouple which was either placed in the bottom of a 6-well plate or in the conical part of a microfuge or centrifuge tube. The temperature was then recorded by a Picotech TC-08 datalogger.

4.3.6 Thermocouple defined approximate freezing point (TdAFP) detection for dimethyl sulfoxide

Materials

Me_2SO *(Sigma, Cat. No154938)*

1xPBS with Mg^{2+} and Ca^{2+} *(Sigma, Cat. No. D8662)*

Controlled Rate Freezer (*Planer, Kryo 10, Series II*)

Picotech TC-08 datalogger

Method

The thermocouple defined approximate freezing point (TdAFP) is an approximation of the equilibrium melting point of a sample. The TdAFP was detected by measuring the release of latent heat. For samples that supercool, the release of latent heat can be seen as a peak on the time/temperature curve. In an ideal set-up, the release of latent heat will increase the sample temperature up to the equilibrium melting point of that solution (Figure 4.7). For more accurate measurements differential scanning calorimetry has to be used to measure the equilibrium melting point. The TdAFP was measured by adding 1.5ml of each solution (10%, 20%, 30%, 40%, 50%, 60% and 70% (v/v) Me_2SO) to a microfuge tube. A thermocouple was inserted into each tube to record the ice nucleation point. Cooling was performed using the Planer Kryo 10 machine at a cooling rate of -2°C/minute. PBS was used as a cryoprotectant carrier solution. Any inadvertent ice nucleation by cooling to below the melting (freezing) point of a given mixture in a LT set-up had to be avoided at all times. Therefore, the temperature at which the Me_2SO concentration had to be increased was determined as follows: for each condition the average temperature was calculated and an offset of +30% of the average temperature was introduced to compensate for any deviation between the actual temperature to the theoretical melting point and to ensure that the Me_2SO increase can be carried out before any nucleation occurs. The Liquidus Tracker can only be programmed with whole numbers and therefore results were rounded.

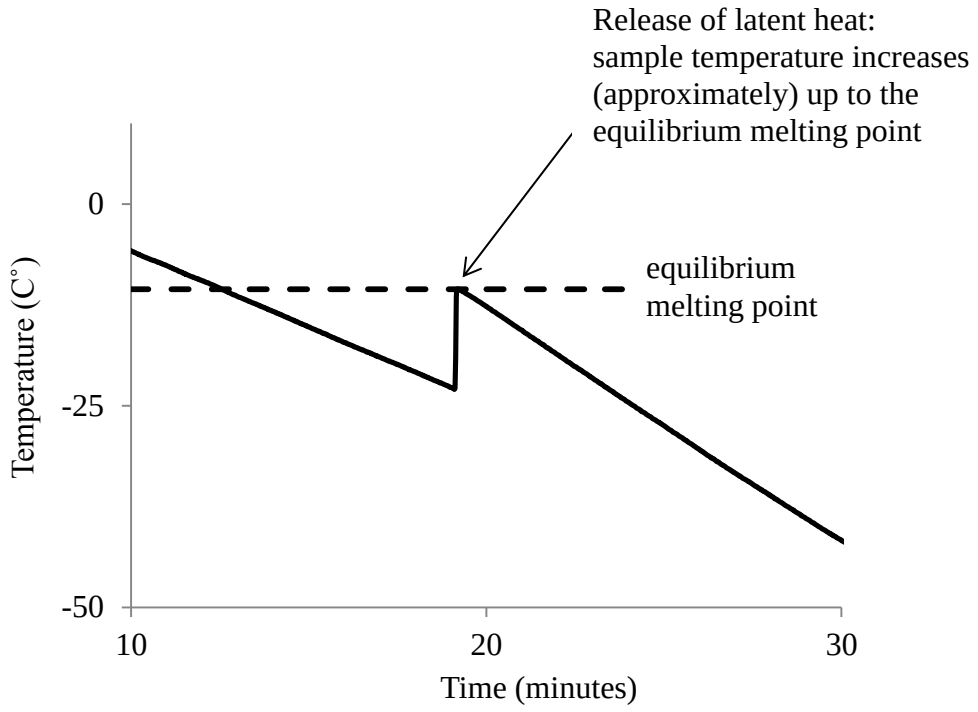

Figure 4.7 Supercooling and release of latent heat

This schematic shows the temperature curve of a supercooled sample and the temperature increase of the sample during the release of latent heat (solid line). The equilibrium melting point of the sample is also shown (dashed line). Upon the release of latent heat the sample temperature is increased approximately to its equilibrium melting point. The actual temperature reached was defined as thermocouple defined approximate freezing point (TdAFP).

4.3.7 Refractive index of dimethyl sulfoxide

Materials

Cole-Pamer Digital Refractometer, Brix, 45.0 to 95.0%, EW-02941-33

Method

To measure the refractive index of a sample, at least 0.4ml of that solution had to be placed on the prism surface of the Cole-Pamer refractometer. The refractometer contains an automatic temperature compensation tool which allows measurements between 0 - 40°C. Samples taken during the LT process were warmed up to at least 0˚C before measurement. Distilled water was used for calibration. A standard curve to determine the Me_2SO concentration of an aqueous solution was established by measuring the refractive index of increasing Me_2SO concentrations at room temperature. The equations for the trendlines were: $y = -0.0029x^2 + 1.0412x + 0.631$($R^2$

= 0.9995) for volume/volume, $y = -0.0023x^2 + 0.9839x + 0.5218$ ($R^2 = 0.9993$) for weight/weight and $y = -0.0027x^2 + 0.9754x + 0.5082$ ($R^2 = 0.9992$) for weight/volume, with y = % Me_2SO and x= refractive index (Figure 4.8).

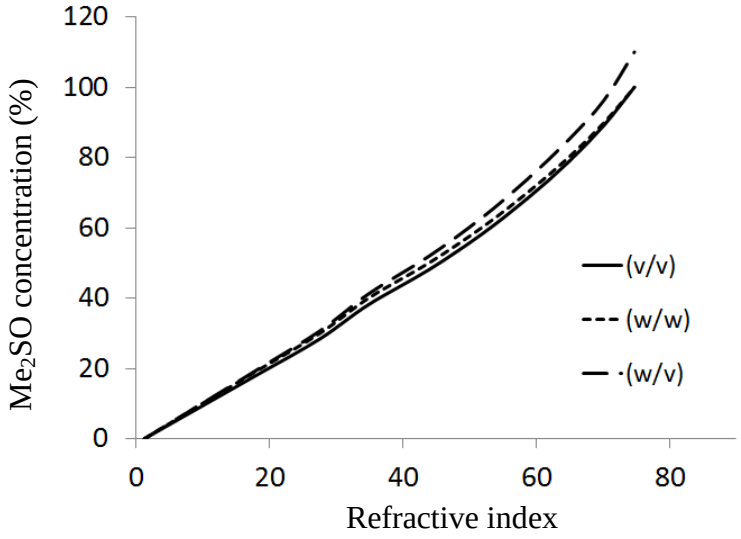

Figure 4.8 Refractive index of Me_2SO

The concentration of an aqueous Me_2SO solution (Me_2SO in 1x PBS at 20°C) as a function of the refractive index. By using the standard curve the CPA concentration of a sample can be determined.

4.3.7.1 Improved manual Liquidus Tracking

Manual LT set-up number 3 has here shown to be the most practical. For a more reliable process the set-up was improved by using a 'thermal buffer - TB' - insulating each 15ml centrifuge tube within a 70% ethanol solution held in a 50ml centrifuge tube. A hole with a diameter of a 15ml centrifuge tube was cut in the 50ml centrifuge tube lid, to keep the 15ml tube fixed in the middle of the 50ml tube. A special stirrer was made by using a 2ml Pasteur pipette which was cut in a specific shape that allowed pressure and suction by up and down movement to provide effective mixing of viscous solutions (Figure 4.9).

A. B.

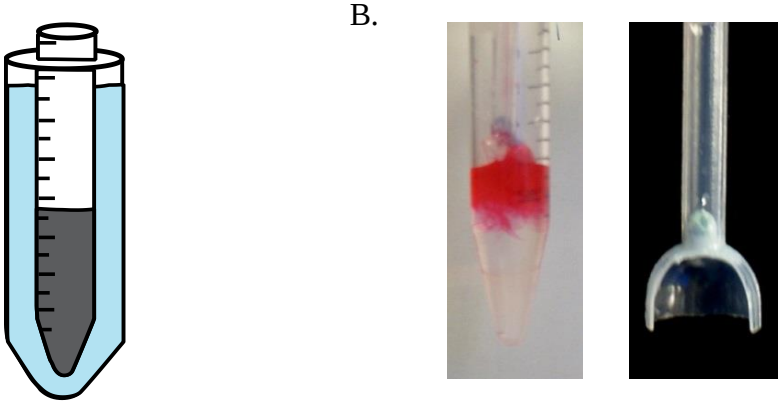

Figure 4.9 Improved manual LT

A.:The insolation system of 70% (v/v) ethanol helped to maintain the sample temperature during the CPA change when the freezer lid is opened. B: A special stirrer made to deal with highly viscous solutions of a 2ml Pasteur pipette; top cut to a length of 1 cm, border cut with a upper diameter of 0.3cm and a lower diameter of 1.2cm. The opening was closed with blue tack. Pressure and suction by up and down movement provided effective and fast mixing even for viscous solutions.

4.4 Results

4.4.1 Can CPA toxicity be reduced by decreasing the temperature?

Alginate encapsulated liver cells (AELC) were incubated at different temperatures in increasing concentrations of dimethyl sulfoxide (Me_2SO) to observe the effect of temperature on Cryoprotectant agent (CPA) toxicity.

4.4.1.1 Me_2SO toxicity at different temperatures and incubation times

AELC were incubated at 37°C in increasing concentrations of Me_2SO (10-70% (v/v)). A sudden viability drop was observed at 40% (v/v) for samples incubated at 37°C, but was delayed to 50% (v/v) Me_2SO when the incubation temperature was set to 4°C. This was independent of whether AELC were incubated for a period of 40 minutes or 6 hours. Recovery of AELC incubated for 6 hours was approximatly 20-30% lower than the recovery of AELC that were incubated for 40 minutes. When exposed to low concentrations of Me_2SO (10-30% (v/v)) viabilities as high as 80% were maintained as long as high incubation temperature (37°C) and long exposure time (6 hours) were not combined. In this case viability decreased to 60% before dropping to 0% at 40% (v/v) Me_2SO. The viability of untreated samples was > 99% (Figure 4.10).

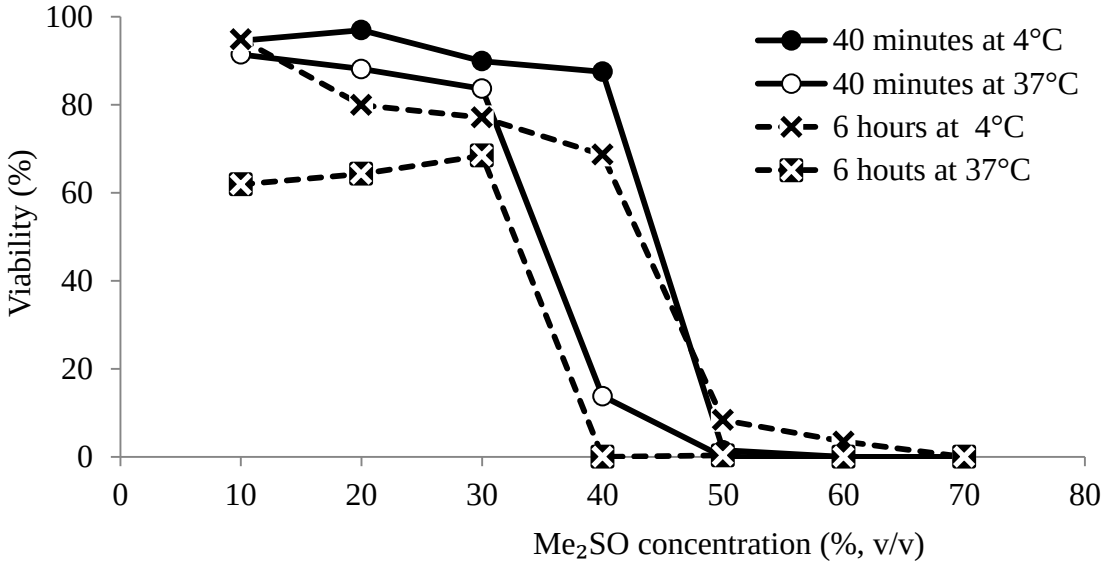

Figure 4.10 AELC viability at increasing Me_2SO concentrations, incubation temperatures and time

Viabilities remained approximately constant until they suddenly dropped to nearly zero percent when reaching a concentration of either 40% or 50% (v/v) Me_2SO at an incubation temperature of 37°C or 4°C, respectively. This was independent of whether the incubation time was set to 40 minutes or 6 hours. AELC were cultured for 24 hours in complete media at 37°C before viability was assessed by FDA/PI staining.

4.4.1.2 Me_2SO toxicity at different temperatures below zero

To verify the results of the previous experiment and to investigate the Me_2SO toxicity at subzero temperatures, AELC were incubated at temperatures between 37°C and -50°C. AELC 2-5 days after encapsulation were used as the purpose was to investigate Me_2SO toxicity. These beads contain less cells and no spheroids and therefore ice formation may have less impact on viability. Moreover lower cell density increases Me_2SO diffusion which is necessary to effectively prevent ice formation inside the cell. The viability of unfrozen samples measured each day was > 97%. Me_2SO toxicity was clearly decreased when exposure temperature was reduced. For example up to 50% (v/v) Me_2SO was well tolerated when alginate encapsulated HepG2 cells were incubated at -20°C but decreased to 0% for all temperatures between -10°C and +37°C. Temperatures lower than -20°C did not prevent further cell death. Some of the samples were frozen after the incubation process as the Me_2SO concentration was too low to

avoid ice formation. These samples showed lower viabilities than unfrozen samples of higher CPA concentration that were incubated at the same temperature (Figure 4.11).

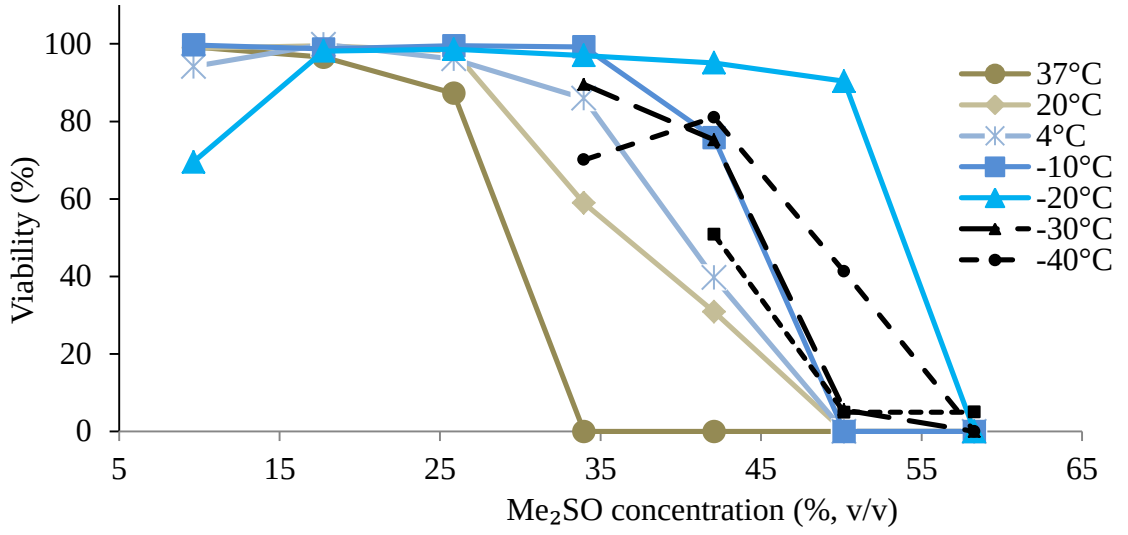

Figure 4.11 Temperature impact on Me_2SO toxicity

AELC were incubated at increasing Me_2SO concentrations at decreasing temperatures for 40 minutes. From 37˚C to -20˚C viability increased, below -20˚C viability decreased. AELC were cultured for 24 hours in complete media at 37˚C before viability was assessed by FDA/PI staining.
** frozen samples*

4.4.1.3 Dimethyl sulfoxide toxicity over time

To estimate the impact of exposure time on Me_2SO toxicity, AELC were incubated for 1, 5, 15 and 40 minutes in 30% to 70% (v/v) Me_2SO at 4°C. Solutions with 10-20% (v/v) Me_2SO were not further investigated as they had shown little effect on cell viability for temperatures lower than 20°C (Figure 4.11). After 1 minute, AELC incubated in 30%, 40% and 50% (v/v) Me_2SO still showed high viabilities of >90%. Instead, recovery of cells incubated in 60% and 70% (v/v) Me2SO decreased to about 50% after 1 minute. After five minutes most of these cells incubated in 70% (v/v) Me_2SO had died whereas those exposed to 60% (v/v) Me_2SO still showed a recovery of 44%. Less toxic were solutions of 30-50% (v/v) Me_2SO with AELC still showing viabilities of approximately 83%. After 15 minutes the difference between the conditions became more evident showing a modest decline to 80% for 30% (v/v) Me_2SO and to 70% for 40% (v/v) Me_2SO. A stronger reduction was seen for 50% and 60% (v/v) Me_2SO with viabilities being reduced to 50% and 14%, respectively. Finally

after 40 minutes, viability of cells incubated in 60% (v/v) Me_2SO was reduced to 0%. AELC exposed to 50% and 40% (v/v) Me_2SO still reached a viability of 12%, and 23% respectively. The exposure to 30% (v/v) Me_2SO showed little additional effect with viabilities still reaching 77%. For 60% and 70% (v/v) Me_2SO viability decreased strongest during the first minute, for 30% and 40% (v/v) Me_2SO during the first five minutes and for 50% during the first 15 minutes (Figure 4.12).

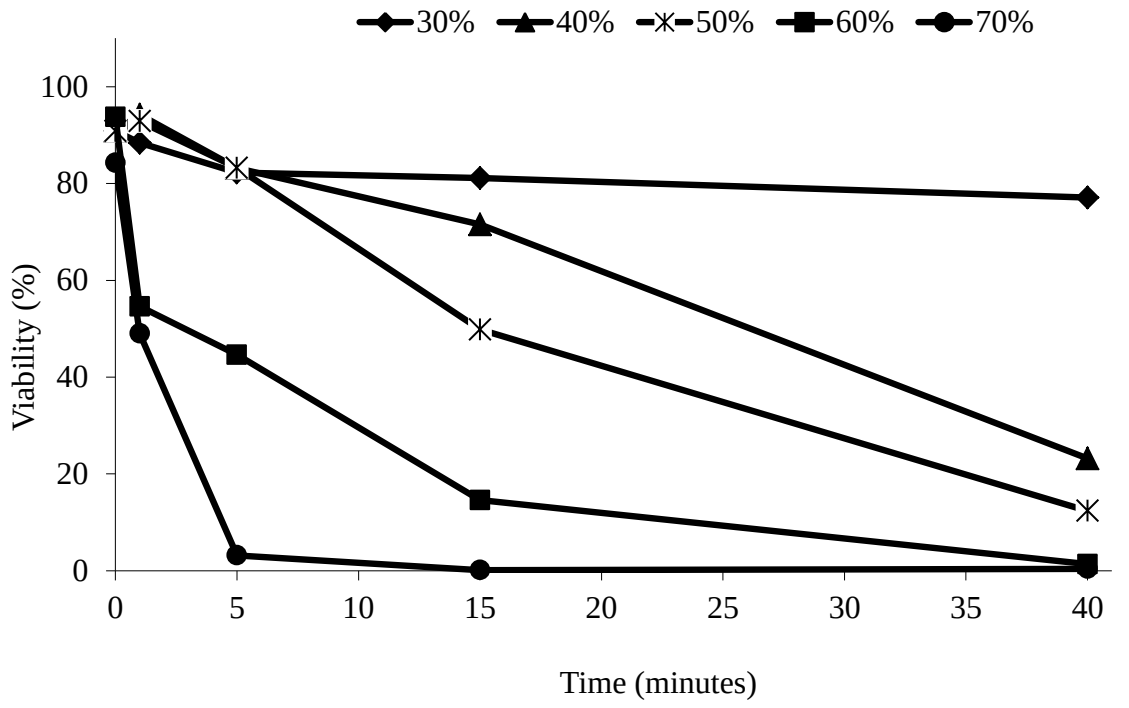

Figure 4.12 Me_2SO toxicity over time at 4˚C

The figure shows Me_2SO toxicity at 4˚C over time. AELC were incubated in 1x PBS solutions containing 10-70% (v/v) Me_2SO. AELC viability slightly decreased over time when exposed to 30% (v/v) Me_2SO, but strongly decreased when 40% and 50% (v/v) Me_2SO was used. Exposure to 60% Me_2SO (v/v) resulted in complete cell death after 40 minutes, whereas AELC incubated in 70% Me_2SO already showed very low recovery after five minutes. AELC were cultured for 24 hours in complete media at 37˚C before viability was assessed by FDA/PI staining.

4.4.2 Determination of osmotic effects

AELC pre-incubated in 20% (v/v) Me_2SO before being incubated in 40% (v/v) Me_2SO showed no significant difference in recovery to those directly exposed to 40% (v/v) Me_2SO when the incubation temperature was set to 0.5°C. This changed when the incubation temperature was set to 37°C. At this temperature the pre-incubation step

significantly reduced cell death and improved recovery from 21% +/- 7% to 45% +/- 7% (n=5) for an incubation period of 15 minutes and from 3 +/- 2% to 36 +/- 2% (n=5) when AELC were incubated for 40 minutes (Figure 4.13).

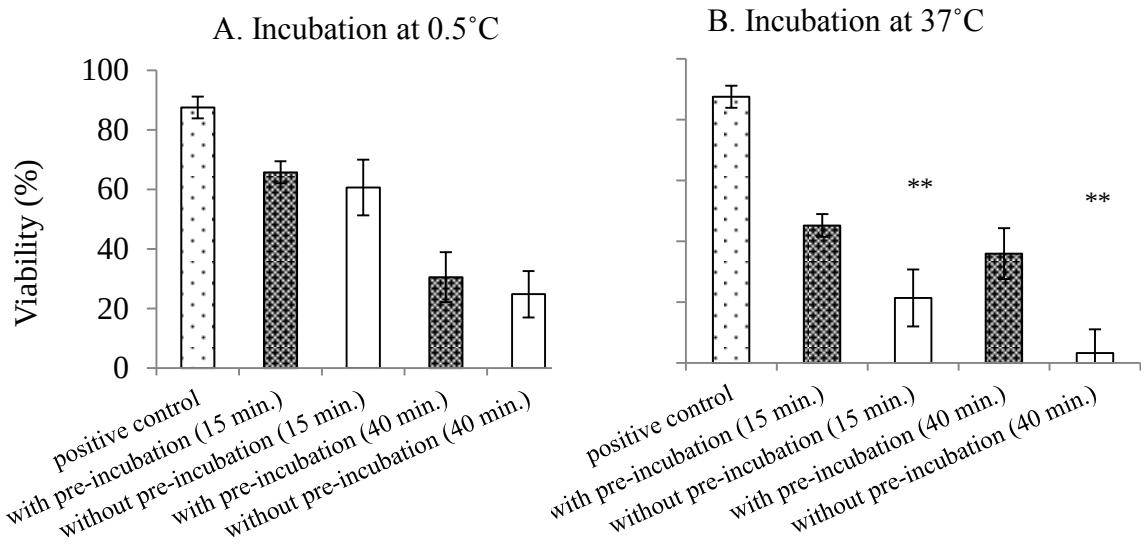

Figure 4.13 Effect of temperature on osmotic injury

Columns in black: with pre-incubation - AELC first incubated for 2 minutes in 20% (v/v) Me_2SO, then in 40% (v/v) Me_2SO for 15 or 40 minutes. Columns in white: without pre-incubation - AELC directly incubated in 40% (v/v) Me_2SO for 15 or 40 minutes. A: There was no significant difference between the two conditions, (pre-incubation and without pre-incubation), when the incubation was carried out at 0.5°C. B: Viability was significantly higher for pre-incubated AELC when the incubation temperature was set to 37°C, with ** p<0.01, (n=5 +/-SD). AELC were cultured for 24 hours in complete media at 37˚C before viability was assessed by FDA/PI staining.

4.4.3 Thermocouple defined approximate freezing point (TdAFP) for dimethyl sulfoxide

Latent heat release was only observed for solutions of 10%, 20% 30% and 40% (v/v) Me_2SO, but not for solutions of 50%, 60% or 70% (v/v) Me_2SO (Figure 4.14). Measured equilibrium melting points were -3.5°C +/- 0.23, -9.2°C +/-0.94, -19.8°C +/- 0.77 and -38.8°C +/-1.85 for 10, 20, 30 and 40% (v/v) Me_2SO, respectively. The equilibrium melting points for 10% and 20% (v/v) Me_2SO were in agreement with those known from literature (10% (-3°C), 20% (-9°C)), whereas 30% and 40% (v/v) Me_2SO were lower (literature: 30% (-16°C), 40% (-30°C)). The equilibrium melting point of a

given concentration was determined by calculating the average of five individual measurements (Figure 4.15).

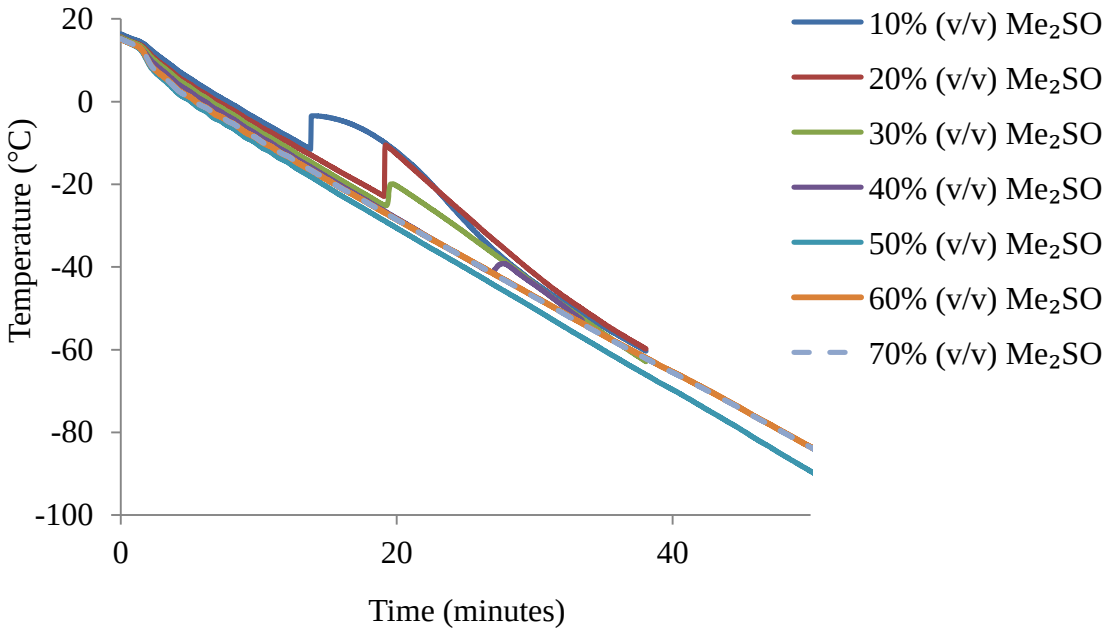

Figure 4.14 Equilibrium melting point detection for increasing concentrations of Me_2SO

The equilibrium melting point for 10, 20, 30, 40, 50, 60 and 70% (v/v) Me_2SO was determined by cooling 1.5ml of each sample at -2˚C/minute in a controlled rate freezer. Thermocouples within the solution measured the temperature during the crystallisation process. Latent heat release was only observed for solutions containing 10%, 20% 30% and 40% (v/v) Me_2SO. Higher concentrated solutions did not show any peak (release of latent heat) in their cooling profile.

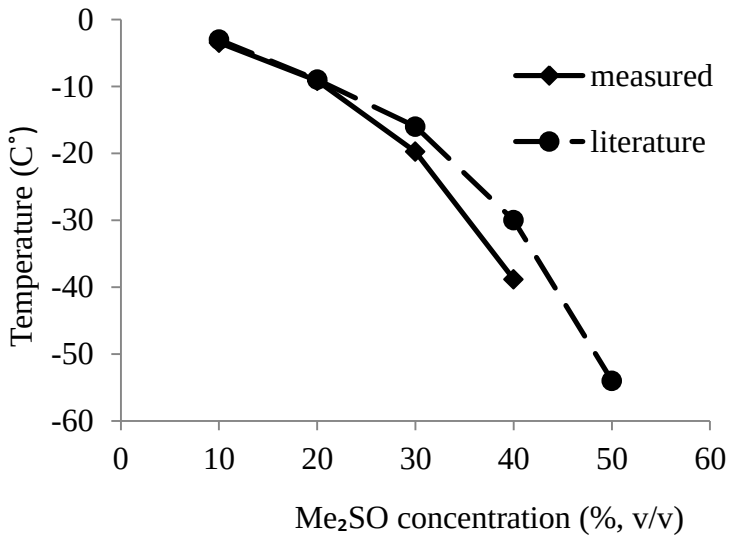

Figure 4.15 Me_2SO Liquidus curve: TdAFP vs. literature data

Thermocouple defined approximate freezing points for 10% and 20% (v/v) Me_2SO were in agreement with the equilibrium melting point for 10% and 20% (v/v) Me_2SO found in literature ((Elford, 1970; Farrant, 1965b), whereas measured values for 30% and 40% (v/v) Me_2SO were lower.

4.4.4 Liquidus Tracking step-by-step (set-up 1)

In order to determine at which step viability is decreased, one sample was taken out of the Planer freezer just before the Me_2SO concentration was increased and temperature further reduced for the remaining samples. Viability remained constant until a concentration of 30% (v/v) Me_2SO, before starting to reduce. An exception to this was LT run five, for which viability was already decreased at 30% (v/v) Me_2SO. Between 30% and 60% (v/v) Me_2SO the strongest viability loss was observed. Recovery remained constant between 60% and 70% (v/v) Me_2SO. There was no notable difference between samples with a final concentration of 70% (v/v) Me_2SO that were cooled to -60°C and directly rewarmed, and those cooled to -160°C and rewarmed after vitrification. An exception was LT run 4, for which viability decreased from 60% to 13% after vitrification. The average viability after vitrification was 23 +/- 16%. The highest value was reached for LT run 1 with a remaining viability of 46% (Figure 4.16).

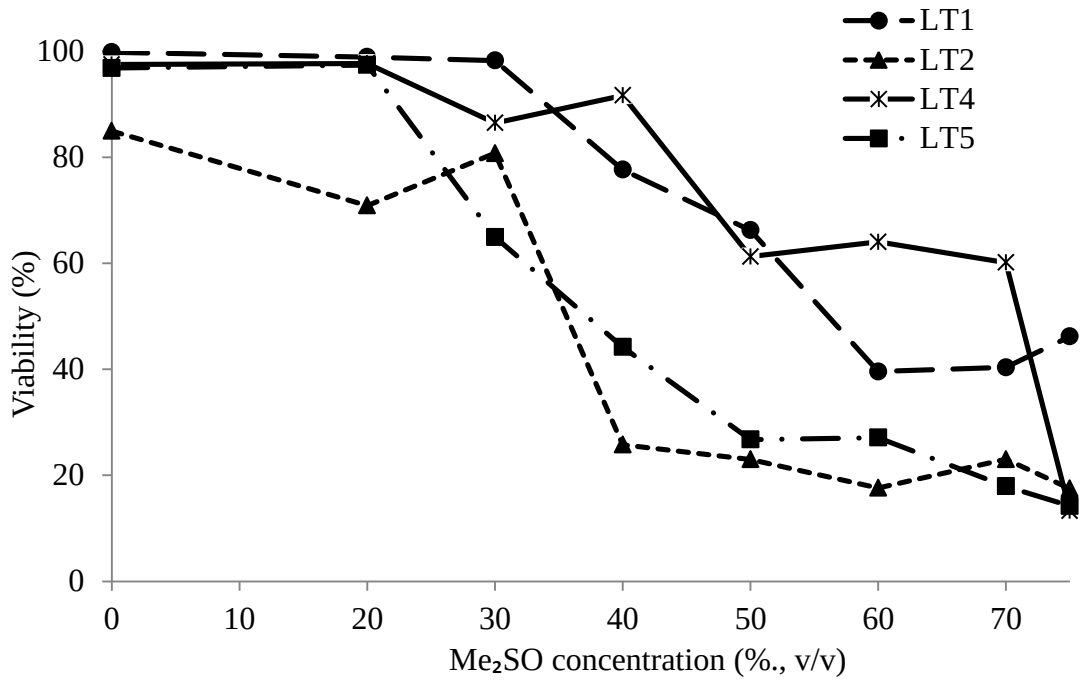

Figure 4.16 LT step-by-step (set-up 1)

The scheme shows how viability decreased during the LT process after each Me_2SO addition step. The figure shows four different runs. Experiment 3 was excluded from evaluation due to strong ice formation. Between 30% and 60% Me_2SO most of the viablity was lost, but remained constant between 60% and 70% (v/v) Me_2SO. Apart from LT run 4, full progress to vitrification did not have an effect on viability. The average viability after vitrification was 23 +/- 16% (n=4). The highest value was reached for LT run 1 with a remaining viability of 46%. AELC were cultured for 24 hours in complete media at 37°C before viability was assessed by FDA/PI staining.

4.4.5 Liquidus Tracking step-by-step (set-up 1, 2 and 3)

Set-up 2 and 3 were compared to results of set-up 1. As for the previous experiments, viability of set-up 2 remained constant until a concentration of 30% (v/v) Me_2SO before starting to drop. For set-up 3 viability decreased continuously until a concentration of 60% (v/v) Me_2SO. For both set-ups (2 and 3) recovery remained constant between 60% and 70% (v/v) Me_2SO and no additional decrease was recorded after vitrification. Viability after vitrification for set-up 2 and 3 was 44% and 23%, respectively (Figure 4.17).

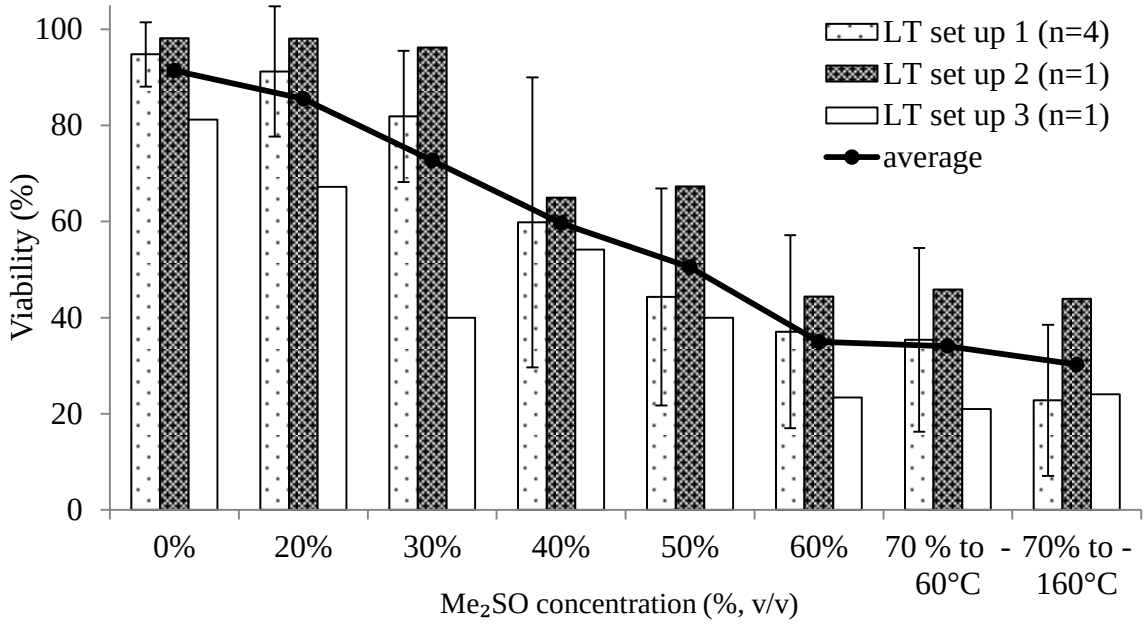

Figure 4.17 LT step-by-step set-up 1, 2 and 3

The Figure shows the data of one run of set-up 2 and 3, the average of set-up 1 (n=4, +/- SD), and the overall average of all runs (solid line). Considerable variability was seen between runs; nevertheless viability dropped mostly between 30% and 60% Me_2SO (v/v). Viability after warming for samples exposed to the final Me_2SO concentration of 70% (v/v) was approximately 30% regardless of whether samples were cooled to -60°C or cooled and stored at -160°C. AELC were cultured for 24 hours in complete media at 37°C before viability was assessed by FDA/PI staining.

4.4.6 Liquidus Tracking step-by-step at 0.5°C.

In this experiment LT was performed on ice (0.5°C) using LT set-up 2. Between each increase, samples were kept on ice for 15 minutes so that the incubation time in CPA would be comparable to LT set-up 2. Warming was performed in the same step wise manner described in section 4.3.3.4, but was carried out at 0.5°C. The experiment was intended to determine whether CPA toxicity decreased due to its stepwise addition of Me_2SO (prevention of osmotic injury) or due to the temperature decrease. As seen before, recovery strongly reduced when the Me_2SO concentration was increased to 40% (v/v). Contrary to manual LT performed at decreasing temperatures (4.4.5), at 50% (v/v) Me_2SO most cells had died and there was no viability observed for cells that reached a final concentration of 60% and 70% (v/v) Me_2SO (Figure 4.18).

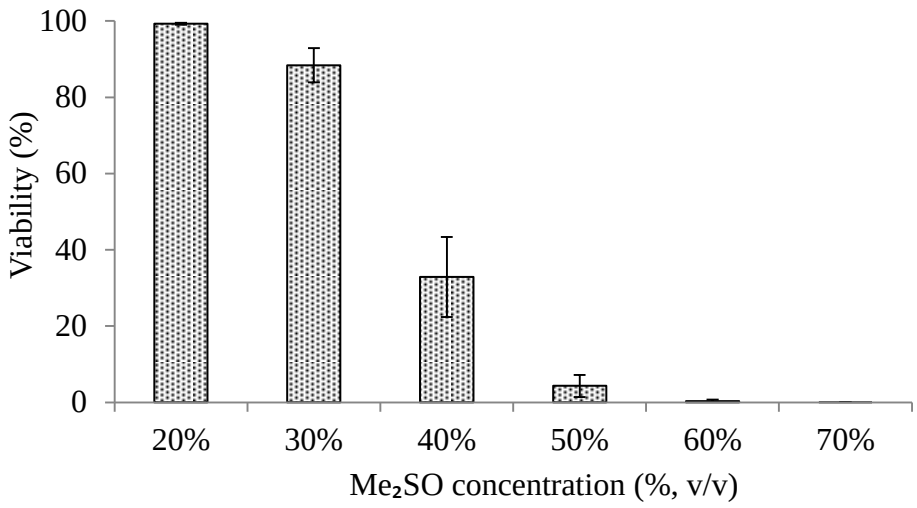

Figure 4.18 LT step-by-step at 0.5°C

The Figure shows data from 5 runs of set-up 2 carried out at 0.5˚C. Viability decreased to 4% +/- 3 when AELC were incubated in 50% (v/v) Me_2SO. No viability was detected for AELC incubated in 60% and 70% (v/v) Me_2SO.

4.4.7 Liquidus Tracking temperature profile

For each manual LT experiment (set-up 1, 2 and 3) the temperature curve was recorded using the Pico Logger software (Figure 4.19, Figure 4.20). A temperature increase of approximately +2°C was measured when cell strainers were transferred between 6-well plates (8ml PBS-Me_2SO per well) while the freezer lid was held open (set-up 1). The temperature was increased by approximately +20°C when 2ml microfuge tubes with a volume of 1.5ml PBS- Me_2SO solution were used. The average cooling rate until the starting temperature was reached was 7.51°C/minute (set-up 2). Set-up 3 showed an average temperature increase of 11.1°C. The average cooling rate until the starting temperature was reached was -2.94°C/minute.

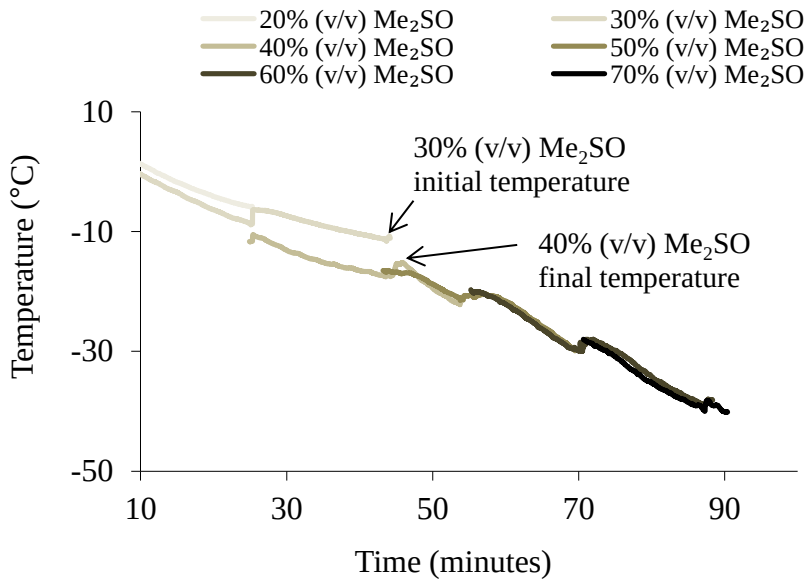

Figure 4.19 LT temperature profile set-up 1

The figure shows the recorded temperature increase during cell strainer transfer. Initial temperature indicates the sample temperature before cell strainers were transferred. Final temperature indicates the temperature of the solution into which cell strainers were placed (temperature was measured after transfer). The temperature difference between initial and final temperature was approximately +2°C.

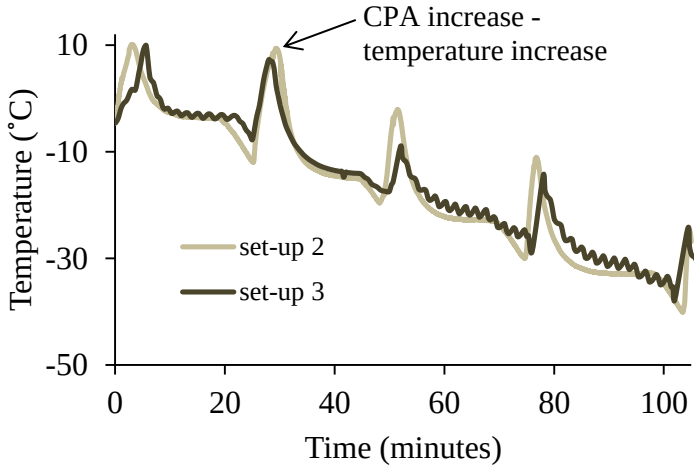

Figure 4.20 LT temperature profile set-up 2 and 3

The figure shows the temperature increase during Me_2SO addition for set-up 2 and 3. The temperature was increased by approximately 20°C when 2ml microfuge tubes with a volume of 1.5ml PBS-Me_2SO solution were used. The average cooling rate until the starting temperature was reached was -7.51°C/minute. Set-up 3 showed an average temperature increase of 11.1°C. The average cooling rate until the starting temperature was reached was -2.94°C/minute.

4.4.8 Improved manual Liquidus Tracking

We determined that manual LT set-up 3 was most practical. Nevertheless temperatures increased by up to 11°C during the addition of Me_2SO. Applying an insolation system helped to decrease temperature variations. When Me_2SO addition was carried out at 2.5°C, -3.5°C and -13°C, the temperature increase was reduced by approximately 3°C, 5°C and 6°C, respectively. At -25°C and -35°C the temperature increase was reduced by 10°C and 13°C, respectively (Figure 4.21). By using the new stirrer made of a Pasteur pipette that uses pressure and suction by up and down movement, the mixing time for viscous solutions was reduced. This was tested by mixing 4ml of uncoloured and 1ml of coloured glycerol. Glycerol has a similar viscosity to Me_2SO at -40°C. Mixing by conventional pipetting took 30 seconds to completely homogenize the sample, when using the new stirrer mixing was completed within 15 seconds. The sample CPA concentration reached with the new mixing technique, determined by refractometry, were 24.7% +/-1.0, 32.7% +/-1.7, 43.5% +/-0.4, 51.1% +/-0.8 and 62.3% +/-0.6 (n=6) and therefore within a range of +/- 4% of the target concentration of 25%, 35%, 45%, 55% and 65% (Figure 4.22).

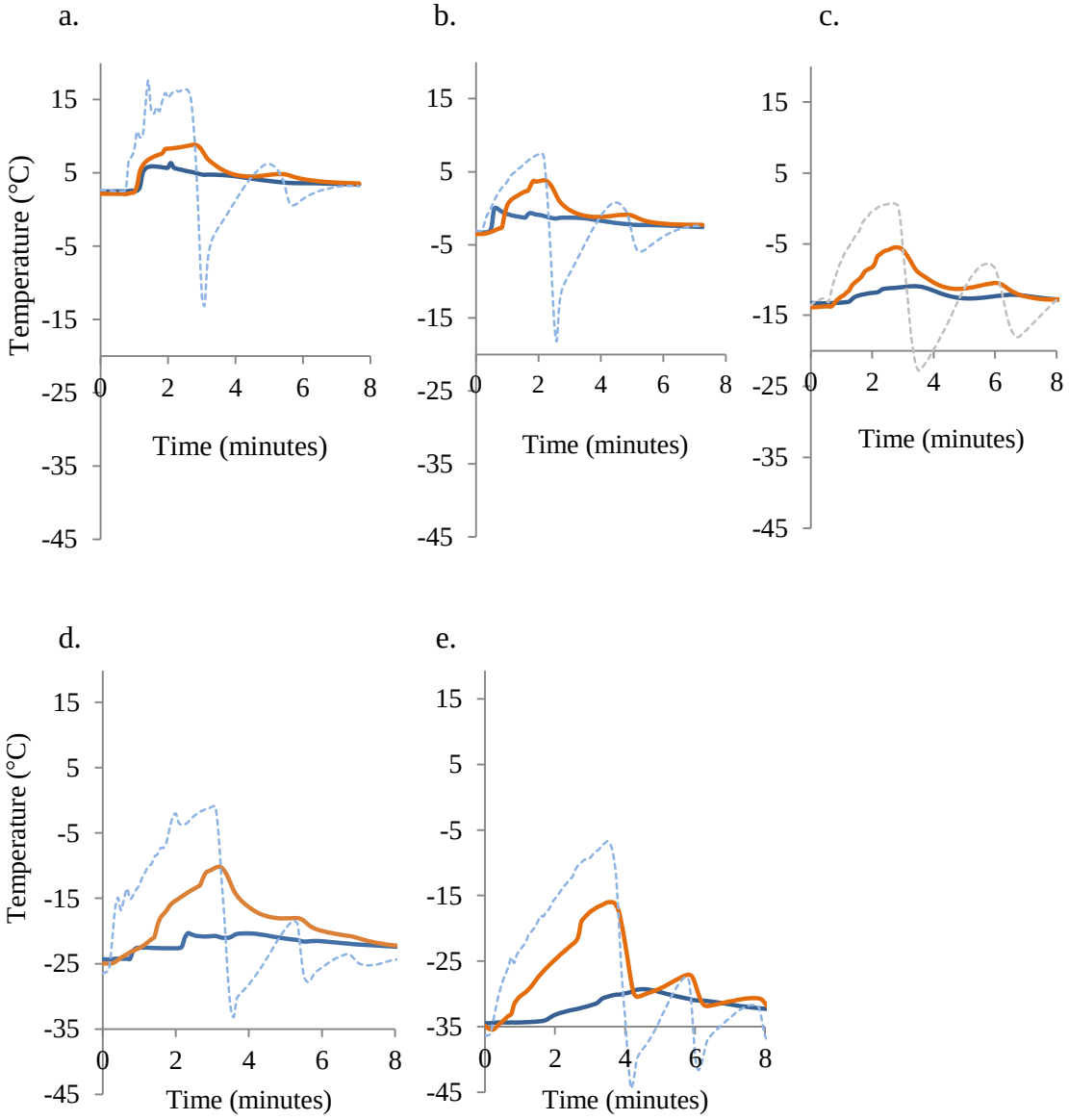

Figure 4.21 LT insolation system

By insolating the sample tube with 70% (v/v) ethanol (TB insolation), the temperature increase during each CPA addition step was reduced. The grey dashed line demonstrates the freezer temperature curve, the red line the temperature curve of samples without TB insolation and the blue line the temperature curve of a sample with insolation system. Each condition was tested in triplicate. This figure shows as an example the temperature curve of one sample. The temperature increase was reduced from a: 7.1°C to 4.5°C, b: 7.9°C to 3.2°C, c: 7.7°C to 2.1°C, d: 14.5°C to 4.4°C and e: 17.8°C to 5.2°C.

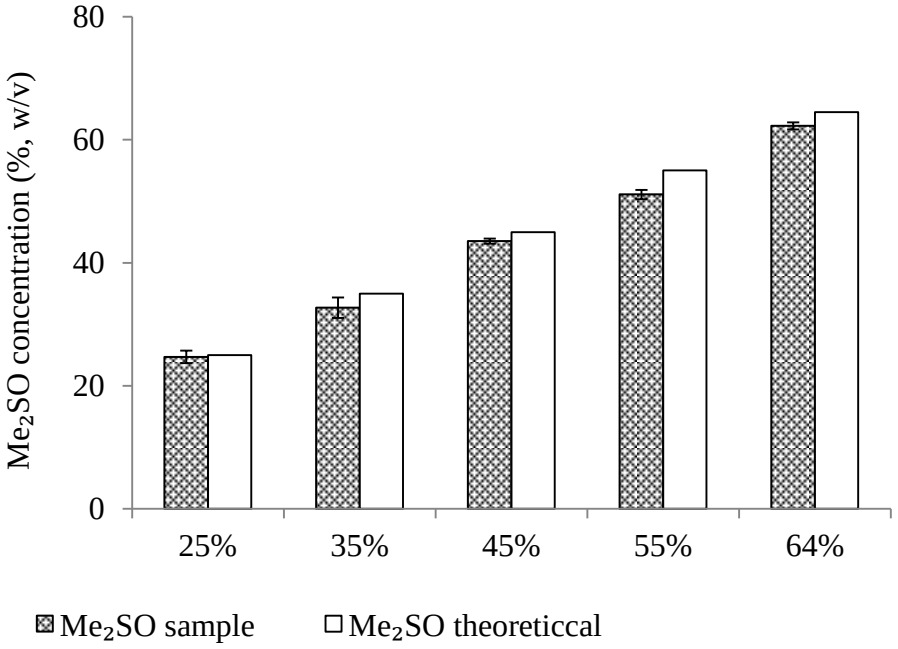

Figure 4.22 Manual LT stirring device.

By using the newly-developed stirrer that uses pressure and suction by up and down movement the sample CPA concentration reached was within +/-4% of the target concentration of 25%, 35%, 45%, 55% and 65% CPA (n=6, +/- SD). The concentration was measured by determining the refractive index.

4.5 Discussion

The first aim of this chapter was to prove the Liquidus Tracking (LT) theory that cryoprotectant agent (CPA) toxicity can be reduced by lowering the temperature. At lower temperatures molecules move slower and therefore less collisions between molecules decrease the possibility of any chemical or biochemical reaction. It has been predicted that by every one degree Celsius drop in human body temperature, cellular metabolism slows by 5% (Erecinska et al., 2003) and it was shown that for hibernating animals for which minimal body temperature can fall as low as -2.9˚C, the metabolism can be reduced to 1% of the euthermic rates (Carey et al., 2003).

To determine the influence of the CPA exposure temperature on our cell system, alginate encapsulated liver cells (AELC) were incubated at increasing dimethyl sulfoxide (Me_2SO) concentrations at decreasing temperatures. When exposed to 40% (v/v) Me_2SO, viability dropped to almost 0% when the incubation was carried out at 37°C, whereas recovery remained above 60% for samples that were kept at 4°C, but then dropped abruptly when the Me_2SO concentration was increased to 50% (v/v). This was independent of time whether AELC were incubated for a period of 40 minutes or 6 hours. The viability drop was further delayed by setting the incubation temperature to -10°C and -20°C. Up to 55% (v/v) Me_2SO was well tolerated when AELC were incubated at -20°C. Apart from the mentioned reasons for reduced CPA toxicity in general, there might be further explanations for Me_2SO in particular. Me_2SO is known to easily permeate cell membranes (Anchordoguy et al., 1992) and it is strongly believed that Me_2SO has the ability to replace water and solvate lipid headgroups (Gordeliy et al., 1998; Tristram-Nagle et al., 1998). A decrease in Me_2SO concentration in the bilayer at lower temperatures has been observed and it has been suggested that Me_2SO is more hydrophilic at lower temperatures. As a consequence less membrane dehydration might account for reduced Me_2SO toxicity at lower temperatures (Sum & de Pablo, 2003). Me_2SO can dissolve DNA at high concentrations and temperatures above 20ºC (Bonner & Klibanov, 2000) and oxidizes sulfhydryl groups (Snow et al., 1975). Those effects can also be expected to reduce when temperature decreases.

Nevertheless reduced toxicity at lower temperatures does not assure effective vitrification, since sufficient CPA has to penetrate the cells to avoid ice nucleation before the temperature is further decreased. It is possible that in these experiments cells incubated at -10°C or -20°C did not reach the same intra-cellular Me_2SO concentration as cells incubated at higher temperatures. For an optimized LT procedure it is therefore necessary to compromise between longer exposure time and higher exposure temperature to achieve sufficient CPA penetration, and a shorter exposure time at lower temperatures for minimum toxicity.

Decreasing the incubation temperature further to -30°C, -40°C or -50°C was unfavourable with a lower recovery than at -20°C. An explanation could be the initial pre-incubation step at which cells were directly incubated in high concentrations of Me_2SO (40-60 w/v %) for one minute at 0.5°C, to achieve some CPA pre-loading to avoid immediate freezing of AELC at the moment they were added to the pre-cooled Me_2SO solutions (-30°C to -50°C). The exposure to high Me_2SO concentrations, although only for one minute, possibly caused cell death by osmotic or chemical toxicity. When AELC were incubated in increasing Me_2SO concentrations at 0.5˚C over time, it was shown that one minute was sufficient to strongly exhibit Me_2SO toxicity (AELC viability reduced by 45%) when the concentrations was 60% (v/v). However, concentrations up to 50% (v/v) were well tolerated for one minute. Lower viability of AELC pre-incubated in 40% and 50% (v/v) Me_2SO which were then added to more concentrated Me_2SO solutions at temperatures below -20˚C could have been caused by insufficient Me_2SO penetration during the pre-incubation step. As a consequence, introducing the AELC bead solution to temperatures < -30°C would have initialized instant intracellular ice formation.

Interestingly viability did not decrease slowly while the Me_2SO concentration was increased, but usually dropped precipitously when a certain Me_2SO concentration at a given temperature was reached. This would suggest a strong influence of osmotic pressure, which will be increased by both higher temperature and Me_2SO concentration. The observation that the viability drop was independent of the exposure time if this was over 40 minutes, suggests a strong instant effect rather than progressive chemical or biochemical toxicity. Similar observations were made by Fahy (Fahy, 1982). In his

studies on rabbit renal cortex 40% Me_2SO was toxic whereas 30% w/v Me_2SO was completely nontoxic.

To investigate the impact of osmotic stress a two-step Me_2SO addition protocol was compared to a one step addition protocol. Upon addition of CPA, cells initially shrink as water leaves the cell by osmosis. Following this, cells swell as CPA crosses the cell membrane to enter the cell. This shrink and swell response occurs as cells possess increased permeability to water than solutes (Meryman, 2007; Paynter et al., 2005). The faster water is drawn out of the cell and the slower CPAs enter the cell, the more the cell will shrink. Currently several different theories of how osmotic injuries occur have been proposed. The minimum volume hypothesis suggests that upon shrinkage in hyper-osmotic condition cytoskeleton components and the shrunken cell membrane irreversibly interact. This compromises cell integrity upon rehydration (Meryman, 2007). The maximum cell surface hypothesis proposes that cell shrinkage induces irreversible membrane fusion and hence reduces the effective area of the cell membrane. When the cells are returned to isotonic condition, the cells lyse before the initial volume is regained as a result of the reduced membrane area (Steponkus & Wiest, 1978). Stepwise CPA addition decreases the difference in solute concentration inside and outside the cell. As a consequence cells do not shrink or swell beyond their osmotic tolerance (Si et al., 2006) and hyperosmotic stress is decreased. Step-wise addition and removal of CPAs have been shown to significantly improve survival of various cell types including oocytes (Isachenko et al., 2004; Wang et al., 2010) and islets (de Freitas et al., 1998).

When AELC were pre-incubated in 20% (v/v) Me_2SO before adding them to 40% (v/v) Me_2SO at 37°C recovery was significantly increased from approximately 21% to 45% for an incubation period of 15 minutes and from approximately 3% to 36% when exposure lasted for 40 minutes. Cells, which underwent the pre-incubation step, were exposed for five minutes longer to toxic Me_2SO. However, these cells showed better recovery which can therefore be explained by decreased osmotic stress as a result of the stepwise increase of Me_2SO. Contrary to this, no significant difference in recovery was observed between the two conditions when the incubation was carried out at 0.5°C, which would strongly suggest that osmotic stress for AELC is reduced at lower

temperature. This might come as a surprise since studies on oocytes have shown more shrink response and therefore higher osmotic damage at lower temperatures (Paynter et al., 2005). However, it has been reported that the conductivity of water and CPA is cell-type and species specific (Si et al., 2006) and is likely to be different for tissue-like material. For example it has been reported that for lung fibroblasts (Rule et al., 1980) and human spermatozoa (Gilmore et al., 1995; Phelps et al., 1999) conductivity in the presence of Me_2SO was half the value of cells in saline. However, in oocytes little or no difference was observed (Benson & Critser, 1994; Paynter et al., 1999; Paynter et al., 1997).

Another theory to explain the process of osmotic stress proposes that the extent of solution influx and efflux in the cell plays a major role. The rate of flux is directly dependent on the temperature of a given solution and has been approximated by the following equation: v = Lp ART(p), where Lp is the hydraulic conductivity, A the membrane surface area, R the gas constant, T the absolute temperature and p the difference in intra and extracellular osmolality. At lower temperatures the water flux rate will therefore be reduced which could reduce cell membrane damage caused by osmotic poration. This theory has been proposed by Muldrew and McGann in 1994, and states that strong water flux and frictional forces between water and potential membrane pores might damage the cell membrane (Muldrew & McGann, 1994). Although their idea was that the formation of pores is damaging as they allow ice crystals to grow inside the cell, the mechanism is often cited for osmotic injury in general. Another theory proposes that, as a result of hyperosmotic stress an influx of non-permeating solutes occurs. This leads the cells to swell beyond their normal isotonic volume and to lyse once they are returned to isosmotic conditions (Mazur et al., 1972). An influx of non-permeating solutes might be further enhanced by pores formed by osmostic poration. At lower temperatures, but also when CPAs are increased in a step-wise procedure, osmotic pressure and consequently the influx rate will be decreased. Thus, an influx of non-permeating solutes should be reduced. Work by Guan (Guan et al., 2013) on precision-cut liver slices showed no effect when a gradient instead of a step-wise loading/unloading protocol was used. Despite the reduction of osmotic stress, the viability of slices did not improve. Liver slices in their study and hepatocyte spheroids at low temperature in my experiments were not sensitive to osmotic changes. On the

other hand the time factor for AELC had a lower impact on viability than the final CPA concentration, possibly suggesting the level of dehydration as the main factor for CPA toxicity. It was noticed that cell viability after incubation in equal concentrations of CPA for the same length of time varied between experiments that were carried out on different days. AELC were used between 9-11 days of growths after encapsulation. Variations in average cell density and bead size might be responsible for varying CPA diffusion rates and thus for CPA toxicity.

The second aim of this chapter was to investigate the practical challenges of manual LT and to establish an optimized and reliable manual protocol. The chosen CPA was Me_2SO as it has been the CPA of choice for other recent LT studies (Pegg et al., 2006; Wang et al., 2007). Three test set-ups were tested and compared. To run a LT experiment the liquidus curve of the CPA solution has to be known. In this chapter the Me_2SO liquidus curve was established by measuring the thermocouple defined approximate freezing point (TdAFP). Temperature values were equal to *differential scanning calorimetry* (DSC) measurements found in the literature for concentrations up to 20% (v/v) Me_2SO (Elford, 1970; Farrant, 1965b). However, the sample temperature did not return the true equilibrium melting point when the concentration was increased to 30% and 40% (v/v) Me_2SO. This can be explained by the chamber temperature, which will be lower than the sample temperature, and thus will cool the sample temperature below the equilibrium melting temperature. No peak of release of latent heat was detected for concentrations of 50% (v/v) Me_2SO and above. Those samples contained low concentrations of water which meant that only small amounts of heat were released - too small to be detectable as samples were simultaneously cooled by low subzero freezer temperatures.

DSC measurements use the melting curve to measure the equilibrium melting point and are more accurate. Therefore literature values were used to define the CPA transfer temperatures. Those were set 5˚C above the equilibrium melting point to avoid any freezing. The transfer temperature of solutions containing 40% (v/v) and more Me_2SO were set +10˚C above the equilibrium melting point as they became otherwise too viscous for pipetting and mixing. Using the refractive index to measure the

concentration of Me_2SO of a sample proved to be efficient and reliable. The coefficient of determination $R^2$of the standard curve, fitted by linear regression, was >0.999.

For set-up 1, AELC to be vitrified were transferred in a cell strainer from one well containing 8ml of CPA solution to the next, each with a higher CPA concentration at a lower temperature. A disadvantage of this set-up is that it is only suitable for tissue pieces, which can be transferred by using forceps or encapsulated cells of a unit size allowing them to be trapped by a suitable cell strainer in which the sample can be transferred. The first observation made was, that the cooling rate of the sample (as opposed to the chamber (-2°C/minute) became very low when the sample temperature approached the next transfer temperature, which was caused by the thermal mass provided by the plastic of the 6-well plates and the CPA volume of 8ml. This was overcome by setting the temperature of the freezer -10°C below the sample temperature to be reached which led to a measured sample cooling rate of approximately -0.75°C/minute. However, to avoid any ice formation close observation of the sample temperature during cooling had to be maintained throughout the experiment which was done by recording temperatures from the thermocouples in dummy wells. A freezer holding time of 10 minutes at -10°C below the transfer temperature allowed enough time for the sample to reach the transfer temperature and to place all six cell strainers into the next plate. Cooling and holding time approximated 30 minutes between each stepwise CPA increase. The length of the total incubation time was chosen on the basis of Pegg's work on articular cartilage (Pegg et al., 2006). Cell densities of alginate encapsulated HepG2 liver cells are lower than those for articular cartilage and therefore it was assumed that sufficient time for CPA penetration was given.

During first experiments random ice formation in some samples was visually noted, possibly caused by a carry-over effect each time the samples were transferred in cell strainers to the next higher CPA concentration. Surface adherence of lower concentrated CPA solution on the cell strainer will result in uncontrolled and successively increasing dilution of the CPA, which at worst might lead to ice formation as lower temperatures are reached. Ice formation could also have been caused from inhomogeneous heat transfer between wells as higher cooling rates were measured for those samples that

were positioned closer to the freezer ventilator. Mixing was not carried out for set-up 1 because this would have taken too long (8ml/well) with a higher risk of sample warming as this step has to be done by opening the lid of the Planer freezer. As a consequence, inhomogeneous CPA distribution could also explain why some of the wells became partially frozen. In order to avoid any ice formation during the LT procedure, the transfer temperature was set 30% above the sample melting point, instead the initial offset of 20%. Reasons given for ice formation can also be listed as potential causes for sample to sample variability. Additionally, inadvertent and variable sample warming, when cell strainers are taken out of solution and placed in the next well can cause sample variability, depending on how fast the samples are transferred. Nevertheless, one can speculate that the sample temperature increase was low, as the transfer per cell strainer took less than five seconds, and the temperature of the solution the cell strainer was placed into only increased by approximately 2°C.

For set-up 2, the CPA increase was achieved by adding a 20% more concentrated Me_2SO solution to the sample. To maintain a constant volume, half of the solution was taken off after mixing was completed. As the volume had to be reduced, this set-up was only feasible for sample material that would accumulate at the bottom of the tube by gravity (in the time given until the next CPA addition step). The sample cooling rate was similar to the cooling rate of the freezer chamber when microfuge tubes and volumes below 1.5ml were used. To allow a diffusion period of approximately 30 minutes, and, to provide a similar cooling profile as set-up 1, the freezer temperature was set on hold for 15 minutes once the average temperature between the starting and the transfer temperature was reached. Then an additional holding step was set at -5˚C below the transfer temperature, for seven minutes to reach the required temperature and to process the samples. As for set-up 1 a freezer cooling rate of -2°C/minute was chosen and the same transfer temperatures were used. The main advantage of set-up 2 was that samples were mixed during each step, which was important to provide homogenous CPA distribution. Another advantage of set-up 2 was that the sample remained within the same solution holder during the whole LT process which made it possible to record the temperature throughout the process. The main disadvantage of set-up 2 became evident: as the freezer chamber was opened to allow manual access whilst CPA concentration was changed, the temperature inside the freezer deviated rapidly,

affecting the temperature of the solutions kept inside the freezer. Extracting and adding half of the sample volume and the mixing process took time and therefore had a considerably impact on the sample temperature. During the CPA addition processes a temperature increase up to +20°C was measured by thermocouples placed inside the sample tubes.

Set-up 3 is a variant of LT set-up 2 whereby only one highly concentrated CPA solution was used to make the stepwise required CPA concentration. However, since the final steps of LT require solutions in the range of 60% CPA, an extremely concentrated CPA (80% v/v) had to be added. The sample remained within the sample container throughout the process and the solution was mixed after each step as for set-up 2. One advantage of set-up 3 is that smaller volumes need to be added at each step, avoiding the problem of accumulating supernatant volumes, therefore the sample volume does not have to be reduced each time as for set-up 2. Several other advantages can be outlined for this approach: - as only one solution has to be added the accuracy of achieving the target CPA improves: there is no loss of cell material and the process is faster which means less sample-to-sample variability due to potential temperature variation. Sample volume (0.75ml to 4.5ml) and the property of the tube (15ml centrifuge tube) provided more thermal buffering against transient temperature fluctuation than set-up 2. This and the faster process explain why the average temperature increase during each CPA addition and mixing step was lower than for set-up 2, at approximately +11°C. Using only one (two) solutions to increase the CPA concentration also simplified the process when different conditions within one run were being compared. A potential disadvantage of this approach is that highly concentrated CPA is added to the sample at relatively high temperatures which could be a problem for cells that are especially prone to osmotic stress and CPA toxicity, if the mixing is not processed quickly enough. As a compromise two different highly concentrated solutions were used; 60% for the first step and 80% for the final increase.

In order to investigate at which step viability was mostly decreased during the LT procedure, step-by-step LT experiments were carried out. All three set-ups; 1, 2 and 3 were tested. Some samples were removed at each stage just before the next addition of Me_2SO, and rewarmed for viability measurements, whilst the remaining cohort stayed

in the controlled rate freezer as the LT run progressed further. In the final step, the two remaining samples were slowly cooled down to -60°C. One sample was warmed up immediately; the other one was directly added to the vapour phase of liquid nitrogen and rewarmed after 3-7 days. A simplified reversal of the LT protocol was used to warm samples after cooling. The Me_2SO was reduced from 70% to 50% at -20°C in a first step and was limited to a 20% concentration reduction for all subsequent steps. This seemed a reasonable approach, based on the observation that osmotic injury was strongly reduced at 0.5°C, although reverse osmotic stress could be more damaging as membranes change and become more brittle when they are exposed to low temperatures.

Manual step-by-step experiments showed that viability was decreased after each LT step, and thus the results did not indicate a specific concentration at which viability was primarily reduced. Still, the data suggests that viability is mainly reduced between 30% and 60% (v/v) Me_2SO but is kept constant between 60% and 70% (v/v) Me_2SO, regardless of whether samples are cooled down to -60°C and immediately re-warmed or stored at -160°C and subsequently rewarmed. The experiments showed that cell viabilities can be ~30% after achieving the vitrified state and reversal via LT. Concentrations of 60% and 70% (v/v) Me_2SO were reached at very low temperatures (< -25°C) and it could be hypothesized that at these low temperatures, the Me_2SO influx is limited which means that full intracellular Me_2SO concentrations of 60-70% (v/v) might not have been achieved (which could explain higher consistency between these steps). In this respect, cells that survived the LT process until the final increase to 70% (v/v) Me_2SO seem to have achieved sufficient Me_2SO penetration to be vitrified. This could of course also be brought about by the high viscosities of the Me_2SO mixture acting to kinetically inhibit ice crystal formation, and the parallel extreme osmotic dehydration of the cells which also prevented organisation of any residual water molecules into ice nuclei. High variability between experiments can be partially explained by temperature profile variations and CPA concentration differences between samples resulting from the different manual approaches to achieving LT and handling variability. Divergent CPA concentrations across the LT steps could have resulted from pipetting difficulties with the highly viscous higher CPA solutions, and ‘carry over’

effects in those experiments where samples were physically moved between different Me_2SO mixtures.

Manual LT set-up 3 was performed on ice (0.5°C) to determine whether the LT protocol decreased CPA toxicity due to its stepwise addition of Me_2SO (prevention of osmotic injury) or due to the temperature decrease. Viabilities after "manual LT" at 0.5°C were similar to those seen in previous experiments, when AELC were directly incubated in increasing concentrations of Me_2SO for 40 minutes at 4˚C. Recovery was strongly reduced at 40% and 50% (v/v) Me_2SO and no viability was observed when cells were incubated in 60% and 70% (v/v) Me_2SO. Contrary, AELC exposed to 70% (v/v) Me_2SO and vitrified following manual LT at decreasing temperatures reached viabilities of approximately 30%. This suggests that stepwise CPA addition to reduce osmotic stress during LT has only a minor influence on CPA toxicity. Instead, CPA exposure at low temperatures might reduce intracellular Me_2SO concentration or/and dehydration and therefore increase cell recovery.

Manual LT set-up 3 was most practical. Nevertheless heat fluctuation during the CPA addition process was observed. The increase in sample temperature was especially strong at lower temperatures. This was mainly caused by a prolonged mixing procedure due to increasing sample viscosity and the larger volumes that had to be mixed. To provide a more reliable process each LT container (15ml centrifuge tube) was externally suspended within a 70% ethanol solution held in a 50ml centrifuge tube. By using the described 'thermal buffer- jacket - TB' for insolation, the temperature fluctuation during CPA change was reduced from a maximum of +18°C (CPA addition at -35°C) to less than + 5°C. When first developing the insolation system the following was considered: the solution used for TB should not freeze during the cooling process as this would affect the cooling rate of the LT sample itself due to altered heat capacities. Also the TB solution should remain liquid so that the LT sample tube could be taken out from the TB at the end of the run and stored in liquid nitrogen. Additionally, the TB system should be as symmetrical as possible to allow a homogenous cooling profile throughout the entire volume. The TB carrier solution should be as low toxic as possible for handling purposes, and the TB system had to be of a size that could fit within a controlled Planer Kryo -10 freezer. It was important that the sample cooling rate during

CPA addition or reduction was affected as little as possible, while the TB insolation should maintain the same temperature for several minutes in an altered environment until the CPA change has been processed. Other combinations of TB carrier solutions and tubes with better thermal buffering abilities might be used. Nevertheless this could lead to lower sample cooling rates causing longer runs and therefore longer exposure times to CPAs and cold temperatures. Using a Pasteur pipette to mix the samples after each addition step became especially complicated at low temperatures due to the increase in CPA viscosity. To overcome this problem a stirrer was designed that uses suction and pressure by up and down movement. For this a Pasteur pipette was used as the material of the Pasteur pipette is inert to most reagents. This was important to assure that as little as possible of the sample solution would stick to the stirrer after mixing to avoid any loss of material as this would change the target CPA concentration. The diameter of the top part of a Pasteur pipette is just slightly smaller than the diameter of a 15ml centrifuge tube. By cutting the top and the border a device was made that could be introduced into a 15ml centrifuge tube. The small space between tube and stirrer border and the up and down movement of the stirrer enabled mixing by pressure and suction. To maximize the mixing effectiveness several different designs were created by cutting more or less of the top and the border of the Pasteur pipette. For example, if the border remains uncut, the pressure is too high and it becomes very difficult to move the stirrer. By using the new stirrer the time needed to mix viscous solutions was reduced, an important measure to maintain the sample temperature during CPA concentration change. Also when mixing is carried out by pipetting, there is a risk that sample solution remains in the top of the Pasteur pipette. Although a small amount of sample solution sticks to the stirrer, the impact was acceptable as the CPA concentration after mixing was in a range of +/- 4% of the target concentration.

Additionally, handling variability can be compensated for by testing a higher number of samples. However, the maximum number of samples that can be processed during one LT run has to be limited to maintain similar sample warming and incubation times for all the processed samples. Thus, in the present manual LT feasibility study, it was found that a maximum of eight samples per experiment, which can all be housed in the chamber of a Kryo 10 cooler and processed within two minutes, including CPA addition and mixing, should not be exceeded.

4.6 Conclusion

In summary experiments proved the Liquidus Tracking (LT) principle that cryoprotectant agent (CPA) toxicity can be reduced by decreasing the temperature. Further experiments led to the assumption that chemical toxicity has a higher impact on cell viability than osmotic pressure.

LT by manual protocols has been shown to be a complex and lengthy procedure. Some of the complications that were observed for manual LT may not apply for an optimized automatic approach, which would minimize inhomogeneous dimethyl sulfoxide (Me_2SO) concentrations and temperature fluctuations during Me_2SO changes. Moreover the Me_2SO concentration will potentially be increased in smaller steps and therefore toxicity should be further reduced. In addition, by its nature, manual LT is complicated and can result in high variability. Nevertheless, this approach offers the possibility of testing several conditions at the same time and can therefore be used to pre-test different LT factors before being taken forward to automatic LT. Improvements made for manual set-up 3 may further increase post-warming cell recoveries.

The possibility to further reduce CPA toxicity by using combination of penetrating and non-penetrating CPAs instead of Me_2SO as a sole reagent will be explored in the next chapter.

CHAPTER 5
Cryoprotectant agent development

5.1 Introduction

Manual Liquidus Tracking (LT) experiments (Chapter 4) have shown that high concentrations of dimethyl sulfoxide (Me_2SO) are highly toxic for alginate encapsulated liver cells (AELC) even at low temperature. As it was conceivable that high Me_2SO toxicity would also occur in an optimized automatic LT process, additional possibilities of cryoprotectant agent (CPA) reduction had to be identified.

5.1.1 Cryoprotectant agent (CPA) toxicity

Several other methods are known for reducing CPA toxicity; for example by decreasing the final CPA concentration and the exposure time to toxic CPAs. However, lower concentrations of CPAs bear a higher risk of ice nucleation before reaching the glass transition range. Effective vitrification is normally achieved once the homogeneous nucleation temperature (T_h) falls below the glass transition temperature (T_g). Ice nucleation can be prevented to some extent and on a kinetic basis by either applying high hydrostatic pressure (Fahy et al., 1984) or by increasing the cooling rate. Both methods decrease the homogenous nucleation temperature, which means that nucleation is more likely to occur at a lower temperature. In order to increase the cooling rate, which consequently also decreases the exposure time to toxic CPAs, normally the sample volume has to be decreased since the minimum temperature that can be reached in a standard laboratory is that of liquid nitrogen (-196˚C). To decrease the sample volume and to increase the heat transfer, thin straws have been used (Jondet, 1965). More recently, promising results have been gained by adding small drops of sample directly to liquid nitrogen (Leunufna & Keller, 2003) or using holders such as cryo-loops (Mavrides & Morroll, 2002). However, both high hydrostatic pressure and high cooling rates are inapplicable for an open, high volume system, such as LT.

A more feasible way to reduce CPA toxicity for our purpose is by using CPAs other than Me_2SO or by using combinations of various CPAs. Combinations of CPAs have

proven to be less toxic than the use of a single CPA (Jomha et al., 2010). It has even been shown that the toxicity of formamide can be reduced by the addition of Me_2SO (Fahy, 2010) and that Me_2SO toxicity can be reduced by the addition of sugars (Clark et al., 1984).

Secondly, toxicity of the vitrification solution can be reduced by partially replacing penetrating CPAs with non-penetrating CPAs. This procedure is limited for use with mammalian cells, as some penetrating CPAs are essential in any vitrification protocol. The combination of 40-50% (w/v) penetrating and up to 10% (w/v) non-penetrating CPA has shown effective vitrification properties and decreased toxicity (Fahy et al., 1984; Kuleshova et al., 1999). Also, evidence exists that CPA toxicity can be decreased by using a different vehicle solution, for example by replacing sodium with choline (Wusteman et al., 2008).

5.1.2 Viscosity; the limiting factor for a CPA solution for Liquidus Tracking

Viscosity is the first limiting factor for the development of a new LT CPA solution because highly viscous material cannot be pipetted or mixed effectively which is important for accurate manual LT. On the other hands, Liquidus Tracker pumps are unable to operate at viscosities much higher than 934mPa*s. This is the viscosity of glycerol at room temperature and is comparable to 70% (w/v) Me_2SO at -40˚C, which is the concentration and the temperature the automatic Liquidus Tracker stops pumping and stirring (S. Butler, personal communication Planer). It was essential for the development of the stirring and pump system of the Liquidus Tracker that experiments were carried out at room temperature and therefore, due to its similar viscosity to Me_2SO at -40˚C, glycerol was used.

5.1.3 CPA concentration for Liquidus Tracking

Combinations of 40-50% (w/v) penetrating CPAs with 10-20% (w/v) non-penetrating CPAs have been largely successful for small volumes when rapid vitrification (by plunging into LN) and fast warming (RT) rates could be applied. Nevertheless, for bulky samples, a final CPA concentration of 50-60% (w/v) used in these protocols (Table 5.4) could be too low to prevent the formation of "double stable glasses" and re-crystallisation during the warming process (Angell, 1981; Boutron & Kaufmann, 1979).

Therefore, it was concluded that LT CPA development should be based on 60-70% (w/v) total CPA concentration with the option to reduce the final CPA concentration if vitrification properties remained unaffected.

5.2 Aims

The aim of Chapter 5 was to develop a CPA solution that has low toxicity for AELC but is also of relatively low viscosity at low temperatures so that it can be used in a liquidus tracking procedure. It was also important to test the vitrification properties of the new CPA solution to estimate whether the vitrified state can be reached within a reasonable concentration of approximately 65% (w/v). Finally, the liquidus curve of the new CPA solutions had to be determined.

5.3 Methods and Materials

5.3.1 CPA toxicity test

Materials

1xPBS with Mg^{2+} and Ca^{2+} *(Sigma, Cat. No. D8662)*

Me_2SO *(Sigma, Cat. No. 154938)*

D+ Trehalose *(Sigma, Cat. No. T95531)*

D+ Raffinose *(Sigma, Cat. No. 83400)*

D+ glucose *(Sigma, Cat. No. 66152)*

D- Fructose *(Sigma, Cat. No. F3510)*

Sucrose *(BDH, Cat. No. 102745C)*

Ethanol *(Fisher Chemicals, Cat. No. E/650DF/17)*

Methanol *(AnalaR Normapur, Cat. No. 2084730)*

Propylene Glycol *(Sigma, Cat. No. 134368)*

Ethylene Glycol *(Sigma, Cat. No. 293237)*

Alginate encapsulated liver cells (8-11 days after encapsulation)

Method

To evaluate the toxicity of a CPA solution a two-step protocol was used to reduce potential osmotic injury. A volume of 0.25ml settled beads (AELC), were incubated in a 30% (w/v) CPA solution first for five minutes at room temperature and then for an additional five minutes at 0.5°C (tubes in ice-water). The concentration was increased to 60% (w/v) CPA using a 70% (w/v) pre-cooled (at 0.5°C) CPA solution (Table 5.1). Beads were incubated for 20 minutes at 0.5°C. By adding 1xPBS the CPA concentration was reduced to 30% (w/v). Samples were left on ice for five minutes. Thereafter samples were washed twice with 4ml of 1xPBS. Finally AELC were incubated in complete media for 24 hours before viability was measured.

Table 5.1: CPA toxicity pipetting scheme

	total volume (ml)	**to come up with**	**70%(w/v) CPA to be added (ml)**
	1.30	30% (w/v) CPA	1
extract 1.3ml	1.00	60% (w/v) CPA	3
final volume	**4.00**		

5.3.2 Viscosity rating of new CPA solutions

Materials

as in section 5.3.1

Controlled Rate Freezer (Planer, Kryo 10, Series II)

Method

CPA solutions with a final CPA concentration of 70% (w/v) were prepared using Sigma 1xPBS (+Mg^{2+}, Ca^{2+}) as a carrier solution. Solutions were cooled to -40°C and viscosity was mechanically tested by pipetting solutions up and down using a 1ml pipette. This allowed a ranking based on applying a standardised suction and pressure (delivered by the barrel of the pipette) to raise the solution to a standard height (defined by the geometry of the pipette tip). As a reference solution 70% (w/v) Me_2SO was used, as this was the standard solution for developing the automatic Liquidus Tracker. A viscosity rating was assigned as follows: 1 = similar to the reference condition (70% (w/v) Me_2SO), easy to pipette; 2 = pipetting not possible but can be easily stirred; 3 = very viscous, pipetting and stirring very difficult; 4 = pipetting and stirring not possible, almost solid.

5.3.3 Viscosity measurement

Materials

as in section 5.3.1

Control Bohlin CVO automated shear rheometer

Method

The viscosities were determined using a Bohlin CVO automated shear rheometer. This type of rheometer measures the friction resistance caused by a liquid placed between a horizontal plate and a graduated cone spinning plate. For more viscous material more force is needed to reach the programmed rotational speed (rpm) of the spinning plate. Experiments were conducted at room temperature and the shear stress (s^{-1}) was increased by 10 rpm every 10 seconds, from 10 to 250 rpm. The viscosity of each sample was obtained by calculating the average viscosity for shear rates between 10 and 250 rpm. Two independent samples of each solution were tested.

5.3.4 Standard vitrification protocol

Materials

as in section 5.3.1

Controlled Rate Freezer (Planer, Kryo 10, Series II)

Method

To evaluate the vitrification properties of a CPA solution a two-step protocol was used in order to reduce potential osmotic injury. Therefore 0.25ml settled beads (unless otherwise stated: 8-11 days after encapsulation) were incubated in a 31.5% (w/v) CPA solution first for five minutes at room temperature and then for an additional five minutes at 0.5°C (tubes in ice-water). The CPA concentration was increased to 63% (w/v) using a 70% (w/v) pre-cooled CPA solution (at 0.5°C). Samples were left on ice for five minutes and then plunged into liquid nitrogen. Samples were warmed for approximately eight minutes until they reached a liquid state. By adding ice cold 1xPBS ($+Mg^{2+}$, Ca^{2+}) the CPA concentration was reduced to 31.5% (w/v). Samples were left on ice for five minutes before washing twice with 4ml 1xPBS ($+Mg^{2+}$, Ca^{2+}). Finally, AELC were incubated in complete media for 24 hours before measuring viability.

5.3.5 Equilibrium melting point measurements by Differential Scanning Calorimetry

Materials

as in section 5.3.1

Q2000 Calorimeter (TA Instruments)

High volume stainless steel pans

Universal Analysis software (TA Instruments)

Crimper

Method

Differential Scanning Calorimetry (DSC) is used to measure the energy flow to and from a sample during a temperature controlled program. In this way exo- or endothermic reactions, such as glass transitions, melting and nucleation events can be identified. A sample of known mass is added to a sealed capsule, the pan. Another pan, the reference pan, remains empty. Both pans are subjected to a cooling and heating cycle over the temperature range of interest whilst the temperature of both pans is

recorded. The energy required to keep both sample and control at the same temperature is plotted *on* a DSC trace against the temperature (°C) of the program, allowing thermal properties to be observed. For this study, modulated DSC (mDSC) was used, which is a technique whereby a sine wave modulation is introduced on top of a linear heating rate. By applying this, small thermal events can be identified even at relatively rapid heating rates.

Each sample pan was loaded with 80µl of CPA solution. Before the addition each pan was weighed. Pans were then crimped, reweighed, sample mass calculated and the values entered into the software. The reference pan and sample pans were loaded onto the calorimeter in an auto-sampler. Analysis was carried out at 5°C/minute with a modulation of 1°C/minute. Data was analysed using the TA Universal Analysis software. Solutions were prepared in triplicate of which each was measured in duplicate.

5.3.6 Improved manual LiquidusTracking

The CPA concentration was increased by adding small amounts of highly concentrated CPA to 15ml centrifuge tubes containing AELC as given in Table 5.2. The cooling protocol is shown in Table 5.3. For both CPA solutions, Me_2SO and No.18, the same protocol was followed and both solutions were tested within the same run. The improved manual LT system described in Chapter 4 was followed, with some modifications in order to simplify the procedure, and were as follows. The first increase to 25% (w/v) CPA was carried out on ice by adding 1ml of 50% (w/v) CPA solution to 1ml of settled beads. The volume was decreased to 1.2ml before adding sample to a precooled chamber (at -3.5˚C).

Table 5.2 Amount of 80% CPA required to increase the sample CPA concentration by increments of 10%

Initial CPA (%)	Initial Vol. (µl)	Vol. (µl) of 80% CPA to add	Target CPA (%)
25	1200	267	35
35	1467	419	45
45	1886	754	55
55	2640	1485	64
final vol.	3925		

*formula to determine the amount of 50% (80%) CPA to be added: B=(A*c-A*a)/(b-c) with B=volume of 80% CPA to add, A=start vol., c= final CPA concentration, a=start CPA concentration, b=80% CPA*

Table 5.3 Me_2SO and mixed CPA transfer temperatures

% (w/v) CPA from:	Transfer temperature	Freezer holding temperature
25 to 35	-3.5°C	-8.5°C
35 to 45	-13°C	-18°C
45 to 55	-25°C*	-30°C
55 to 64	-30°C*	-35°C

**transfer temperatures were determined empirically, as viscosities at colder temperatures have been shown to be too difficult to handle.*

5.3.7 Most commonly used CPAs for vitrification

In PubMed 41 review papers about vitrification were studied of which eight included technical information and references of further technical papers. The most commonly and successfully used penetrating CPAs mentioned in these papers were dimethyl sulfoxide (Me_2SO), glycerol, ethylene glycol (EG), propylene glycol (PG) and formamide. In most protocols the disaccharide, sucrose, was used as a non-penetrating CPA. For the vitrification of hepatocytes the combination of 40% (v/v) EG and 0.6M sucrose has been shown to be especially successful (Kuleshova et al., 2004; Magalhães et al., 2009). Vitrification protocols including CPAs, cooling and warming protocols and cell type are summarized in Table 5.4.

Table 5.4 Summary of vitrification protocols

CPA	Cell type	Cooling, Warming	Viability	Article
Me_2SO, Propylene Glycol, Glycerol (Li et al., 1990) Sucrose, Ficoll	Human blastocytes	cooling: to LN warming at 37°C	Depending on blastocyte type and protocol	(Kader et al., 2009)
40% (v/v) Ethylene Glycol, 0.6M Sucrose	Mouse NSCs	cooling: to LN	>99%	(Kuleshova et al., 2009)
2M Me_2SO, 1M Acetamide, 3M Propylene Glycol	Human ESCs	cooling: to LN warming at 37°C Container volume 200µl	12.2% normal morphology and karyotype	(Fujioka et al., 2004)
3.1M Me_2SO, 3.2M Formamide, 2.21M Propylene Glycol in EuroCollins solution	Rabbit cartilage	six sequential 15 min steps of CPA addition, then fast cooling (-43°C/min) to -100°C, then slow cooling to 3°C/min to -135°C. Warming: slow (30°C/min) to -100°C then fast 225°C/min) Container volume : 2ml	No significant difference in the performance of fresh and cryopreserved cartilage, successful transplantation, no immune reaction	(Song et al., 2004)
40% (v/v) Ethylene Glycol, 0.6 M Sucrose	Hepatocytes	Gradual increase of 15% CPA cooling: 400°C/min, warming: 650°C/min	Almost 100% retention of cell function	(Kuleshova et al., 2004)
CPA screen: best CPA combination: 20% EG, 20% Me_2SO 10% 1,3-butanediol (v/v)	Mouse blastocytes	Equilibrated for 3 min at RT in 25% CPA conc. then directly to LN. Warming in a water bath at 20°C (in straws)	96.2% developmental rate after 24 hours	(Valdez et al., 1992)
VS1: 40% EG (v/v), 0.6M Sucrose) VS2: same as VS1 + 9% (w/v) Ficoll: shown that 1,2Propanediol is not better than EG	Rat Hepatocytes	Pre-equilibration in 10%, 25% EG (each 3min) before exposure to VS1 or VS2-then to LN, warming at 38°C	N/A	(Magalhães et al., 2009)
14% Me_2SO, 14% Formamide, 17% Propylene Glycol, 10% colloid (w/v)	Rabbit kidney	Vitrification with cooling rate<10°C/min	50% of rabbit kidneys tolerate perfusion at -25°C with VS4A1	(Arnaud et al., 2003)
72% Me_2SO (w/v)	Articular cartilage (lambs)	Liquidus Tracking	Functionality 60%	(Wang et al., 2007)
20% Me_2SO, 20% EG, 0.5M Sucrose	Human embryonic stem cells	In a straw to LN warming at 37°C	All clumps revcovered	(Reubinoff et al., 2001)

5.3.8 Viscosity of commonly used Cryoprotectant agents

Viscosity data of some known penetrating CPAs and sugars at different concentrations and temperatures were compared (Table 5.5 and Table 5.6) in order to develop a CPA

solution with a comparable viscosity to 70% (w/v) Me_2SO. Table 5.5 informs about molecular structure, weight, and specific density.

Table 5.5 Specifications of penetrating CPAs

Name	Mol. Formula	Structure	Mol. Weight	Specific Density	Viscosity (mPa*s)
Methanol	CH_4O	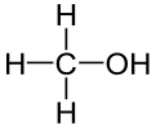	32.04	0.787	**0.54**
N,N-Dimethyl-formamide (DMF)	C3H7NO	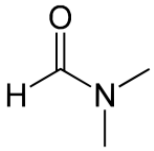	73.09	0.945	**0.79**
Water	H2O	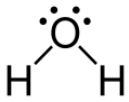	18.02	0.999	**0.89**
Ethanol	C2H6O	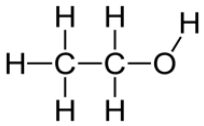	46.07	0.787	**1.07**
Dimethyl sulfoxide (Me_2SO)	C2H6OS	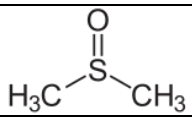	78.13	1.095	**1.99**
Formamide	CH3NO	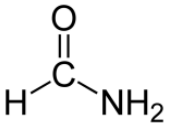	45.04	1.129	**3.34**
Ethylene glycol	C2H6O2	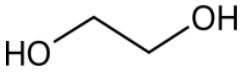	62.07	1.111	**16.1**
1,2-Propanediol (propylene glycol)	C3H8O2	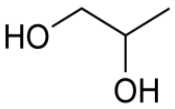	76.1	1.033	**40.4**
1,3-Butanediol	C4H10O2	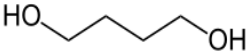	90.12	1.002	**98.3**
Glycerol	C3H8O3	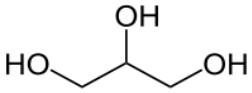	92.09	1.257	**934**

Data from Thermophysical Properties of Chemicals and Hydrocarbons, Carl L. Yaw, William Andrew, Norwich, NY, 2008

Table 5.6 Viscosity of sugars at different concentrations and temperatures

Sugar/water (w/w)	Viscosity (mPa*s)
10% Fructose at 20°C	1.43
10% Fructose at 0°C	2.89
20% Fructose at 20°C	2.09
30% Fructose at 20°C	3.07
10% Glucose at 20°C	1.58
10% Glucose at 0°C	2.78
20% Glucose at 20°C	2.13
30% Glucose at 20°C	3.46
10% Sucrose at 20°C	1.48
10% Sucrose at 0°C	2.98
20% Sucrose at 20°C	2.38
30% Sucrose at 20°C	3.46
30% Propylene glycol at 20°C	2.7*

*Data from Migliori et al.2007, *Curme and Johnston 1952*

5.3.9 CPAs for Liquidus Tracking

Formamide is highly corrosive and can be deadly if ingested. Dimethyl formamide is a possible carcinogen, and has been associated with birth defects. Both reagents are categorized as toxic by the European Dangerous Substances Directive and therefore were regarded as too hazardous for the cryopreservation of a biomass to be used in a bioartificial liver device that will be connected to a patient. The CPAs 1,3-Butandiol and glycerol are already highly viscous at room temperature and would become too viscous at low subzero temperature to be used in a LT procedure. Propylene glycol (1,2-Butandiol) was chosen, despite its high viscosity, due to its very good vitrification and stabilization properties (Boutron & Kaufmann, 1979). High molecular weight non-penetrating CPAs like dextran, polyethylene glycol and ficoll were rejected due to their high viscosities and were also deemed unnecessary since sugars have been shown to be successful non-penetrating cryoprotectants. Sugars are well tolerated even at high concentrations and can be used to partially replace penetrating CPAs without substantially modifying the vitrification properties of the solution (Kuleshova et al., 1999). Methanol and ethanol were tested because of their low viscosity despite the fact that only few papers refer to them as useful CPAs.

5.4 Results

5.4.1 Methanol vs. ethanol as penetrating low viscosity CPAs

High concentrations of dimethyl sulfoxide, ethylene glycol, propylene glycol and sugars at low sub-zero temperatures can become too viscous to be used for LT. Methanol and ethanol are both of much lower viscosity and could therefore offer a means to reduce the viscosity by partially replacing high viscous CPAs. Significantly higher viability was obtained when methanol was used instead of ethanol in a mixture of Me_2SO/glucose/ethanol or methanol in a ratio of 5/1/1, regardless of whether the final concentration was 60% or 70% (w/v). Hence, methanol was used to reduce viscosity of potential CPA mixtures in further experiments (Figure 5.1).

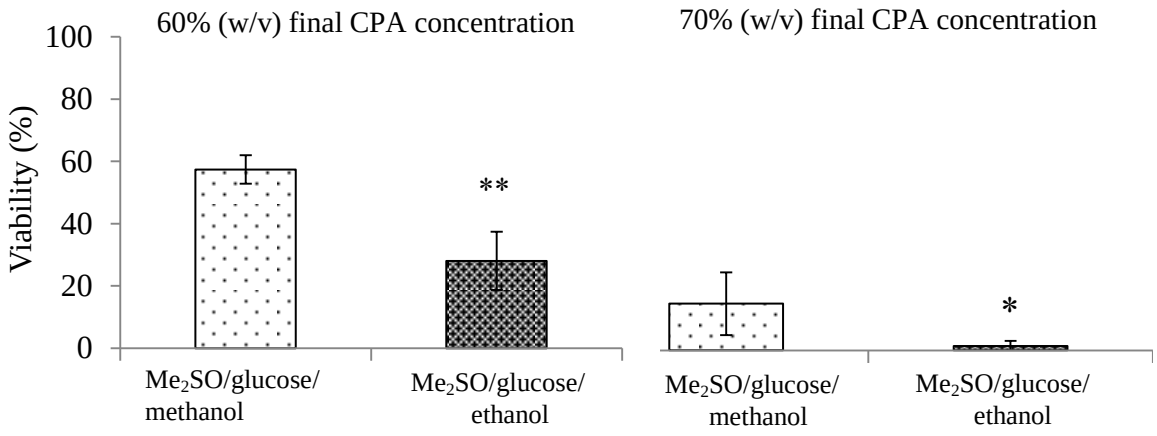

Figure 5.1 Toxicity test methanol vs. ethanol

AELC were incubated for 20 minutes at 0.5°C in 60% (w/v) and 70% (w/v) final CPA concentration using a step-wise CPA addition and reduction process (5.3). AELC were cultured for 24 hours in complete media at 37˚C before measuring viability by FDA/PI staining. The combination of Me_2SO/glucose/ethanol (ratio 5/1/1) showed significantly higher toxicity than the same combination with methanol. Data are n=5 +/- SD. **p<0.01, *<0.05.

5.4.2 Testing different sugars and sugar combinations

The addition of 10% (w/v) sugar (glucose, fructose, raffinose, sucrose, trehalose) to 50% (w/v) Me_2SO had a strong impact on cell viability when AELC were incubated for 20 minutes on ice in different CPA mixtures. The viability of AELC incubated in 50% (w/v) Me_2SO without sugar decreased from 90% +/- 2.15 (n=3), untreated AELC to

4.9% +/-3.56 (n=3). The addition of 10% (w/v) of any sugar to 50% (w/v) Me_2SO increased cell viability markedly by up to 50% although the final CPA concentration was increased to 60% (w/v). Results suggest that the combination of two sugars (average viability of 60% +/-4.36 (n=10)) was more beneficial than the use of a single sugar (average viability of 51% +/-3.15 (n=5)). Otherwise, viability within the two groups was comparable. The highest average viability for the group of individual sugars was reached with glucose, yielding 58% +/- 6.1 (n=3). In the group of two sugars the highest viability value was reached with the combination of sucrose and fructose reaching 66% +/-9 (n=3). However, in both cases the difference within the group was not significant (Figure 5.2).

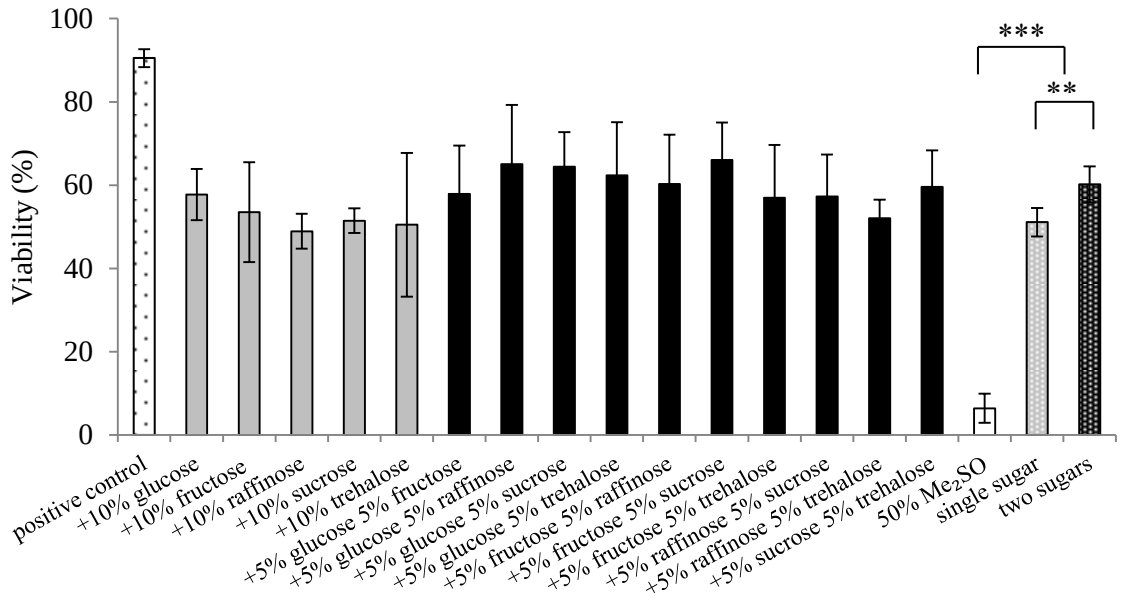

Figure 5.2 Sugars and sugar combination as non-penetrating CPA

AELC were incubated in 50% (w/v) Me_2SO (white) or 50% (w/v) Me_2SO plus 10% (w/v) sugar, either of one single sugar (grey) or two different sugars (black). AELC were incubated for 20 minutes at 0.5˚C, using a step-wise CPA addition and reduction procedure (5.3). AELC were cultured for 24 hours in complete media at 37˚C before measuring viability by FDA/PI staining. Data were n=3 +/- SD. Viability obtained with 50% (w/v) Me_2SO (n=3 +/- SD) was significantly lower than with solutions containing one sugar (grey dotted, average of single sugar solutions, n=5 +/-SD) or two sugars (black dotted, average of two sugar solutions n=10 +/-SD). One sugar (grey dotted) resulted in significantly lower viability than solutions with two sugars (black dotted) ***p<0.001, **p<0.01.

5.4.3 Viscosity rating of candidate CPA combinations

The viscosities of 21 combinations of penetrating CPAs (Me_2SO, EG, PG) with the non-penetrating CPA glucose were compared to the reference solution of 70% (w/v) Me_2SO (Table 5.7). Viscosity comparison was carried out by using a simple mechanical procedure described in section 5.3.2. It was predicted that at least 40% (w/v) penetrating CPAs and a maximum total concentration of 70% (w/v) CPA should be used to obtain sufficient vitrification for large volumes and slow cooling rates (>10˚C/min) as explained in section 5.1.3. Glucose was chosen as the non-penetrating CPA as it gave the highest viability within the group of individual sugars. Only the condition with 60% (w/v) Me_2SO and 10% (w/v) glucose showed a similar viscosity to 70% (w/v) Me_2SO and was rated with "1" (easy to pipette at -40˚C). Combinations with high amounts of glucose and PG were more viscous than those which contained mainly EG and Me_2SO. Out of the 20 solutions tested, eight were rated with "2" (difficult to pipette at -40˚C), 11 were rated with "3" (difficult to stir at -40˚C), and one was rated with "4" (not possible to stir). The last contained the highest amount of PG which is of much higher viscosity than Me_2SO and EG (Table 5.5) and comparable to the viscosity of glucose (Table 5.6).

Table 5.7 Viscosity rating part 1: The viscosity of 21 combinations of penetrating and non-penetrating CPAs tested at -40°C

Penetrating CPA (single)	Non-penetrating CPA	Viscosity rating
40% CPA	**30% Glucose**	
40% Me_2SO	30% Glucose	2
40% EG	30% Glucose	3
40% PG	30% Glucose	3
50% CPA	**20% Glucose**	
50% Me_2SO	20% Glucose	2
50% EG	20% Glucose	2
50% PG	20% Glucose	3
60% CPA	**10% Glucose**	
60% Me_2SO	10% Glucose	1*
60% EG	10% Glucose	2
60% PG	10% Glucose	4
70% CPA	**0% Glucose**	
70% Me_2SO	0% Glucose	1*
Penetrating CPA (combination)	**Non-penetrating CPA**	**Viscosity rating**
40% CPA	**30% Glucose**	
20% Me_2SO, 20% EG	30% Glucose	3
20% Me_2SO, 20% PG	30% Glucose	3
20% EG, 20% PG	30% Glucose	3
13.3% Me_2SO, 13.3% EG, 13.3% PG	30% Glucose	3
50% CPA	**20% Glucose**	
25% Me_2SO, 25% EG	20% Glucose	2
25% Me_2SO, 25% PG	20% Glucose	3
25% EG, 25% PG	20% Glucose	3
16.7% Me_2SO, 16.7% EG, 16.7% PG	20% Glucose	3
60% CPA	**10% Glucose**	
30% Me_2SO, 30% EG	10% Glucose	2
30% Me_2SO, 30% PG	10% Glucose	3
30% EG, 30% PG	10% Glucose	2
20% Me_2SO, 20% EG, 20% PG	10% Glucose	2

Solutions were compared to the reference solution (70% (w/v) Me_2SO). Viscosity was assessed by trying to pipette or stir the solution at -40˚C.Viscosity was rated 1-4 (1=similar to 70% (w/v) Me_2SO, easy to pipette; 2= pipetting not possible but can be easily stirred, 3 = very viscous, stirring very difficult, 4 = stirring not possible, almost a solid). Highlighted data indicates a group of CPA combinations with the same concentration (w/v) of penetrating and non-penetrating CPAs. Optimal mixes*

5.4.4 CPA mixtures of low viscosity

The eight solutions with a viscosity rating of "2" identified in the previous experiment (5.4.3) were modified by replacing highly viscous CPAs with less viscous CPAs. In most cases 10% (w/v) glucose or PG was replaced with either EG, Me_2SO or methanol. EG was replaced with Me_2SO or methanol, and Me_2SO replaced with methanol. Thus, in a range of 10% (w/v) all possible combinations were tested and the viscosity of all but two solutions (No.3, No.17) was sufficiently reduced for LT, resulting in a viscosity rating of "1" or "1-2" (Table 5.8).

Table 5.8 Viscosity rating part 2: solutions of reduced viscosity

Solution No.	Me_2SO, EG, PG	Methanol	Glucose	Viscosity rating
	0% Me_2SO			
1	25% EG, 25% PG	10% Methanol	10% Glucose	1-2
2	30% EG, 30% PG	10% Methanol	-	1-2
3	50% EG	10% Methanol	10% Glucose	2
4	60% EG	10% Methanol	-	1
	20% Me_2SO			
5	20% Me_2SO, 20% EG, 10% PG	10% Methanol	10% Glucose	1-2
6	20% Me_2SO, 30% EG	10% Methanol	10% Glucose	1-2
	30% Me_2SO			
7	30% Me_2SO, 20% EG	10% Methanol	10% Glucose	1
8	30% Me_2SO, 20% PG	10% Methanol	10% Glucose	1
9	30% Me_2SO, 10% EG, 10%PG	10% Methanol	10% Glucose	1-2
	40% Me_2SO			
10	40% Me_2SO	10% Methanol	20% Glucose	1
11	40% Me_2SO, 10% EG	10% Methanol	10% Glucose	1
12	40% Me_2SO, 10% PG	10% Methanol	10% Glucose	1-2
13	40% Me_2SO, 20% EG	10% Methanol	-	1
14	40% Me_2SO, 20% PG	10% Methanol	-	1
15	40% Me_2SO, 10% EG, 10%PG	10% Methanol	-	1
16	40% Me_2SO, 10% EG, 10%PG	5% Methanol	5% Glucose	1-2
17	40% Me_2SO, 20%EG, 10%PG	-	-	2
18	40% Me_2SO, 20%EG	-	10% Glucose	1-2
	50% Me_2SO			
19	50% Me_2SO	10% Methanol	10% Glucose	1
20	50% Me_2SO 10% EG	10% Methanol	-	1
21	50% Me_2SO 10% PG	10% Methanol	-	1
22	50% Me_2SO, 10% EG	-	10% Glucose	1-2
23	50% Me_2SO, 10% PG	-	10% Glucose	1-2
24	50% Me_2SO, 20% EG	-	-	1
25	50% Me_2SO, 20% PG	-	-	1-2
26	50% Me_2SO, 10% EG, 10%PG	-	-	1-2
	60% Me_2SO			
27	60% Me_2SO	-	10% Glucose	1
28	60% Me_2SO	5% Methanol	5% Glucose	1
29	60% Me_2SO 5%PG	-	5% Glucose	1-2
30	60% Me_2SO 5%EG	-	5% Glucose	1-2

Viscosity of solutions rated with 2 from Table 5.7was reduced by partially replacing highly viscous CPAs (e.g. PG) with less viscous CPAs (e.g. methanol). Solutions were compared to the reference solution (70% (w/v) Me_2SO) at -70°C. Viscosity was rated 1-3 ((1=similar to 70% (w/v) Me_2SO, 2= pipetting not possible but can be easily stirred, 3 = very viscous). In **bold**: indicates a group of CPA combinations with the same concentration of Me_2SO.

5.4.5 Toxicity test of low viscous CPA solutions

The toxicity of CPA solutions with a viscosity rating of "1" and "1-2" was assessed by comparing AELC recovery after incubation in 60% (w/v) CPA. A 70% (w/v) starting

solution (Table 5.8) was used to make up the final concentration of 60% (w/v) CPA. Starting solutions were used in the following assessments for comparisons in order to be in line with the concentrations used for the viscosity studies (Table 5.8). A Me_2SO/sugar ratio of 6:1 as for solution No.27 had previously proven to be substantially lower in toxicity than Me_2SO alone (Figure 5.2). Hence, the aim was to find a solution of even lower toxicity. Solutions listed in Table 5.8 were too numerous to be tested in duplicate within one experiment. For this reason solutions were separated in two groups; those containing more and those containing less penetrating CPAs than solution No.27.

5.4.5.1 Solutions with higher predicted toxicity than reference solution No.27

As expected, most solutions with higher concentrations of penetrating CPAs than solution No.27 showed higher toxicity to AELC. Exceptions to this were solutions with 65% (w/v) penetrating CPAs and only 5% (w/v) glucose (No.16, No.29, No.30). After being incubated in these solutions, AELC exhibited similar (No.29, No.30) or better recovery (No16) than solution No.27, suggesting that 5% (w/v) glucose is sufficient to markedly improve viability. Incubating AELC in solutions without glucose led to a decrease in viability from 99.8% to 22.3% or less. In contrast, the lowest viability attained for a solution containing glucose was 59.9% (No.30). The highest viability was obtained with solution No.16, which contained only 5% glucose but less Me_2SO than the reference solution. AELC incubated in solution No.13, No.20 and No.24 showed higher viabilities (17.2%, 4.26% and 22.3%) than AELC incubated in solution No.14, No.21 and No.25 (2.3%, 0.7% and 8.8%). For the latter, EG had completely or partially been replaced with PG (Table 5.9).

Table 5.9 Solutions predicted to have higher toxicity effects than reference solution No.27

Solution No.	Me_2SO, EG, PG	Methanol	Glucose	% Viability (n=2)
+ control	untreated	untreated	untreated	99.8
2	30% EG, 30% PG	10% Methanol	-	2.1
13	40% Me_2SO, 20% EG	10% Methanol	-	17.2
14	40% Me_2SO, 20% PG	10% Methanol	-	2.3
15	40% Me_2SO, 10% EG, 10%PG	10% Methanol	-	7.5
16	**40% Me_2SO, 10% EG, 10%PG**	**5% Methanol**	**5% Glucose**	**83.7**
20	50% Me_2SO 10% EG	10% Methanol	-	4.3
21	50% Me_2SO 10% PG	10% Methanol	-	0.7
24	50% Me_2SO, 20% EG	-	-	22.23
25	50% Me_2SO, 20% PG	-	-	8.8
26	50% Me_2SO, 10% EG, 10%PG	-	-	10.4
27	**60% Me_2SO**	-	**10% Glucose**	**63.0**
29	**60% Me_2SO 5%PG**	-	**5% Glucose**	**61.1**
30	**60% Me_2SO 5%EG**	-	**5% Glucose**	**59.8**

Toxicity of CPA solutions with a viscosity rating of 1 and 1-2 which were predicted to be more toxic than solution No 27. A 70% (w/v) CPA starting solution was used to increase the sample CPA concentration to 30% and then to 60% (w/v). AELC were incubated for 20 minutes at 0.5°C before the concentration was reduced in a two-step procedure (5.3). AELC were cultured for 24 hours in complete media at 37˚C before measuring viability by FDA/PI staining. In **bold:** solutions of low toxicity (addition of glucose).

5.4.5.2 Solutions with lower predicted toxicity than reference solution No.27

In this group of solutions (Table 5.10) all but one (No.10 with 20% w/v glucose) contained the same amount of glucose (10% w/v). Seven of the 12 solutions were equally or less toxic than the reference solution and five were substantially more toxic. Of these five all contained the same amount of methanol (10% w/v) and high concentrations of Me_2SO (>= 40% w/v) or Me_2SO and PG (>=50% w/v). Methanol was only well tolerated when the Me_2SO concentration was equal or less than 30% (w/v) and with at least 10% (w/v) EG. An exception was solution No.10 that contained 10% (w/v) more glucose than all other solution and for which 40% Me_2SO was well tolerated by AELC exhibiting a viability of 86.0%. Solutions without methanol all maintained high viabilities. As in the previous experiment, solutions containing PG (No.8, No.12 and No.23) were more toxic to cells than solutions where PG had been replaced with ethylene glycol (No.7, No.11 and No.22). Recoveries given in per cent viability for AELC incubated in PG-containing CPA solutions were: 53.8%, 48.6% and 78.7%. For the same CPA solution but with EG recoveries were 90.3%, 66.3% and 92.8%. EG also

seemed to exhibit lower toxicity to AELC than Me_2SO, as solution No19 (viability: 42.1%) showed less viability than solution No11 (viability: 66.3%), which in turn showed lower viability than solution No7 (viability: 90.3%). In each case 10% (w/v) Me_2SO was replaced with 10% (w/v) EG (Table 5.10).

Table 5.10 Solutions with lower or similar toxicity than reference solution No.27

Solution No.	Me_2SO, EG, PG	Methanol	Glucose	% Viability (n=2)
1	25% EG, 25% PG	10% Methanol	10% Glucose	57.7
5	**20% Me_2SO, 20% EG, 10% PG**	**10% Methanol**	**10% Glucose**	**97.9**
7	**30% Me_2SO, 20% EG**	**10% Methanol**	**10% Glucose**	**90.3**
8	30% Me_2SO, 20% PG	10% Methanol	10% Glucose	53.8
9	**30% Me_2SO, 10% EG, 10%PG**	**10% Methanol**	**10% Glucose**	**89.7**
10	**40% Me_2SO**	**10% Methanol**	**20% Glucose**	**86.1**
11	40% Me_2SO, 10% EG	10% Methanol	10% Glucose	66.3
12	40% Me_2SO, 10% PG	10% Methanol	10% Glucose	48.6
18	**40% Me_2SO, 20% EG**	**-**	**10% Glucose**	**97.2**
19	50% Me_2SO	10% Methanol	10% Glucose	42.5
22	**50% Me_2SO, 10% EG**	**-**	**10% Glucose**	**92.8**
23	50% Me_2SO, 10% PG	-	10% Glucose	78.7
27	**60% Me_2SO**	**-**	**10% Glucose**	**80.5**

Toxicity of CPA solutions with a viscosity rating of 1 and 1-2. showed lower or similar levels of toxicity than the reference solution No.27. EG was the least toxic penetrating CPA in this set-up. By adding EG the Me_2SO concentration was reduced to 20-30%. Methanol was only well tolerated in combination with EG and Me_2SO. AELC were cultured for 24 hours in complete media at 37˚C before measuring viability by FDA/PI staining. **Bold** type denotes solutions with low toxicity.

5.4.6 Optimal CPA solutions

Solutions of lower toxicity than reference solution No.27 were tested again using the same protocol as before to define the solution of lowest toxicity. A new solution (No.6: 20% Me_2SO + 30% EG + 10% methanol +10% glucose (w/v)) with a viscosity rating of "1-2" was included. A total of nine solutions were tested with the same batch of AELC on day 8, 9 (cell density: 10^6cell/ml beads), and 13 (cell density 14^6cell/ml beads) after encapsulation. Values gained from day 8 and 9 were comparable and therefore an average was calculated (n=3). Recovery was higher and differences between solutions were less pronounced at day 13 after encapsulation than on the days before and therefore data was evaluated separately (n=2). Solution No.18 and No.6 showed markedly better performance than the reference solution No.27 with viabilities of up to

80%. AELC recovery was also higher for solution No.22, No.5 and No.7, although to a lesser extent (Figure 5.3, Figure 5.4).

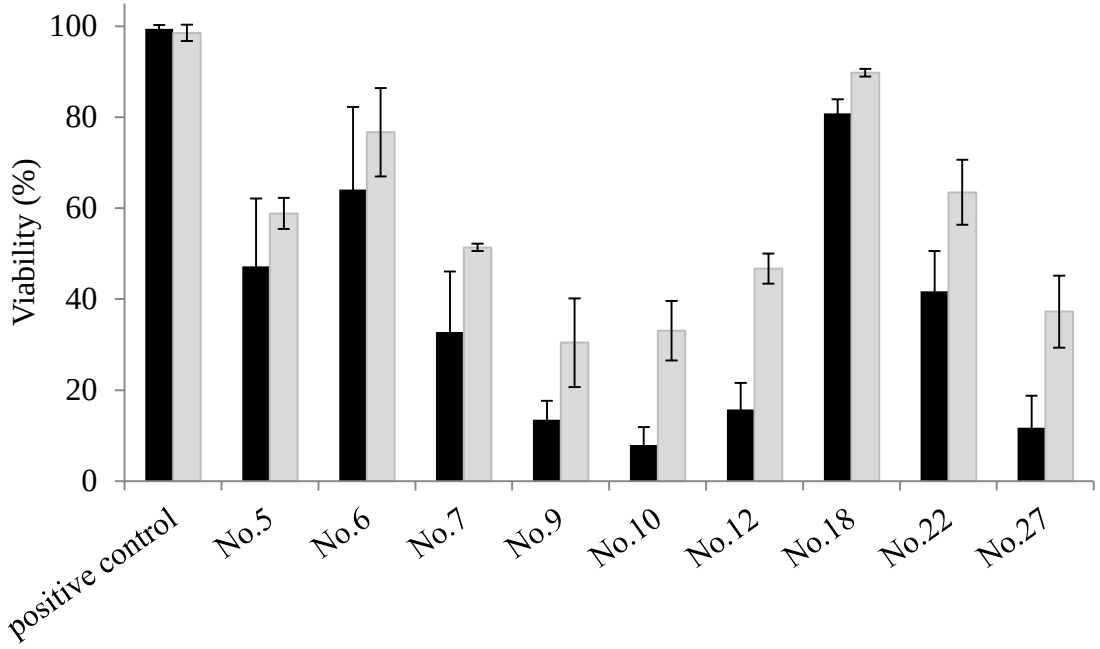

Figure 5.3 Toxicity comparison of low toxic CPA solutions

All solutions with lower toxicity than solution No 27 were tested, with the same batch of AELC on day 8-9 (black, n=3 +/- SD) and 13 (grey n=2 +/- SD) after encapsulation. Cell density was lower on day 8 and 9 (cell density: 10^6cell/ml beads) than on day 13 (cell density: 14^6cell/ml beads).AELC were incubated in 60% (w/v) CPA solution for 20 minutes at 0.5˚C; a step-wise CPA addition and reduction procedure was used (5.3). Solutions No.6 and No.18 were the least toxic, with viability levels of up to 90%, followed by solutions No22, No5 and No7. AELC were cultured for 24 hours in complete media at 37˚C before measuring viability by FDA/PI staining.

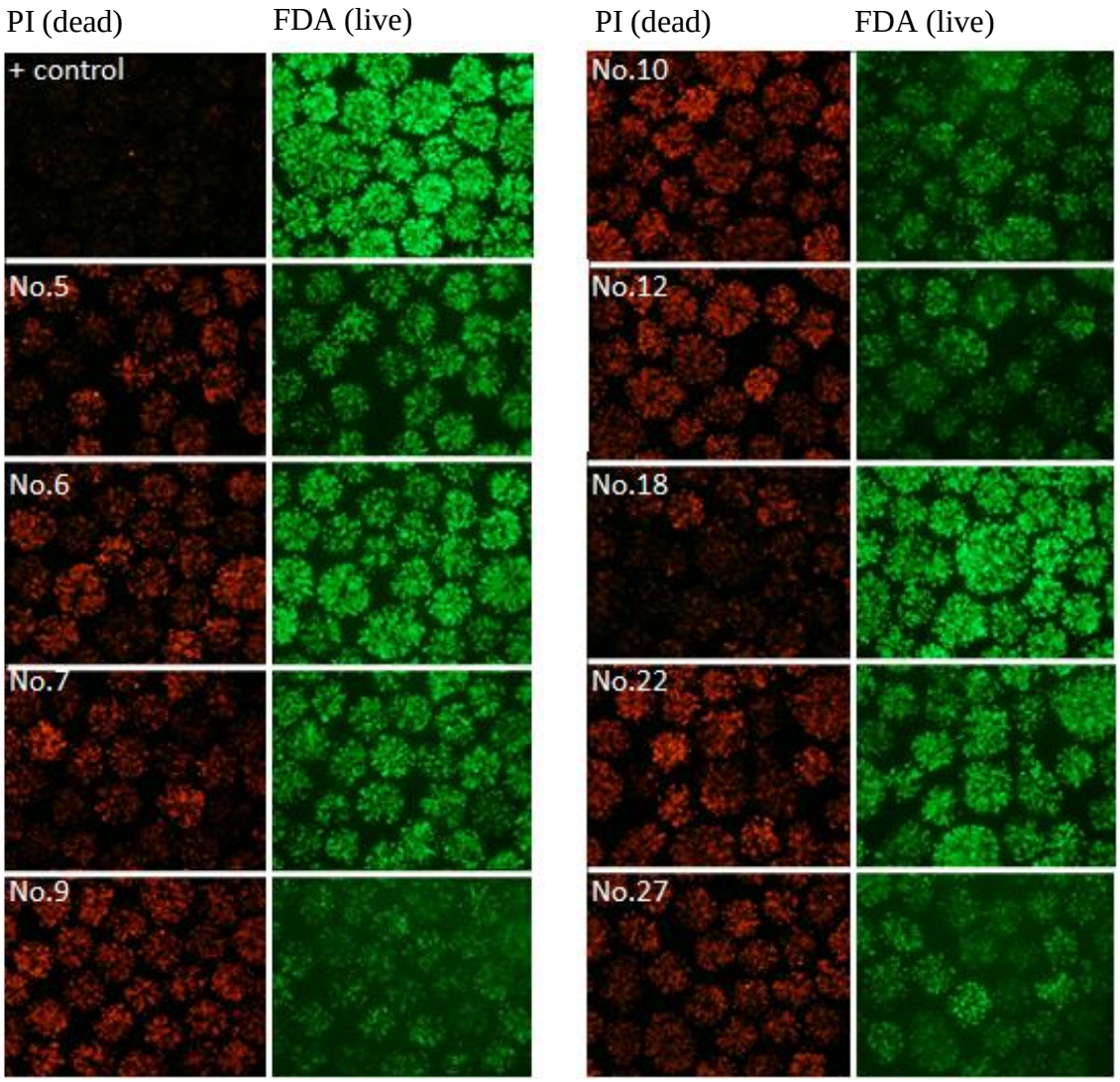

Figure 5.4 Fluorescent microscope images of CPA solutions exhibiting lowest toxicity to AELC

Viability was assessed using FDA (green/live) and PI (red/dead) stains. Images are representative of four further repeats. Original magnification 40x. Solution No.6 and No.18 show highest viability.

5.4.7 Viscosity of optimal CPA solutions

The viscosity of the CPA solutions (concentration 70% (w/v) tested in 5.4.9 was measured using a Bohlin® CVO automated shear rheometer. The viscosity of reference solution (70% (w/v) Me_2SO) was the lowest among the CPA solutions. Nevertheless, differences between sample conditions were less than 3mPa*s (Table 5.5).

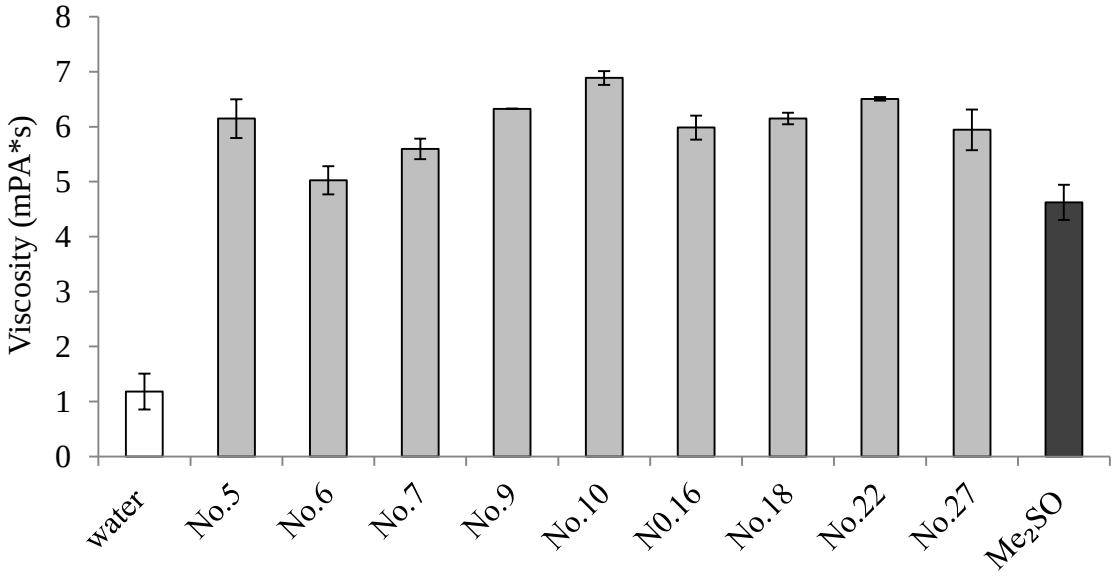

Figure 5.5 Viscosity of the nine best CPA solutions

Viscosity of water (standard), CPA solutions and Me_2SO was measured at 20˚C using a Bohlin CVO automated shear rheometer. Data was n=2. The viscosity of low toxic CPA solutions at a concentration of 70% (w/v) was comparable to the viscosity of Me_2SO.

5.4.8 Toxicity of dimethyl sulfoxide and ethylene glycol

One possibility to permit the use of more viscous CPAs is by running the LT experiment at a higher temperature. However, this will compromise the effect of low temperatures to decrease CPA toxicity and is only useful if the new CPA solution is of significantly lower toxicity. Ethylene glycol seemed to be less toxic than all other tested penetrating CPAs (Table 5.9 and Table 5.10). For this reason EG as a sole agent and in combination with Me_2SO and glucose with a final concentration of 40% (w/v) and 60% (w/v) was tested. As seen in Figure 5.6, recovery of AELC when both EG and Me_2SO were used as a sole agent, was very low, with viabilities of less than 3%. AELC incubation in EG with glucose in a ratio of 6/1 resulted in significantly higher viabilities

than Me_2SO and glucose with a ratio of 6/1. Both solutions were more toxic to AELC than the combination of Me_2SO/EG with glucose in a ratio of 4/2/1 as used for CPA solution No.18.

A.

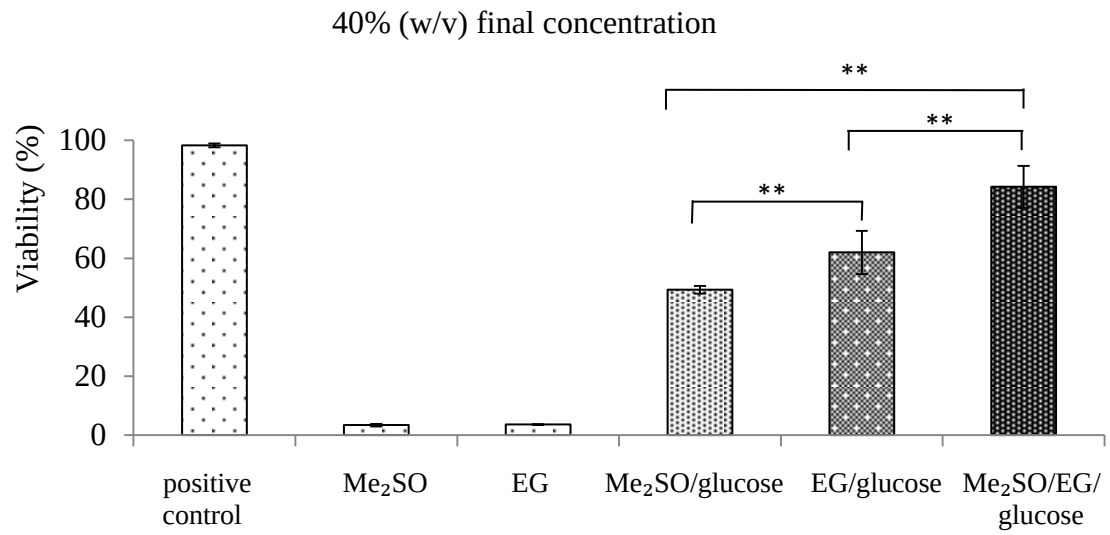

B.

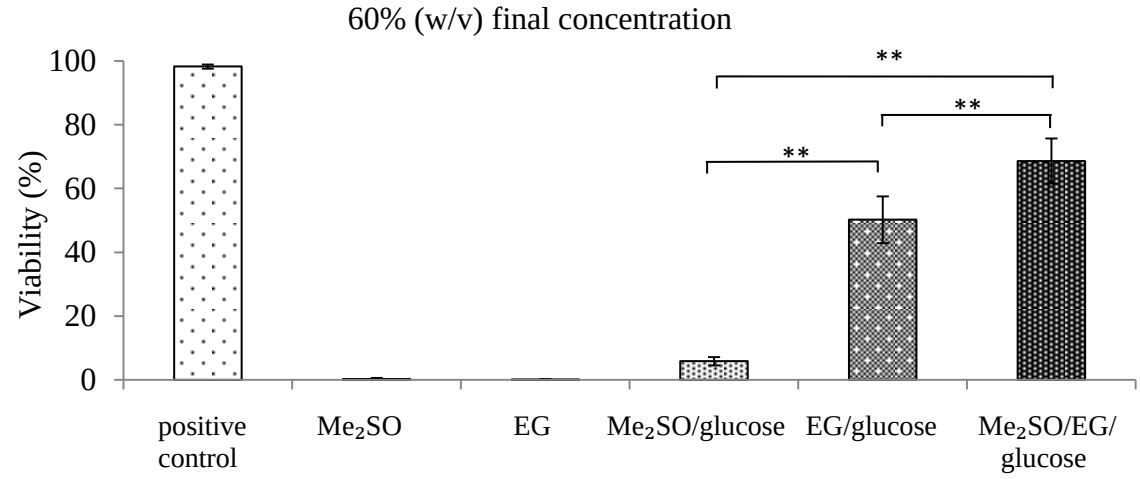

Figure 5.6 CPA toxicity Me_2SO versus EG

AELC were incubated at 0.5^{0}C in A: 40% and B: 60% (w/v) CPA solution for 1 hour, and 20 minutes, respectively. A step-wise addition and reduction procedure was used. AELC were cultured for 24 hours in complete media at 37˚C before measuring viability by FDA/PI staining. In both experiments AELC recovery for Me_2SO/EG/glucose vs. Me_2SO/glucose or EG/glucose was significantly higher, ** p<0.01, (n=5 +/-SD). Toxicity of EG plus glucose was significantly higher than Me_2SO and glucose, ** p<0.01, (n=5 +/-SD).

5.4.9 Vitrification properties of low toxic CPA solutions

Solutions No.5, No.6, No.7, No.18 and No.22 were chosen for further studies as they were the least toxic to AELC (5.4.6). AELC were vitrified in the new CPA mixtures in order to estimate their vitrification properties. As observed in the toxicity studies, solution No.18 exhibited the best results with an average viability of 53% +/-9, followed by solution No.6 (43% +/-8), No.22 (31% +/-12), No.5 (23% +/-5) and No.7 (16% +/-5). Lowest viability was reached with Me_2SO (1% +/-3) (Figure 5.7).

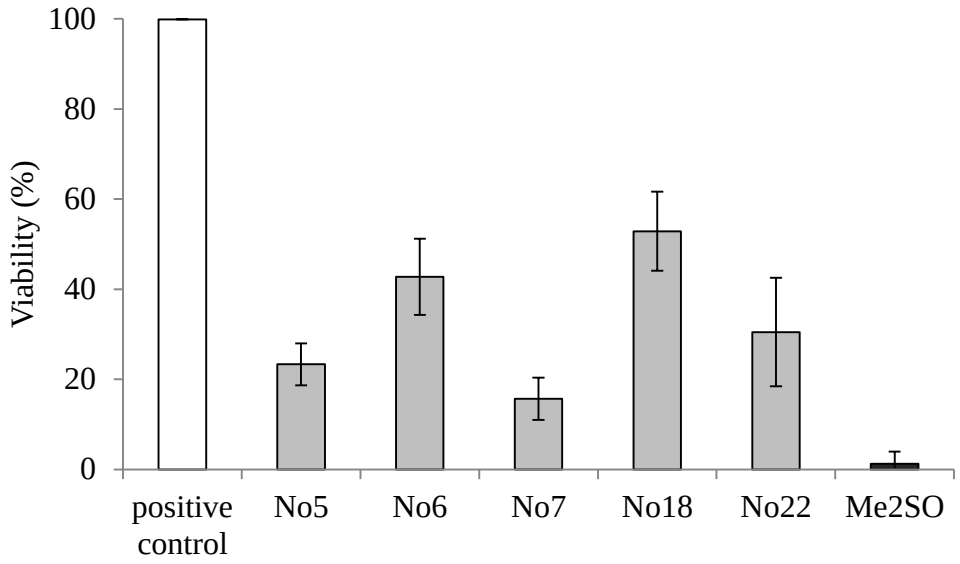

Figure 5.7 CPA solutions of low toxicity used to vitrify AELC

AELC were vitrified in CPA solutions of lowest toxicity (5.4.8). A step-wise CPA addition and reduction procedure was used (5.3.4). The final CPA concentration was 63% (w/v). AELC were cultured for 24 hours in complete media at 37˚C before measuring viability by FDA/PI staining. Solution No.6 and No.18 showed best performance, followed by solution No.22, No.5 and No.7 (n=5 +/-SD).

5.4.10 Vitrification and devitrification properties of low toxic CPA solutions

The vitrification properties of solutions No.5, No.6, No.7, No.18 and No.20 were visually compared to Me_2SO by cooling 4ml of each solution in a 6-well plate at -10°C/min to -160°C. All solutions vitrified at a concentration of 70% (w/v), but only solution No.22 and Me_2SO vitrified at 60% (w/v). Unlike Me_2SO and solution No.22, all other solutions contained 20% (w/v) or more EG. During the warming process, the rate of ice disappearance for the 60% (w/v) solutions was, in descending order: No.5,

No.7, No.6 and No.18. Solution No.18 was the only one of the four that did not contain 10% (w/v) methanol (Figure 5.8).

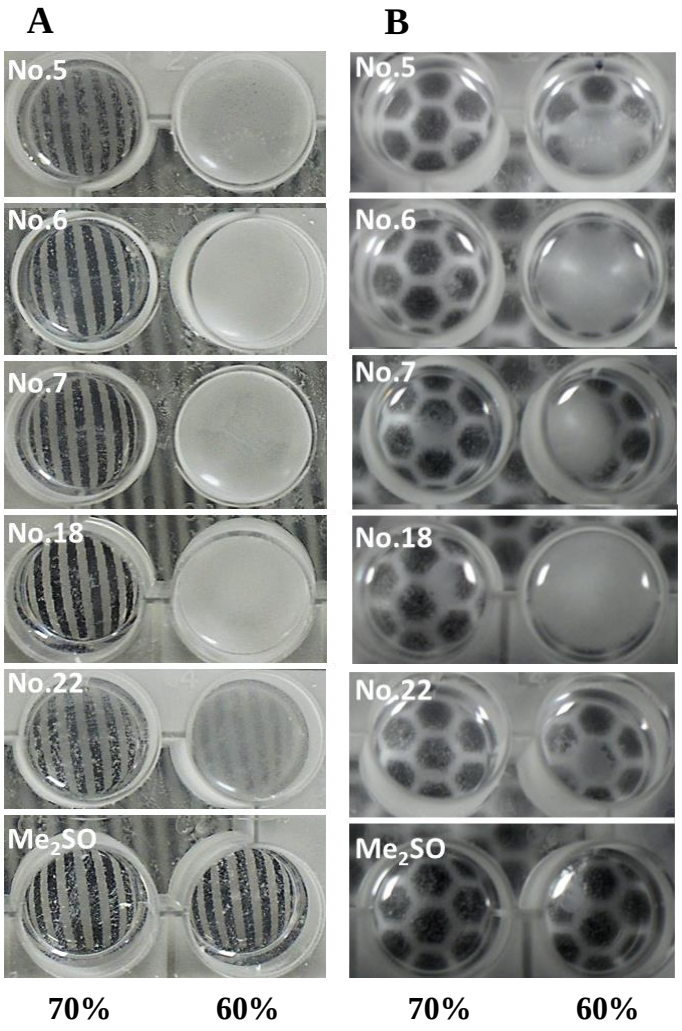

No5	20% Me_2SO, 20% EG, 10% PG, 10% methanol, 10% glucose
No6	20% Me_2SO, 30% EG 10% methanol 10% glucose
No7	30% Me_2SO, 20% EG, 10% methanol, 10% glucose
No18	40% Me_2SO, 20% EG, 10% glucose
No22	50% Me_2SO, 10% EG, 10% glucose

CPA composition of solutions used in Figure 5.8.

Figure 5.8 Vitrification properties of low toxic CPA solutions

A volume of 4ml of each solution was vitrified in a 12-well plate. A: solutions after being cooled at -10˚C/min to -160˚C. All solutions vitrified when at a concentration of 70% (w/v), but only solution No.22 and Me_2SO vitrified at 60% (w/v). B: solutions after 10 minutes at room temperature, showing a different velocity at which any nucleated ice melted during warming. Ice of solution No.7 and No.5 melted faster than ice of No.6 and No.18. Images are representative of four further repeats.

5.4.11 Liquidus curve of optimized CPA solution No.18

The liquidus curve of solution No.18 had to be established in order to use the new solution for LT. The fastest method to establish the working definition for the liquidus

curve of a new solution was by measuring the release of latent heat (4.3.6) to determine the thermocouple defined approximate freezing point (TdAFP) of increasing CPA concentrations. The melting point of 12.5% (w/v) and 37.5% (w/v) CPA No.18 was compared to data gained from differential diffraction scanning calorimetry (DSC). DSC was used as an alternative and more accurate method for determining the equilibrium melting point (Figure 5.9). This method could not be used at all times as the equipment required was not available in-house. Data was therefore compared to the TdAFP to estimate the accuracy of this method. The temperature difference between the two methods was 0.19˚C for 12.5% (w/v) and 0.93˚C for 37.5% (w/v) (n=3) (Figure 5.10). No peaks as a result of release of latent heat or during the endothermic reaction as ice melts (DSC) were obtained for 50% (w/v) CPA.

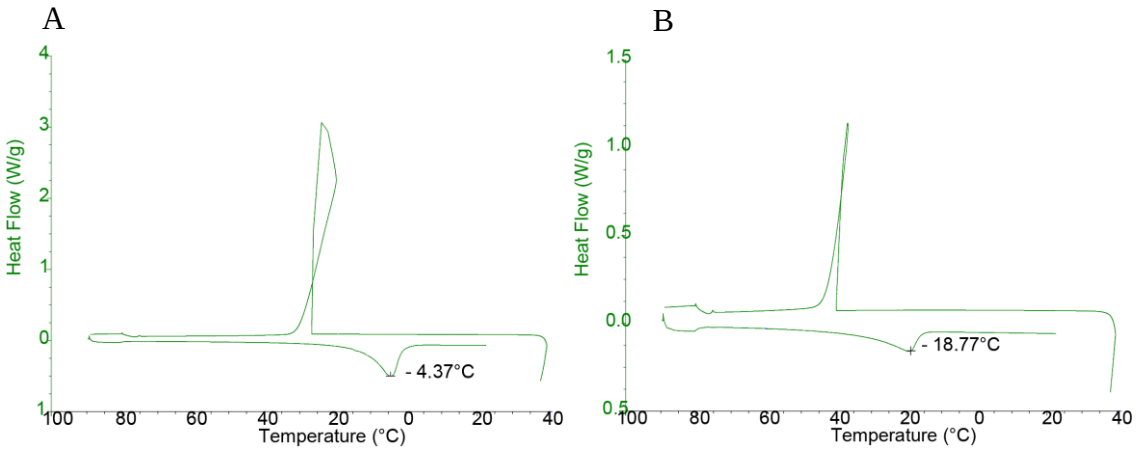

Figure 5.9 Determination of equilibrium melting point using differential scanning calorimetry (DSC).

The equilibrium melting point was determined from the melt curve and was defined as the temperature at which the trough was greatest. Figure A is an example of a thermogram of 12.5% (w/v) CPA and figure B is an example of a thermogram of the 37.5% (w/v) CPA solution. The y-axis shows the release of heat and the x-axis the temperature from -100˚C to +40˚C.

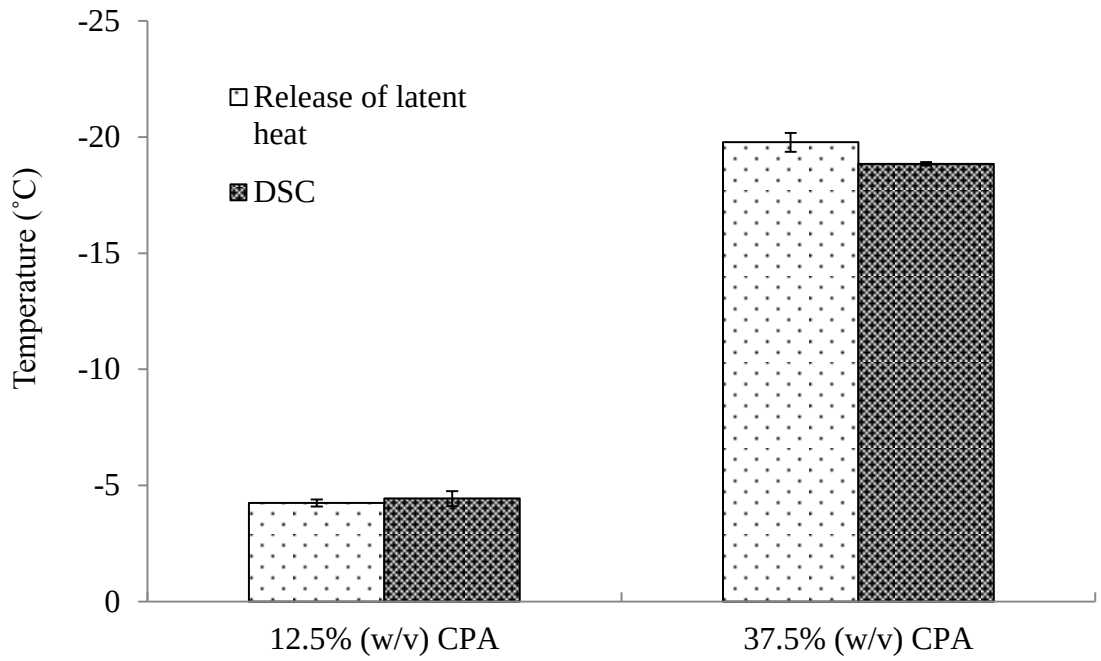

Figure 5.10 TdAFP and equilibrium melting point determination using "release of latent heat" and "DSC".

Each solution was prepared in triplicate, and was tested in duplicate for DSC and five times for "release of latent heat" measurements. The temperature difference between the averages of the two methods was 0.19˚C for 12.5% (w/v) and 0.93˚C for 37.5% (w/v). Data were n=3 +/- SD.

5.4.12 Liquidus curve of CPA solution No.18 in comparison to dimethyl sulfoxide

The data obtained from DSC and release of latent heat measurements were used to set up the liqidus curve for CPA solution No.18. No peaks as a result of release of latent heat or during the endothermic reaction as ice melts (DSC) were obtained for 50% (w/v) CPA. Nevertheless, from optical investigation it was observed that a 50% (w/v) CPA solution froze at approximately -30˚C. This was in accordance with the trendline value of solution No.18 (Figure 5.11). The melting points of 12.5% and 25% (w/v) CPA No.18 were comparable to those of Me_2SO. For higher concentrations the melting curve of Me_2SO runs below that of No.18.

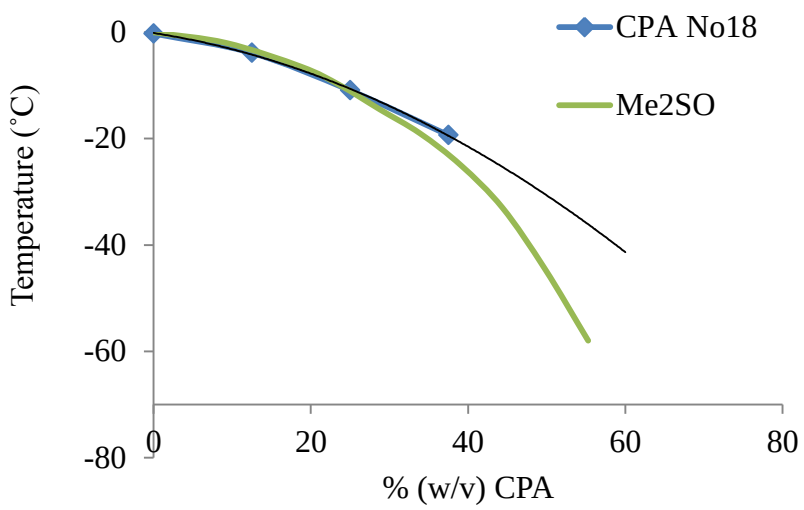

Figure 5.11 Liquidus curve of CPA No.18 in comparison to the liquidus curve of Me_2SO

At low CPA concentrations (<=25% (w/v) the melting point of CPA No.18 are comparable to those of Me_2SO (Chapter 4). For lower concentrations the predicted melting curve of No.18 runs above that of Me_2SO.

5.4.13 Manual Liquidus Tracking with CPA solution No.18 and dimethyl sulfoxide

The CPA solutions No.18 and Me_2SO were compared using the modified manual LT protocol as described in section 5.3.6. Viability, cell number, methylthiazol tetrazolium (MTT) and alpha-fetoprotein (AFP) production were measured 24 and 48 hours after rewarming from -160˚C. The following values, expressed as percentage of the positive control (un-treated), were obtained: AELC viability 24 hours post-warming was 74% +/-3 for solution No.18 and 29% +/-6 for Me_2SO. After 48 hours viability increased to 76% +/- 5 for solution No.18 and decreased to 23% +/-5 for Me_2SO. Cell numbers 24 hours after vitrification was 79% +/- 2 for No.18 and 51% +/- 7 for Me_2SO. The cell number increased to 85% +/- 8 for No.18 and 59% +/- 6.3 for Me_2SO after 48 hours. MTT values of 68% +/-13 and 45% +/-9 after 24 hours and 68% +/-12 and 45% +/-9 after 48 hours were reached for solution No.18 and Me_2SO respectively. AFP production was 34% +/- 1.6 for No.18 and 21% +/- 3 for Me_2SO after 24 hours and increased to 78% +/- 9.5 and 48% +/- 4.3 after 48 hours (Figure 5.12).

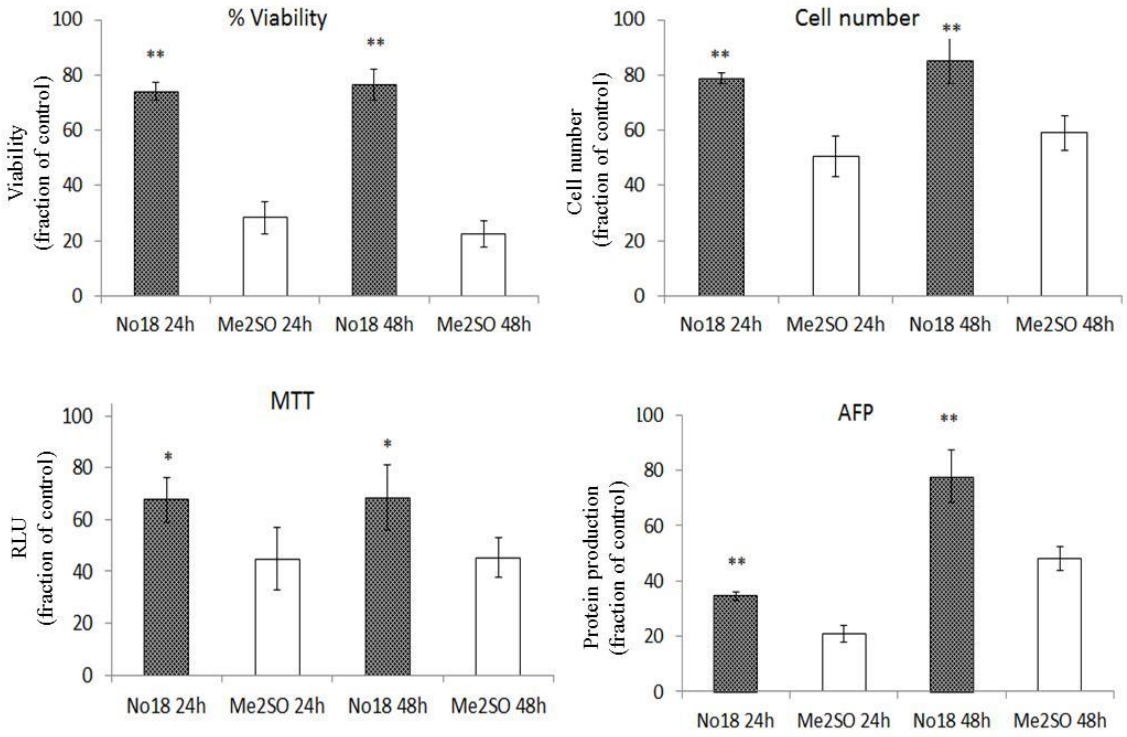

Figure 5.12 Manual LT with CPA solution No.18 vs. Me_2SO

CPA solutions No.18 and Me_2SO were compared using the modified manual LT protocol as described in section 5.3.6. Viability, cell number, MTT and AFP production were significantly higher for CPA solution No.18 than for Me_2SO. Data are n=5 +/- SD **p<0.01 and *p<0.05.

5.5 Discussion

The purpose of this chapter was to develop a new CPA solution with optimized properties for Liquidus Tracking (LT). An iterative series of experiments were designed to investigate the practicalities of using different CPA solution within the LT principle, to be balanced by differential toxicities seen at high concentrations. As a result of the time-consuming stepwise CPA addition and reduction process and the high concentrations that are needed to vitrify bulky materials, it was important to develop a CPA solution with minimal toxicity. However, the first limiting factor for the new CPA solution was viscosity, as the pumps and stirrer of the automatic Liquidus Tracker (see later work in Chapter 6 and 7) do not work when a viscosity of approximately 900 mPa*s is surpassed. Also, highly viscous material cannot be pipetted or mixed accurately when using the manual LT approach. A good CPA solution was considered to be of low viscosity, low toxicity and of good vitrifying capability. After a literature search to identify commonly used CPAs and by comparing the viscosity of these CPAs with Me_2SO, three penetrating CPAs including dimethyl sulfoxide (Me_2SO), ethylene glycol (EG), propylene glycol (PG) and sugars as non-penetrating CPA were chosen as promising CPAs for further studies.

In regard to toxicity the addition of sugars displayed an overwhelming protective effect by increasing viabilities to up to 60%. When AELC were incubated in 50% (w/v) Me_2SO for 20 minutes on ice, viability dropped to less than 5%, but remained high when 10% sugar was added. One main reason sugars are used in vitrification protocols is to decrease the amount of penetrating CPAs while keeping similar final CPA concentrations and vitrification properties. Here, Me_2SO was not replaced, but instead 10% w/v sugar was additionally included. Comparable to reduced toxicity of formamide through the addition of Me_2SO (Fahy et al., 1995) this is an actual account of toxicity neutralisation. It is possible that the protective effect is caused by osmotically reducing the cell volume, and therefore triggering reduced uptake of penetrating CPA, which leads to less intracellular dehydration through CPAs and also reduced osmotic stress when CPAs are washed out. The type of sugar used appeared to be irrelevant; however the combination of two sugars seemed to be slightly more effective than the use of one single sugar. Sugars were selected based on different positive effects. Fructose and

Raffinose have shown to minimize the amount of reactive oxygen species (ROS) (Nishizawa et al., 1997). ROS are known to increase substantially during environmental stress, potentially causing significant damage to the cell (Devasagayam et al., 2004). Trehalose and sucrose are thought to stabilize cell membranes by interacting with polar head groups of phospholipids during dehydration (Rudolph & Crowe, 1985). Glucose has been reported to prevent irreversible binding of Me_2SO to proteins (Clark et al., 1984). The fact that no significant difference between sugars was detected might hint at a more general influence of the non-penetrating CPA, such as less CPA influx and reduced osmotic stress. More specific actions, as described above, might play a minor role and might therefore be more detectable when the effects of two sugars are combined.

In order to simplify the procedure, glucose was chosen as the non-penetrating CPA for further studies. Reasons for this were several: as a single sugar glucose showed the highest average viability for AELC, although the difference to that of other sugars was not significantly relevant. Large CPA volumes are needed for automatic LT and glucose is inexpensive in comparison to raffinose and trehalose and is also cheaper than sucrose and fructose. Moreover, the use of raffinose and trehalose in concentrations exceeding 0.5M and 1M respectively has been advised against, because the sugars precipitate (Kuleshova et al., 1999). Glucose has been successfully used in several vitrification protocols (Dhali et al., 2000; Fan et al., 2009). Produced by the liver, glucose is a natural cryoprotectant in wood frogs (Conlon et al., 1998). The addition of natural levels of glucose to the incubation media prevented freezing damage of wood frog hepatocytes at -4˚C. In addition, glucose might serve to a certain degree as a penetrating CPA, as it has been demonstrated that liver cells have glucose channels (Sugimachi et al., 2006). Conversely, being a reducing sugar, glucose could have adverse effects. Reducing sugars can unfold proteins via Maillard reaction between the carbonyl group of the reducing sugar and primary amines of aminoacids. Irreversible protein unfolding can have a negative impact on cell viability (Carpenter et al., 1988).

The evaluation of different sugars was stopped at that point due to the high costs for trehalose and raffinose, and because results between sugars had shown to be comparable. Instead, combinations of commonly used penetrating CPAs (Me_2SO, EG,

PG) with increasing concentrations of glucose to a final concentration of 70% (w/v) were tested on viscosity. The studies accessibility to a viscometer or rheometer was limited and no means were available to measure viscosities either in large numbers of samples at the same time or at low subzero temperatures. Nevertheless, the mechanical evaluation by standardised pipetting and stirring these mixtures at -40˚C and comparing them to Me_2SO provided a simple way to quickly test a high number of solutions at low subzero temperatures. The reliability of the mechanical test was verified by rheologically measuring the viscosity of the nine least toxic CPA solutions. On the basis of the mechanical test these solutions had been considered to be fairly similar in viscosity to Me_2SO, which was confirmed by the rheological measurements. Although Me_2SO proved to be the least viscous, the difference to the most viscous solution (No.12) was less than 3mPa*s.

When testing the first set of CPA solutions it became obvious that all but one mixture containing more than 10% (w/v) glucose were substantially more viscous than Me_2SO and only one mixture (60% (w/v) Me_2SO + 10% (w/v) glucose) of the 21 combinations was of similar viscosity. To obtain more solutions of low viscosity, 10% of a more viscous CPA was systematically replaced with 10% of a less viscous CPA. Both PG and EG as well as glucose exhibit high viscosities in comparison to Me_2SO. Therefore methanol was selected as a low viscosity CPA as a means to reduce the overall viscosity of the CPA mixture. Ethanol is less viscous than methanol but proved to be more toxic to AELC. Monovalent alcohols like methanol and ethanol are not commonly used in cryopreservation protocols, mostly due to their known high toxic effects on many biological systems. However, methanol has shown to be effective for non-mammalian cells such as protozoa (Kirsop & Henry, 1984; Polge & Soltys, 1960) yeast (Kirsop & Snell, 1984). cyanobacteria and algae (Bodas et al., 1995; Konev et al., 1975). It has also been used successfully in fish semen and embryo preservation (Lahnsteiner, 2008; Lahnsteiner et al., 2002; Seki et al., 2011). In these applications, the concentration used was 10% or less, which justified the concentration used for new LT CPA solutions. Ethanol in comparison to methanol has only been used in very few cryopreservation protocols (Lewis et al., 1993) due to its higher toxicity, which corresponds to the data found in this chapter. By replacing more viscous CPAs with less viscous CPAs,

including methanol, the viscosity of all but two solutions was reduced, resulting in 28 different CPA solutions with a similar viscosity to Me_2SO.

When testing the toxicity of these solutions it was shown that, as expected, higher concentrations of penetrating CPAs resulted in lower AELC viability. Interestingly the addition of just 5% (w/v) glucose was sufficient to substantially increase viability, whereas the increase from 10% to 20% (w/v) glucose did not show much further improvement. Results also suggest that for AELC, EG is less toxic than Me_2SO or PG. This observation corresponds to previous findings from other authors in chondrocytes and alginate encapsulated HepG2 and β-TC-cells (Jomha et al., 2010; Lawson et al., 2011; Valdez et al., 1992). As stated by Fahy, the non-specific toxicity of a given solution is dependent on the strength of hydrogen bonding between water and the polar groups of the permeating cryoprotectants (Fahy, 2010). According to this theory, viability increases when the average polar group of a CPA is interacting less strongly with water which in general means that weaker glass formers favour higher viability. Group polarity of CPAs is as follows: propylene glycol > Me_2SO> ethylene glycol > amides. This seems to correlate with the toxicity results and vitrification properties of the newly developed CPA solutions for AELC. Replacing PG with Me_2SO did not make much difference in AELC viability, but EG seemed to be superior to PG and Me_2SO. As discussed later in more detail, Me_2SO vitrified best among six selected CPA solutions, but was more toxic. In contrast CPA solutions No.18 and No.6 were the least toxic, but seemed to be the least effective for vitrification.

The combination of Me_2SO with EG (No.18) has shown to be less toxic than other combinations. EG has been stated to be the least toxic CPA for hepatocyte virtification (Kuleshova et al., 2004; Magalhães et al., 2008) but for AELC, the combination of Me_2SO and EG resulted in significantly higher viability than either of the CPAs on its own. This combination has also shown good results for the vitrification of cumulus cells using 22% EG and 18% Me_2SO (Saeed et al., 2000) and in equine embryos with a concentration of 17.5% for both EG and Me_2SO (Oberstein et al., 2001). There has been no explication so far about the interaction between EG and Me_2SO, but both solutions are also main components of the well-known and commercially available vitrification solutions VS55 and M22 (Fahy et al., 1995; Fahy et al., 2004). These solutions

additionally contain non-penetrating CPAs and also formamide, which was regarded as too toxic for our purpose, and ice-blockers which are deemed too expensive for the development of a large scale preservation method. Although of general high toxicity, methanol was well tolerated when in combination with EG and low amounts (>=30% w/v) of Me_2SO. Solution No.6 containing 10% (w/v) methanol was the second least toxic after solution No.18. Methanol has a very high rate of permeability, exceeding that of Me_2SO as demonstrated in algal cells (Brand & Diller, 2004) which might explain to some extent its high toxicity. Nevertheless, high penetration rates and low viscosity might be necessary for some vitrifiction protocols, and for those protocols methanol might be a considerably useful CPA.

When developing new CPA solutions it is necessary to assess toxicity of cryoprotectants at the concentrations needed to vitrify. CPA concentrations in the literature are given in different units such as volume per volume (v/v), weight per weight (w/w), weight per volume (w/v) or moles per volume. In respect to laboratory practicability, the use of weight/volume is preferable, which is why it has been used in this work. However, in regard to vitrification properties, it might be more meaningful to use weight/weight as the amount of water in comparison to CPAs is kept constant. Important work regarding the vitrification properties of CPAs has been done by Boutron and others (Baudot & Boutron, 1998; Baudot et al., 2000; Boutron, 1986; Wowk et al., 1999; Wowk et al., 2000) who used weight/weight for their comparability studies. Fahy, who has mainly concentrated on the toxicity of CPA mixtures, normally used weight/volume (Fahy et al., 2004). He determined the minimum concentration needed to vitrify a solution at a given volume at maximum cooling rates and then used the minimum concentration to compare the toxicity of different CPA mixtures. Others have used molarities (Fujioka et al., 2004; Kuleshova et al., 2004), which can be helpful to predict osmotic pressure. If little is known about the toxicity of a potential CPA solution, it might be more efficient to first test the toxicity of different mixtures at the same concentration in order to make a pre-selection before testing a variety of concentrations. This strategy was pursued in this work on the grounds that exact final CPA concentrations for LT are of less importance than for conventional vitrification, as final concentrations are reached at very low temperatures (<-30˚C), at which CPA penetration and toxicity are suspected to be strongly reduced. Furthermore, exact final

concentrations are difficult to achieve as the procedure itself, manually as well as automatically, implies pipetting and pumping inaccuracies. It was, nonetheless, important to get an estimation of the vitrification properties of the potential CPA solutions. Me_2SO and the five CPA solutions of lowest toxicity to AELC were therefore vitrified and compared. Whilst all solutions vitrified at 70% (w/v), only Me_2SO and the mixture of Me_2SO/EG/glucose with a ratio of 5:1:1 vitrified at 60% (w/v). One reason why the other four solutions did not vitrify is probably the higher concentration of EG and methanol. EG has been described as a less effective vitrifier than Me_2SO and PG (Baudot et al., 2000) and methanol only vitrifies on its own under high pressure (Brugmans & Vos, 1995). However, CPA solutions No.5 and No.9, and to a smaller extent No.6, melted faster than solution No.18, which did not contain methanol. This might suggest a positive effect of methanol during the warming phase by increasing the velocity at which ice melts, and thus decreasing the amount of potential devitrification.

As a next step in the investigation the CPA solutions were used to vitrify AELC. The same order in viability as previously seen for toxicity studies, with highest viabilities gained from solution No.18, was observed. Reduced incubation time before plunging AELC into liquid nitrogen could be beneficial for solutions with higher concentrations of fast penetrating CPAs (Me_2SO, methanol), and some of the solutions might vitrify also at lower concentrations which would reduce CPA toxicity and increase viability. However, for the chosen set-up solution No.18 was superior to the other solutions and proved to be an efficient vitrifier. Vitrification experiments can only give an indication whether a CPA solution is suitable for LT. Ultimately only the LT procedure itself can be used to determine the best CPA solution. However testing all CPA solutions in a LT set up would have been too time-consuming. Automatic LT only allows testing of one CPA solution per experiment, and even the manual LT set up is very limited in sample number (maximum 10). Due to the long LT process and consequently long exposure times to toxic concentrations of CPA, it was concluded that the CPA solution of lowest toxicity (No.18) would be more beneficial to cryopreserve AELC using LT than the best vitrifier (No.22 or Me_2SO). Also CPA concentrations for LT can be adjusted to a level that allows vitrification at very low subzero temperatures (<-30˚C) at which CPA toxicity might be completely reversed.

The next challenge was to determine the liquidus curve for solution No.18. Unfortunately, it was not always possible to conduct DSC measurements. For this reason, using the release of latent heat was established as an alternative method. The equilibrium melting point of 12.5% and 37.5% (w/v) were determined using both methods; DSC and the release of latent heat. The temperature difference between the two methods was less than 1˚C. This seemed to be acceptable considering that the temperature for each LT CPA increase was set +5˚C above the equilibrium melting point to account for pipetting and pumping deviations. When using release of latent heat to measure the equilibrium melting temperature of high concentrations of Me_2SO (Chapter 4), values were lower than the literature DSC values. Conversely, measurements for 37.5% (w/v) of CPA solution No.18 were comparable between methods. Two reasons would explain this observation. First, the sample temperature does not return to the true equilibrium melting point since the chamber temperature cools the sample temperature during the warming process. The longer the warming process and the colder the chamber temperature, the stronger this effect will be. Concentration above 25% (w/v) of Me_2SO freeze at lower temperatures than the same concentration of solution No.18. This means that the freezer will be at a lower temperature for Me_2SO than for solution No.18. Contrary to Me_2SO, CPA solution No.18 contains high concentrations of sugars, which might act as nucleation points when supersaturated (for example at low temperatures), reducing the amount of supercooling. Both a shorter warming process (less supercooling) and a higher chamber temperature at the time of nucleation (higher melting point) will reduce the amount of heat loss and result in more comparable values between the true equilibrium melting point, given by DSC measurements - a precise method to measure the equilibrium melting point - and measured values by release of latent heat.

Finally, manual LT was used to compare CPA solution No.18 with Me_2SO. After vitrification, cell number, AFP and MTT production was significantly higher for solution No.18 than for Me_2SO, showing that No.18 is the better CPA solution for the LT approach.

5.6 Conclusion

By using viscosity as a limiting factor the immense number of possible CPA combinations was reduced to a reasonable number of 28. By systematically replacing highly viscous CPAs with less viscous CPAs, all combinations in a range of 10% (w/v) were tested. Toxicity studies identified nine particularly useful CPA solutions of low toxicity of which five were further investigated regarding their vitrification properties. CPA solution No.18, a mixture of Me_2SO, EG and glucose in a ratio of 4/2/1 was predicted to be the most suitable for LT due to its low toxicity, although it was less efficient as a vitrifier than other solutions. It can be assumed that, with respect to the main components, there is little possibility to develop a better CPA solution for Liquidus Tracking. Although solutions were developed to be first of low viscosity and second of low toxicity, solution No 18 resembled those vitrification solutions that are commercially sold. Using a manual LT system clearly demonstrated that CPA solution No.18 is superior to Me_2SO as a sole agent.

The final CPA concentration that is required to obtain a stable glass and to avoid devitrification for volumes up to 400ml for automatic LT still has to be determined.

CHAPTER 6
The automatic Liquidus Tracker

6.1 Introduction

Automatic Liquidus Tracking (LT) is the up-scaled and automated version of the manual LT approach described in Chapter 4. The Liquidus Tracker is an almost completely automated vitrification machine that has been developed by Planer plc in cooperation with David Pegg as a means of cryopreserving biological samples that are not suitable for conventional slow-rate freezing or for ultra-fast vitrification such as organs and tissues or large volumes. The Liquidus Tracker prototype used for the work of this chapter was developed for use with articular cartilage connected to parts of knee-bone. This is reflected in the design of the stirrer, the inlet and outlet system and the volume of the sample container. The inlet and outlet system can be operated by two different methods - the dual solution mode which is similar to the manual LT set-up 2, and the single solution mode which is similar to the manual LT set-up 3 (Chapter 4). For the work of this chapter the single solution mode was used which has the advantage of being less complex in terms of the inlet pump system and more cost effective as less reagents are needed to increase the cryoprotectant agent (CPA) concentration of the sample (Figure 6.1, Figure 6.2). New approaches needed to be developed to enable automatic LT to be used with AELC, and these are described.

6.1.1 The dual solution mode

The dual solution mode works with three peristaltic pumps, of which two operate the inlet and one the outlet. A highly concentrated CPA solution and a buffer are mixed by pumping the two inlet solutions into a combined inlet tube to obtain a solution that is slightly more concentrated than the solution within the sample container. The sample container is completely filled with the inlet solution before the volume is reduced. High amounts of CPA and buffer solutions are needed to increase the sample CPA concentration (Figure 6.1).

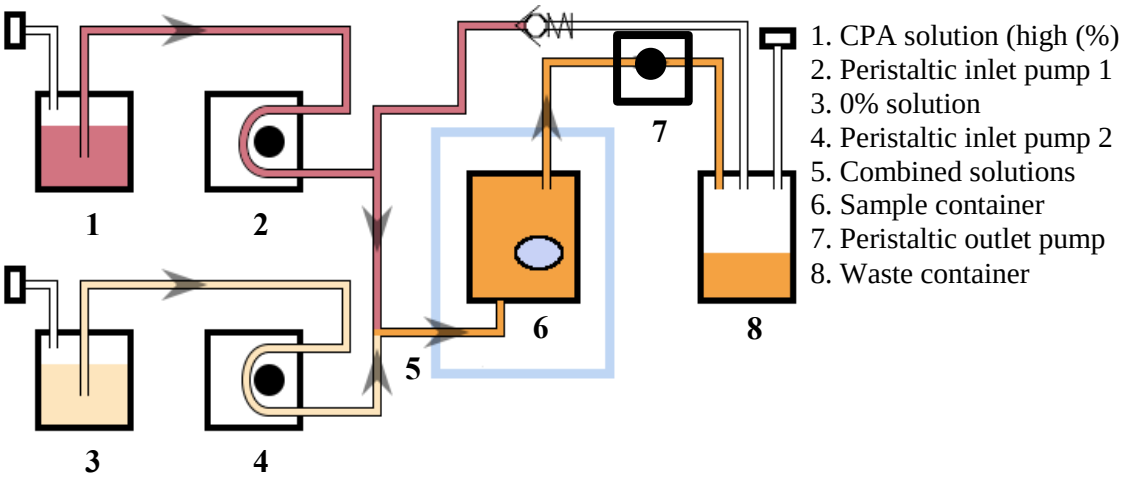

Figure 6.1 The dual solution mode

High concentrated CPA (1) is pumped by a peristaltic inlet pump (2) towards the sample carrier. Before passing the sample carrier inlet port, the CPA solution is mixed and diluted with a buffer solution (3) being pumped (4) from a separate container to the combined inlet tube. The new solution (5) which is slightly more concentrated than the sample itself, is added to the sample carrier (6) to increase the CPA concentration before the sample reaches its melting point. After the mixing process, sample is extracted by the outlet pump (7) and led to the waist container (8).

6.1.2 The single solution mode

The single solution mode only uses one highly concentrated CPA solution to increase the CPA concentration within the sample. Therefore only two peristaltic pumps are needed, one for the inlet and one for the outlet. The outlet volume is determined by the volume of the next infusion so that sufficient CPA can be added to increase the sample CPA concentration. Both, inlet and outlet volume increase after each step as more CPA has to be added when targeting the same percentage increase during each step. The stirrer operates throughout the entire process (Figure 6.2).

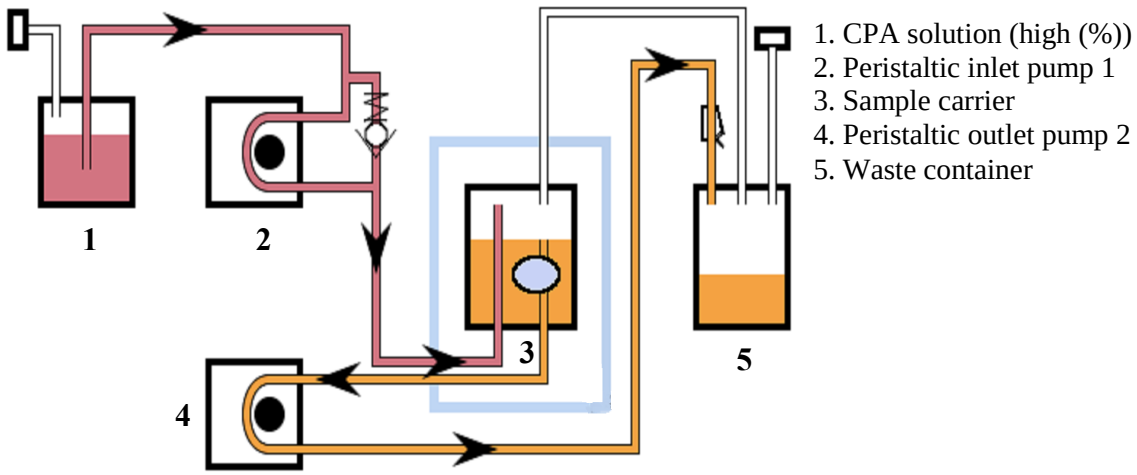

Figure 6.2 The single solution mode

High concentrated CPA (1) is pumped by a peristaltic inlet pump (2) into the sample carrier (3) to increase the CPA concentration before the temperature is reduced. After mixing the sample, some of the solution is extracted by the outlet pump (4) and lead to the waist container (5).

6.1.3 The Liquidus Tracker

The Liquidus Tracker (single solution mode) consists of one inlet and one outlet pump, a magnetic stirrer, a controlled rate freezer and a personal computer. All of these units are connected to the controller. The LT device is controlled by the computer software CfgPid and Delta T. The temperature-CPA-profile, which determines the CPA concentration that has to be reached at a certain temperature to prevent freezing, is entered into the CfgPid table. Commands are sent to the controller which in turn operates the peristaltic pumps. High concentrated CPA solution is pumped into the sample carrier to increase the CPA concentration. After mixing, solution is extracted by the outlet pump and is led to the waist container. The system stirs continuously through all three phases: injection, hold phase and extraction until the final target CPA concentration is reached. Commands to operate the stirrer are sent from the CfgPid software to the controller and from the controller to the stirrer. For the stirring process the sample carrier has to be maintained in a fixed position – this is provided by the sample holder. Information about start temperature and cooling rates are managed by the DeltaT software. Once the controller obtains the information from the computer, they are sent to the controlled rate freezer. Before being added to the sample, the inlet

CPA solution has to be cooled down. This is achieved by keeping the inlet tube, wounded around the sample holder, within the freezer. The longer the inlet tube and the slower the cooling rate, the closer is the inlet temperature to the freezer temperature. The LT system also includes two measures of security, a pressure relief valve for the event of inlet solution freezing while pumping and an overflow port inside the sample carrier that is connected to an outlet tube. This prevents pressure build up inside the container and CPA solution to leak into the freezer. The temperature of the inlet and the outlet solution, as well as the temperature of the solution inside the sample carrier are measured via thermocouples which are connected to a Pico Logger (Figure 6.3).

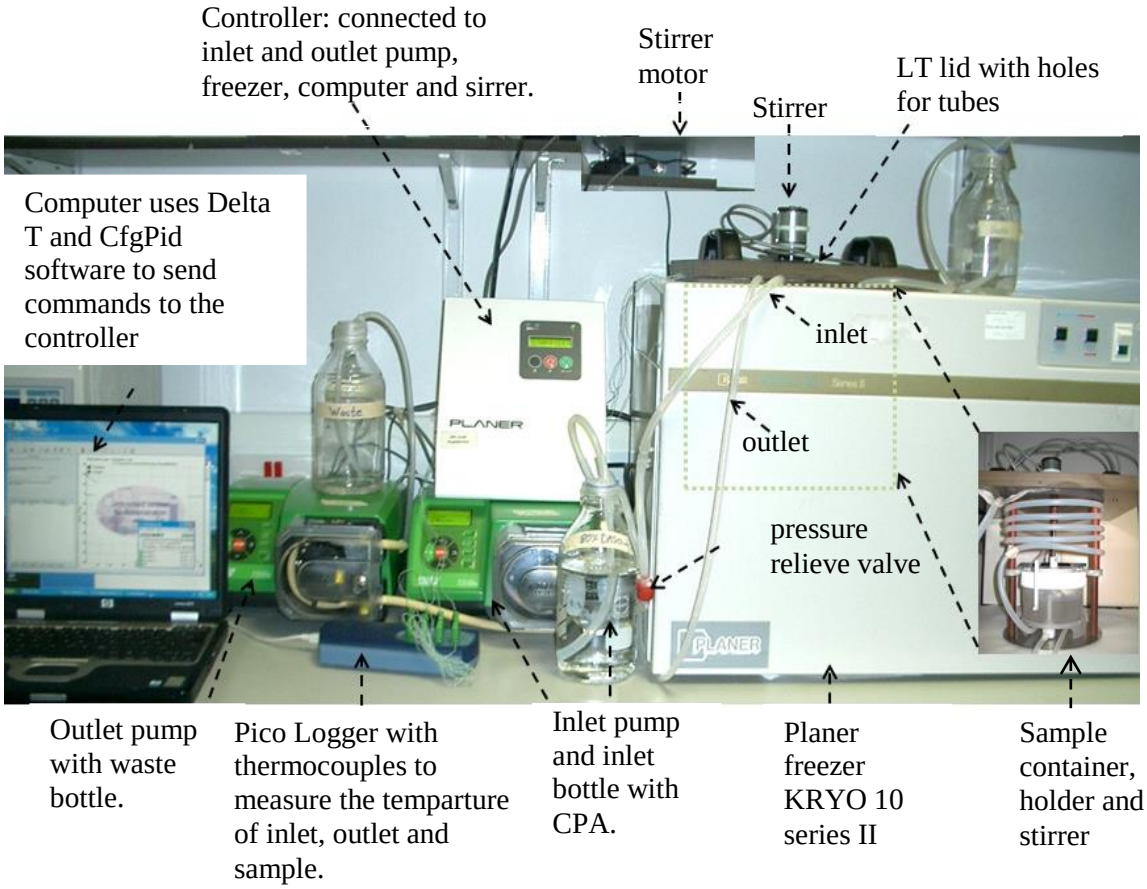

Figure 6.3 The Liquidus Tracker

The graph shows the automatic LT device displaying the one solution mode. Watson-Marlow pumps, Planer stirrer and Planer freezer (Kryo10, series II) are operated by the controller which gets its commands from the computer software CfgPid and DeltaT. The sample carrier has to be inserted in the sample holder which is placed inside the Planer freezer. The inlet tube goes from a highly concentrated CPA solution into the pump and to the sample container. The outlet tubes goes directly to the pump and from there into a waste bottle. The CPA concentration of the sample is increased by pumping high concentrated CPA solution into the sample carrier. The stirrer consists of a plastic part that turns around within the sample container and a magnetic part which is powered by a motor. A pressure relief valve is added between the inlet pump and the freezer as a measure of security. The temperature of inlet, outlet and sample are measured by the Pico Logger.

6.1.4 The stirrer

To fully mix large volumes, mechanical stirring is required to ensure that the solution is thoroughly mixed. A stirrer for cryopreservation purposes has to withstand (to -160˚C) and work (to -40˚C) at very low subzero temperatures, which is normally not provided by any electrical application. This is overcome by placing the motor outside the freezer and by magnetically coupling the motor to a stirring system held inside the freezer. The motor rotates a metal plate inside the freezer, which in turn magnetically drives the stirrer inside the sample carrier. The stirrer is made of a bottom part and an upper part. The bottom part of the stirrer contains three holes through which the inlet, outlet and overflow ports are introduced and which hold this part of the stirrer in static position. The upper part is made of a disc which holds several small magnets and four paddles which rotate between the sample carrier wall and the static paddles. This way the solution is being mixed, while tissues and organs can be placed in the centre of the sample carrier. To increase the mixing effect, the rotation direction is constantly changed (Figure 6.4).

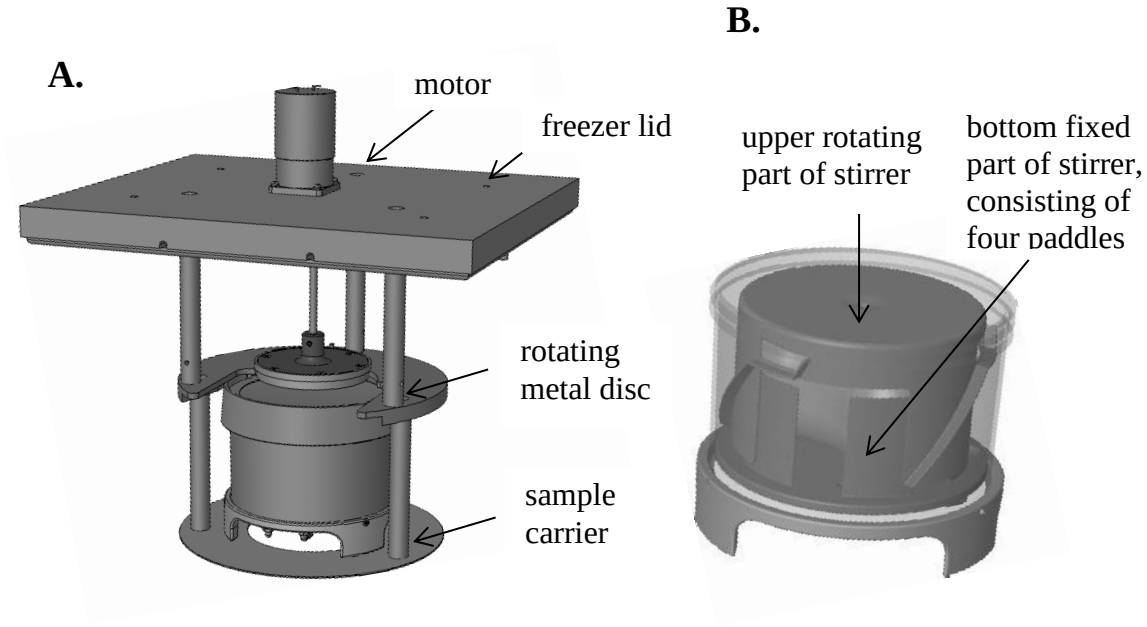

Figure 6.4 Sample holder and stirrer

Figure A: demonstrates the sample carrier holder, the sample carrier and part of the motor which rotates the metal disc inside the freezer. The metal disc and the motor are separated by the freezer lid. Figure B: shows the stirrer inside the sample carrier. The paddles of the upper stirrer move between the sample carrier wall and the paddles of the bottom stirrer part.

6.1.5 Heat transfer

Heat or thermal energy is the motion of atoms or molecules (kinetic energy) that can be transmitted to another system. The amount of thermal energy depends on how fast the molecules move, on the specific heat capacity and on the mass of an object. The specific heat capacity is defined as the amount of energy that is required to increase the temperature of one kg of that substance by one degree. The temperature is the average value of energy for all the atoms and molecules in a given system and is independent of the amount of matter. Heat always flows from the body of higher temperature to the body of lower temperature. This continues until the temperatures equalize each other. Heat can be transferred in three ways: conduction, convection and radiation. Both conduction and convection require matter to transfer heat. Instead, radiation does not rely upon any contact between the heat source and the heated object. Heat is transferred by means of electromagnetic waves such as the sun light. Conduction is the transfer of energy that occurs when two particles collide with each other. The particle of higher kinetic energy transfers some of its kinetic energy to the particle of lower kinetic energy. This is how heat energy is transferred from the sample solution, to the sample carrier and finally to the controlled rate freezer. An increase of the freezer temperature is prevented by controlled addition of vaporous nitrogen that has just been released from liquid nitrogen. Convection is a way of energy transfer that occurs when warmer areas of a liquid or gas rise to cooler areas in the liquid or gas, whereby both mix with each other. Heat transfer by convection is provided by the stirring process of the LT device. Heat transfer is an important aspect of cooling and warming of larger volumes. Slow cooling and warming rates are easy to achieve but there are limitations for high cooling and warming rates. Normally higher rates can be achieved by increasing the temperature difference between sample and freezer, between sample and inlet solution and by increasing the amount of inlet solution. Regardless the stirring process, heat gradients may still exist within samples, making devitrification and/or ice recrystallization more likely.

6.2 Aims

The aim of this chapter was to set-up the Liquids Tracker and to run the standard single solution mode cooling profile with dimethyl-sulfoxide (Me_2SO) as developed by Planer. Following this, the Liquidus Tracking system was adapted to the use of alginate encapsulated liver cell (AELC). This included the development of a filter system and a new protocol to increase in the sample cooling rate. Finally the newly developed cryoprotectant agent solution (CPA No18 – Chapter 5) was compared to Me_2SO.

6.3 Methods and Materials

6.3.1 Liquidus Tracker set-up

Materials

Controlled Rate Freezer (Planer, Kryo 10, Series II)

Watson Marlow pumps 520Du

Inlet tube: Plat Silicon tube; bore 4.8mm, wall.2.4 mm,

(Watson Marlow, Cat. No. 913.AJ48.024)

Outlet tube (outside pump): Plat Silicon tube; bore 4mm, wall 1.6mm,

(Watson Marlow, Cat. No. 913.A048.016

Oulet tube (inside pump): Santropene tube, bore 6.3mm, wall 2.4mm,

(Altec, Cat. No. 01992042)

Pressure relieve valve *(Smart products, Cat. No. 303303PS-1700S020-2368)*

Ten barbed Tee tubing connectors for bore size 4.95mm *(Altec, Cat. No. 05-405123)*

Barbed straight tube connectors for bores size 6.3mm and 4.3mm

(Altec Cat. No. 05-42-5355)

Method

The Liquidus Tracker was set up following the operator's manual if not otherwise noted. The inlet pump was equipped with an inlet tube of three meter length, which was wrapped five times around the sample holder before being connected to the sample container. The pressure relief valve was installed between the tube that goes into and out of the inlet pump. For the loop the same tube type as for the inlet was used. Tubes were connected with barbed striped tube connectors. For the outlet two different tube types were used. Inside the Waston Marlow pump a certain tube thickness had to be reached to allow perelistic pumping. For that reason a tube with a larger bore size of 6.3mm and a wall thickness of 2.4mm from Altec Santroprene was used inside the pump which was connected to a silicon tube of 4mm bore size and a wall thickness of 1.6mm. For the connections barbed straight tube connector from Altec were used.

6.3.1.1 The CfgPid profile

The following data was added to the CfgPid software: Kstart - the CPA concentration of the starting solution, F1 and F2, the pump calibration factors, the

temperature/concentration values, the start volume (Ksol1), (same for each new cycle) and the temperature at which the stirrer was supposed to stop (Off1). The single solution mode was selected. The CfgPid software uses the temperature/concentration table to calculate the amount of CPA that is needed for the next inlet. The points (T1, K1) to (T10, K10) define points on the curve and linear interpolation is used by the software to determine the concentration between these points (Figure 6.5).

Figure 6.5 The CfgPid software

Data added in the CfgPid table were needed to operate the perelistic pumps and the stirrer. The temperature/concentration table described the sample temperature that was supposed to be reached at a certain CPA concentration. The start volume (Ksol1) and a start concentration (Kstart) had to be defined. Pump calibration factors (F1 and F2) described the flow throughput for a given set-up.

6.3.1.2 Delta T

Freezer information such as start temperature and the cooling rate were added to the Delta T software, which provided a PC interface to the Planer controlled rate freezers.

6.3.1.3 Pump calibration

Pumps were calibrated with the final LT set-up in respect to tube type, lengths and geometry (wounded around the sample holder). The inlet and outlet tube volume was determined by pumping a sequence of normal water and coloured water into a

volumetric flask. Once either, the normal or coloured water had finished, the time was stopped and the volume was measured. Calibration values F (flow factors in ml/minute) were entered into the CfgPid software, to determine the pump speed needed to obtain the necessary amount of inlet and outlet during the LT process.

6.3.1.4 Freezer connection

The data cable 12-pin connector of the Kryo10 series II freezer was exchanged with a new 10-pin connector to be compatible with the Planer controller.

6.3.1.5 Filling the sample carrier

The sample carrier has a volume of 500ml and was filled manually for each run with the starting solution. Then the upper part of the stirrer was placed on top. The container was closed tightly with an inner and an outer lid. Before filling, the inlet, outlet and overflow ports were connected to the tubes to prevent the solution to leaking out (Figure 6.6).

empty sample carrier- sample volume 500ml	starting solution filled up to the outlet port level	magnetic stirrer placed above static part of the	internal plastic lid for protection placed above	closed tightly with cover lid

Figure 6.6 Filling the sample carrier

The Figure describes how the sample was added to the sample container and how the stirrer was put together before being placed into the sample holder.

6.3.1.6 The CPA concentration/temperature curve

To evaluate the outcome of each LT run, the temperature/concentration curve was determined. Therefore a sample of extracted solution was taken at the end of each extraction cycle and the CPA concentration was determined by measuring the refraction index. This value was correlated to the temperature of the sample inside the sample carrier at the beginning of the inlet cycle. The length of a complete cycle was seven minutes and followed the subsequent sequence: inlet over one minute - mixing for three

minutes-outlet over three minutes. Consequently the temperature at the beginning of the inlet cycle when new CPA solution was pumped in was higher than at the end of the outlet cycle. To obtain the lowest temperature reached for a given CPA concentration the temperature had to be recorded at the end of the extraction cycle. The temperature-concentration curve for each run was then compared to the liquidus curve of the CPA solution and the CfgPid profile used in the experiment.

6.3.2 Changes made to the original Liquidus Tracker set-up

6.3.2.1 Temperature measurement

Materials

Type K thermocouple (*Pico Technology, Cat. No. SE027*)

TC-08 data logger (*Pico Technology*)

PicoLog recorder software (*Pico Technology*)

Method

To measure the temperature of the inlet solution a thermocouple was inserted into the inlet tube just a few centimetres before the inlet port, to measure the temperature just before being pumped into the sample carrier. The temperature inside the sample carrier was measured by introducing a thermocouple through the overflow tube and port. The thermocouple was fixed one centimetre from the bottom and on to the overflow port to prevent the thermocouple to interfere with the stirring system. The outlet solution was measured by a thermocouple inside the outlet tube just after the outlet port exit (Figure 6.7).

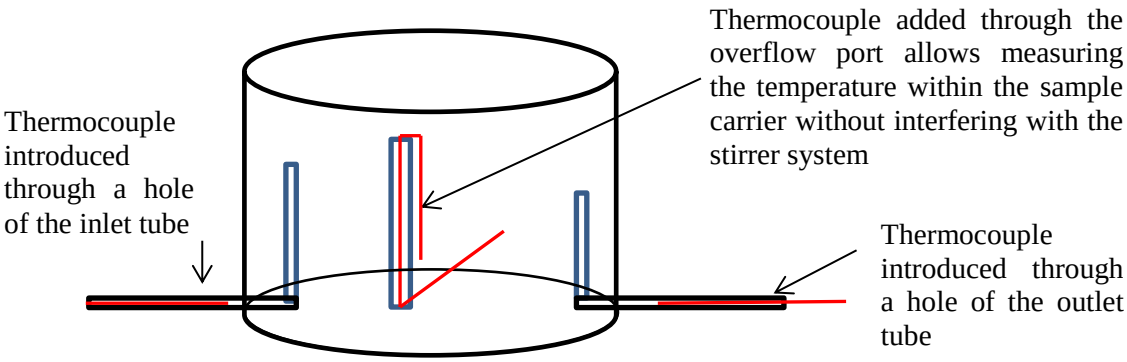

Figure 6.7 Monitoring inlet, outlet and sample temperature

The graph demonstrates where thermocouples (in red) were placed to measure the temperature of inlet, outlet and sample solution. To measure the inlet and outlet temperature, thermocuples were inserted into the tubes (in black) just before the ports (in blue). The thermocouple to measure the sample temperature was introduced through the overflow port.

6.3.2.2 Outlet filter system

Materials

plastic tube: length 3cm, diameter 3cm

mesh: 200µm Nylon mesh

Method

Unlike larger constructs, alginate encapsulated liver cells (AELC) do not remain statically on the bottom of the sample carrier while being stirred. Therefore a mesh system was needed to keep the beads inside the sample carrier. The first filter system for AELC was made out of a piece of mesh which was directly attached to the outlet port opening. However within the first few extraction cycles the filter would block despite occasional starting a short reversed flow to unblock the filter. A new filter system of increased filter area was designed. The filter area was increased from 0.20cm^2 to 9.82cm^2 by using a plastic tube which was covered from both ends with a mesh. The outlet port was introduced through the mesh at the outer edge to maintain most of the mesh closer to the inner part of the sample carrier so that the filter system would not interfere with the stirrer. By increasing the filter area and by keeping the filter away from the opening of the port where the suction force was highest, filter blockage was avoided (Figure 6.8).

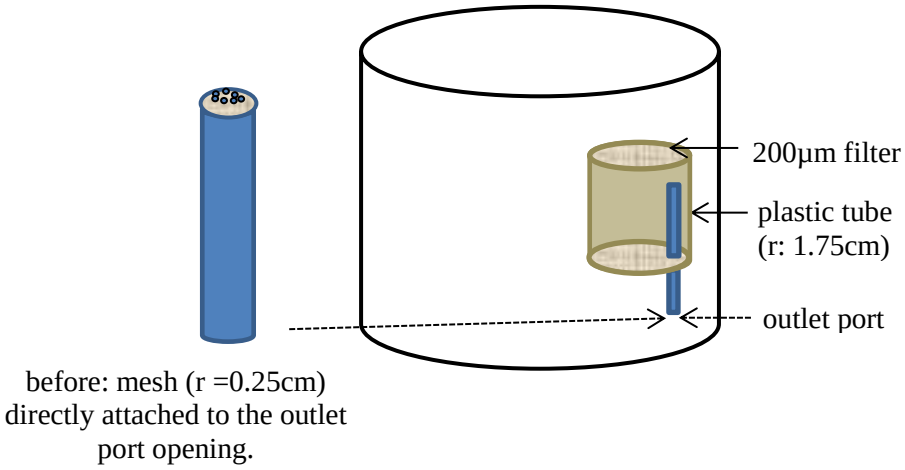

Figure 6.8 Outlet port filter system

A filter directly attached to the outlet port resulted in filter blockage. By increasing the filter area and by keeping the filter away from the opening of the port, filter blockage was prevented.

6.3.2.3 Increasing inlet tube lengths

The original tube length was designed for cooling rates of approximately -0.1˚C /minute. However for faster cooling rates (> -0.5˚C) and higher inlet speed (up to 150ml/minute) which were more appropriate for AELC, insufficient cooling was provided. Therefore the inlet tube length was increased from originally three meters to six meters to assure that the inlet temperature was close to the freezer temperature.

6.3.3 Automatic Liquidus Tracking cooling

Materials

Liquidus Tracker *(Planer plc)*

Me_2SO or CPA No.18 *(see Chapter 5)*

1xPBS with Mg^{2+} and Ca^{2+} *(Sigma, Cat. No. D8662)*

15ml Centrifuge tubes

AELC

6.3.3.1 Standard Planer Liquidus Tracking procedure

Method

The standard method was as following: 400ml of 15% (w/v) CPA containing AELC was added to the sample carrier. Larger volumes of beads were not always available and therefore 6ml of beads 12-15 days after encapsulation were used if not otherwise noted. The start temperature was set to 20˚C and a cooling rate of -0.5˚C/minute was chosen. The sample concentration was increased automatically by following the CfgPid curve (Table 6.1), pumping in a 80% (w/v) CPA solution into the sample carrier until a concentration of 65% (w/v) was reached. Once a temperature of -40˚C was reached the stirrer was stopped and aliquots of 2.5ml were added to 15ml Mircofuge tubes hold in a bucket of liquid nitrogen for vitrification and storage.

Table 6.1 CfgPid table (standard program) one-solution mode using 80% (w/v) Me_2SO

CfgPid modified	
Temperature (˚C)	Concentration (%, w/v)
4	15
-1.84	21
-4.84	26.96
-9.04	32.96
-14.8	38.96
-22.41	44.96
-32.18	50.96
-44.53	56.96
-59.72	62.96
-65.35	65.96

6.3.3.2 Combined manual/automatic Liquidus Tracking

Method

To avoid outlet pump freezing and to maintain the sample temperature/concentration curve close to its liquidus curve a combined manual/automatic LT cooling approach was followed. First infusions were carried out by operating the pumps manually, while the outlet was primed with 50% (w/v) CPA and remained unused to avoid freezing. The freezer temperature was set on hold at -20˚C. Once a concentration of 35% (w/v) CPA was reached the automatic program (CfgPid curve) was started (for details see Appendix 6.3.3.2).

6.4 Results

6.4.1 The temperature-concentration curve

For each LT run the temperature/concentration (T/C) curve was determined by measuring the refraction index of the extracted solution and by correlating this value to the sample temperature reached at the end of the extraction cycle. For this the CPA concentration of the collected sample, had to coincide with the CPA concentration of the sample inside the sample carrier. For the first runs this was not the case as the extraction volume at the beginning of the LT cooling procedure was lower than the outlet tube volume of originally 80ml, which led to a deviation to the predicted T/C curve. The outlet tube was therefore shortened to a minimum length of 60cm and an outlet tube volume of 35ml, which exceeded the minimum outlet volume by 5ml. For approximation the CPA sample concentration was calculated by using the inlet volume and concentration and the sample volume and concentration. The calculation was based on the assumption that perfect mixing was achieved (Figure 6.9).

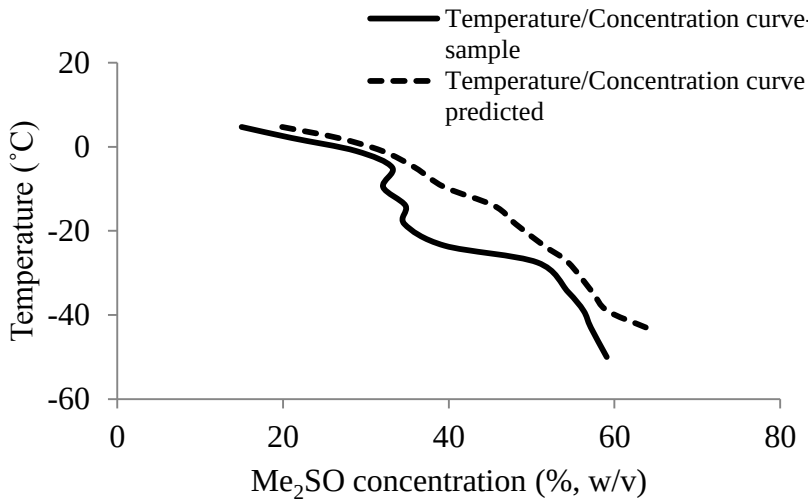

Figure 6.9 The temperature/concentration curve

The graph shows the temperature/concentration curve of a LT run for which the outlet tube volume was higher than the extraction volume. Measured refraction index values (used to calculate the Me_2SO concentration) did not correspond to the Me_2SO concentration inside the sample carrier and the temperature measured at the beginning of the inlet cycle. This lead to strong deviations to the predicted T/C curve (blue curve), which had been calculated by using the known inlet volume and concentration and the known sample volume and concentration.

6.4.2 Devitrification

An initial concentration of 60% (w/v) Me_2SO to vitrify a volume of 400ml CPA solution using automatic LT was insufficient to prevent devitrification. An increase to 62.5% (w/v) was needed to prevent any visual ice formation. However this was insufficient for the same solution with addition of 200ml of alginate beads. By visual inspection it was observed that beads became opaque during the warming process before the ice started to form in the surrounding solution, obviously reacting as a nucleation centre. To avoid devitrification the final CPA concentration had to be increased to 64% (w/v). Stirring could not be carried out at temperatures below -40˚C for Me_2SO (<-35˚C for CPA No.18) due to increased CPA viscosity. As the temperature was gradually decreased, a gradual CPA increase had to be followed which resulted in a stronger deviation of the CfgPid curve from the liquidus curve (Figure 6.10).

A.

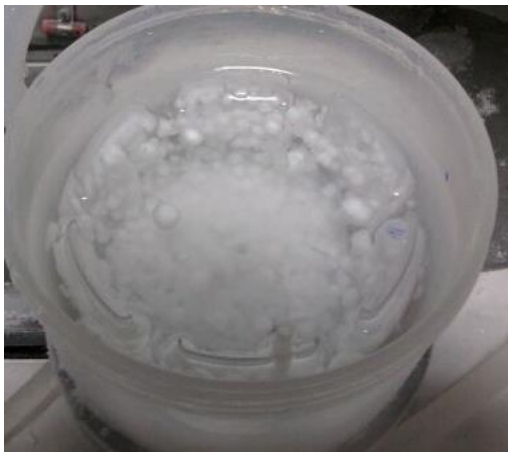

B.

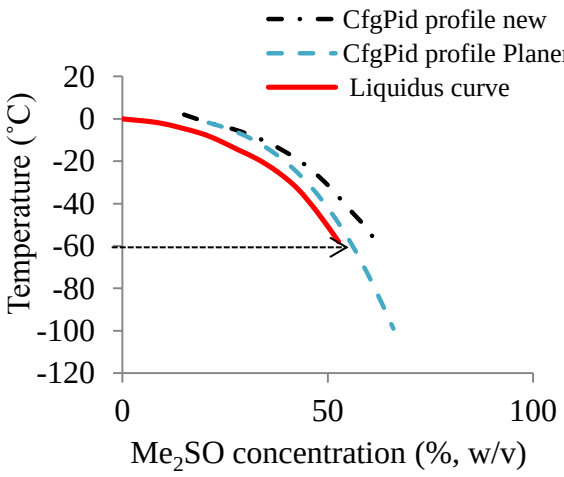

Figure 6.10 Devitrification during the warming process

Figure A shows the sample carrier filled with 60% Me_2SO (w/v) that was cooled down to -130˚C. Ice formed during the warming process (at room temperature) when the sample temperature was between -90˚C and -60˚C. The CPA concentration for samples with beads had to be increase to 64% (w/v) Me_2SO to prevent devitrificatio. Figure B shows the change made to the original CfgPid profile (dashed line in blue) used by Planer. The final inlet temperature was maintained at -60˚C while the Me_2SO concentration was gradually increased (dashed line in black), resulting in a stronger deviation to the Me_2SO liquidus curve (line in red).

6.4.3 Liquidus Tracking temperature measure

The concept of Liquidus Tracking (LT) is to keep temperature and concentration of the CPA solution close to its liquidus curve to minimize CPA toxicity. However, once thermocouples were used to measure the temperature of inlet, outlet and sample solution, it became evident that the temperature of the sample differed by more than 15˚C from the temperature of the programmed profile (CfgPid curve) and was approximately 20˚C higher than the temperature of the liquidus curve. These results were achieved with a freezer cooling rate of -0.5˚C/minute. A freezer cooling rate of -0.1˚C/minute had previously been used to predict the temperature difference between freezer and sample. The predicted sample temperature was displayed by the controller and was seen to conform to the programmed CfgPid curve (Figure 6.11).

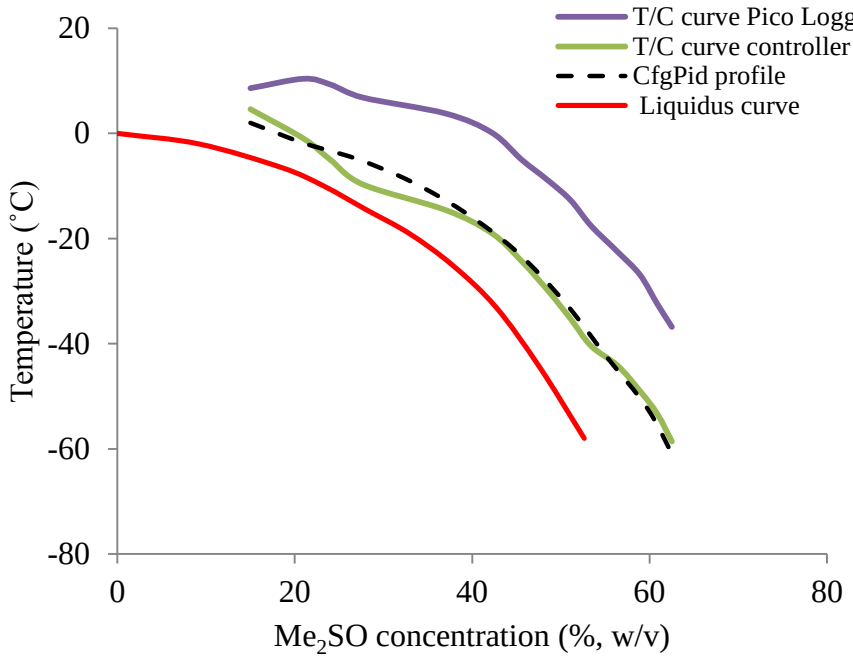

Figure 6.11 CfgPid curve and sample T/C curve temperature difference

The graph shows the difference between the programmed CfgPid curve (dashed black line) and the temperature/concentration (T/C) curve obtained when measuring the temperature inside the sample carrier (purple line -Pico Logger). The measured Me_2SO concentration but in correlation with the temperature displayed by the controller (green line -controller)) overlaped with the programmed concentration (CfgPid curve). The temperature difference between the T/C Pico Logger curve and the CfgPid curve reached from initially 10˚C to finally 20˚C.

6.4.4 Reducing the temperature difference between liquidus curve and temperature/concentration curve

Without the option to change the volume of the sample and the geometry of the sample carrier, the only way to increase the sample cooling rate and to run a T/C profile closer to the liquidus curve was to reduce the freezer temperature. This was done by defining lower target temperatures for the same CPA concentrations in the temperature/concentration table of the CfgPid software tool. Over the first runs the freezer temperature was reduced by first 4˚C and then 6˚C in respect to the starting profile (A-1), while the freezer temperature was kept above the liquidus curve of Me_2SO. The changes only had a marginal impact on the sample cooling rate - the difference to the liquidus curve remained above 18˚C (Figure 6.12 A).

Subsequently the freezer temperature was set 20˚C below the temperature of the CfgPid A-1 profile and up to 10˚C below the Me_2SO liquidus curve (B-1). The solution inside the outlet tube froze at a freezer temperature of -47˚C. The freezer temperature was therefore increased above the liquidus curve of Me_2SO once the freezer reached a temperature of -44˚C (B-2). Additionally the outlet tube was isolated which helped to increase the temperature by approximately +5˚C in respect to the freezer temperature. The implemented measures did not prevent the outlet tube from freezing. This was finally achieved by further increasing the freezer temperature (B-3) in respect to the B-2 profile (Figure 6.12 A). However, the T/C curve achieved with CfgPid B-3 was only 5˚C closer to the Me_2SO liquidus curve than the T/C curve of the starting CfgPid profile A-1 (Figure 6.13).

A.

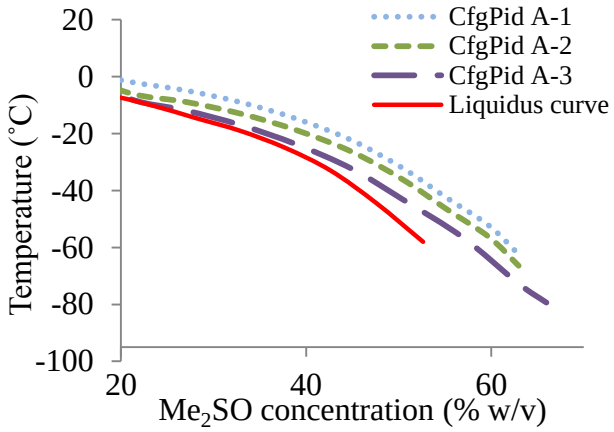

Table to Figure 6.11 A

run	change	Temp. difference sample to liquidus curve
A-1	Starting CfgPid curve	approx. 20˚C
A-2	CfgPid curve set 4˚C below A-1 curve	approx. 18˚C
A-3	CfgPid curve set 6˚C below A-1 curve	approx. 18˚C

B.

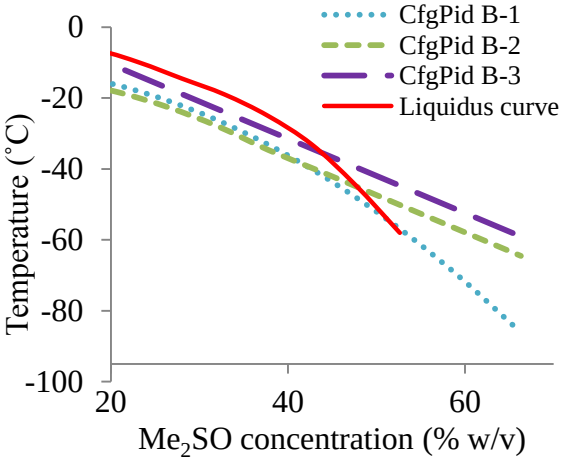

Table to Figure 6.11 B

run	change	result
B-1	-20˚C below CfgPid A-1 and below liquidus curve	Outlet tube freezing at the end of the run
B-2	As B-1but higher temperature at the end of the run	Outlet tube freezing
B-3	+8˚C above CfgPid B-1 below liquidus curve	No outlet tube freezing 5˚C to 30˚C above the liquidus curve

Figure 6.12 LT temperature/CPA concentration profiles

Figure A and B show CfgPid profiles that were used for automatic LT. Figure A: The freezer temperature was programmed to remain above the liquidus curve of Me_2SO. The freezer temperature was reduced (A-2 and A-3) to obtain a T/C curve that runs closer to the Me_2SO liquidus curve. Figure B: The freezer temperature was programmed to be below or partially below the Me_2SO liquidus curve. Using the profile CfgPid B-1 and B-2 resulted in outlet tube freezing. CfgPid B-3 was the profile with the lowest possible temperature that would not lead to outlet tube freezing. Table A and B summarize changes and outcome of changes made to the CfgPid profiles.

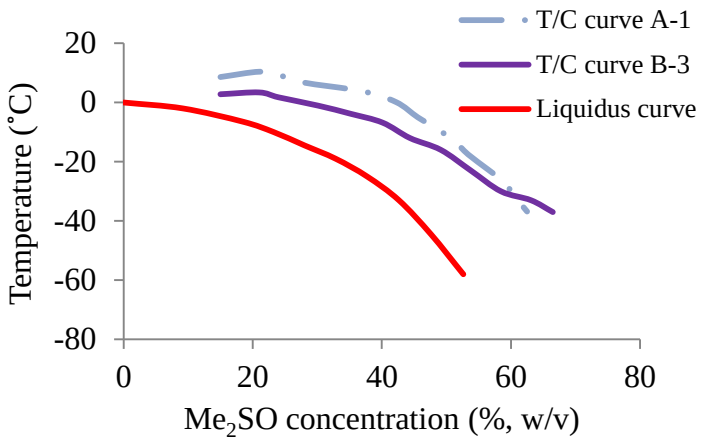

Figure 6.13 Temperature/concentration curve achieved with LT CfgPid profile A-1 and B-3

The graph shows the T/C curves achieved with Cfgpid profile A-1 and B-3. T/C curve B-3 (light blue dashed line) ran approximately 5˚C below the T/C curve A-1 (purple line). At a concentration of 50% Me_2SO (w/v) the temperature difference started to equalize. T/C curve B-3 remained 5˚C to 30˚C (from 15 to 65% (w/v) Me_2SO) above the liquidus curve of Me_2SO.

6.4.5 The combined manual/automatic Liquidus Tracking approach

Outlet tube freezing occurred when the freezer temperature fell below the melting point of the solution held inside the tube. The solution inside the sample carrier was not affected due to lower cooling rates, which were a result of the higher sample volume and the sample carrier geometry. The solution inside the inlet tube remained liquid, as it contained much higher concentrations of CPA. To prevent the outlet tube from freezing a combined manual and automatic approach was used. The outlet tube was primed with a highly concentrated CPA solution and was not used for the first four inlet cycles. The CPA concentration was increased manually by operating the pumps once the required sample temperature was reached. This way the T/C curve was kept close to the liquidus curve of the CPA solution especially at the beginning of the run (Figure 6.14).

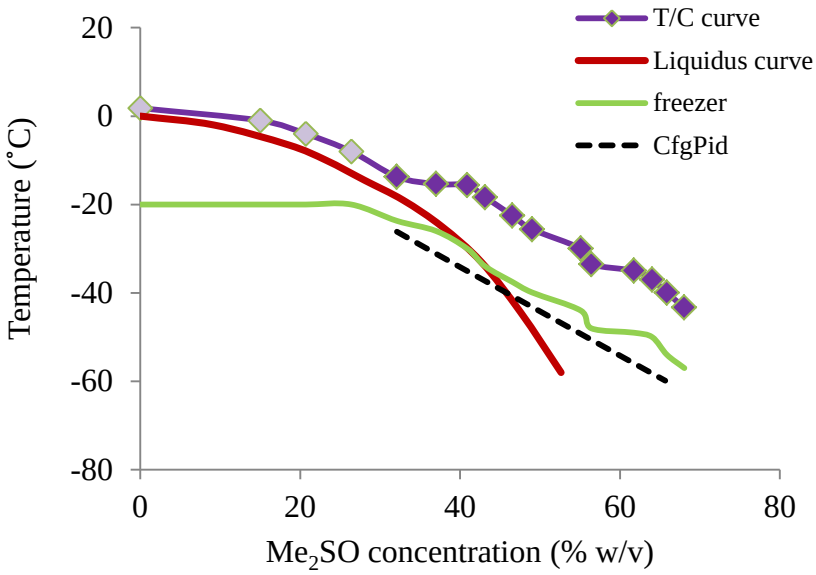

Figure 6.14 Combined manual and automatic LT

To increase the cooling rate of the sample inside the sample carrier the freezer temperature was set to -20˚C. The CPA concentration was increased manually over four inlet cycles (squares in grey) until a concentration of approximately 37% (w/v) CPA at -17˚C was reached, without operating the outlet pump to avoid outlet tube freezing. The automatic process (purple squares) was started to increase the CPA concentration from 37% to 65% CPA (w/v) by using a linear CfgPid profile (dashed black line). This way the sample T/C curve followed closely the Me_2SO liquidus curve (red curve).

6.4.6 Combined manual/automatic Liquidus Tracking temperature profile

As a means to increase the sample cooling rate the freezer temperature was set to -20˚C while the manual inlet cycles were carried out. Due to the inlet tube lengths of six meters the inlet solution cooled down to the freezer temperature before passing the inlet port even at high inlet pump rates (up to 140ml/minute). The CPA solution inside the sample carrier cooled down as a result of the inlet solution temperature of -20˚C and as a result of the temperature difference between the freezer and the sample. Once manual inlet cycles were finished, automatic LT with a freezer cooling rate of -0.5˚C/minute was started. The freezer temperature was kept at -60˚C for 20 minutes to provide sufficient mixing before the freezer was set to -160˚C, which as a consequence increased the sample cooling rate to -3˚C/minute (from -40˚C to -125˚C). The outlet was not used until the automatic profile was started and therefore the temperature was the

same as the freezer temperature. Once the outlet was started, the sample solution which was of higher temperature increased the temperature inside the outlet tube. This, and the insolation around the outlet tube which helped to decrease the cooling rate, maintained the temperature above the solution's melting point (Figure 6.15).

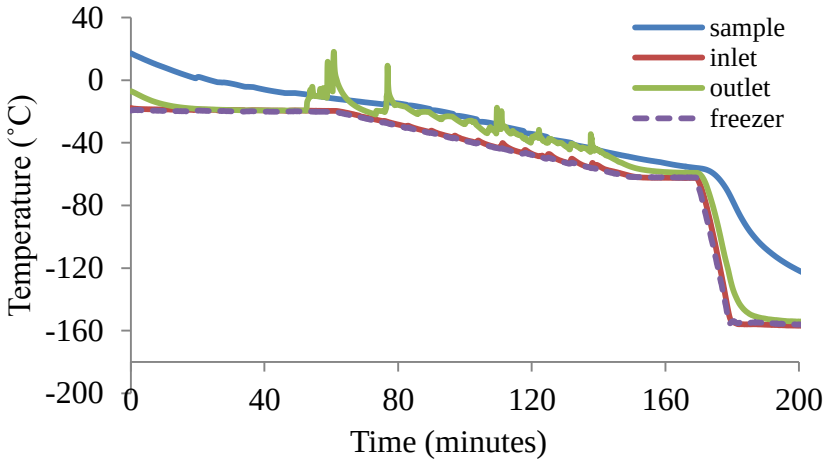

Figure 6.15 Combined manual/automatic LT temperature profile

The graph shows the freezer, inlet, outlet and sample temperature profiles of a typical manual/automatic LT run. The freezer temperature (dashed blue line) was kept at -20˚C until the automatic profile with a freezer cooling rate of -0.5˚C/minute was started. The sample temperature (blue line) decreased almost linear with an average cooling rate of -0.5˚C/minute until a temperature of -50˚C was reached, then the cooling rate increased in response to the increased freezer cooling rate (-10˚C/minute) to -3˚C/minute. The temperature of the inlet solution (red line) closely followed the freezer temperature curve. The temperature of the outlet solution (green line) increased each time solution was extracted and then followed a faster cooling rate than the freezer, however remained above the Me_2SO liquidus curve throughout the run.

6.4.7 First runs with dimethyl sulfoxide and CPA solution No.18

First LT runs using the combined set-up with AELC using Me_2SO as a single CPA resulted in no post-warming cell viability. When the newly developed CPA solution CPA No.18 (Chapter 5) was used, cell viability was increased to approximately 40% (Figure 6.16).

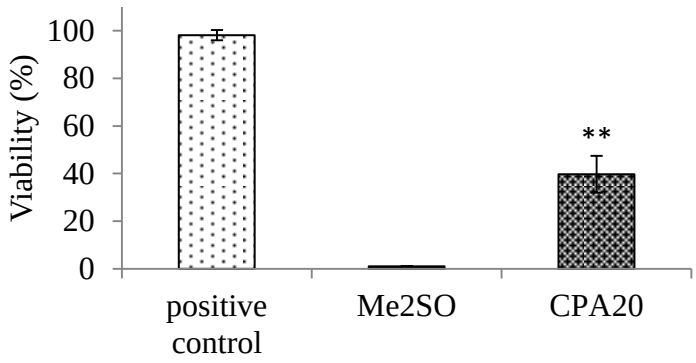

Figure 6.16 Automatic Liquidus Tracking-Me_2SO vs. CPA No.18

Cell viability increased from 1.0% +/- 0.1 to 40% +/- 7.7 when combined manual/automatic LT was carried out using CPA No.18 instead of Me_2SO. After cooling to -40˚C, aliquots of 2.5ml were immediately vitrified (6.3.3.1). A two-step warming protocol (from 65% to 44% (w/v) CPA at -20˚C, then to 20% (w/v) glucose at 0.5˚C) was used and AELC were cultured for 24 hours in complete media at 37˚C before measuring viability. Data are n=3 +/- SD **p<0.01.

6.5 Discussion

The first part of this chapter was to install the Liquidus Tracker and to run the Planer Liquidus Tracking (LT) cooling protocol. This pre-set method uses high concentrated dimethyl sulfoxide (80% (w/v) Me_2SO) to increase the sample CPA concentration (single solution mode). It is important to mention that this standard method but also the design of the stirrer and the sample carrier were developed to meet the requirements for cryopreserving larger constructs, and in particular articular cartilage (connected to chunks of bones). Me_2SO was chosen as a single cryoprotectant as promising results had previously been achieved for cartilage preservation using manual LT (Pegg et al., 2006; Wang et al., 2007). Thus, Me_2SO was used by Planer to develop the pump and stirring system and the LT cooling protocol.

One of the main issues for the development of the Liquidus Tracker was the increasing viscosity of Me_2SO at decreasing temperatures. Pump cycles had to be adjusted as it was shown that the extraction cycle at low subzero temperatures became increasingly inaccurate. The outlet time was therefore set to 180 seconds - three times longer than the inlet cycle - to allow a slower pump rate and reduce air bubbles that were distorting the extraction volume. The minimum temperature at which the stirrer operated flawlessly in respect to viscosity had been defined and translated to the temperature and concentration profile (CfgPid table) the sample was supposed to follow. To avoid the need to re-develop these parameters, viscosity was selected as the first limiting factor when a new CPA solution (CPA No.18 - Chapter 5) was developed.

Although manual LT experiments (Chapter 4) already demonstrated better suitability of CPA No.18 to cryopreserve AELC, Me_2SO was used to improve the LT system. On the one hand as it had been used by Planer for the development of the LT system, but also because the preparation was faster (no dilution of glucose), it was cheaper and the solution could easily be reused by simply adding more Me_2SO until the required concentration (measured with the refractometer) was reached. As for the large amounts of CPA needed for one LT run (approximately 1l of 80% (w/v) CPA) and the numerous LT runs that were carried out, this was a considerable time and cost-saving measure.

Contrary to larger constructs for which the system had been designed, alginate beads are not held in a fixed position, which made it necessary to introduce a filter system. The first filter, of the size of the outlet port (d=0.5cm) and directly attached to the outlet port opening was blocked with beads shortly after the start of the LT cooling procedure. Initially it was tried to unblock the filter by occasionally reversing the outlet flow, however the success was limited due to the following reasons: firstly the original filter area was small in comparison to the number of beads (approximately 300ml of settled beads) and the volume that had to be extracted (up to 140ml in 3 minutes). Secondly alginate beads became increasingly sticky at higher CPA concentrations. Thus, to overcome filter blockage the filter area was substantially increased whilst the mesh was hold several centimetres away from the opening of the outlet port. With several centimetres and solution between the opening of the port and the filter, the suction was distributed more evenly over the whole mesh. As a result suction per filter area was reduced sufficiently to allow the cross-flow produced by the stirring system to keep the filter free of beads. Due to the geometry of the stirrer, space inside the sample carrier was limited, which restricted the size of the filter system. To increase the filter area, two meshes, connected with a plastic ring, one above and one below the outlet port opening, were used.

A surprising but positive effect encountered with CPA solution No.18 in comparison to Me_2SO was that beads were less sticky at high CPA concentrations. This was advantageous in respect to outlet filter blockage and the filter area needed. This is also an important aspect in terms of upscaling. In order to keep the same cooling rate much higher volumes have to be pumped though the system, as cooling will mainly be achieved by the low temperature of the inlet solution (convection) and not by conduction (heat transfer from sample to sample carrier to the freezer). This means that the filter system has to be substantially increased though with the requirement not to interfere with the stirrer system.

One of the main issues that was encountered when using the pre-set Planer method was the substantial difference between the freezer cooling rate and the cooling rate of the sample solution inside the sample carrier. First runs performed with the Planer standard CfgPid profile for Me_2SO with a freezer cooling rate of -0.5˚C/minute resulted in a

temperature offset from the melting point by +20˚C, which meant that an already critical Me_2SO concentration of 40% (w/v) (melting point of -25˚C) was reached at 0˚C. In an attempt to increase the sample cooling rate, the freezer temperature was decreased and set closer to the Me_2SO liquidus curve. At first the freezer temperature was maintained above the temperature of the sample liquidus curve, but the effect on the sample cooling rate was negligible. In a different approach the freezer temperature was set 15˚C below the sample liquidus curve to maintain the sample temperature 5˚C above its melting point to avoid any freezing inside the sample carrier. The sample solution remained liquid but ice formed inside the outlet tub, so that the experiment had to be stopped. The solution inside the outlet tube being from the previous extraction cycle contained the lowest CPA concentration within the LT system; however the cooling rate inside the tube was comparable to the freezer cooling rate due to the tube geometry and material. Insolating the outlet tube reduced the cooling rate but did not prevent freezing, manual priming the outlet tube after each extraction cycle with high concentrated CPA strongly interfered with the automatic program and again did only delay freezing but would not completely prevent it. As a consequence the freezer temperature was increased until outlet freezing was avoided, but the sample cooling rate that was achieved with the new CfgPid profile was comparable to the original Planer profile.

AELC incubated in CPA concentrations of up to 55% (v/v) demonstrated high survival rates when the incubation temperature was set to -10˚C or -20˚C (Chapter 4). Thus, the conclusion was drawn that it was especially important at the begging of the cooling process - at temperature above -10˚C - to keep the sample temperature close its melting point. To prevent the outlet tube from freezing a combined manual and automatic approach was used. The outlet tube was primed with a high concentrated CPA solution and was not used for the first four inlet cycles until a concentration of 35% (w/v) and a temperature of -12˚C were reached. The CPA concentration was increased manually by operating the pumps once the required sample temperature was reached. This way the sample temperature was kept close to its melting point (liquidus curve) and outlet freezing was avoided.

Although the combined manual/automatic LT kept the sample temperature/concentration curve close to the liquidus curve and despite the fact that

automatic LT increased the CPA concentration continuously and without the temperature fluctuation seen for manual LT, no viability was detected when Me_2SO was used as a single CPA. However when Me_2SO was replaced with the newly developed CPA No.18 solution (Chapter 5) viability was increased to approximately 40%.

6.6 Conclusion

The Liquids Tracker was set-up and a new LT protocol of faster sample cooling rate as well as a filter system was established and tested. Viability was increased from 0% to 40% post-warming by using the newly developed CPA solution No18 instead of Me2SO. Despite these improvements, recovery is insufficient for AELC to be used within a bioartificial liver device. Therefore, the aim of the next chapter was to identify other mechanisms to improve recovery and in addition, to establish the warming protocol, so that the complete LT process, including cooling, vitrification and warming, could be tested.

CHAPTER 7
Automatic Liquidus Tracking

7.1 Introduction

In Chapter 6 it was described how the Liquidus Tracker was set up and the system was adapted for the use of encapsulated liver cells (AELC). Apart from installing a filter system to retain AELC in the sample carrier, the cooling rate was increased so that the sample would run closer to the samples liquidus curve. Nevertheless, no post-warming viability was detected when Me_2SO was used to vitrifiy AELC. Viability increased to 40% when the newly developed cryoprotectants agent (CPA) solution No.18 (Chapter 5) was used instead. However recovery was still too low for a potential use of AELC in a bioartificial liver device.

Further possibilities to increase cell recovery could be the use of organ preservation solutions like Viaspan (University of Wisconsin solution) or HTK instead of PBS as a CPA carrier solution. Those solutions were designed to reduce chilling injury during hypothermic storage and could therefore be useful to maintain cell viability through the lengthy LT cooling and warming process. Additionally important is to investigate whether sufficient CPA penetration is provided during the cooling process and what effect stirring has on cell survival.

7.2 Aims

The aim of this chapter was to identify other potential mechanisms to increase cell recovery following cryopreservation. For this a simplified manual Liquidus Tracking (LT) procedure to pre-test conditions for automatic LT was established. Finally the automatic warming LT process had to be established in order to test the complete LT process including cooling and vitrification on warming.

7.3 Methods and Materials

7.3.1 The 50-60-66% CPA inlet

Materials

Liquidus Tracker *(Planer plc)*

CPA No.18 *(see Chapter 5)*

1xPBS with Mg^{2+} and Ca^{2+} *(Sigma, Cat. No. D8662)*

15ml Centrifuge tubes

AELC

Method

AELC in 280ml of PBS were added to the sample carrier and both inlet and outlet were primed with 50% (w/v) CPA.

Delta T program:

Freezer start temperature was set to 1˚C (on hold)

Manual inlet:

First 50% (wv) CPA was manually pumped in until a sample concentration of 40% (w/v) was reached. Then a 60% (w/v) CPA solution was used to increase the sampel to 50% (w/v) and finally a 66% CPA solution was added to reach a final sample concentration of 65% (w/v) (for details see Appendix 7.3.1).

7.3.2 Automatic Liquidus Tracking warming

Materials

Liquidus Tracker *(Planer plc)*

vitrified AELC

CPA No.18 *(see Chapter 5)*

1xPBS with Mg^{2+} and Ca^{2+} *(Sigma, Cat. No. D8662)*

7.3.2.1 The single solution reverse mode

Method

Vitrified AELC were added to a pre-cooled solution (-25˚C) of 65% (w/v) CPA No.18. The freezer temperature was set to -25˚C. Once the sample (volume 400ml at 65% (w/v)

CPA No.18) reached a temperature of -25˚C, manually 60ml PBS (at room temperature) were pumped through the outlet port into the sample carrier. The outlet port with a inside freezer tube length of 40cm (inlet tube length = 6m), was used to avoid any freezing while pumping in PBS at subzero temperatures. An inlet pump speed of 20ml/minute was used. After one minute of stirring, 60ml were pumped out to prevent the outlet port from freezing, to reduce the sample volume and to measure the refraction index. During the addition the temperature increased and time was given until the temperature decreased again (Table 7.1). The warming procedure, when started at -25˚C took approximately one hour.

Table 7.1 One solution mode warming protocol

Freezer temperature	Sample temperature		CPA concentration (%, w/v)
-25˚C	-25˚C		65
-25˚C	-17˚C	Inlet of 60ml 1xPBS	57
-25˚C	-22˚C	Wait 12 minutes	57
-25˚C	-16˚C	Inlet of 60ml 1xPBS	49
-25˚C	-20˚C	Wait 12 minutes	49
-25˚C	-13˚C	Inlet of 60ml 1xPBS	42
-25˚C	-20˚C	Wait 12 minutes	36
-25˚C	-13˚C	Inlet of 60ml 1xPBS	30
-10˚C	-13˚C	Continuous inlet until a CPA concentration of 0% and temperature of 10˚C was reached.	

Finally 0.25ml of beads were added to a cell strainer and washed three times with fresh 1xPBS (ice-cold) to remove all CPA. Finally AELC were incubated in 8ml of complete media at 37˚C until measurement.

7.3.2.2 The four step reverse mode

Method

The freezer was set to -25˚C to warm up the sample temperature. Once the sample had reached a temperature of -35˚C the stirrer was started. The CPA solution inside the inlet tube was extracted and the tube was primed with 150ml of a 50% (w/v) CPA No.18 solution. The freezer was set to -30˚C and the inlet was started once the inlet temperature had reached -30˚C. The inlet and outlet speed were set to 20ml/minute if not otherwise noted. After the addition of 250ml 50% (w/v) CPA No.18, the freezer temperature was set to -25˚C while the remaining 250ml of the 50% (w/v) CPA No.18 solution was added. This helped to increase the sample temperature to approximately -25˚C. The freezer was set to -20˚C and 40% (w/v) CPA No.18 was added. After the addition of 250ml the freezer temperature was set to -15˚C while the remaining 250ml were added. This helped to increase the sample temperature to approximately -15˚C. After the addition of 250ml 30% (w/v) CPA No.18, the freezer temperature was set to -10˚C while the remaining 250ml of the 30% (w/v) CPA No.18

solution was added. The sample temperature increased to approximately -10˚C and 1L PBS hold at room temperature was added at an inlet speed of 40ml/minute. The outlet speed was also increased to 40ml/minute.

7.3.3 The complete Liquidus Tracking procedure

The LT process was divided into: LT cooling to -40˚C (cooling rate -0.5˚C CPA increase from 0% to 65% (w/v), fast cooling to -125˚C (below the expected glass transition point), slow warming to -95˚C, in order to obtain a homogenous temperature across the sample before the fast warming phase was started, fast warming to -40˚C and the LT reverse warming process from -40˚C to >4˚C (CPA decrease from 65% to 0% (w/v). When the vitrification cooling step was included the whole process was carried out, as otherwise the sample carrier had to be disconnected from the inlet, outlet and overflow tube and be taken out from the sample holder. As this included additional challenges, the whole process was followed in the one run. The amount of one liquid nitrogen drewar (35L) was insufficient to support the entire process. Therefore the tank was disconnected from the controlled rate freezer to be re-filled, once the sample had reached a temperature of -125˚C and the warming process was started. Slow cooling (warming rate +0.35˚C/minute) was obtained by disconnecting the liquid nitrogen tank from the freezer and keeping the freezer lid closed. Slow warming was chosen until -95˚C to equilibrate the temperature across the sample carrier before the freezer temperature was set to -25˚C. The reason for this was that devitrification had been observed at a temperature range between -95˚C and -60˚C, consequently a faster warming rate was chosen for temperature above -95˚C. At -40˚C the reverse LT warming process was started by putting the stirrer in operation (Figure 7.1).

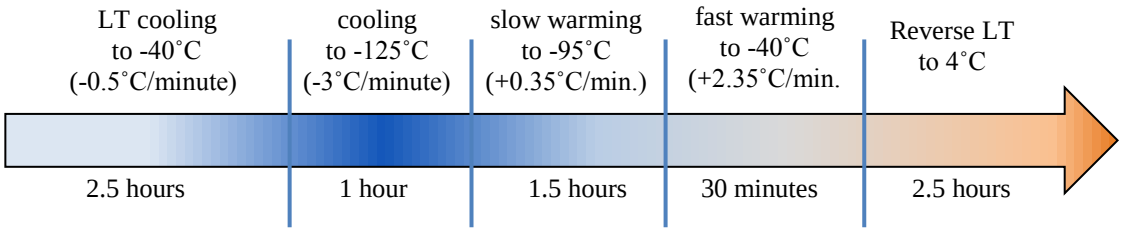

Figure 7.1 Complete LT process

The complete LT process consisting of: LT cooling to -50˚C, (duration: 2.5 hours), fast cooling to -125˚C (duration: 1 hour), slow warming to -95˚C (duration: 1.5 hours), fast warming to -40˚C (duration: 30 minutes) and LT reverse warming process (duration 2.5 hours).

7.3.4 Manual two-step Liquids Tracking

Materials

Liquidus Tracker *(Planer plc)*

AELC

15ml Centrifuge tubes

50ml Centrifuge tubes

100 um cell strainers *(BD Bioscience, Cat. No. 352360)*

Ethanol *(Fisher Chemicals, Cat. No. E/650DF/17)*

1xPBS with Mg^{2+} and Ca^{2+} *(Sigma, Cat. No. D8662)*

CPA No.18 *(see Chapter 5)*

for CPA No.18 variations:

Me_2SO *(Sigma, Cat. No. 154938)*

Ethylene Glycol *(Sigma, Cat. No. 293237)*

D+ glucose *(Sigma, Cat. No. 66152)*

D+ Trehalose *(Sigma, Cat. No. T95531)*

D+ Raffinose *(Sigma, Cat. No. 83400)*

D+ glucose *(Sigma, Cat. No. 66152)*

Sucrose *(BDH, Cat. No. 102745C)*

for sample carrier variations:

HEPES *(Gibco, Cat. No.15630)*

ViaSpan = UW solution: Belzer Germany

HTK

for pre-incubation experiments:

Alginic acid albumin *(Sigma, Cat. No. A2033)*

L-Proline *(Sigma, Cat. No. P0380)*

D+ Trehalose *(Sigma, Cat. No. T95531)*

Culture media (see Chapter 2)

Method

In order to process several samples at the same time and to pre-test conditions for automatic LT, a two-step manual cooling and warming protocol proved to be more practical than a multi-step manual LT protocol as used in Chapter 4 (manual LT) (for details see Appendix 7.3.4).

7.4 Results

7.4.1 Pre-testing conditions with manual Liquidus Tracking

Although the usage of CPA No.18 substantially improved cell recovery, viability was still low (40%). To increase post-warming viability several measures were taken. In a first attempt the concentration of the non-penetrating CPA glucose was increased while the penetrating CPA concentration (Me_2SO) was decreased. When AELC were incubated for one hour at a temperature of 0.5˚C, cell viability was significantly higher in comparison to CPA No.18 but recovery was significantly lower when AELC were vitrified using the two-step manual LT protocol (Figure 7.2), but also when the automatic LT approach was used (Figure 7.3). Different results between the test systems pointed out the necessity of including the vitrification step in the cooling procedure when evaluating CPAs and sample carrier composition. As automatic LT was not suitable to screen a variety of different conditions, the two-step manual LT approach was used.

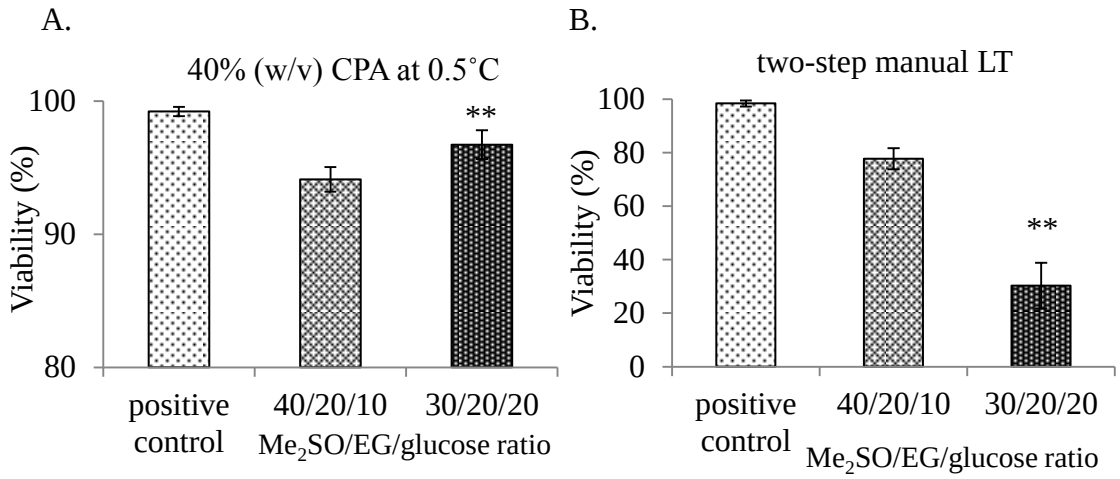

Figure 7.2 Decreased Me_2SO and increased glucose concentration

A.) AELC incubation in CPA No.18 (Me_2SO/EG/glucose ratio 40/20/10) for 1h at 0.5˚C was more toxic than a CPA solution with a ratio of 30/20/10 (Me_2SO/EG/glucose ratio). Data was n=5+/-SD, **p<0.01. B.) Using a two-step manual LT protocol (from 0% to 40% (w/v) CPA at 0.5˚C, then to 65% (w/v) at -20˚C, to LN at -40˚C; warming: from 65% to 44% (w/v) CPA at -22˚C, then to 20% (w/v) glucose at 0.5˚C), indicated significantly better post-warming results for CPA No.18 than for a

Me_2SO/EG/glucose solution with a ratio 30/10/20. Data was n=5+/-SD, **p<0.01. A. and B: AELC were cultured for 24 hours in complete media at 37˚C before measuring viability.

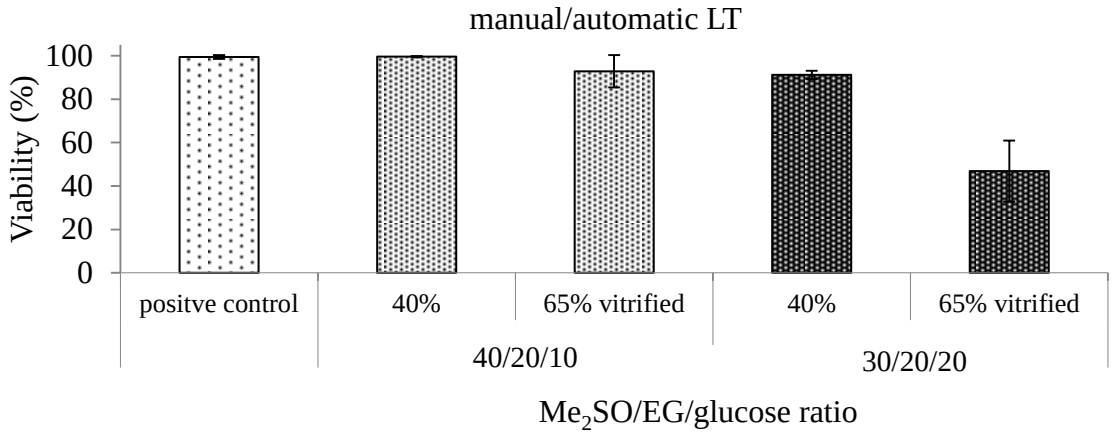

Figure 7.3 Automatic LT-decreased Me_2SO and increased glucose concentration

AELC vitrified using the combined manual/automatic LT approach showed much lower viability when the new CPA solution (Me_2SO/EG/glucose ratio 30/20/20) was used instead of CPA No.18 (ratio of 40/20/10). Each condition was tested once. Five sample were taken after the increase to 40% CPA (w/v) and five samples were vitrified at -40˚C at a concentration of 65% (w/v) (n=5 +/-SD). Non-vitrified samples were warmed within one step (directly to 20% glucose at 0.5˚C). Vitrified samples were warmed in a two-step warming protocol (from 65% to 44% (w/v) CPA at -22˚C, then to 20% (w/v) glucose at 0.5˚C). AELC were cultured for 24 hours in complete media at 37˚C before measuring viability.

In Chapter 5 it was shown that the combination of two sugars showed better cell recovery than the use of a single sugar when the incubation was carried out at 0.5˚C, however, no improvement was observed when the three best glucose combinations (glucose-trehalose, glucose-raffinose and glucose-sucrose) were compared in a two-step manual LT set-up. Exchanging 1xPBS with ViaSpan, HTK (Histidine-tryptophan-ketoglutarate) or HEPES buffer did not show any improvement either. Adding 40mM proline to the culture media 24 hours pre-testing slightly decreased cell viability while the addition of 30mM (w/v) trehalose and an increased concentration of linoleic acid-albumin by 2.5-fold (8.75mM) in the culture media increased cell viability slightly, but not statistically significantly. As no substantial improvements were noted, none of the conditions was re-tested using the automatic LT approach (Figure 7.4).

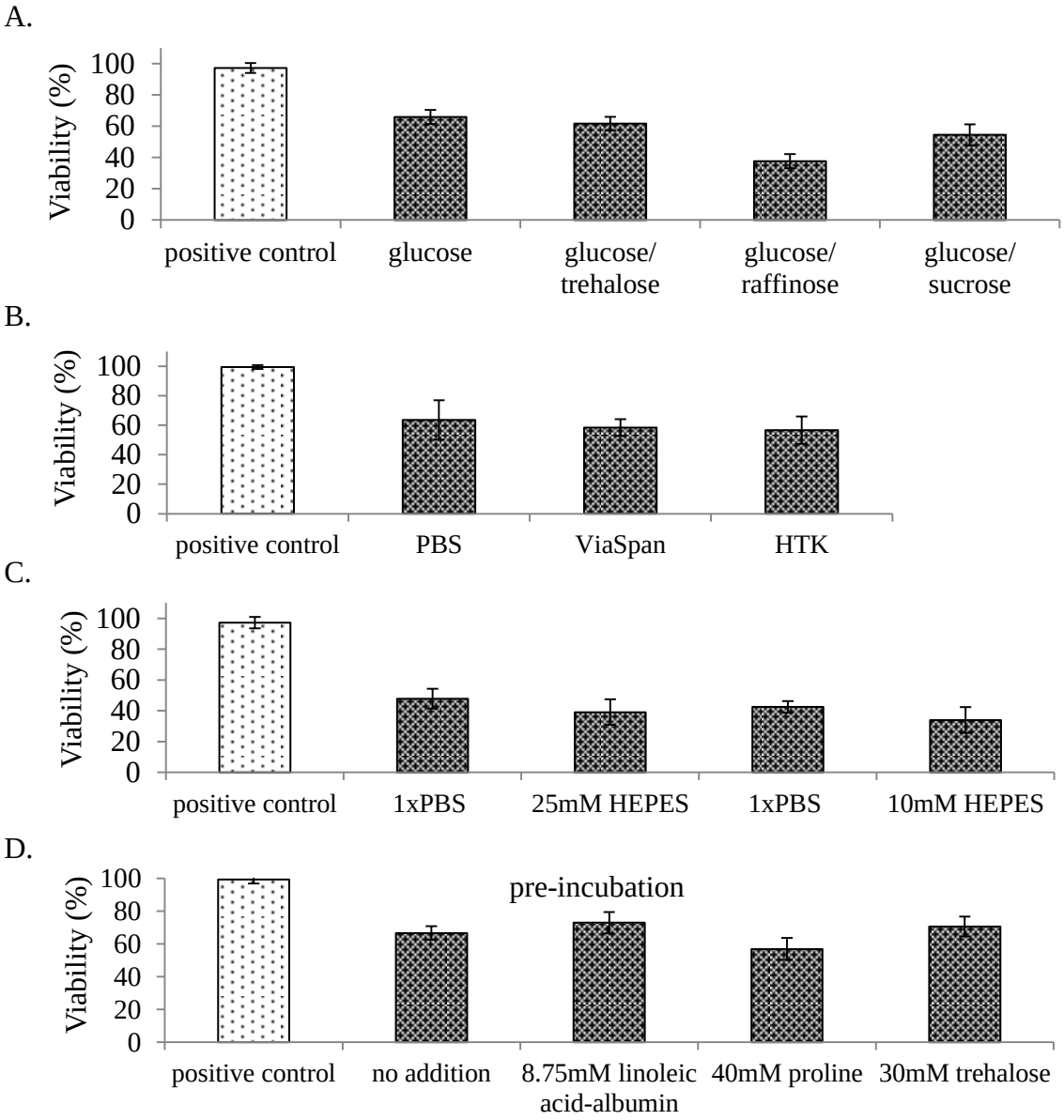

Figure 7.4 Pre-test of CPA No.18 variations, sample carrier solutions, pre-incubation additives

Two-step manual LT (from 0% CPA to 40% CPA at 0.5˚C, then to 65% at -20˚C, to LN at -40˚C) was used to pre-evaluate sugars, buffers and pre-incubation additives. After warming (from 65% CPA to 45% CPA at -22˚C, then to 20% glucose at 0.5˚C), AELC were cultured for 24 hours in complete media at 37˚C before measuring viability. Graph A: Glucose alone or in combination with trehalose, sucrose or raffinose was used as a penetrating CPA for CPA No.18 (same w/v concentration for both sugars, Me_2SO/EG/sugar ratio was 40/20/10). Graph B: As a CPA carrier 1xPBS, ViaSpan or HTK was used. Graph C: As a buffer 1XPBS, 10mM and 25mM HEPES was used. Graph D: AELC were cultured in complete media for 24 hours prior testing, containing either 8.75mM linoleic acid-albumin, 40mM proline or 30mM trehalose. Changes made to the standard condition (CPA No.18 with 1xPBS) did not significantly improved post-warming viability. Data was n=5 +/-SD.

7.4.2 Minimum CPA addition and inlet temperature

The usage of different sugars and buffers or the pre-incubation in sugars and proteins did not improve LT cell survival. Another consideration was therefore that the temperature of the sample was too low to provide sufficient CPA penetration to prevent intracellular ice formation or that the CPA toxicity was still too high. Two-step manual LT was used to determine whether the CPA addition temperature had an effect on cell recovery. AELC first incubated in 40% and 50% CPA No.18 (w/v) at 0.5˚C (for 5 minutes) were cooled at -2˚C/minute to -11˚C, -16˚C and -22˚C and to -22˚C, -27˚C and -33˚C, respectively before the CPA concentration was increased to 65%. Subsequently samples were cooled to -40˚C at -1˚C/minute before they were vitrified in liquid nitrogen. Cell recovery increased significantly at lower CPA addition temperatures from -11˚C to -22˚C, but remained equal between -22˚C and -27˚C and was reduced at -33˚C (Figure 7.5). Similar results were obtained for automatic LT. In a first experiment cell recovery was lower when the minimum inlet temperature was set to -15˚C, increased when set to -25˚C and clearly decreased at -37˚C. In a second experiment slightly lower viability was measured when the minimum inlet temperature was set to -33˚C instead to -25˚C (Figure 7.6).

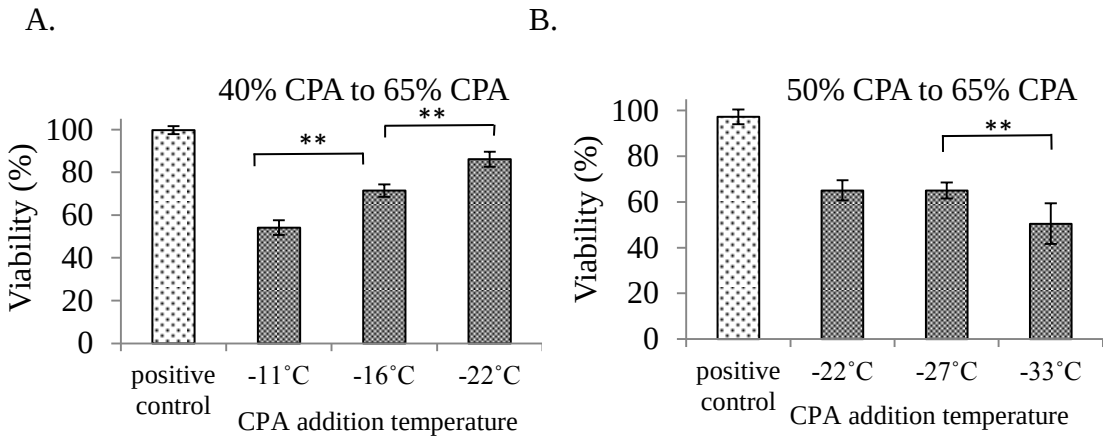

Figure 7.5 Final CPA addition temperature – manual LT

Graph A and B: CPA concentration was increased from 0% to 40% or 0% to 50% (w/v) CPA No.18 at 0.5˚C. Samples were then cooled at -2˚/minute to -11˚C, -16˚C and -22˚C or -22˚C, -27˚C and -33˚C, respectively, before the CPA concentration was increased to 65% (w/v) CPA No.18. Finally samples were cooled to -40˚C at -2˚/minute and introduced into LN. Viability significantly increased from -11˚C to -16˚C and from -16˚C to -22˚C, but was significantly reduced at -33˚C (n=5+/- SD p<0.01). AELC were cultured for 24 hours in complete media at 37˚C before measuring viability.**

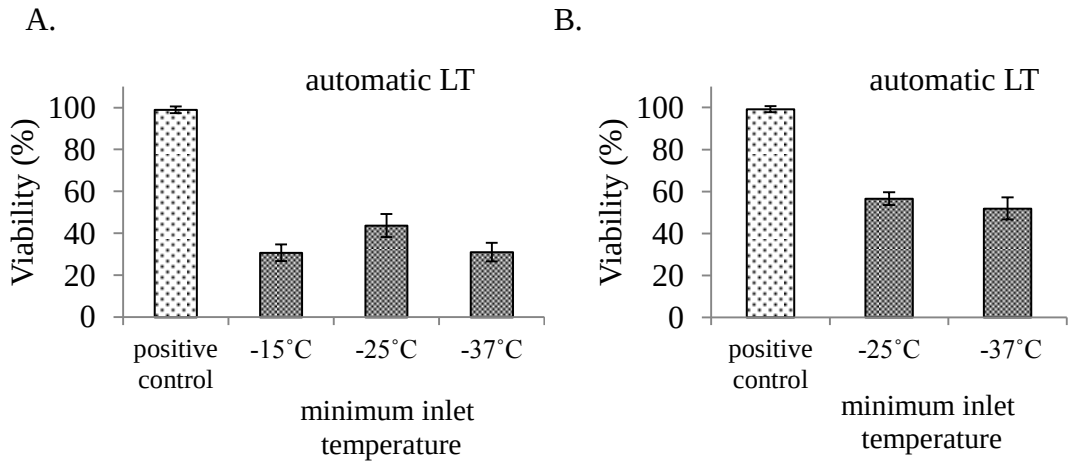

Figure 7.6 Final CPA addition temperature – automatic LT

Graph A and B show two sets of automatic LT runs. For each run five samples were vitrified, warmed and viability measured (n=5 +/- SD). Combined manual/automatic LT with a maximum inlet temperature of -15˚C, -25˚C and -37˚C showed an improvement in viability from -15˚C to -25˚C but was lower at -37˚C. Samples were vitrified at -40˚C and were then warmed in a two-step warming protocol (from 65% to 45% (w/v) CPA at -22˚C, then to 20% (w/v) glucose at 0.5˚C). AELC were cultured for 24 hours in complete media at 37˚C before measuring viability.

7.4.3 Impact of sample volume on cell viability

Several litres of CPA were needed to perform a single automatic LT run. One aim was therefore to reduce the starting volume from initially 280ml to 140ml. This had an unexpected effect on cell viability as recovery was substantially reduced (Figure 7.7).

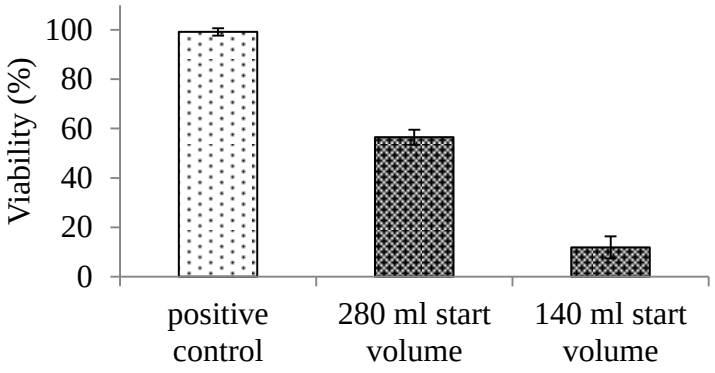

Figure 7.7 Impact of sample volume on cell viability

Lower viability was obtained when the sample volume was reduced from 280ml to 140ml. Each condition was tested once. Five samples were vitrified after being increased to 65% (w/v) CPA and after being cooled to -40˚C. Vitrified samples were warmed in a two-step warming protocol (from 65% to 44% (w/v) CPA at -22˚C, then to 20% (w/v) glucose at 0.5˚C). AELC were cultured for 24 hours in complete media at 37˚C before measuring viability.

7.4.4 Inhomogeneous "cell per bead" survival

AELC viability was observed after each LT run using the fluorescent microscope. It was noted that some of the beads contained a high proportion of viable cells, while others contained almost exclusively dead cells. This observation was independent of whether AELC were vitrified after the cooling process to -40˚C (at 65% (w/v) CPA) or directly warmed. It was assumed that the effect was caused by the temperature difference within the sample carrier (colder at the carrier wall, bottom or surface and warmer at the centre) or by the temperature difference between inlet and sample solution. Viability, up to a CPA concentration of 40% (w/v) remained high and inhomogeneous AELC viability in beads was not observed. The inlet temperature was therefore maintained at -15˚C once a CPA concentration of 35% (w/v) was reached. That way the freezer temperature and consequently the temperature inside the sample carrier and of the inlet

solution was maintained constant during the CPA addition process from 35% and 65% (w/v). Nevertheless strong variation between beads remained (Figure 7.8).

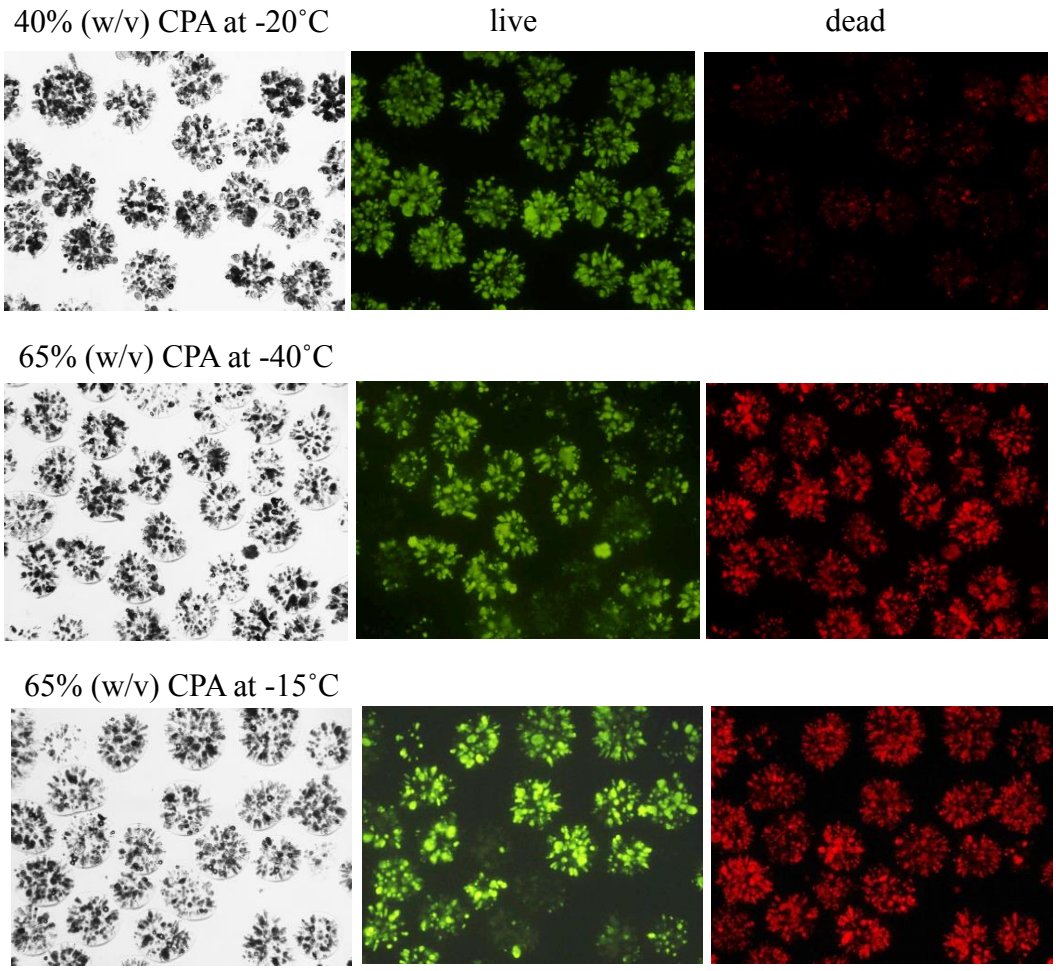

Figure 7.8 Inhomogeneous "cell per bead" survival

AELC survival at 40% (w/v) CPA No.18 at -20˚C was high and there was visually little difference between the numbers of cells per bead that had survived the LT process. Once AELC were exposed to 65% CPA at -40˚C, beads strongly varied in their number of viable cells. This was also seen when the freezer and inlet temperature was restricted to -15˚C. The figure shows phase images, and images of live (green, stained with FDA) and dead (red, stained with PI) cells.

7.4.5 High concentrated CPA inlet solution

It was shown that a temperature gradient across the sample carrier did not cause the strong variation seen between beads in respect to AELC survival. In an initial experiment the inlet CPA concentration had been investigated with the prediction that

an inlet of 80% (w/v) CPA No.18 would cause immediate damage to AELC as a cause of strong CPA concentration differences between inlet and sample solution. Instead an inlet solution 50% (w/v) CPA No.18 was used to increase the sample concentration to 40% (w/v). Viability and cell numbers were measured; however, both were only slightly higher when a 50% (w/v) CPA inlet solution was used. Changing the CPA composition from Me_2SO/EG/glucose to EG/glucose (ratio 4/1) did not show any difference in viability or cell number to the 80% inlet (Figure 7.9).

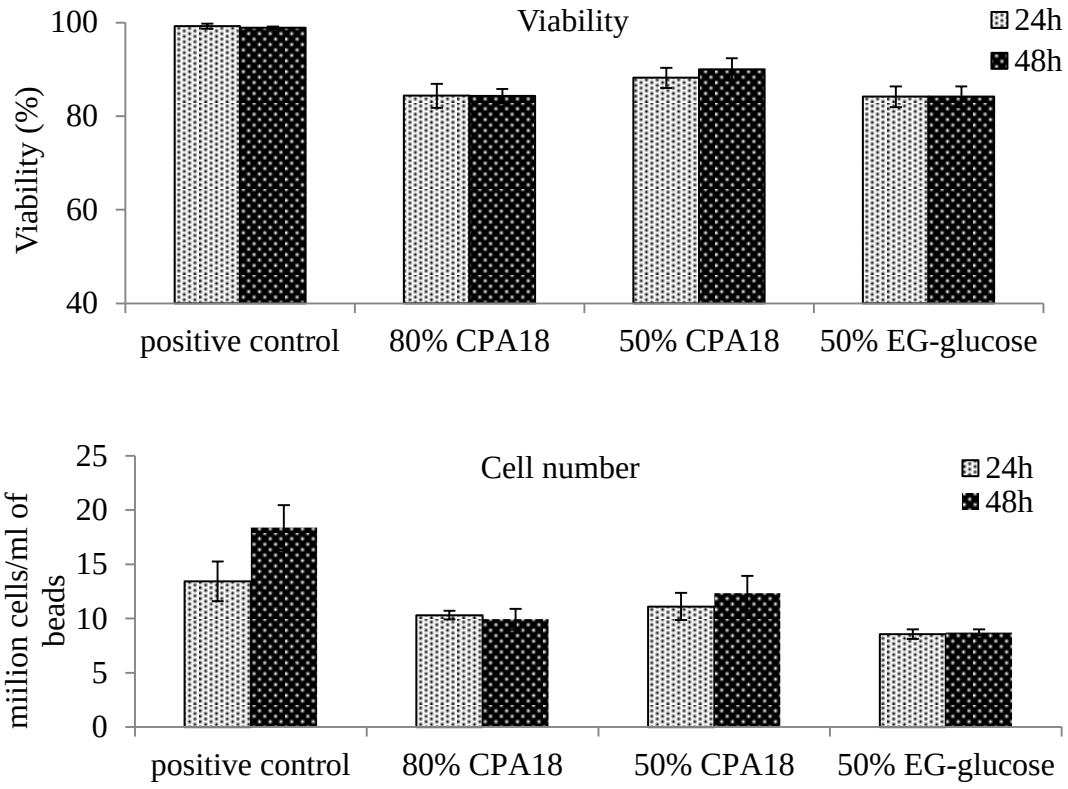

Figure 7.9 CPA inlet reduced from 80% to 50% (w/v)

AELC were processed using the combined manual/automatic LT approach until a concentration of 40% (w/v) CPA No.18 at -20˚C was reached. Viability and cell numbers 24 and 48 hours post-warming were slightly higher when the concentration of the inlet solution was reduced from 80% to 50% (w/v). Using a 50% (w/v) EG/glucose (ratio 4/1) solution had no beneficial effect. The data presents one run for each condition. For each run five samples (n = 5+/-SD) were warmed following a one-step warming protocol (from 40% (w/v) CPA No.18 at -20˚C to 20% (w/v) glucose at 0.5˚C). AELC were cultured for 24 and 48 hours in complete media at 37˚C before measuring viability and cell number.

Changing the initial inlet from 80% to 50% (w/v) CPA until a concentration of 40% was reached did not show a clear impact on cell survival. However, when the final inlet was reduced to a concentration of 66% (w/v), viability was substantially increased and "viable cell per bead" distribution was more homogenous. The inlet sequence was finally changed to a sequence of 50%, 60% and finally 66% (w/v) CPA to further improve cell viability (Figure 7.10).

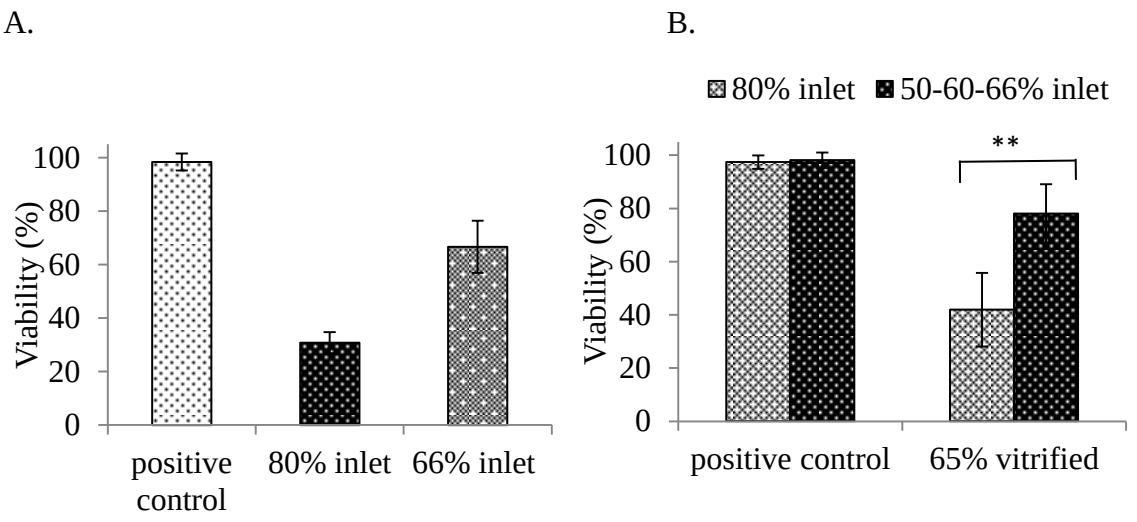

Figure 7.10 Reduced inlet CPA concentration

A: Viability increased by approximately 40% +/-4 when an inlet solution of 66% +/-10 instead of 80% (w/v) CPA No.18 was used for combined manual/automatic LT. Data presents one run, for each run five samples were tested for viability (n=5 +/- SD). B: Instead of using an inlet of 80% CPA No.18, an inlet sequence of 50%, 60% and finally 66% (w/v) CPA No.18 was used which significantly increased viability from 42%+/-14 to 78%+/-11 The data presents four separate runs (n=4+/-SD, p<0.01). A and B: For each run five samples were vitrified and warmed following a two-step warming protocol (from 65% to 45% (w/v) CPA at -22˚C, then to 20% (w/) glucose at 0.5˚C). AELC were cultured for 24 hours in complete media at 37˚C before measuring viability.**

7.4.6 Reduced outlet port height

The height of the outlet port was reduced to ensure that the filter system was submerged in CPA solution throughout the LT process. This was done to prevent alginate beads, stuck to the upper filter, being exposed to the temperature of the surrounding air, which was expected to be close to the freezer temperature and below the melting point of the solution inside the sample carrier (Figure 7.11).

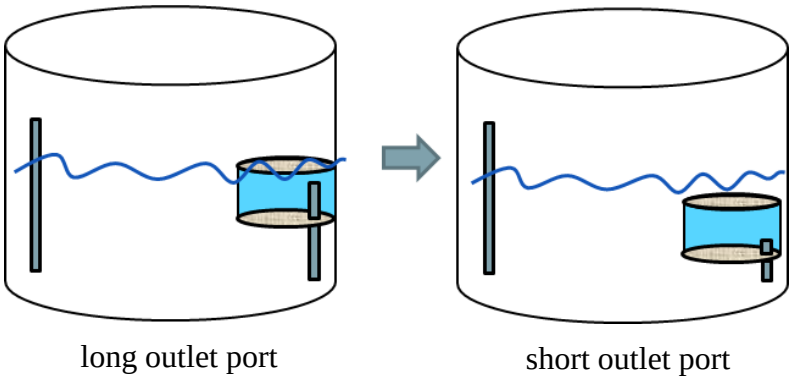

Figure 7.11 Long versus short outlet port design

The outlet port was shortened to make sure that the filter unit was submerged in CPA throughout the LT process to prevent beads that stick to the upper filter from being exposed to the temperature of the surrounding air.

7.4.6.1 Short outlet port-diminishes viability

Changes made to the outlet system reduced viability from approximately 80% to 40%. Strong differences between the distribution of viable and dead cells per bead were noted, just as it was observed before the final inlet concentration was reduced from 80% to 66% (Figure 7.12).

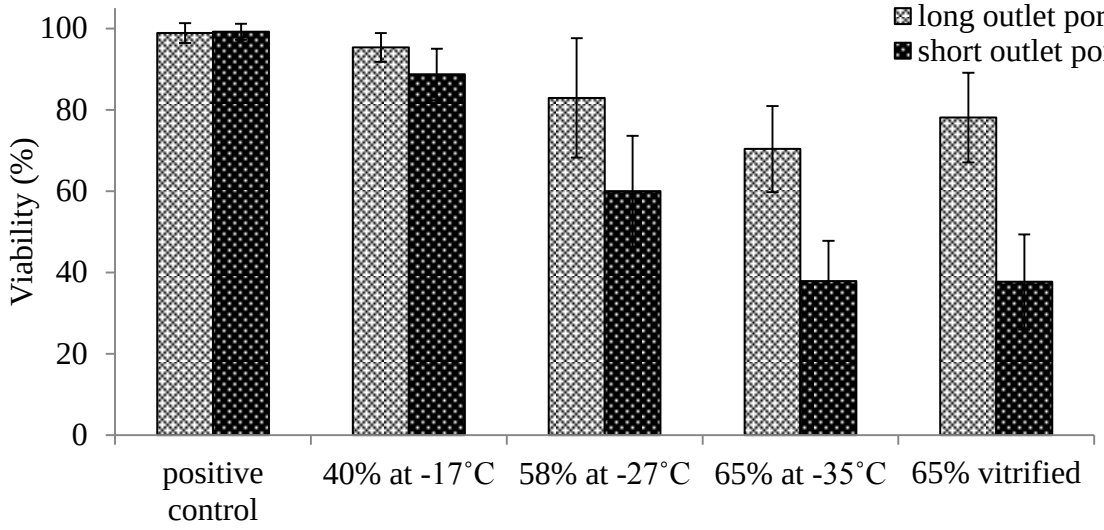

Figure 7.12 Long versus short LT outlet port: impact on cell viability

Viability was decreased when the outlet port was reduced. The data presents four separate runs (n=4+/-SD). For each run five sample were taken after the increase to 40%, 58% and 65% (w/v) CPA No.18, five samples were vitrified at -40˚C. Non-vitrified samples were warmed within one step (directly to 20% (w/v) glucose at 0.5˚C). Vitrified samples were warmed in a two-step warming protocol (from 65% to 44% (w/v) CPA at -22˚C, then to 20% (w/v) glucose at 0.5˚C). AELC were cultured for 24 hours in complete media at 37˚C before measuring viability.

7.4.6.2 Inhomogeneous CPA extraction

Firstly we hypothesized that changing the filter height had an effect on the CPA component that would predominantly be taken out during the extraction process due to different densities of glucose, Me_2SO and ethylene glycol. In a first attempt the glucose concentration was increased from a ratio of 40/20/10 to 35/20/15 (Me_2SO/EG/glucose) for the 50% and 60% CPA inlet solution, but was kept as before for the 66% inlet solution (ratio 40/20/10). This was done to reduce CPA toxicity at higher temperatures and to improve vitrification properties by increasing the Me_2SO concentration during the final inlet steps. However, this resulted in lower viability throughout the process. An increase in Me_2SO to a ratio of 45/20/5 resulted in the same final viability obtained with CPA No.18 (Figure 7.13).

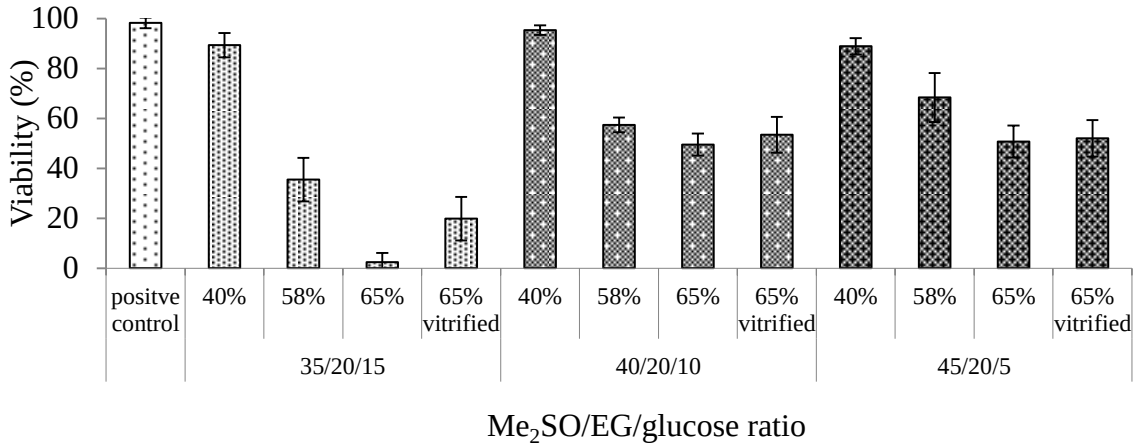

Figure 7.13 Inhomogeneous LT extraction

Increasing the sugar to Me_2SO and EG concentration decreased viability, while higher Me_2SO concentrations did not have any effect. Each condition was tested once. Five sample were taken after the increase to 40%, 58%, 65% CPA (w/v) and five samples were vitrified (n=5 +/- SD) at -40˚C. Non-vitrified samples were warmed within one step directly to 20% (w/v) glucose. Vitrified samples were warmed in a two-step warming protocol (from 65% to 45% (w/v) CPA No.18 at -22˚C, then to 20% (w/v) glucose at 0.5˚C). AELC were cultured for 24 hours in complete media at 37˚C before measuring viability.

7.4.7 The Liquidus Tracking stirrer

Increased concentrations of Me_2SO or glucose in comparison to CPA No.18 did not improve cell recovery, suggesting that the changes made to the outlet port height did not affect the Me_2SO/EG/glucose ratio of the CPA solution inside the sample carrier. Therefore the assumption was made that the mixing process in itself might have been changed by decreasing the inlet port height. Instead of the original stirrer a simple propeller stirrer was designed to achieve more homogenous mixing conditions. By using the propeller stirrer viability was significantly improved and strong variations in viable cell numbers per bead, as it was noted before, were no longer observed (Figure 7.14, Figure 7.15).

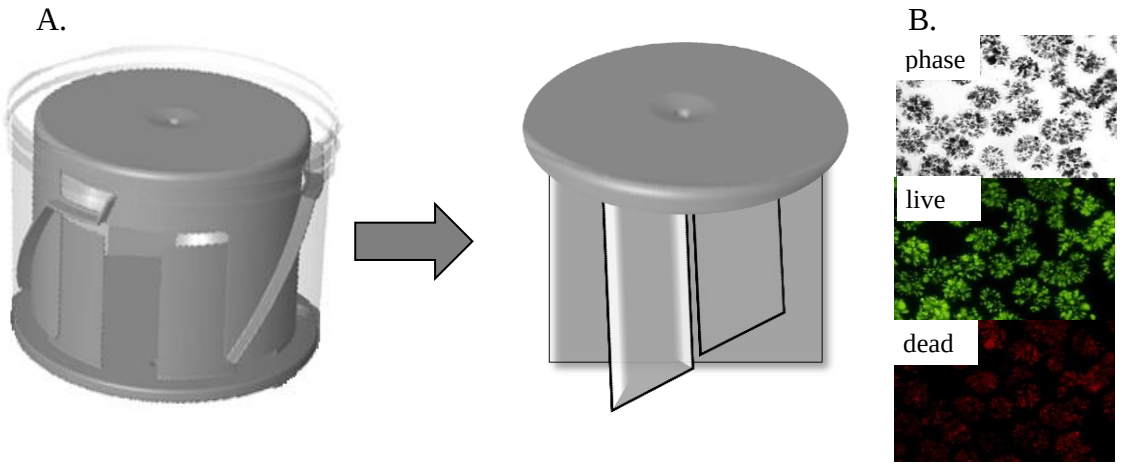

Figure 7.14 Planer stirrer versus propeller stirrer

A. The Planer stirrer was designed to hold larger constructs in the middle of the sample carrier while providing efficient CPA homogenisation. Strong differences between the sample carrier centre and on the outside (between the static pedals and the moving part of the stirrer) in respect to mixing behaviour and shear forces were expected to affect AELC. The propeller stirrer provided more homogenous mixing of beads and solution. B. The images show AELC after being warmed from vitrification using combined manual/automatic LT with the new propeller stirrer. Viable and non-viable cells were evenly distributed across alginate beads. The figure shows phase images, and images of live (green, stained with FDA) and dead (red, stained with PI) cells.

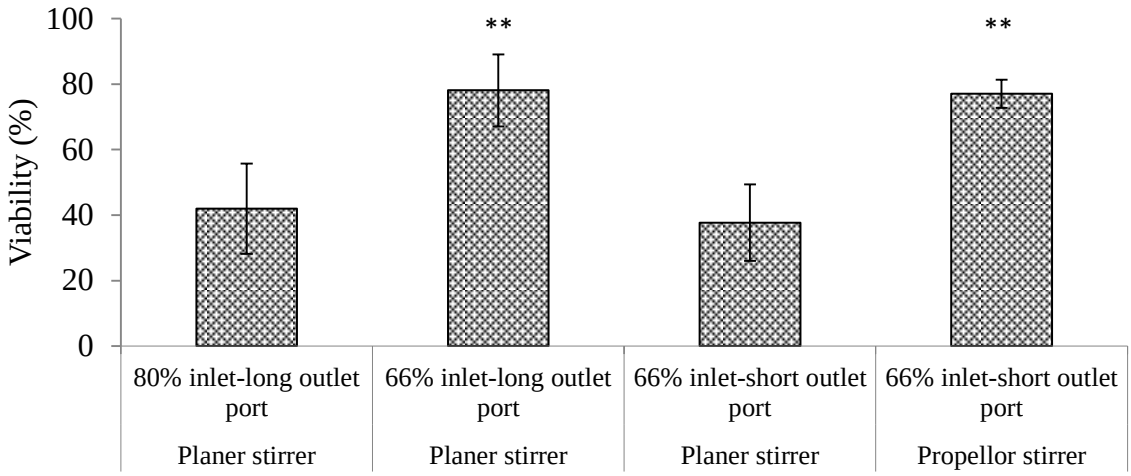

Figure 7.15 Propeller stirrer- increased cell viability

Using a short outlet port in combination with a propeller stirrer, instead of the Planer stirrer, increased post-warming cell viability significantly from 38% +/-11.7 (n=4+/- SD) to 77% +/- 4.3 (n=4 +/-SD), ** p<0.01. Comparable values were obtained with a long outlet port in combination with the Planer stirrer (78% +/- 11.1 (n=5 +/-SD) when the maximum inlet CPA concentration was to 66% (w/v). Viabilities were significantly lower when the Planer stirrer and a short outlet port (42%+/-13.8 (n=4 +/-SD) was used, ** p<0.01 For each run five samples were vitrified at -40˚C and warmed in a two-step warming protocol (from 65% CPA to 45% CPA at -22˚C, then to 20% glucose at 0.5˚C). AELC were cultured for 24 hours in complete media at 37˚C before measuring viability.

7.4.8 Manual Liquidus Tracking warming process

Different manual warming procedures were tested by using aliquots of vitrified AELC. The more steps were used to warm AELC and to reduce the CPA concentration, the higher was the post-warming viability. A two-step procedure (first to 40% (w/v) CPA18 then to 20% (w/v)) glucose significantly improved post-warming viability in comparison to the one-step procedure (directly to 20% (w/v) glucose) and showed similar results to the three step procedure (50-40-20% (w/v) CPA) (Figure 7.16). A 20% (w/v) glucose solution was used as a last step to reduce osmotic stress while decreasing the concentration of penetrating CPAs.

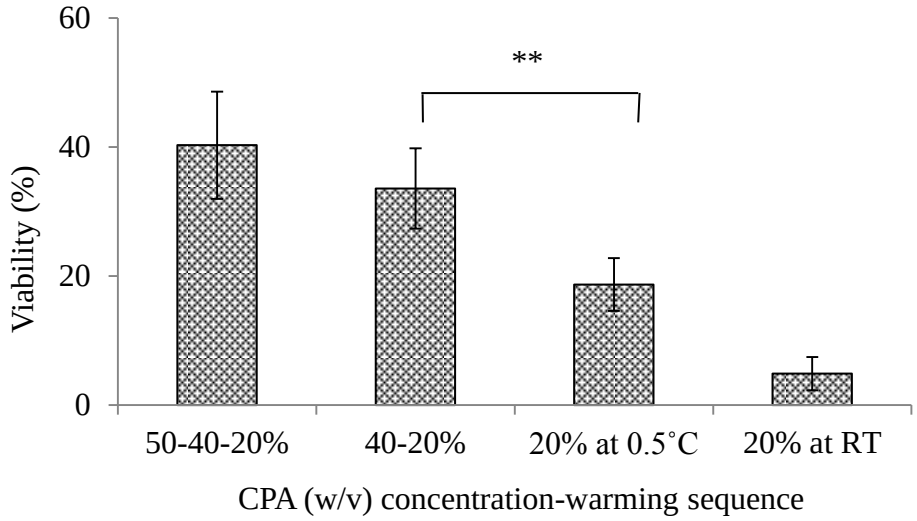

Figure 7.16 Manual LT warming sequence

The use of more warming steps resulted in higher AELC post-warming viability. Aliquots of vitrified AELC were warmed to -20˚C in the controlled rate freezer. Condition "50-40-20%": CPA No.18 concentration was reduced from 65% to 50% and then to 40% (w/v) CPA No.18 by adding 35% (w/v) CPA No.18. Incubation at each step was 15 minutes at-20˚C. Samples were poured through cell strainers and placed in 8ml of ice cold 20% (w/v) glucose solution for 10 minutes before being washed 3 times with 1xPBS (ice-cold) to remove all CPA. Finally AELC were incubated in 8ml of complete media at 37˚C until measurement. Condition "40-20%": as condition "50-40-20%" but the CPA No.18 concentration was reduced directly reduced from 65% to 40% (w/v). Condition "20% at 0.5˚C" and "20% at RT": sample were warmed to -20˚C and poured through cell strainers and placed in 8ml 20% (w/v) glucose solution for 10 minutes either at 0.5˚C or room temperature. Data was n=5 +/-SD, ** p<0.01.

7.4.9 Automatic Liquidus Tracking warming process

It is more complicated to keep the sample temperature close to the melting point during automatic LT warming than during cooling. This is for the following reasons: in order to dilute the sample the inlet solution has to be of lower CPA concentration than the sample. To avoid freezing the freezer has to be set several degrees above the melting point of the inlet solution. The smaller the concentration difference is, between inlet and sample solution, the closer the sample can be kept to its liquidus curve. However, this means that more solutions steps have to be carried out.

7.4.9.1 The one solution reverse mode

To simplify the LT warming procedure the attempt was made to use only 20% (w/v) glucose to reduce the sample CPA concentration while keeping the sample close to its liquidus curve. The method was based on the theory that two solutions of equal volume but of different temperature and CPA concentration do not freeze if the average temperature remains above the melting point. This was tested by pumping 20% glucose (at 20˚C) into a container holding 120ml of 65% (w/v) CPA No.18, while the solution was continuously mixed by a magnetic stirrer. Inlet was started at a sample temperature of either -35˚C, 30˚C or -25˚C, while the sample itself was kept at -25˚C during the inlet process. The temperature/concentration (T/C) profile closest to the liquidus curve for CPA No.18 was achieved with an initial sample temperature of -35˚C and an inlet speed of 20ml/minutes. Some ice formed when the initial sample temperature was set to -35˚C but disappeared once the sample reached a temperature of -20˚C. The process was successfully transferred to automatic LT, albeit the initial sample temperature had to be decreased from -35˚C to -25˚C to avoid ice formation. Strong ice formation was noted when stirrer and pumps stopped operating. Aliquots of vitrified AELC for which a maximum post-warming viability of 40% had been reached in previous experiments were used to test the one solution reverse LT mode, but no viability was measured 24 hours post-warming (Figure 7.17).

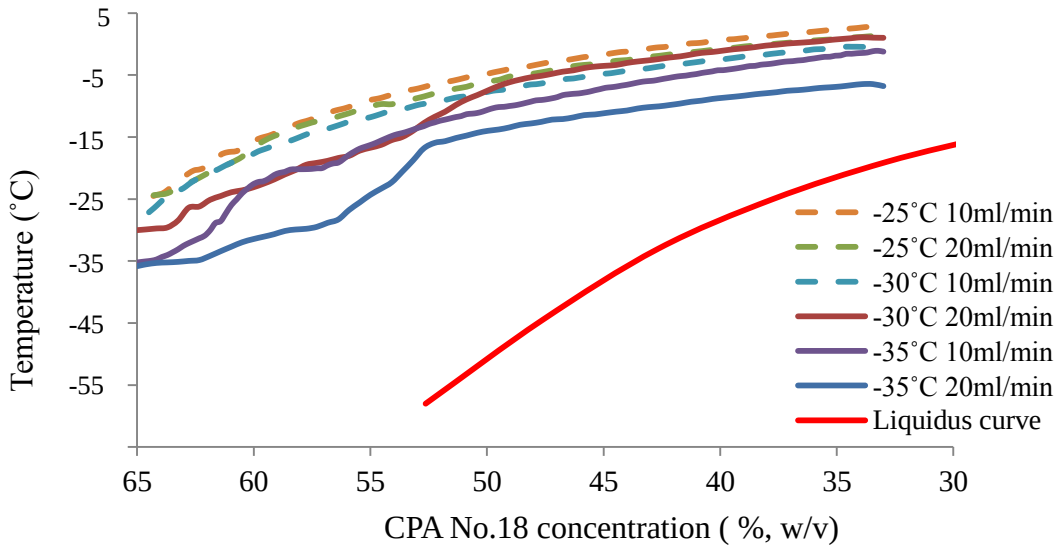

Figure 7.17 PBS inlet into subzero CPA solution

The graph shows T/C curves of samples that were warmed up by the inlet of 1xPBS (20˚C) while the surrounding temperature was kept at -25˚C. The initial CPA volume of the 65% (w/v) CPA solution was 120ml. Inlet temperature was started at a sample temperature of either -25˚C, 30˚C or 35˚C while the inlet speed was set to either 20ml/minute or 25ml/minute. The T/C profile closest to the liquidus curve was achieved with an initial sample temperature of -35˚C and an inlet speed of 20ml/minutes.

7.4.9.2 The four-step reverse mode

In a second approach the CPA concentration was reduced by adding in the following order 50%, 40%, 30% (w/v) CPA No.18 and 1xPBS. The freezer but also the sample temperature had to be maintained above the melting point of the inlet solution to avoid freezing, even though the average concentration of inlet and sample CPA concentration suggested a lower melting point for the incoming solution. The solution inside the inlet port froze several times as it did not mix with the higher concentrated sample solution but was cooled down by it. A temperature difference of 5˚C between sample and inlet solution was sufficient to initiate inlet port freezing as the inlet solution was already close to its freezing point before entering the sample carrier though the inlet port. To overcome this problem the inlet solution was used to increase the sample temperature before the next lower concentrated inlet CPA solution was connected to the inlet pump. This was achieved by setting the freezer temperature 4˚C above the melting temperature of the next lower inlet CPA solution whilst 200ml of the previous CPA solution still had

to be pumped in. Following this approach freezing was avoided while the T/C curve was kept close to the liquidus curve. When vitrified AELC were warmed with the four-step warming method viabilities of 60% and higher were obtained (Figure 7.18).

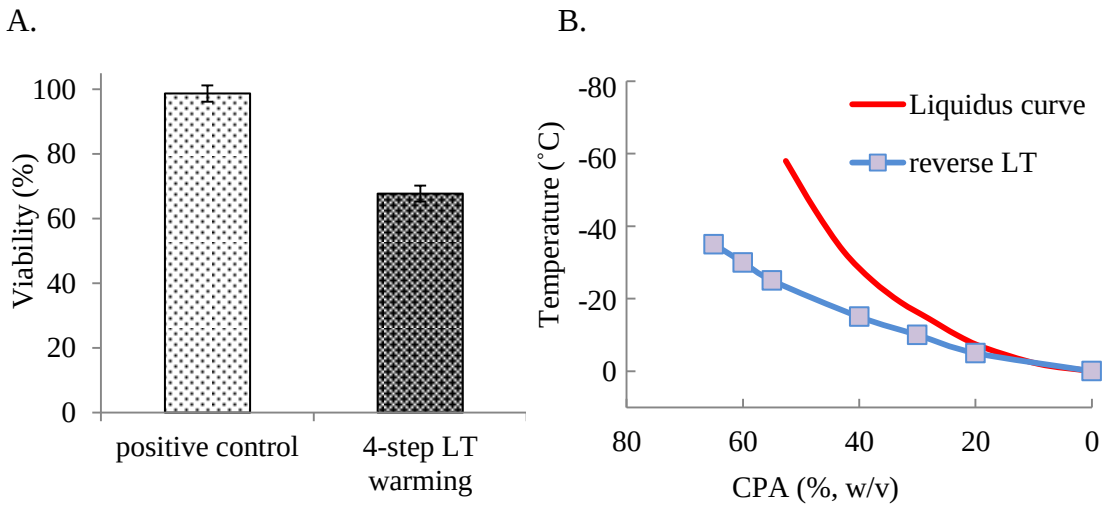

Figure 7.18 LT warming protocols

A. When using a four-step LT warming protocol post-warming viabilities of 68% +/- 2.5 (n=4 +/- SD) were achieved. B. Lower concentrated CPA No.18 solutions were used to reduce the sample CPA concentration while maintaining the sample T/C curve close to the liquidus curve of CPA No.18.

7.4.10 CPA toxicity over time

Both, the automatic cooling and the warming LT process for large volumes can take several hours depending on the volume that has to be vitrified. It is therefore of importance to know whether viability is diminished over time at a certain temperature and concentration when the conditions remain unchanged. For this reason AELC were incubated over time at -7˚C, -15˚C, -20˚C and -25˚C in 35%, 50% , 55% and 65% (w/v) CPA. Viability was reduced at -7˚C at a concentration of 35% (w/v) CAP20 after one hour but remained constant at -15˚C (50% CPA), -20˚C (55%) and -25˚C (65%) (Figure 7.19).

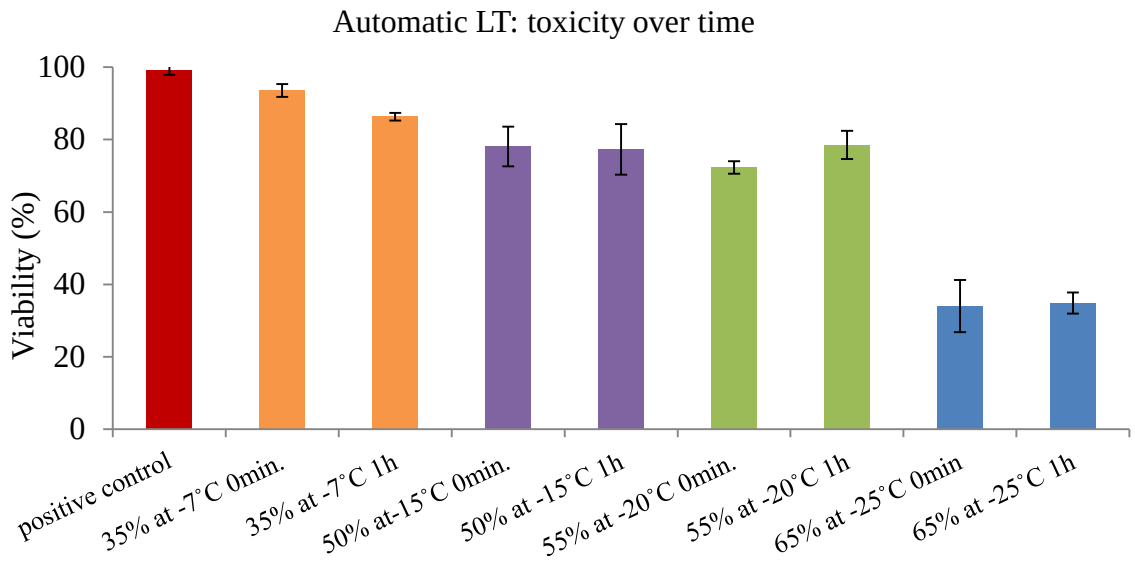

Figure 7.19 Toxicity over time using automatic LT

Automatic LT was used to cool down AELC to -7˚C, -15˚C, -20˚C and -25˚C. Each time five samples were taken once the temperature was reached and after one hour of incubation. Samples incubated in 35% (w/v) CPA were warmed by adding AELC to 20% glucose at 0.5˚C (10 minutes). For samples incubated in 50-65% (w/v) CPA the two-step warming protocol was used. Viability was reduced after one hour at -7˚C (35% CPA) but remained constant at -15˚C (50% CPA), -20˚C (55%) and -25˚C (65%). Data was n=5 +/-SD.

7.4.11 Cell density impacts cell survival

AELC of high cell densities were less affected by LT treatment than AELC of low cell density which was shown when beads of high and low cell density were processed within the same run. Beads of either type were easily distinguished under the microscope, which made it possible to take images of single beads and determine the viability using the established FDA/PI method. Viabilities for high cell densities beads were significantly higher than for low cell density beads. Although this procedure allowed testing two populations of beads under exactly the same conditions, cell number and albumin production could not be measured because beads could not be physically separated (Figure 7.20, Figure 7.21).

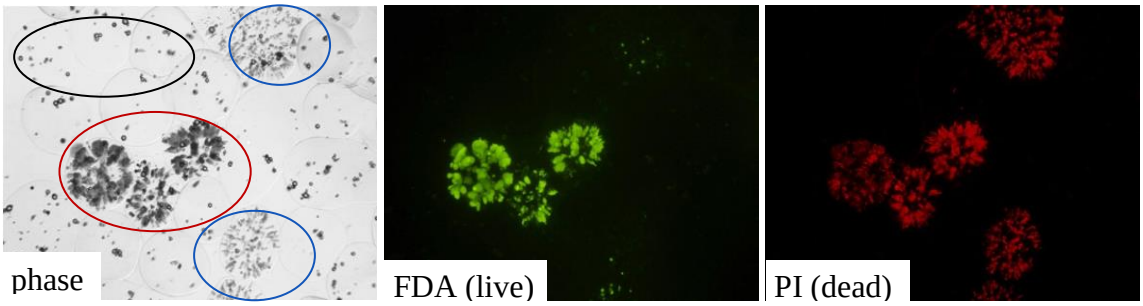

Figure 7.20 High vs. low cell density beads for LT

The phase image shows the three types of alginate beads that were processed at the same time in the sample carrier: empty beads with small pieces of silica (black circle), low cell density beads (circle in blue) and high cell density beads (circle in red). Cell numbers were $4*10^6$ cells/ml of beads for low cell density beads and $15*10^6$ cells/ml of beads for high cell density beads. High cell density beads showed better survival rates (strong FDA signal) than low cell density beads (low FDA signal but strong PI signal).

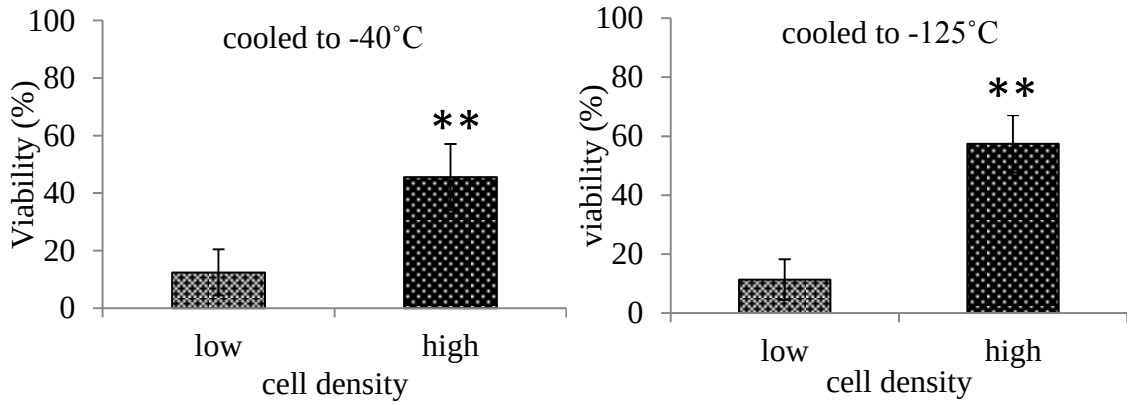

Figure 7.21 Impact of low and high cell densities on post-LT viability

Cell viability was significantly higher for beads of high cell density (-40˚C: 46% +/-11.5, n=17) and (-125˚C: 57%+/-9.7, n=17) than beads of low cell density (-40˚C: 12% +/-8.0, n=17) and (-125˚C: 11+/- 6.9, n=17), ** $p<0.01$. This was independent of whether AELC were warmed up in a two-step warming process directly after reaching 65% CPA (w/v) and -40˚C or after being vitrified (cooled to -125˚C) and then warmed up. There was no difference in post-warming viability in respect to the minimum cooling temperature.

7.4.12 Complete automatic Liquidus Tracking procedure

The complete LT process was carried out with AELC of increasing cell numbers. Higher cell density resulted in higher cell numbers, viability, albumin and alpha-fetoprotein production with respect to the positive control. For cell densities of $17*10^6$ and $20*10^6$ cells/ml of beads) viability was 70% and 90%, viable cell number 61% and 79% and albumin and alpha-fetoprotein production 48% and 54%, and 67% and 75%, respectively (fraction of the untreated control after 48 hours of post warming) (Figure 7.22).

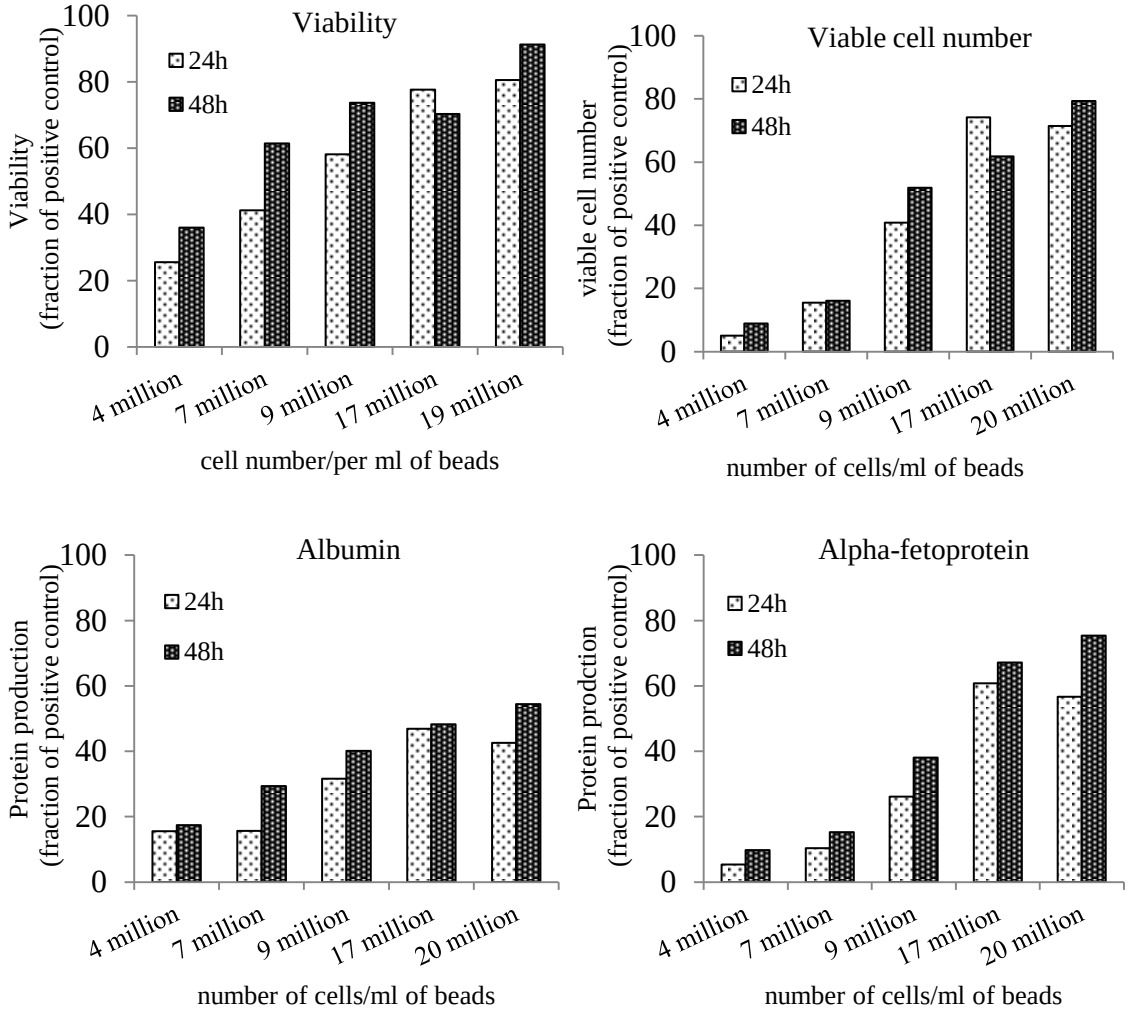

Figure 7.22 Impact of low and high cell densities on cell recovery

The higher the cell number the higher was the post-warming viability, cell number, Albumin and Alpha-fetoprotein production. AELC were cooled to -40˚C and then vitrified using the combined manual/automatic LT approach and warmed using the four-step LT process. For each cell density one run was performed.

7.5 Discussion

Although the combined manual/automatic LT approach kept the sample temperature/concentration curve close to the liquidus curve and despite the fact that automatic LT increased the CPA concentration continuously and without the temperature fluctuation seen for manual LT, no viability was detected when Me_2SO was used as a single CPA (Chapter 6). When Me_2SO was replaced with the newly developed CPA No.18 solution (Chapter 5) viability was increased to approximately 40%, suggesting that CPA toxicity was not fully suppressed by the automatic LT process. The possibility was considered that viability had mainly been compromised during the two-step manual warming process and that an optimized warming procedure would result in high viabilities for Me_2SO. However, for manual LT a similar warming process was used and post-warming viabilities between 20% and 50% were reached, whilst no viable cells were detected after the automatic LT cooling process, suggesting a stronger impact of automatic LT cooling than manual two-step warming.

The question of whether cell viability is reduced during the cooling or warming process is important, but sometimes difficult to answer. One process cannot be carried out without the other, and there will always be some uncertainty at which step viability is reduced as long as viability is not increased substantially when trying different cooling or warming methods. Nevertheless, there might be some indication which process might be more detrimental. For example, different warming protocols were used to warm aliquots of AELC that had previously been vitrified by automatic LT (CPA No.18), but viability never increased to more than 40%. Manual warming can be considered to be subject to some deviation and some replicates were expected to be warmed up in a more beneficial way than others and should have exceeded 40% viability, if the cooling process had not already reduced viability close to this value. When, in combination with the two-step warming process, a two-step manual LT cooling approach was used instead of automatic LT cooling, viability was increased to more than 80%. This proved the suitability of the warming process but also demonstrated the necessity for a simplified manual LT process which can be easily modified and carried out rapidly to improve automatic LT.

CPA addition steps for the manual two-step cooling and warming set-up were based on several observations and considerations: firstly AELC had shown good tolerance to 40% (w/v) CPA No.18 for up to one hour at an incubation temperature of 0.5˚C (Chapter 5). Moreover, 40% and 80% (w/v) CPA No.18 were still liquid enough at -20˚C to allow efficient mixing and accurate addition. An extra addition step at a concentration of 20% (w/v) CPA was carried out at -5˚C but proved to be of little benefit, as the additional procedure caused the temperature to increase close to 0˚C. Instead it was more practical to use a starting mixture of AELC at 0.5˚C (on ice water), and to increase the CPA concentration in two steps to 40% (w/v), before aliquots of AELC were added to precooled tubes (0˚C). Cooling was carried out at 0.5˚C/minute and the CPA concentration was increased to 65% (w/v) by adding 80% (w/v) at -20˚C. Samples were were further cooled and finally vitrified at -40˚C to simulate the automatic LT process. The warming step was also carried out at -20˚C by adding 50% (w/v) CPA to the sample (at 65% (w/v)). Although an additional step from 65% to 50% (w/v) CPA during the warming process resulted in higher post-warming viabilities, the two-step warming process was used for practical reasons. At temperatures below -20˚C, CPA No.18 was too viscous to be poured though a cell strainer. This meant that a lower concentrated CPA solution had to be added to decrease the sample CPA concentration. This as a consequence, increased the sample volume. However, when using the manual insulation system, 15ml microfuge tubes were used. The tube capacity was only sufficient to add 9ml of 50% (w/v) CPA to decrease the sample CPA concentration to 44% (w/v). Increasing and decreasing the CPA solution only once at low subzero temperatures proved to be both more feasible and reliable. Manual LT includes the vitrification process in the procedure and was therefore superior to CPA toxicity testing at 0.5˚C. It was shown that changing the Me_2SO/EG/glucose ratio towards more glucose was beneficial when AELC were incubated at 0.5˚C, but post-warming viability was decreased when AELC were vitrified. The same findings were obtained when the automatic LT process was used.

Replacing half of the glucose amount with sucrose, raffinose or trehalose for their beneficial effects discussed in Chapter 5, did not improve cell viability. Viaspan and HTK, which are organ preservation solutions designed to reduce chilling injury during

hypothermic storage, were used to replace PBS as a carrier solution. Apart from different sugars to reduce osmotic stress (also contained in CPA No.18), HTK contains a histidine-HCL buffer with extended buffering capacity, tryptophan to support cell membrane integrity and alpha-ketoglutarate which serves as a substrate for aerobic energy production (HTK data sheet, www.custodiol.com, (Ringe et al., 2005), while Viaspan contains the antioxidant glutathione (Ceballos-Picot et al., 1996; Southard et al., 1990). Although both solutions have shown good results in liver and hepatocyte cold storage (Abrahamse et al., 2003; den Butter et al., 1995), they are not commonly used in vitrification procedures. HEPES buffer ((4-(2-hydroxyethyl)-1piperazineethanesulfonic acid) at a concentration of 10mM and 25mM, which is within the suggested rate of 5mM and 30mM, was also used to replace PBS. HEPES has similar dissociation characteristics to water at low temperatures, and has shown superior buffering capacity at low temperatures (Baicu & Taylor, 2002; Swan et al., 1994; Taylor, 1982). Nonetheless, none of the solutions used to replace PBS indicated any advantage. The addition of other antioxidants such catalase (Michael et al., 2007; Paudel et al., 2010; Roca et al., 2005) and Trolox (water-soluble vitamin E) (Peña et al., 2004; Thuwanut et al., 2008) which have been used successfully for cryopreservation of sperm cells from various species, or the use of a temperature independent pH buffer, designed for biomedical applications at low temperatures (Sieracki et al., 2008) might be more beneficial. However, it is questionable whether non-CPA components can reveal much of their specific effects at low sub-zero temperatures and high CPA concentrations. It is most likely that those effects are restricted to the beginning of the cooling and the end of the warming procedure when CPA levels are lower and temperatures higher. Yet, at these concentrations cell survival is still high and cell death negligible in comparison to the viability decrease noted when the CPA concentration is increased to 65% (w/v).

Pre-incubating AELC in proline, tehalose or linoleic acid in order to “prepare” cells for the cooling procedure including the later phase of the process was therefore estimated as a more effective way to improve post-warming viability. Feeding the larva of the drosophilid fly Chymomyza costata proline-augmented diets before vitrification had increased their freeze tolerance significantly (Kostál et al., 2011). It is believed that prolin binds to remaining unfrozen water and thus, increases vitrification efficacy.

Promising results were also obtained when cells were pre-incubated in trehalose and linoleic acid-albumin before they were slowly cooled to subzero temperatures. Intracellular trehalose has reportedly improved the survival of cryopreserved mammalian cells (Eroglu et al., 2000) and the pre-incubation in linoleic acid-albumin has enhanced the post-thaw survival of in vitro-produced bovine embryos (Tominaga et al., 2000). However, none of the additives used for pre-incubation indicated any beneficial effect for AELC cryopreservation. The concentration of trehalose, proline and linoloic acid, although used in the range described in the literature, might not have been adequate. However, even after optimization benefit was expected to be low in respect to the 60% viability decrease noticed for AELC after automatic LT.

As the viability loss during auomatic LT was high and mainly seen when the solution was increased from 40% to 65% (w/v) at temperatures below -20˚C it was assumed that the CPA addition temperature was too cold to provide sufficient CPA cell penetration or too high to sufficiently reduce CPA toxicity. Hence, different CPA addition temperatures (-11˚C, -16˚C, -22˚C, -25˚C, -33˚C) were tested at which the CPA concentration was manually increased either from 40% to 65% or 50% to 65% (w/v). Cell recovery was significantly higher when CPA addition was carried out at -25˚C (86%) than at -11˚C (54%) or -16˚C (71%), was comparable at -22˚C (65%) and -27˚C (65%) but was significantly reduced at -33˚C (50%). Similar results were obtained for automatic LT. In a first experiment viability was much lower at -37˚C (31%) than at -25˚C (44%). In a second experiment viability was slightly reduced from 57% (-25˚C) to 54% (-37˚C). Data suggested that CPA penetration was insufficient to prevent intracellular ice formation at temperatures below -27˚C (-25˚C). Fahy has used a similar minimum temperature (-22˚C) for the perfusion and vitrification of kidneys (Fahy et al., 2004). No explanation was given why this temperature was chosen. It is known that at lower temperatures viscosity becomes higher and perfusion more challenging. However it is also possible that lower temperatures in respect to toxicity have not shown any beneficial effect.

When AELC viability was determined using the fluorescent microscope, a markedly inhomogeneous distribution of viable and dead cells between alginate beads was observed. Whilst some beads contained mainly viable cells, others contained

exclusively dead cells. At first it was assumed that the following temperature differences had caused this effect. The inlet temperature during the cooling process is much colder than the sample temperature and there is also a temperature gradient across the sample carrier with lower temperatures at the outside and higher temperatures at the inside of the sample container. Inhomogeneous distribution of viable and dead cells was not noted for CPA concentrations below 40% (w/v), normally reached at -15˚C. Consequently the inlet and sample solution temperature was maintained at -15˚C, thus offsetting the temperature difference inside the sample carrier while the sample CPA concentration was increased from 40% to 65% (w/v). However, strong variations in the number of viable cells per bead were detected. It also seemed possible that bead inhomogeneity was caused by the difference in sample and inlet CPA concentration. In a first experiment the CPA concentration of the inlet solution was reduced from 80% to 50% (w/v) to increase the sample concentration to 40%, but almost no difference in viability between the two conditions was noted. This changed once the inlet CPA concentration was reduced from 80% to 66% (w/v) to increase the sample concentration to 65%. Post-warming viability increased from approximately 40% to 80% and the distribution of viable and dead cells per bead demonstrated good homogeneity. Findings that a reduced inlet CPA concentration to 50% at the beginning of the run had no impact on cell survival, and the observation that viability was strongly reduced when the initial sample volume was reduced from 280ml to 140ml, might be explained thus; when the CPA concentration is low, high concentrated CPA can be diluted quickly enough to avoid CPA toxicity. This also applies for larger volumes in comparison to smaller volumes, when the inlet speed is kept the same.

Surprisingly viability was reduced to its previous low level (40%) when the height of the outlet port was reduced from 8cm to 3cm. Firstly it was believed that the lower outlet level had changed the Me_2SO/EG/glucose ratio of the sample solution as a result of different CPA densities. It was hypothesized that throughout the lengthy LT cooling and CPA addition procedure more glucose would accumulate at the bottom of the sample carrier and more Me_2SO at the top of the sample solution. Increasing the Me_2SO concentration while decreasing the glucose concentration or vice versa was predicted to either improve or reduce cell recovery, respectively. Ethylene glycol was not tested as it was assumed that a change in viability would mainly be caused by the penetrating to

non-penetrating CPA ratio and for this Me_2SO and glucose concentrations were increased and reduced by 5% (w/v). Viabilities were strongly reduced when the glucose concentration was increased, which was in accordance with previous observations, whilst an increase in Me_2SO had no impact on cell survival, suggesting extensive dehydration as likely cause of cell demage.

Another possibility was that the outlet port height had changed the mixing conditions inside the sample container. With the longer outlet port the incoming CPA solution had been approximately at the same level as the inlet port which might have helped to draw the incoming CPA solution to the centre of the sample carrier. The Planer stirrer was designed to operate alongside the sample carrier wall to avoid any interference with larger, static constructs in the middle of the sample carrier. However this design implies strong differences across the sample carrier in respect to mixing behaviour and shear forces. For example, AELC trapped between the static pedals and the moving part of the stirrer are subject to stronger mixing and higher shear forces than AELC that are located at the centre of sample carrier. To overcome these mixing differences a self-made propeller stirrer was used instead. Findings were comparable to those obtained with the combination of long outlet port and Planer stirrer. Viabilities were increased to 80% and viable and non-viable cells were evenly distributed across alginate beads.

When viabilities were increased from 40% to 80% by reducing the maximum inlet concentration to 66% (w/v) it was initially believed that this was due to the 80% (w/v) CPA No.18 solution not being diluted fast enough to prevent chemical or osmotic injury. However viabilities were at 40% when a 66% (w/v) CPA inlet solution in combination with the shorter outlet port was used, indicating that the inlet CPA concentration per se did not cause cell death. By using the 66% (w/v) CPA inlet a stronger flow through was created, which possibly helped to homogenize the inlet CPA solution. Higher viability as a result of improved homogenization is compliant with better suitability of the propeller stirrer as a more uniform mixing approach. Still, the question remained how cell viability was affected by the given mixing conditions.

Viable cell per bead distribution was inhomogeneous although the temperature was maintained constant at -15˚C when the Planer stirrer was used. Chemical toxicity (Fahy et al., 1995), dehydration and osmotic stress (Song et al., 2009) as a result of

temperature was therefore excluded as a main cause for cell death, however those factors may have been reinforced through strong mixing. The inlet port being in close proximity to the Planer stirring system supports the theory that AELC located in the "intense mixing zone" and close to the inlet of high concentrated CPA, experience high intra- and extracellular CPA concentration differences and an enhanced mass transport across membranes as a result of high kinetic energy caused by intensive stirring. Wang demonstrated that stirring of the sample during LT cooling increases the Me_2SO concentration in cartilage of osteochondral dowels. When no stirring was used, the Me_2SO concentration in the tissue was 49.5 ± 6.9 % but when stirred the Me_2SO concentration in the tissue increased to 58.9 ± 1.2% (Wang et al., 2007).

Shear stress is also likely to cause cell death by membrane disruption (Park et al., 2011) and would account for a more homogenous distribution of viable and dead cells amongst beads when the propeller stirrer was used. In addition shear stress reportedly increases cell membrane fluidity. This effect is commonly seen in endothelial cells (Butler et al., 2001; Haidekker et al., 2000; Yamamoto & Ando, 2013) and L. polyedrum (Mallipattu et al., 2002). Higher membrane fluidity would allow for more CPA and water movement across the plasma membrane, thus excessive dehydration (Fathallah et al., 1995) but also hyperosmotic stress through an influx of non-permeating solutes occuring are possible causes for cell death (Mazur et al., 1972).

Most experiments used to improve the automatic cooling process were carried out by using the simplified two-step warming method. Once acceptable viabilities were reached an automatic LT warming process was developed. Attempts to solely use a 20% glucose solution, which was held at room temperature and pumped into the sample carrier at temperature between -25˚C and 0˚C, failed not because of ice formation but because no post-warming viability was detected. As a second approach the sample CPA concentration was reduced by adding in the following order 50%, 40%, 30% (w/v) CPA No.18 and 1xPBS while keeping the sample as close to its liquidus curve as possible. For practical reasons the difference of inlet and sample CPA concentration was selected to be at least 10% - similar to the cooling process - as otherwise the dilution process and the entire LT process would have taken too long. High viabilities similar to the two-step manual LT process were achieved.

An important aspect of LT, due to its overall time length is the question of whether cell survival is reduced over time once the conditions are maintained constant. For automatic LT it was shoen that viability was lower at higher CPA concentrations, but did not change over time at -15˚C, -20˚C and -25˚C at CPA concentrations of 50%, 55%, and 65% (w/v). Only at -7˚C and 35% (w/v) CPA No.18 viability was significantly reduced after one hour. For the final LT cooling set up, 35% CPA is reached at approximately -12˚C and concentration over 50% at temperatures below -20˚C. It is therefore most likely that the time factor of the final cooling process is successfully suppressed which means that upscaling could be possible in principle.

An interesting effect was seen when beads of varying cell densities were used for automatic LT. Low cell density beads tested in the same experiment and therefore undergoing exactly the same procedure than high cell density beads, showed significantly reduced cell survival. This was regardless whether AELC were cooled to -40˚C or below the glass transition point (-125˚C). To measure cell numbers and protein production exclusively beads of the same cell density had to be used, but the effect was the same. 3D cell cultures of higher cell density undergoing the complete automatic LT process including cooling to -40˚C, vitrification and warming, showed higher post-warming viability, cell number and protein production. For cell densities of $17*10^6$ and $20*10^6$ cells/ml of beads, viability was 70% and 90%, viable cell number 61% and 79% and albumin and alpha-fetoprotein production 48% and 54%, and 67% and 75%, respectively (fraction of the untreated control after 48 hours of post warming). Higher cell recovery of spheroid hepatocytes in comparison to single cell suspension following cryopreservation has previously been reported by Lee and colleagues (Lee et al., 2012). Higher cell activity as noted in 3-D cell cultures (Bokhari et al., 2007; Coward et al., 2009; Lee et al., 2012; Selden et al., 1999) has been previously linked to higher cell recovery following cryopreservation in single cell suspension. Cells cultures during their exponential growth are metabolically more active and showed higher post warming viability than cells cryopreserved when reaching the lag phase (Cho et al., 2000). Vitrification studies by Magalhães have shown better post-cryopreservation viability for tissue-like culture than for single cells. They concluded that cell-to-cell contact is beneficial in the maintenance of viability (Magalhães et al., 2012).

In respect to shear forces created by the stirrer during LT, it can be expected that higher cell density is beneficial, as the outer cells may provide protection to those located closer to the centre. This also applies in respect to excessive dehydration. In 3-dimensional cell constructs, water diffuses sequentially from one cell to its neighborhood. Cells in the surface layer respond to osmotic changes in the extracellular medium, interior cells respond only to osmotic changes in cells of surfaces, and thus are exposed to slower rates of dehydration (Levin et al., 1977).

7.6 Conclusion

In this chapter the different parts of the LT process – cooling, vitrification and warming – were investigated and improved individually before they were finally set together to form the entire LT process. The set-up was changed from the "one-solution" to the "two-solution" mode for both the cooling and warming process. Important aspects of the automatic LT process were examined which included CPA toxicity over time, cell density and most importantly the mixing effects. Changes to the CPA No.18 solution and pre-incubation conditions showed little effect. Higher post-warming viability and performance are still expected for a further optimized stirring and CPA inlet system and for 3D cultures of higher cell density (< 20 million cells/ml beads). The addition of ice blockers or antifreeze proteins might provide an additional possibility to reduce the CPA concentration throughout the LT process and to further reduce CPA toxicity. Overall Liquidus Tracking can be regarded as a promising tool for large scale cryopreservation of 3D cell cultures.

CHAPTER 8
General Discussion

The overall aim of this thesis was to establish a large scale cryopreservation protocol for alginate encapsulated liver cells that would deliver high functional recovery sufficient to replace liver function when used within a bioartificial liver device. For this purpose the new technique of automatic Liquidus Tracking was applied, which allows to vitrify a volume of 500ml in a slow cooling process.

8.1 Viability assessment

The first aspect of this thesis was to establish a rapid and conclusive method to evaluate cell recovery after cryopreservation to improve the Liquidus Tracking (LT) process (Chapter 3). In this respect the use of a membrane integrity test proved to be the most suitable with the additional advantage that disaggregation of cell spheroids and dissolving of the alginate capsule was unnecessary. A digital imaging system, a combination of a microscope, a charge-coupled device (CCD) camera, a computer and an imaging software program, was used to detect and quantify the fluorescence signal of fluorescein and propidium iodide. It was shown that the standardized method was sufficiently reliable to describe post-stress viability to compare experimental conditions. This was verified by ELISA, cell count and MTT measurements. Similar to the digital imaging system a method for the use of a fluorescent plate reader was developed.

Other possibilities to evaluate cell recovery are various and might give a more detailed estimation of cell death and vitality. For example, changes in protein kinase cascades and cell cycle but also markers for apoptosis and inflammation have previously been used to determine hepatocellular stress and injury (Beyer et al., 2007; de Longueville et al., 2003; Heinloth et al., 2004; Kiyosawa et al., 2006; Reilly et al., 2001). Gene expression patterns could be used to investigate those changes in an effective manner. DNA microarrays or reverse transcription quantitative real-time PCR (RT-qPCR) are reliable techniques and have been previously used for the validation of toxicity biomarkers (Guo et al., 2009; Rokushima et al., 2007). Two examples for HepG2

toxicity biomarkers are cytokine receptor IL-11RA which was strongly increased upon exposure to acetaminophen while the transcription factor Myc was reduced by 30% (Fox et al., 2010). However those systems are likely to be more time consuming and expensive and are therefore more useful to evaluate the LT method once fully established. For the developing process itself our system was considered the better choice.

8.2 Cryoprotectant agents for Liquidus Tracking

First experiments with alginate encapsulated liver cells (AELC) demonstrated strong Me_2SO toxicity. By combining commonly used CPAs of relatively low viscosity (Chapter 5) so that effective mixing was provided at low subzero temperatures, nine particularly useful CPA solutions of low toxicity and viscosity were defined. Although developed to be first of low viscosity and then of low toxicity as well as being a good vitrifier, solution No18 (containing Me_2SO, ethylene glycol and glucose in a ratio of 4/2/1), resembled those vitrification solutions that are commercially available. It is therefore questionable whether a better CPA solution for LT can be developed by replacing one of these main components.

However the addition of synthetic ice-blockers (SIB) to prevent heterogenous ice nucleation or antifreeze proteins (AFP) to modify ice growth creates the possibility of reducing the amount of toxic CPAs (Wowk et al., 2000). Examples of commonly used SIBs are 1,3 cyclohexanediol (1,3 CHD), 2,3 butanediol and polyethylene glycol (PEG-400) (Eisenberg et al., 2012; Fahy, 2004). Most active AFPs so far have been found in insects (Knight, 2000; Lin et al., 2011). One of the most potent AFPs (*Ri*AFP) was found in the longhorn beetle *Rhagium inquisitor* which can be supercooled to below -25°C (Hakim et al., 2013). However AFP from insects cannot be produced in sufficient quantities and AFPs from other sources such as fish or monoclonals are expensive and can only be used for small volume vitrification. Thus, for large scale cryopreservation synthetic ice blockers are a better choice.

In general, SIBs and AFPs have a greater effect on influencing ice nucleation and growth than accounted for on a colligative basis, which favours reduced osmotic stress. This offers the possibility not only to replace toxic CPAs but also to reduce the amount

of CPAs needed to suppress ice formation during the LT process and to achieve a stable vitrified state. The addition of SIBs and AFPs might be especially valuable for the warming process, when devitrification has to be avoided. While in my studies a final concentration of 62% (w/v) Me_2SO was sufficient to avoid visible ice formation during the cooling process to -125˚C for a volume of 400ml, the concentration had to be increased to 64% to avoid devitrification during warming. This points to important factors of the kinetics for ice nucleation at cryogenic temperatures which require further study.

8.3 Liquidus Tracking

Cryo-banking of larger structures, such as tissues or organs, remains elusive with only rare claims of success (Fahy et al., 2004) and dispersed, cellular systems, in volumes above 10ml, have required sample size manipulation (e.g. into a thin film volume format (Massie et al., 2014; Sputtek et al., 2011). For dispersed cell system of large volumes, inhomogeneous warming and cooling rates are problematic. When using a slow cooling protocol, cells that are cooled too fast may not dehydrate sufficiently to avoid intracellular ice formation and others may be exposed for too long to high concentrations of injurious CPAs (Karlsson et al., 1993; Koshimoto & Mazur, 2002; Pegg et al., 2006; Toner et al., 1990). During warming, devitrification and/or ice recrystallisation becomes more likely. For 3-dimensional structures the formation of extracellular ice in liquid spaces within the tissue, such as within small capillary blood vessels inside an organ (Hunt, 1984; Jacobsen et al., 1984; Pegg, 2010) physically destroys the internal structure.

Ice formation can be avoided by vitrification but, high cooling rates must be imposed to avoid toxic effects. This is neither possible for tissues nor for tissue like cell constructs as enough time must be given for CPAs to penetrate into the cells, nor for large sample volumes (>1ml) where high cooling and warming rates cannot be achieved. Those obstacles are overcome by Liquidus Tracking (LT), a method of achieving vitrification at minimized toxicity by decreasing the sample temperature to just above the melting point before the CPA concentration of the sample is increased (Farrant, 1965a; Pegg et al., 2006; Wang et al., 2007).

8.4 Manual Liquidus Tracking

To understand the LT process but also to pre-test conditions for automatic LT, different methods to carry out manual LT were established and evaluated (Chapter 4). The most practical approach to increase the sample CPA concentration was to add highly concentrated CPA (60-80%) while the sample was being cooled in a controlled rate-freezer. The method was further improved by using an insulation thermal buffer system to reduce temperature fluctuation during the addition of new CPAs and a special stirrer was invented to increase mixing effectiveness of viscous solution. A two-step LT cooling and warming process proved to be more suitable to pre-test conditions for automatic LT than a multistep LT process. Although fewer addition and reduction steps were used, (higher CPA concentration at the same temperature) viabilities of up to 90% were reached. A two-step (possibly a three step process for cells that are more sensitive to CPAs) has the additional advantage, that the volume during CPA addition does not increase greatly and thus, making a reduction step at subzero temperatures unnecessary. Although this is possible for encapsulated cells, this is not suitable for single cells, which do not sink to the bottom of the sample carrier by gravity, so that the CPA solution on top can be taken off. In my work manual LT was only used for pre-testing purposes. However, to be used as an independent protocol for long-term preservation, sterility has to be maintained. For this either a cooled laminar flow or a small portable cooling system that can be placed under a conventional laminar flow could be used.

8.5 Automatic Liquidus Tracking

Automatic Liquidus Tracking (Chapter 6 and 7) provides a promising possibility to cryopreserve large volumes, tissues and organs in the future. Interestingly incubation temperature once below -20˚C, and incubation time had no or only a small impact on cell survival, whereas changes made to the mixing properties by using a propeller instead of a Planer stirrer or by changing the outlet port height, drastically increased post-warming viability by 40%. More work is required to fully characterize stirring effects, which could also enlighten the process of sample preparation for conventional vitrification. An investigation at the National Institute of Biological Standards and

Controls (NIBSC) has shown that cell recovery after vitrification varied considerably between technicians (Fleck et al., 2013). It is possible that mixing formed part of these differences. A better understanding could help to improve cell recovery and lead to better standardization of vitrification protocols.

Changes made to the original automatic LT protocol developed by Planer, such as the use of a two-step instead of a single-step solution mode, would need to be automated. This would markedly facilitate the test procedure and enhance reliability. It also has to be considered whether it can be ensured that all CPAs are washed off from AELC before starting to treat the patient.

Careful consideration ought to be given to how the process can be maintained under sterile conditions when disconnecting and reconnecting the sample carrier from the outlet and inlet tubes, to be stored at subzero temperatures. In addition benefits of different storage temperatures should be tested. While storage at -80˚C could be more accessible in laboratories and clinics and the CPA concentration could be potentially be reduced, ice formation during storage and thus recrystallization during warming could have an impact on cell survival especially for long-term storage.

8.6 Improving the Liquidus Tracking procedure

For the use in a bioartificial liver (BAL) device cell viability following cryopreservation by LT has to be further improved. At the moment the system can achieve viabilities of more than 70% and a alpha-fetoprotein production of approximately 70% when AELC with a cell densities of more than $17*10^6$ cells/ml of beads are used (fraction of the untreated control after 48 hours of post warming). However, for the use in a BAL viability and a protein production of more than 90% should be reached. As bioreactor size and thus, the bead volume are limited, high cell density and viability are required to deliver sufficient biomass to replace liver function. In addition debris and DNA from dead cells contained in the plasma may be returned to the patient and trigger an immune or inflammatory response. Hepatoblastoma HepG2 DNA poses an additional risk of tumourigenesis. Although a filter system will be part of the BAL circuit, less cell fragments within the plasma would reduce the risk of a filter overload and thus the potential risk to the patient.

To improve the LT system it would be highly advantageous if the intracellular CPA and water concentration over the LT process could be monitored. For example, if it can be shown that CPA toxicity is negligible once CPA and water flux are (nearly) reversed and in case this happens within the temperatures range (0 to -40˚C) of CPA addition and reduction, LT protocols could be adapted. The CPA concentration could be increased at a higher temperature to assure intracellular vitrification before cooling the sample to a temperature of reversed membrane flux. Once reached, the concentration needed to prevent devitrification during warming may be realised.

Proton nuclear magnetic resonance spectroscopy (NMR) has been used to measure the Me_2SO in rat liver and cornea (Fuller et al., 1989; Walcerz et al., 1995). A more recent approach makes use of the Me_2SO sulfur atom which strongly increases the mass attenuation, making the concentration measurable by x-ray computed tomography (CT). This method has the advantage of being non-invasive and precise, making it possible to measure the concentration inside a single cell. In addition ice crystals are detectable so that CPA addition and cooling rate can be adjusted to provide sufficient CPA penetration (Sousa, 2013). The water content can be measured by differential scanning calorimetry (DSC) and Fourier transform infrared spectroscopy (FTIR) (Akhoondi et al., 2011; Devireddy et al., 1998). However, it is questionable as to how any of these applications could be used for "in-process" measurements of automatic large scale LT, but samples might be taken and vitrified in liquid nitrogen to be measured later at a predefined subzero temperature at which no further changes are expected or by warming the samples using DSC. Raman spectroscopy seems to be an even more promising method. Used to monitor sample quality during cold storage at temperatures as low as -140˚C, Raman is able to "visualize" single cells and distinguish between water, ice and different cryoprotectants (Dorr et al., 2012).

Although not an option for manual LT, as it works with an open system, applying higher sample pressure (Fahy et al., 1984) could help to reduce CPA toxicity, provided that LT pumps and stirrer remain unaffected. The approach of supercooling facilitated by a variable magnetic field (Kobayashi & Kirschvink, 2014) seems promising and has shown good success for the vitrification of ovarian cortex tissue (Moriguchi et al., 2012). Programmed freezers with an oscillating magnetic field have already been built

and used for human embryonic stem cells preservation (Lin et al., 2013), so the combination of LT and supercooling might be an interesting approach.

However, at the moment still the most promising approach to improve LT cell recovery is the use of different stirrer types and speed; for example a higher speed would be useful to increase homogenisation and a lower speed would be preferable to reduce membrane permeability.

8.7 Further methods to increase cell recovery

Cell death can result following either apoptosis or necrosis. While necrotic cell death is uncontrolled and results from external influences, apoptosis (programmed cell death) is initiated by intracellular and extracellular signalling pathways. Apoptosis can be stimulated by cytokines and hormones but also by environmental stress factors. For example, apoptosis following cryopreservation was reported for liver cells and slices (Fujita et al., 2005; Martin et al., 2000; Vanhulle et al., 2006), embryonic stem cells (Xu et al., 2010) and sperm (Khan et al., 2009; Martin et al., 2007). The release of reactive oxygen species (ROS), is known to trigger apoptosis in liver (San-Miguel et al., 2006) and HepG2 cells (Oh & Lim, 2006) and oxidative stress following hypothermia was shown to lead to apoptosis (Fujita et al., 2005; Rauenet al., 1999).

The addition of antioxidants such as Trolox and N-acetyl-cysteine to the cryopreservation media to reduce ROS is one approach to improve cell recovery and has been shown to be successful for sperm cells (Peña et al., 2004; Thuwanut et al., 2008) and rat hepatocytes (Vairetti et al., 2001). Although the use of Viaspan (containing glutathione as an antioxidant) instead of PBS (Chapter 6) did not increase cell viability after LT, the use of different types of antioxidants possibly at a different concentration might be more successful.

Other possibilities to influence the signalling pathway or to reduce apoptosis-triggering factors might be more effective for LT. For example, the addition of caspase inhibitors proved successful for the cryopreservation of primary liver cells (Matsushita et al., 2003; Yagi et al., 2001), porcine hepatocytes (Yagi et al., 2001), human haematopoietic stem cells (Stroh et al., 2002) and mice ovarian tissue (Zhang et al., 2009), while the

upregulation of heat shock proteins (HSPs) reportedly improved liver cell and tissue recovery after hypothermia (Chen & Gao, 2004; Kao et al., 2008). In addition, the hepatocyte growth factor (HGF) was shown to be an effective anti-apoptotic agent for adult human hepatocytes (Saich et al., 2007; Schulze-Bergkamen et al., 2004). Rho-associated kinase (ROCK) inhibitors have also been shown to reduce apoptosis and improve recovery of cryopreserved human stem cells (Gauthaman et al., 2010; Martin-Ibañez et al., 2008).

However, costs for the reagents have to be considered as large amounts are needed and due to the constant exchange of solution the best moment for addition has to be evaluated.

8.8 Further applications for Liquidus Tracking

Apart from our intended use to cryopreserve AELC for the use in a BAL, there are many more applications for encapsulated 3D cell cultures and the necessity for long-term storage. It has been recognized that two-dimensional cell culture (2D) systems do not accurately reproduce the functions and physiology of living tissues. In recent years three-dimensional cell culture systems have been developed that better reflect complex tissue structures with normal differentiation, polarization, cell behaviour and intercellular interactions (Bokhari et al., 2007; O'Brien et al., 2006; Pampaloni et al., 2007). Those 3D tissue-like cell cultures can provide valuable information for basic research but also for tissue organ engineering, stem cell research and drug discovery. In vitro cell types such as primary hepatocytes and immortalized cell lines are useful means for initial screening of the hepato-toxic effects of drugs, however culturing cells three-dimensional is more comparable to its natural architecture environment and was shown to improve the morphological characteristics of human HepG2 cells in culture (Khalil et al., 2001; Guillouzo & Guguen-Guillouzo, 2008).

Moreover, encapsulation as a means to isolate transplanted cells from the patient's immune system has generated an emerging interest in cell-based medicine for the treatment of diseases such as diabetes, liver failure, neurodegenerative, musculoskeletal, and cardiovascular diseases (Lim & Sun, 1980; Murua et al., 2008; Orive et al., 2003). The host immune rejection of transplanted donor cells is a problem that is often

addressed by administrating drugs for immunosuppression, but a suppressed immune system also puts the patient at risk for other diseases. Cell encapsulation with potentially higher cell density could offer an alternative to protect the transplanted cells from being damaged by the host's immune system while allowing free diffusion of nutrients, metabolites and metabolic waste. In addition encapsulation protects the cells from physical damage, which is an important aspect of automatic LT, but also has the potential advantage of enhancing cell growth. Studies have focused on the use of stem cells and induced pluripotent stem cells for their potential in cellular therapy and the favorable effect that micro-environment has on survival and functioning (Yagi et al., 2009).

Another application for which the LT system might be useful is the preservation of skin allografts. Perfusion as needed for other organs is not required and the cell thickness of skin (2mm) is comparable to that of cartilage (7mm) and AELC (0.5mm). Skin transplants for the treatment of burns and other wounds are not always available in adequate quantities making skin graft preservation important in meeting the need for skin transplantation. Vitrification (Fujita et al., 2000) and slow freezing protocols (Ben-Bassat et al., 1996, 2001) have been successfully used to cryopreserve cadaveric half skin but there is still a need to cryopreserve larger pieces of skin allograft and skin grafts of greater thickness (e.g full skin).

References

Abrahamse, S.L., van Runnard Heimel, P., Hartman, R.J., Chamuleau, R.A.F.M., and van Gulik, T.M. (2003). Induction of necrosis and DNA fragmentation during hypothermic preservation of hepatocytes in UW, HTK, and Celsior solutions. Cell Transplant. *12*, 59–68.

Acker, J.P., and McGann, L.E. (1989). The role of cell-cell contact on intracellular ice formation. 1989 *19*, 367–374.

Acker, J.P., and McGann, L.E. (2000). Cell-cell contact affects membrane integrity after intracellular freezing. Cryobiology *40*, 54–63.

Acker, J.P., Elliott, J.A., and McGann, L.E. (2001). Intercellular ice propagation: experimental evidence for ice growth through membrane pores. Biophys. J. *81*, 1389–1397.

Adam, R., and Hoti, E. (2009). Liver transplantation: the current situation. Semin. Liver Dis. *29*, 3–18.

Akhoondi, M., Oldenhof, H., Stoll, C., Sieme, H., and Wolkers, W.F. (2011). Membrane hydraulic permeability changes during cooling of mammalian cells. Biochim. Biophys. Acta *1808*, 642–648.

Allen, J.P., Litten, R.Z., Strid, N., and Sillanaukee, P. (2001). The role of biomarkers in alcoholism medication trials. Alcohol. Clin. Exp. Res. *25*, 1119–1125.

Anchordoguy, T.J., Carpenter, J.F., Crowe, J.H., and Crowe, L.M. (1992). Temperature-dependent perturbation of phospholipid bilayers by dimethylsulfoxide. Biochim. Biophys. Acta *1104*, 117–122.

Angell, C.A. (1981). The Glass Transition: Comparison of Computer Simulation and Laboratory Studies*. Ann. N. Y. Acad. Sci. *371*, 136–150.

Arnaud, F.G., Khirabadi, B., and Fahy, G.M. (2003). Physiological evaluation of a rabbit kidney perfused with VS41A. Cryobiology *46*, 289–294.

Baertschiger, R.M., Berney, T., and Morel, P. (2008). Organ preservation in pancreas and islet transplantation. Curr. Opin. Organ Transplant. *13*, 59–66.

Baicu, S.C., and Taylor, M.J. (2002). Acid-base buffering in organ preservation solutions as a function of temperature: new parameters for comparing buffer capacity and efficiency. Cryobiology *45*, 33–48.

Balasubramanian, S.K., Bischof, J.C., and Hubel, A. (2006). Water transport and IIF parameters for a connective tissue equivalent. Cryobiology *52*, 62–73.

Bañares, R., Nevens, F., Larsen, F.S., Jalan, R., Albillos, A., Dollinger, M., Saliba, F., Sauerbruch, T., Klammt, S., Ockenga, J., et al. (2013). Extracorporeal albumin dialysis with the molecular adsorbent recirculating system in acute-on-chronic liver failure: the RELIEF trial. Hepatol. Baltim. Md *57*, 1153–1162.

Barry J. Fuller, Nick Lane, Erica E. Benson (2004). Life in the frozen state (London: CRC Press).

Ben-Bassat, H., Strauss, N., Ron, M., Chaouat, M., Breiterman, S., Israeli, A., Wexler, M.R., and Eldad, A. (1996). Transplantation performance of human skin cryopreserved by programmed or stepwise freezing and stored at -80 degrees C or -180 degrees C. J. Burn Care Rehabil. *17*, 421–428.

Ben-Bassat, H., Chaouat, M., Segal, N., Zumai, E., Wexler, M.R., and Eldad, A. (2001). How long can cryopreserved skin be stored to maintain adequate graft performance? Burns J. Int. Soc. Burn Inj. *27*, 425–431.

Baudot, null, and Boutron, null (1998). Glass-forming tendency and stability of aqueous solutions of diethylformamide and dimethylformamide. Cryobiology *37*, 187–199.

Baudot, A., Alger, L., and Boutron, P. (2000). Glass-forming tendency in the system water-dimethyl sulfoxide. Cryobiology *40*, 151–158.

Belle, S.H., Beringer, K.C., and Detre, K.M. (1995). An update on liver transplantation in the United States: recipient characteristics and outcome. Clin. Transpl. 19–33.

Benson, C.T., and Critser, J.K. (1994). Variation of water permeability (Lp) and its activation energy (Ea) among unfertilized golden hamster and ICR murine oocytes. Cryobiology *31*, 215–223.

Bentley-Mowat JA (1982). Application of fluorescence microscopy to pollution studies on marine phytoplankton. Bot Mar *25*, 2003–2004.

Beyer, R.P., Fry, R.C., Lasarev, M.R., McConnachie, L.A., Meira, L.B., Palmer, V.S., Powell, C.L., Ross, P.K., Bammler, T.K., Bradford, B.U., et al. (2007). Multicenter study of acetaminophen hepatotoxicity reveals the importance of biological endpoints in genomic analyses. Toxicol. Sci. Off. J. Soc. Toxicol. *99*, 326–337.

Bird, T.G., Lorenzini, S., and Forbes, S.J. (2008). Activation of stem cells in hepatic diseases. Cell Tissue Res. *331*, 283–300.

Bodas, K., Brenning, C., Diller, K.R., and Brand, J. (1995). Cryopreservation of blue-green and eukaryotic algae in the culture collection at the University of Texas at Austin. CryoLetters *16*, 267–274.

Bokhari, M., Carnachan, R.J., Cameron, N.R., and Przyborski, S.A. (2007). Culture of HepG2 liver cells on three dimensional polystyrene scaffolds enhances cell structure and function during toxicological challenge. J. Anat. *211*, 567–576.

Bonner, G., and Klibanov, A.M. (2000). Structural stability of DNA in nonaqueous solvents. Biotechnol. Bioeng. *68*, 339–344.

Boutron, P. (1986). Comparison with the theory of the kinetics and extent of ice crystallization and of the glass-forming tendency in aqueous cryoprotective solutions. Cryobiology *23*, 88–102.

Boutron, P., and Kaufmann, A. (1979). Stability of the amorphous state in the system water--1,2-propanediol. Cryobiology *16*, 557–568.

Brand, J.J., and Diller, K.R. (2004). Application and theory of algal cryopreservation. Nova Hedwig. *79*, 175–189.

Brugmans, M.J.P., and Vos, W.L. (1995). Competition between vitrification and crystallization of methanol at high pressure. J. Chem. Phys. *103*, 2661–2669.

Butler, P.J., Norwich, G., Weinbaum, S., and Chien, S. (2001). Shear stress induces a time- and position-dependent increase in endothelial cell membrane fluidity. Am. J. Physiol. Cell Physiol. *280*, C962–C969.

Den Butter, G., Saunder, A., Marsh, D.C., Belzer, F.O., and Southard, J.H. (1995). Comparison of solutions for preservation of the rabbit liver as tested by isolated perfusion. Transplant International *8*, 466–471.

Carey, H.V., Andrews, M.T., and Martin, S.L. (2003). Mammalian hibernation: cellular and molecular responses to depressed metabolism and low temperature. Physiol. Rev. *83*, 1153–1181.

Carpenter, J.F., Martin, B., Loomis, S.H., and Crowe, J.H. (1988). Long-term preservation of dried phosphofructokinase by sugars and sugar/zinc mixtures. Cryobiology *25*, 372–376.

Ceballos-Picot, I., Witko-Sarsat, V., Merad-Boudia, M., Nguyen, A.T., Thévenin, M., Jaudon, M.C., Zingraff, J., Verger, C., Jingers, P., and Descamps-Latscha, B. (1996). Glutathione antioxidant system as a marker of oxidative stress in chronic renal failure. Free Radic. Biol. Med. *21*, 845–853.

Chen, K., and Gao, X. (2004). Exogenous endothelin-1 induced pulmonary hemorrhage in newborn rats and the antagonizing effect of calcitonin gene-related peptide. J. Pediatr. *42*, 446–449.

Cho, J.-S., Chun, S.-H., Lee, S.-J., Kim, I.-H., and Kim, D.-I. (2000). Development of cell line preservation method for research and industry producing useful metabolites by plant cell culture. Biotechnol. Bioprocess Eng. *5*, 372–378.

Clark, P., Fahy, G.M., and Karow, A.M. (1984). Factors influencing renal cryopreservation. II. Toxic effects of three cryoprotectants in combination with three vehicle solutions in nonfrozen rabbit cortical slices. Cryobiology *21*, 274–284.

Conlon, J.M., Yano, K., Chartrel, N., Vaudry, H., and Storey, K.B. (1998). Freeze tolerance in the wood frog Rana sylvatica is associated with unusual structural features in insulin but not in glucagon. J. Mol. Endocrinol. *21*, 153–159.

Coward, S.M., Selden, C., Mantalaris, A., and Hodgson, H.J.F. (2005). Proliferation rates of HepG2 cells encapsulated in alginate are increased in a microgravity environment compared with static cultures. Artif. Organs *29*, 152–158.

Coward, S.M., Legallais, C., David, B., Thomas, M., Foo, Y., Mavri-Damelin, D., Hodgson, H.J., and

Selden, C. (2009). Alginate-encapsulated HepG2 cells in a fluidized bed bioreactor maintain function in human liver failure plasma. Artif. Organs *33*, 1117–1126.

Crowe, J.H., Crowe, L.M., Carpenter, J.F., and Aurell Wistrom, C. (1987). Stabilization of dry phospholipid bilayers and proteins by sugars. Biochem. J. *242*, 1–10.

David, B., Doré, E., Jaffrin, M.Y., and Legallais, C. (2004). Mass transfers in a fluidized bed bioreactor using alginate beads for a future bioartificial liver. Int. J. Artif. Organs *27*, 284–293.

Demetriou, A.A., Brown, R.S., Busuttil, R.W., Fair, J., McGuire, B.M., Rosenthal, P., Am Esch, J.S., Lerut, J., Nyberg, S.L., Salizzoni, M., et al. (2004). Prospective, randomized, multicenter, controlled trial of a bioartificial liver in treating acute liver failure. Ann. Surg. *239*, 660–670.

Devasagayam, T.P.A., Tilak, J.C., Boloor, K.K., Sane, K.S., Ghaskadbi, S.S., and Lele, R.D. (2004). Free radicals and antioxidants in human health: current status and future prospects. J. Assoc. Physicians India *52*, 794–804.

Devireddy, R.V., Raha, D., and Bischof, J.C. (1998). Measurement of water transport during freezing in cell suspensions using a differential scanning calorimeter. Cryobiology *36*, 124–155.

Dhali, A., Manik, R.S., Das, S.K., Singla, S.K., and Palta, P. (2000). Vitrification of buffalo (Bubalus bubalis) oocytes. Theriogenology *53*, 1295–1303.

Diller, K.R. (1975). Intracellular freezing: effect of extracellular supercooling. Cryobiology *12*, 480–485.

Dorr, D., Stracke, F., and Zimmermann, H. (2012). Noninvasive Quality Control of Cryopreserved Samples. Biopreservation Biobanking *10*, 529–531.

Dowgert, M.F., and Steponkus, P.L. (1984). Behavior of the Plasma Membrane of Isolated Protoplasts during a Freeze-Thaw Cycle. Plant Physiol. *75*, 1139–1151.

Edgar, D.H., and Gook, D.A. (2012). A critical appraisal of cryopreservation (slow cooling versus vitrification) of human oocytes and embryos. Hum. Reprod. Update *18*, 536–554.

Ehrhart, F., Schulz, J.C., Katsen-Globa, A., Shirley, S.G., Reuter, D., Bach, F., Zimmermann, U., and Zimmermann, H. (2009). A comparative study of freezing single cells and spheroids: towards a new model system for optimizing freezing protocols for cryobanking of human tumours. Cryobiology *58*, 119–127.

Eisenberg, D.P., Taylor, M.J., and Rabin, Y. (2012). Thermal expansion of the cryoprotectant cocktail DP6 combined with synthetic ice modulators in presence and absence of biological tissues. Cryobiology *65*, 117–125.

Elford, B.C. (1970). Diffusion and distribution of dimethyl sulphoxide in the isolated guinea-pig taenia coli. J. Physiol. *209*, 187–208.

Elford, B.C., and Walter, C.A. (1972). Effects of electrolyte composition and pH on the structure and function of smooth muscle cooled to -79 degrees C in unfrozen media. Cryobiology *9*, 82–100.

Ellis, A.J., Hughes, R.D., Wendon, J.A., Dunne, J., Langley, P.G., Kelly, J.H., Gislason, G.T., Sussman, N.L., and Williams, R. (1996). Pilot-controlled trial of the extracorporeal liver assist device in acute liver failure. Hepatol. Baltim. Md *24*, 1446–1451.

Erecinska, M., Thoresen, M., and Silver, I.A. (2003). Effects of hypothermia on energy metabolism in Mammalian central nervous system. J. Cereb. Blood Flow Metab. *23*, 513–530.

Eroglu, A., Russo, M.J., Bieganski, R., Fowler, A., Cheley, S., Bayley, H., and Toner, M. (2000). Intracellular trehalose improves the survival of cryopreserved mammalian cells. Nat. Biotechnol. *18*, 163–167.

Erro, E., Bundy, J., Massie, I., Chalmers, S.-A., Gautier, A., Gerontas, S., Hoare, M., Sharratt, P., Choudhury, S., Lubowiecki, M., et al. (2013). Bioengineering the liver: scale-up and cool chain delivery of the liver cell biomass for clinical targeting in a bioartificial liver support system. BioResearch Open Access *2*, 1–11.

Fahy, G.M. (2004). Methods of using ice-controlling molecules. Organ Recovery Systems, Inc. Patent number 6773877.

Fahy, G.M. (2010). Cryoprotectant toxicity neutralization. Cryobiology *60*, S45–S53.

Fahy, G.M., MacFarlane, D.R., Angell, C.A., and Meryman, H.T. (1984). Vitrification as an approach to cryopreservation. Cryobiology *21*, 407–426.

Fahy, G.M., daMout, C., Tsonev, L., Khirabadi, B., Mehl, P., and Meryman, H.T. (1995). Cellular injury associated with organ cryopreservation: chemical toxicity and cooling injury. In J.J. Lemasters, C. Oliver (Eds.), Cell Biology of Trauma.

Fahy, G.M., Wowk, B., Wu, J., Phan, J., Rasch, C., Chang, A., and Zendejas, E. (2004). Cryopreservation of organs by vitrification: perspectives and recent advances. Cryobiology *48*, 157–178.

Fan, W.-X., Ma, X.-H., Ge, D., Liu, T.-Q., and Cui, Z.-F. (2009). Cryoprotectants for the vitrification of corneal endothelial cells. Cryobiology *58*, 28–36.

Farrant, J. (1965a). Permeability og guinea pig smooth muscle to non-electrolytes. J. Physiol. *178*, 1–13.

Farrant, J. (1965b). Mechanism of Cell Damage During Freezing and Thawing and its Prevention. Nature *205*, 1284–1287.

Farrant, J., and Woolgar, A.E. (1972). Human red cells under hypertonic conditions; a model system for investigating freezing damage. I. Sodium chloride. Cryobiology *9*, 9–15.

Fathallah, H., Coezy, E., de Neef, R.S., Hardy-Dessources, M.D., and Giraud, F. (1995). Inhibition of

deoxygenation-induced membrane protein dephosphorylation and cell dehydration by phorbol esters and okadaic acid in sickle cells. Blood *86*, 1999–2007.

Fleck, R.A., Stacey, G.S., Hunt, C.J., Jung, L., and Healy, L. (2013). Comparison of cryopreservation and vitrification methods for preservation of human embtyonic stem cell lines. Cryo-Letters *34*, 174–216.

Fox, B.C., Devonshire, A.S., Schutte, M.E., Foy, C.A., Minguez, J., Przyborski, S., Maltman, D., Bokhari, M., and Marshall, D. (2010). Validation of reference gene stability for APAP hepatotoxicity studies in different in vitro systems and identification of novel potential toxicity biomarkers. Toxicol. Vitro. *24*, 1962–1970.

De Freitas, R.C., Diller, K.R., Lachenbruch, C.A., and Merchant, F.A. (1998). Network thermodynamic model of coupled transport in a multicellular tissue--the islet of Langerhans. Ann. N. Y. Acad. Sci. *858*, 191–204.

Fujioka, T., Yasuchika, K., Nakamura, Y., Nakatsuji, N., and Suemori, H. (2004). A simple and efficient cryopreservation method for primate embryonic stem cells. Int. J. Dev. Biol. *48*, 1149–1154.

Fujita, R., Hui, T., Chelly, M., and Demetriou, A.A. (2005). The effect of antioxidants and a caspase inhibitor on cryopreserved rat hepatocytes. Cell Transplant. *14*, 391–396.

Fujita, T., Takami, Y., Ezoe, K., Saito, T., Sato, A.K., Takeda, N., Yamamoto, Y., Homma, K., Jimbow, K., and Sato, N. (2000). Successful preservation of human skin by vitrification. J. Burn Care Rehabil. *21*, 304–309.

Fuller, B.J. (1987). Storage of cells and tissues at hypothermia for clinical use. Symp. Soc. Exp. Biol. *41*, 341–362.

Fuller, B.J., Busza, A.L., and Proctor, E. (1989). Studies on cryoprotectant equilibration in the intact rat liver using nuclear magnetic resonance spectroscopy: a noninvasive method to assess distribution of dimethyl sulfoxide in tissues. Cryobiology *26*, 112–118.

Fuller, B.J., Petrenko, A.Y., Rodriguez, J.V., Somov, A.Y., Balaban, C.L., and Guibert, E.E. (2013). Biopreservation of hepatocytes: current concepts on hypothermic preservation, cryopreservation, and vitrification. Cryo Letters *34*, 432–452.

Gauthaman, K., Fong, C.-Y., Subramanian, A., Biswas, A., and Bongso, A. (2010). ROCK inhibitor Y-27632 increases thaw-survival rates and preserves stemness and differentiation potential of human Wharton's jelly stem cells after cryopreservation. Stem Cell Rev. *6*, 665–676.

Gilbert F., Galgani F., and Cadiou Y. (1992). Rapid assessment of metabolic activity in marine microalgae: application in ecotoxicological tests and evaluation of water quality. Marine Bioloy. *112*, 199–205.

Gilmore, J.A., McGann, L.E., Liu, J., Gao, D.Y., Peter, A.T., Kleinhans, F.W., and Critser, J.K. (1995).

Effect of cryoprotectant solutes on water permeability of human spermatozoa. Biol. Reprod. *53*, 985–995.

Gordeliy, V.I., Kiselev, M.A., Lesieur, P., Pole, A.V., and Teixeira, J. (1998). Lipid membrane structure and interactions in dimethyl sulfoxide/water mixtures. Biophys. J. *75*, 2343–2351.

Greenfield Sluder, David E. Wolf (2007). Digital Microscopy: Methods in Cell Biology (Academic Press,).

Guan, N., Blomsma, S.A., Fahy, G.M., Groothuis, G.M.M., and de Graaf, I.A.M. (2013). Analysis of gene expression changes to elucidate the mechanism of chilling injury in precision-cut liver slices. Toxicol. In Vitro. *27*, 890–899.

Guillouzo, A., and Guguen-Guillouzo, C. (2008). Evolving concepts in liver tissue modeling and implications for in vitro toxicology. Expert Opin. Drug Metab. Toxicol. *4*, 1279–1294.

Guo, L., Song, L., Wang, Z., Zhao, W., Mao, W., and Yin, M. (2009). Panaxydol inhibits the proliferation and induces the differentiation of human hepatocarcinoma cell line HepG2. Chem. Biol. Interact. *181*, 138–143.

Haidekker, M.A., L'Heureux, N., and Frangos, J.A. (2000). Fluid shear stress increases membrane fluidity in endothelial cells: a study with DCVJ fluorescence. Am. J. Physiol. Heart Circ. Physiol. *278*, H1401–H1406.

Hakim, A., Nguyen, J.B., Basu, K., Zhu, D.F., Thakral, D., Davies, P.L., Isaacs, F.J., Modis, Y., and Meng, W. (2013). Crystal structure of an insect antifreeze protein and its implications for ice binding. J. Biol. Chem. *288*, 12295–12304.

Hart, S.N., Li, Y., Nakamoto, K., Subileau, E., Steen, D., and Zhong, X. (2010). A comparison of whole genome gene expression profiles of HepaRG cells and HepG2 cells to primary human hepatocytes and human liver tissues. Drug Metab. Dispos. Biol. Fate Chem. *38*, 988–994.

Hazell, A.S., and Butterworth, R.F. (1999). Hepatic encephalopathy: An update of pathophysiologic mechanisms. Proc. Soc. Exp. Biol. Med. *222*, 99–112.

Heinloth, A.N., Irwin, R.D., Boorman, G.A., Nettesheim, P., Fannin, R.D., Sieber, S.O., Snell, M.L., Tucker, C.J., Li, L., Travlos, G.S., et al. (2004). Gene expression profiling of rat livers reveals indicators of potential adverse effects. Toxicol. Sci. *80*, 193–202.

Hunt, C.J. (1984). Studies on cellular structure and ice location in frozen organs and tissues: the use of freeze-substitution and related techniques. Cryobiology *21*, 385–402.

Isaacson, Y., Salem, O., Shepherd, R.E., and Van Thiel, D.H. (1989). Lactobionic acid as an iron chelator: a rationale for its effectiveness as an organ preservant. Life Sci. *45*, 2373–2380.

Isachenko, V., Montag, M., Isachenko, E., Nawroth, F., Dessole, S., and van der Ven, H. (2004). Developmental rate and ultrastructure of vitrified human pronuclear oocytes after step-wise versus direct

rehydration. Hum. Reprod. *19*, 660–665.

Jacobsen, I.A., Pegg, D.E., Starklint, H., Chemnitz, J., Hunt, C., Barfort, P., and Diaper, M.P. (1984). Effect of cooling and warming rate on glycerolized rabbit kidneys. Cryobiology *21*, 637–653.

Jalan, R., Gines, P., Olson, J.C., Mookerjee, R.P., Moreau, R., Garcia-Tsao, G., Arroyo, V., and Kamath, P.S. (2012). Acute-on chronic liver failure. J. Hepatol. *57*, 1336–1348.

Jochem F.J. (1999). Dark survival strategies in marine phytoplankton assessed by cytometric measurement of metabolic activity with fuorescein diacetate. Marine Biology. *135*, 721–728.

Jomha, N.M., Weiss, A.D.H., Fraser Forbes, J., Law, G.K., Elliott, J.A.W., and McGann, L.E. (2010). Cryoprotectant agent toxicity in porcine articular chondrocytes. Cryobiology *61*, 297–302.

Jondet, R. (1965). A simplified method of freezing bull semen conditioned in plastic straws. Anim. Breed. *33*, 227.

Kader, A.A., Choi, A., Orief, Y., and Agarwal, A. (2009). Factors affecting the outcome of human blastocyst vitrification. Reprod. Biol. Endocrinol. *7*, 99.

Kao, Y.-H., Goto, S., Jawan, B., Nakano, T., Hsu, L.-W., Lin, Y.-C., Pan, M.-C., Lai, C.-Y., Sun, C.-K., Cheng, Y.-F., et al. (2008). Heat preconditioning ameliorates hepatocyte viability after cold preservation and rewarming, and modulates its immunoactivity. Transpl. Immunol. *18*, 220–231.

Karlsson, J.O., Cravalho, E.G., Borel Rinkes, I.H., Tompkins, R.G., Yarmush, M.L., and Toner, M. (1993). Nucleation and growth of ice crystals inside cultured hepatocytes during freezing in the presence of dimethyl sulfoxide. Biophys. J. *65*, 2524–2536.

Karmazsin, L., Balla, G., and Szöllösi, J. (1979). Cellular esterase activity: estimation by fluorescein diacetate hydrolysis. Acta Paediatr. Acad. Sci. Hung. *20*, 249–253.

Van de Kerkhove, M.P., Di Florio, E., Scuderi, V., Mancini, A., Belli, A., Bracco, A., Dauri, M., Tisone, G., Di Nicuolo, G., Amoroso, P., et al. (2002). Phase I clinical trial with the AMC-bioartificial liver. Int. J. Artif. Organs *25*, 950–959.

Khalil M, Shariat-Panahi A, Tootle R, Ryder T, McCloskey P, Roberts E, Hodgson H, Selden C. (2001). Human hepatocyte cell lines proliferating as cohesive spheroid colonies in alginate markedly upregulate both synthetic and detoxificatory liver function. J Hepatol. *34*, 68-77.

Khan, D.R., Ahmad, N., Anzar, M., and Channa, A.A. (2009). Apoptosis in fresh and cryopreserved buffalo sperm. Theriogenology *71*, 872–876.

King, T.W., Brey, E.M., Youssef, A.A., Johnston, C., and Patrick, C.W. (2002). Quantification of vascular density using a semiautomated technique for immunostained specimens. Anal. Quant. Cytol. Histol. *24*, 39–48.

Kirsop, B.E., and Snell, J.J.S. (1984). Maintenance of Microorganisms. (Academic Press, New York).

Kirsop, B., and Henry, J. (1984). Development of a miniaturised cryopreservation method for the maintenance of a wide range of yeasts. Cryo-Letters *5*, 191–200.

Kiyosawa, N., Shiwaku, K., Hirode, M., Omura, K., Uehara, T., Shimizu, T., Mizukawa, Y., Miyagishima, T., Ono, A., Nagao, T., et al. (2006). Utilization of a one-dimensional score for surveying chemical-induced changes in expression levels of multiple biomarker gene sets using a large-scale toxicogenomics database. J. Toxicol. Sci. *31*, 433–448.

Klammt, S., Stange, J., Mitzner, S.R., Peszynski, P., Peters, E., and Liebe, S. (2002). Extracorporeal liver support by recirculating albumin dialysis: analysing the effect of the first clinically used generation of the MARSystem. Liver *22 Suppl 2*, 30–34.

Knight, C.A. (2000). Structural biology. Adding to the antifreeze agenda. Nature *406*, 249, 251.

Kobayashi, A., and Kirschvink, J.L. (2014). A ferromagnetic model for the action of electric and magnetic fields in cryopreservation. Cryobiology *68*, 163–165.

Koester M., Jensen P., and Meyer-Reil LA (1991). Hydrolytic activities of organisms and biogenic structures in deep-sea sediments. Microbial enzymes in aquatic environments, 298–310.

Konev, I.E., Zhilina, Z.A., and Chamin, N.N. (1975). [Some characteristics of using polyalcohols as cryoprotectors in preserving Actinomyces noursei LIA-0471]. Antibiotiki *20*, 342–345.

Kordes, C., Sawitza, I., and Häussinger, D. (2009). Hepatic and pancreatic stellate cells in focus. Biol. Chem. *390*, 1003–1012.

Koshimoto, C., and Mazur, P. (2002). Effects of cooling and warming rate to and from -70 degrees C, and effect of further cooling from -70 to -196 degrees C on the motility of mouse spermatozoa. Biol. Reprod. *66*, 1477–1484.

Kostál, V., Zahradnícková, H., and Šimek, P. (2011). Hyperprolinemic larvae of the drosophilid fly, Chymomyza costata, survive cryopreservation in liquid nitrogen. Proc. Natl. Acad. Sci. U. S. A. *108*, 13041–13046.

Kuleshova, L.L., MacFarlane, D.R., Trounson, A.O., and Shaw, J.M. (1999). Sugars exert a major influence on the vitrification properties of ethylene glycol-based solutions and have low toxicity to embryos and oocytes. Cryobiology *38*, 119–130.

Kuleshova, L.L., Wang, X.W., Wu, Y.N., Zhou, Y., and Yu, H. (2004). Vitrification of encapsulated hepatocytes with reduced cooling and warming rates. Cryo Letters *25*, 241–254.

Kuleshova, L.L., Tan, F.C.K., Magalhães, R., Gouk, S.S., Lee, K.H., and Dawe, G.S. (2009). Effective cryopreservation of neural stem or progenitor cells without serum or proteins by vitrification. Cell Transplant. *18*, 135–144.

Lahnsteiner, F. (2008). The effect of internal and external cryoprotectants on zebrafish (Danio rerio) embryos. Theriogenology *69*, 384–396.

Lahnsteiner, F., Mansour, N., and Weismann, T. (2002). The cryopreservation of spermatozoa of the burbot, Lota lota (Gadidae, Teleostei). Cryobiology *45*, 195–203.

Lawson, A., Ahmad, H., and Sambanis, A. (2011). Cytotoxicity effects of cryoprotectants as single-component and cocktail vitrification solutions. Cryobiology *62*, 115–122.

Lee, J.-H., Jung, D.-H., Lee, D.-H., Park, J.-K., and Lee, S.-K. (2012). Effect of spheroid aggregation on susceptibility of primary pig hepatocytes to cryopreservation. Transplant. Proc. *44*, 1015–1017.

Leise, M.D., Poterucha, J.J., Kamath, P.S., and Kim, W.R. (2014). Management of hepatic encephalopathy in the hospital. Mayo Clin. Proc. *89*, 241–253.

Leunufna, S., and Keller, E.R.J. (2003). Investigating a new cryopreservation protocol for yams (Dioscorea spp.). Plant Cell Rep. *21*, 1159–1166.

Levin, R.L., Cravalho, E.G., and Huggins, C.E. (1977). Water transport in a cluster of closely packed erythrocytes at subzero temperatures. Cryobiology *14*, 549–558.

Lewis, J.G., Learmonth, R.P., and Watson, K. (1993). Role of growth phase and ethanol in freeze-thaw stress resistance of Saccharomyces cerevisiae. Appl. Environ. Microbiol. *59*, 1065–1071.

Lim, F., and Sun, A.M. (1980). Microencapsulated islets as bioartificial endocrine pancreas. Science *210*, 908–910.

Lin, F.-H., Davies, P.L., and Graham, L.A. (2011). The Thr- and Ala-rich hyperactive antifreeze protein from inchworm folds as a flat silk-like β-helix. Biochemistry (Mosc.) *50*, 4467–4478.

Lin, P.-Y., Yang, Y.-C., Hung, S.-H., Lee, S.-Y., Lee, M.-S., Chu, I.-M., and Hwang, S.-M. (2013). Cryopreservation of human embryonic stem cells by a programmed freezer with an oscillating magnetic field. Cryobiology *66*, 256–260.

Liu, B.L., and McGrath, J.J. (2005). Ice formation of vitrification solutions for cryopreservation of tissues. Conf. Proc. Annu. Int. Conf. IEEE Eng. Med. Biol. Soc. *7*, 7501–7504.

Liu, C.-C., Hsu, P.-K., Huang, W.-C., Huang, M.-H., and Hsu, H.-S. (2007). Two-layer method (UW solution/perfluorochemical plus O2) for lung preservation in rat lung transplantation. Transplant. Proc. *39*, 3019–3023.

De Longueville, F., Atienzar, F.A., Marcq, L., Dufrane, S., Evrard, S., Wouters, L., Leroux, F., Bertholet, V., Gerin, B., Whomsley, R., et al. (2003). Use of a low-density microarray for studying gene expression patterns induced by hepatotoxicants on primary cultures of rat hepatocytes. Toxicol. Sci. *75*, 378–392.

Lovelock, J.E. (1953). The mechanism of the protective action of glycerol against haemolysis by freezing

and thawing. Biochim. Biophys. Acta *11*, 28–36.

Lovelock, J.E., and Bishop, M.W. (1959a). Prevention of freezing damage to living cells by dimethyl sulphoxide. Nature *183*, 1394–1395.

Lovelock, J.E., and Bishop, M.W. (1959b). Prevention of freezing damage to living cells by dimethyl sulphoxide. Nature *183*, 1394–1395.

Luyet, B. (1937). The ultrarapid freezing of organic colloids and of protoplasm. Biodynamica 1–14.

Luyet, B., and Gehenio PM. (1940). Life and death at low temperatures. Biodynamica.

Magalhães, R., Wang, X.W., Gouk, S.S., Lee, K.H., Ten, C.M., Yu, H., and Kuleshova, L.L. (2008). Vitrification successfully preserves hepatocyte spheroids. Cell Transplant. *17*, 813–828.

Magalhães, R., Anil Kumar, P.R., Wen, F., Zhao, X., Yu, H., and Kuleshova, L.L. (2009). The use of vitrification to preserve primary rat hepatocyte monolayer on collagen-coated poly(ethylene-terephthalate) surfaces for a hybrid liver support system. Biomaterials *30*, 4136–4142.

Magalhães, R., Nugraha, B., Pervaiz, S., Yu, H., and Kuleshova, L.L. (2012). Influence of cell culture configuration on the post-cryopreservation viability of primary rat hepatocytes. Biomaterials *33*, 829–836.

Malkiel, S., Har-el, R., Schwalb, H., Uretzky, G., Borman, J.B., and Chevion, M. (1993). Interaction between allopurinol and copper: possible role in myocardial protection. Free Radic. Res. Commun. *18*, 7–15.

Mallipattu, S.K., Haidekker, M.A., Von Dassow, P., Latz, M.I., and Frangos, J.A. (2002). Evidence for shear-induced increase in membrane fluidity in the dinoflagellate Lingulodinium polyedrum. J. Comp. Physiol. A Neuroethol. Sens. Neural. Behav. Physiol. *188*, 409–416.

Manns, M.P. (2013). Liver cirrhosis, transplantation and organ shortage. Dtsch. Ärztebl. Int. *110*, 83–84.

Martin, G., Cagnon, N., Sabido, O., Sion, B., Grizard, G., Durand, P., and Levy, R. (2007). Kinetics of occurrence of some features of apoptosis during the cryopreservation process of bovine spermatozoa. Hum. Reprod. *22*, 380–388.

Martin, H., Bournique, B., Sarsat, J.P., Albaladejo, V., and Lerche-Langrand, C. (2000). Cryopreserved rat liver slices: a critical evaluation of cell viability, histological integrity, and drug-metabolizing enzymes. Cryobiology *41*, 135–144.

Martin-Ibañez, R., Unger, C., Strömberg, A., Baker, D., Canals, J.M., and Hovatta, O. (2008). Novel cryopreservation method for dissociated human embryonic stem cells in the presence of a ROCK inhibitor. Hum. Reprod. *23*, 2744–2754.

Massie, I., Selden, C., Hodgson, H., and Fuller, B. (2011). Cryopreservation of encapsulated liver

spheroids for a bioartificial liver: reducing latent cryoinjury using an ice nucleating agent. Tissue Eng. Part C Methods *17*, 765–774.

Massie, I., Selden, C., Hodgson, H., and Fuller, B. (2013). Storage temperatures for cold-chain delivery in cell therapy: a study of alginate-encapsulated liver cell spheroids stored at -80°c or -170°c for up to 1 year. Tissue Eng. Part C Methods *19*, 189–195.

Massie, I., Selden, C., Hodgson, H., Fuller, B., Gibbons, S., and Morris, G.J. (2014). GMP Cryopreservation of Large Volumes of Cells for Regenerative Medicine: Active Control of the Freezing Process. Tissue Eng. Part C Methods *20*, 693–702.

Matheny, J., Karow, A.M., and Carrier, O. (1969). Toxicity of dimethyl sulfoxide and magnesium as a function of temperature. Eur. J. Pharmacol. *5*, 209–212.

Matsushita, T., Yagi, T., Hardin, J.A., Cragun, J.D., Crow, F.W., Bergen, H.R., Gores, G.J., and Nyberg, S.L. (2003). Apoptotic cell death and function of cryopreserved porcine hepatocytes in a bioartificial liver. Cell Transplant. *12*, 109–121.

Mavri-Damelin, D., Eaton, S., Damelin, L.H., Rees, M., Hodgson, H.J.F., and Selden, C. (2007). Ornithine transcarbamylase and arginase I deficiency are responsible for diminished urea cycle function in the human hepatoblastoma cell line HepG2. Int. J. Biochem. Cell Biol. *39*, 555–564.

Mavrides, A., and Morroll, D. (2002). Cryopreservation of bovine oocytes: is cryoloop vitrification the future to preserving the female gamete? Reprod. Nutr. Dev. *42*, 73–80.

Mazur, P. (1960). Physical factors implicated in the death of microorganisms at subzero temperatures. Ann. N. Y. Acad. Sci. *85*, 610–629.

Mazur, P. (1965). CAUSES OF INJURY IN FROZEN AND THAWED CELLS. Fed. Proc. *24*, S175–S182.

Mazur, P. (1984). Freezing of living cells: mechanisms and implications. Am. J. Physiol. *247*, C125–C142.

Mazur, P., Leibo, S.P., and Chu, E.H. (1972). A two-factor hypothesis of freezing injury. Evidence from Chinese hamster tissue-culture cells. Exp. Cell Res. *71*, 345–355.

Meryman, H.T. (2007). Cryopreservation of living cells: principles and practice. Transfusion (Paris) *47*, 935–945.

Michael, A., Alexopoulos, C., Pontiki, E., Hadjipavlou-Litina, D., Saratsis, P., and Boscos, C. (2007). Effect of antioxidant supplementation on semen quality and reactive oxygen species of frozen-thawed canine spermatozoa. Theriogenology *68*, 204–212.

Michalopoulos, G.K. (2013). Principles of liver regeneration and growth homeostasis. Compr. Physiol. *3*, 485–513.

Migliori, M., Gabriele, D., Sanzo, R., Cindio, B., and Correra, S. Viscosity of Multicomponent Solutions of Simple and Complex Sugars in Water. J. Chem. Eng. Data. *57*, 1347-1353

Moore K., A.A.M.R. (2007). Essential Clinical Anatomy (Lippincott Williams and Wilkins).

Moriguchi, H., Zhang, Y., Mihara, M., and Sato, C. (2012). Successful cryopreservation of human ovarian cortex tissues using supercooling. Sci. Rep. *2*, 537.

Mukherjee, I.N., Song, Y.C., and Sambanis, A. (2007). Cryoprotectant delivery and removal from murine insulinomas at vitrification-relevant concentrations. Cryobiology *55*, 10–18.

Muldrew, K., and McGann, L.E. (1994). The osmotic rupture hypothesis of intracellular freezing injury. Biophys. J. *66*, 532–541.

Muldrew, K., Novak, K., Yang, H., Zernicke, R., Schachar, N.S., and McGann, L.E. (2000). Cryobiology of articular cartilage: ice morphology and recovery of chondrocytes. Cryobiology *40*, 102–109.

Murua, A., Portero, A., Orive, G., Hernández, R.M., de Castro, M., and Pedraz, J.L. (2008). Cell microencapsulation technology: towards clinical application. J. Control. Release Off. J. Control. Release Soc. *132*, 76–83.

Nei, T. (1981). Mechanism of freezing injury to erythrocytes: effect of initial cell concentration on the post-thaw hemolysis. Cryobiology *18*, 229–237.

Neuberger, J., Farber, L., Corrado, M., and O'Dell, C. (2003). Living liver donation: a survey of the attitudes of the public in Great Britain. Transplantation *76*, 1260–1264.

Nishizawa, A., Yabuta, Y., and Shigeoka, S. (2008). Galactinol and raffinose constitute a novel function to protect plants from oxidative damage. Plant Physiol. *147*, 1251–1263.

Nyberg, S.L., Shatford, R.A., Payne, W.D., Hu, W.S., and Cerra, F.B. (1993). Staining with fluorescein diacetate correlates with hepatocyte function. Biotech. Histochem. Off. Publ. Biol. Stain Comm. *68*, 56–63.

O'Brien, L.E., Yu, W., Tang, K., Jou, T.-S., Zegers, M.M.P., and Mostov, K.E. (2006). Morphological and biochemical analysis of Rac1 in three-dimensional epithelial cell cultures. Methods Enzymol. *406*, 676–691.

O'Grady, J. (2006). Personal view: current role of artificial liver support devices. Aliment. Pharmacol. Ther. *23*, 1549–1557.

O'Grady, J.G. (2005). Acute liver failure. Postgrad. Med. J. *81*, 148–154.

O'Grady, J.G., Schalm, S.W., and Williams, R. (1993). Acute liver failure: redefining the syndromes. Lancet *342*, 273–275.

Oh, S.-H., and Lim, S.-C. (2006). A rapid and transient ROS generation by cadmium triggers apoptosis

via caspase-dependent pathway in HepG2 cells and this is inhibited through N-acetylcysteine-mediated catalase upregulation. Toxicol. Appl. Pharmacol. *212*, 212–223.

Orive, G., Gascón, A.R., Hernández, R.M., Igartua, M., and Luis Pedraz, J. (2003). Cell microencapsulation technology for biomedical purposes: novel insights and challenges. Trends Pharmacol. Sci. *24*, 207–210.

Pampaloni, F., Reynaud, E.G., and Stelzer, E.H.K. (2007). The third dimension bridges the gap between cell culture and live tissue. Nat. Rev. Mol. Cell Biol. *8*, 839–845.

Pan, J., Naik, S., Santangini, H., Trenkler, D., and Jauregui, H. (1996). Flow cytometric characterization of isolated porcine hepatocyte suspensions for liver support. Artif. Organs *20*, 1173–1180.

Park, J., Fan, Z., and Deng, C.X. (2011). Effects of shear stress cultivation on cell membrane disruption and intracellular calcium concentration in sonoporation of endothelial cells. J. Biomech. *44*, 164–169.

Paudel, K.P., Kumar, S., Meur, S.K., and Kumaresan, A. (2010). Ascorbic acid, catalase and chlorpromazine reduce cryopreservation-induced damages to crossbred bull spermatozoa. Reprod. Domest. Anim. Zuchthyg. *45*, 256–262.

Paynter, S.J., Fuller, B.J., and Shaw, R.W. (1997). Temperature dependence of mature mouse oocyte membrane permeabilities in the presence of cryoprotectant. Cryobiology *34*, 122–130.

Paynter, S.J., Cooper, A., Gregory, L., Fuller, B.J., and Shaw, R.W. (1999). Permeability characteristics of human oocytes in the presence of the cryoprotectant dimethylsulphoxide. Hum. Reprod. *14*, 2338–2342.

Paynter, S.J., Borini, A., Bianchi, V., De Santis, L., Flamigni, C., and Coticchio, G. (2005). Volume changes of mature human oocytes on exposure to cryoprotectant solutions used in slow cooling procedures. Hum. Reprod. *20*, 1194–1199.

Peak, E. (2012). Dual fluorescence assay for determining viability of parasitic or non- parasitic worms.

Pegg, D. (2010a). Cryobiology, Essentials of Tissue Banking (Springer).

Pegg, D.E. (1981). The effect of cell concentration on the recovery of human erythrocytes after freezing and thawing in the presence of glycerol. Cryobiology *18*, 221–228.

Pegg, D.E. (2010b). The relevance of ice crystal formation for the cryopreservation of tissues and organs. Cryobiology *60*, S36–S44.

Pegg, D.E., Wusteman, M.C., and Boylan, S. (1997). Fractures in cryopreserved elastic arteries. Cryobiology *34*, 183–192.

Pegg, D.E., Wang, L., Vaughan, D., and Hunt, C.J. (2006a). Cryopreservation of articular cartilage. Part 2: mechanisms of cryoinjury. Cryobiology *52*, 347–359.

Pegg, D.E., Wang, L., and Vaughan, D. (2006b). Cryopreservation of articular cartilage. Part 3: the liquidus-tracking method. Cryobiology *52*, 360–368.

Peña, F.J., Johannisson, A., Wallgren, M., and Rodriguez Martinez, H. (2004). Antioxidant supplementation of boar spermatozoa from different fractions of the ejaculate improves cryopreservation: changes in sperm membrane lipid architecture. Zygote Camb. Engl. *12*, 117–124.

Petrenko, Y.A., Jones, D.R.E., and Petrenko, A.Y. (2008). Cryopreservation of human fetal liver hematopoietic stem/progenitor cells using sucrose as an additive to the cryoprotective medium. Cryobiology *57*, 195–200.

Phelps, M.J., Liu, J., Benson, J.D., Willoughby, C.E., Gilmore, J.A., and Critser, J.K. (1999). Effects of Percoll separation, cryoprotective agents, and temperature on plasma membrane permeability characteristics of murine spermatozoa and their relevance to cryopreservation. Biol. Reprod. *61*, 1031–1041.

Polge, C., and Soltys, M.A. (1960). Protective action of some neutral solutes during the freezing of bull spermatozoa and trypanosomes. In Recent Research in Freezing and Drying, (Blackwell, Oxford), pp. 87–100.

Polge, C., Smith, A.U., and Parkes, A.S. (1949). Revival of spermatozoa after vitrification and dehydration at low temperatures. Nature *164*, 666.

Rauen, U., Polzar, B., Stephan, H., Mannherz, H.G., and de Groot, H. (1999). Cold-induced apoptosis in cultured hepatocytes and liver endothelial cells: mediation by reactive oxygen species. FASEB J. *13*, 155–168.

Reilly, T.P., Bourdi, M., Brady, J.N., Pise-Masison, C.A., Radonovich, M.F., George, J.W., and Pohl, L.R. (2001). Expression profiling of acetaminophen liver toxicity in mice using microarray technology. Biochem. Biophys. Res. Commun. *282*, 321–328.

Reubinoff, B.E., Pera, M.F., Vajta, G., and Trounson, A.O. (2001). Effective cryopreservation of human embryonic stem cells by the open pulled straw vitrification method. Hum. Reprod. *16*, 2187–2194.

Rifai, K., Ernst, T., Kretschmer, U., Bahr, M.J., Schneider, A., Hafer, C., Haller, H., Manns, M.P., and Fliser, D. (2003). Prometheus--a new extracorporeal system for the treatment of liver failure. J. Hepatol. *39*, 984–990.

Ringe, B., Braun, F., Moritz, M., Zeldin, G., Soriano, H., and Meyers, W. (2005). Safety and efficacy of living donor liver preservation with HTK solution. Transplant. Proc. *37*, 316–319.

Roca, J., Rodríguez, M.J., Gil, M.A., Carvajal, G., Garcia, E.M., Cuello, C., Vazquez, J.M., and Martinez, E.A. (2005). Survival and in vitro fertility of boar spermatozoa frozen in the presence of superoxide dismutase and/or catalase. J. Androl. *26*, 15–24.

Rokushima, M., Omi, K., Araki, A., Kyokawa, Y., Furukawa, N., Itoh, F., Imura, K., Takeuchi, K., Okada, M., Kato, I., et al. (2007). A toxicogenomic approach revealed hepatic gene expression changes mechanistically linked to drug-induced hemolytic anemia. Toxicol. Sci. *95*, 474–484.

De Rougemont, O., Lehmann, K., and Clavien, P.-A. (2009). Preconditioning, organ preservation, and postconditioning to prevent ischemia-reperfusion injury to the liver. Liver Transplant. *15*, 1172–1182.

Roussel, J.C., Moran, C.J., Salvaris, E.J., Nandurkar, H.H., d' Apice, A.J.F., and Cowan, P.J. (2008). Pig thrombomodulin binds human thrombin but is a poor cofactor for activation of human protein C and TAFI. Am. J. Transplant. *8*, 1101–1112.

Ruifrok, A.C. (1997). Quantification of immunohistochemical staining by color translation and automated thresholding. Anal. Quant. Cytol. Histol. *19*, 107–113.

Saeed, A.M., Escribá, M.J., Silvestre, M.A., and Garcia-Ximénez, F. (2000). Vitrification and rapid-freezing of cumulus cells from rabbits and pigs. Theriogenology *54*, 1359–1371.

Saich, R., Selden, C., Rees, M., and Hodgson, H. (2007). Characterization of pro-apoptotic effect of liver failure plasma on primary human hepatocytes and its modulation by molecular adsorbent recirculation system therapy. Artif. Organs *31*, 732–742.

San-Miguel, B., Alvarez, M., Culebras, J.M., González-Gallego, J., and Tuñón, M.J. (2006). N-acetyl-cysteine protects liver from apoptotic death in an animal model of fulminant hepatic failure. Apoptosis Int. J. Program. Cell Death *11*, 1945–1957.

Sarin, S.K., Kumar, A., Almeida, J.A., Chawla, Y.K., Fan, S.T., Garg, H., de Silva, H.J., Hamid, S.S., Jalan, R., Komolmit, P., et al. (2009). Acute-on-chronic liver failure: consensus recommendations of the Asian Pacific Association for the study of the liver (APASL). Hepatol. Int. *3*, 269–282.

Saruyama, N., Sakakura, Y., Asano, T., Nishiuchi, T., Sasamoto, H., and Kodama, H. (2013). Quantification of metabolic activity of cultured plant cells by vital staining with fluorescein diacetate. Anal. Biochem. *441*, 58–62.

Schnürer, J., and Rosswall, T. (1982). Fluorescein diacetate hydrolysis as a measure of total microbial activity in soil and litter. Appl. Environ. Microbiol. *43*, 1256–1261.

Schulze-Bergkamen, H., Brenner, D., Krueger, A., Suess, D., Fas, S.C., Frey, C.R., Dax, A., Zink, D., Büchler, P., Müller, M., et al. (2004). Hepatocyte growth factor induces Mcl-1 in primary human hepatocytes and inhibits CD95-mediated apoptosis via Akt. Hepatol. Baltim. Md *39*, 645–654.

Seki, S., Kouya, T., Tsuchiya, R., Valdez, D.M., Jin, B., Koshimoto, C., Kasai, M., and Edashige, K. (2011). Cryobiological properties of immature zebrafish oocytes assessed by their ability to be fertilized and develop into hatching embryos. Cryobiology *62*, 8–14.

Selden, C., Shariat, A., McCloskey, P., Ryder, T., Roberts, E., and Hodgson, H. (1999). Three-

dimensional in vitro cell culture leads to a marked upregulation of cell function in human hepatocyte cell lines--an important tool for the development of a bioartificial liver machine. Ann. N. Y. Acad. Sci. *875*, 353–363.

Shah, D., Naciri, M., Clee, P., and Al-Rubeai, M. (2006). NucleoCounter-An efficient technique for the determination of cell number and viability in animal cell culture processes. Cytotechnology *51*, 39–44.

Si, W., Hildebrandt, T.B., Reid, C., Krieg, R., Ji, W., Fassbender, M., and Hermes, R. (2006). The successful double cryopreservation of rabbit (Oryctolagus cuniculus) semen in large volume using the directional freezing technique with reduced concentration of cryoprotectant. Theriogenology *65*, 788–798.

Al Sibae, M.R., and McGuire, B.M. (2009). Current trends in the treatment of hepatic encephalopathy. Ther. Clin. Risk Manag. *5*, 617–626.

Sieracki, N.A., Hwang, H.J., Lee, M.K., Garner, D.K., and Lu, Y. (2008). A temperature independent pH (TIP) buffer for biomedical biophysical applications at low temperatures. Chem. Commun. Camb. Engl. 823–825.

Slany, A., Haudek, V.J., Zwickl, H., Gundacker, N.C., Grusch, M., Weiss, T.S., Seir, K., Rodgarkia-Dara, C., Hellerbrand, C., and Gerner, C. (2010). Cell characterization by proteome profiling applied to primary hepatocytes and hepatocyte cell lines Hep-G2 and Hep-3B. J. Proteome Res. *9*, 6–21.

Snow, J.T., Finley, J.W., and Friedman, M. (1975). Oxidation of sulfhydryl groups to disulfides by sulfoxides. Biochem. Biophys. Res. Commun. *64*, 441–447.

Song, Y.C., An, Y.H., Kang, Q.K., Li, C., Boggs, J.M., Chen, Z., Taylor, M.J., and Brockbank, K.G.M. (2004). Vitreous preservation of articular cartilage grafts. J. Investig. Surg. *17*, 65–70.

Song, Y.S., Moon, S., Hulli, L., Hasan, S.K., Kayaalp, E., and Demirci, U. (2009). Microfluidics for cryopreservation. Lab. Chip *9*, 1874–1881.

Songsasen, N., and Leibo, S.P. (1997). Cryopreservation of mouse spermatozoa. I. Effect of seeding on fertilizing ability of cryopreserved spermatozoa. Cryobiology *35*, 240–254.

Sousa, A.C. (2013). X-ray Computed Tomography as a Method of cryoprotectant concentration measurement and ice detection. Application to organ cryopreservation-PhD Thesis. Sevilla.

Southard, J.H., van Gulik, T.M., Ametani, M.S., Vreugdenhil, P.K., Lindell, S.L., Pienaar, B.L., and Belzer, F.O. (1990). Important components of the UW solution. Transplantation *49*, 251–257.

Sputtek, A., Lioznov, M., Kröger, N., and Rowe, A.W. (2011). Bioequivalence comparison of a new freezing bag (CryoMACS(®)) with the Cryocyte(®) freezing bag for cryogenic storage of human hematopoietic progenitor cells. Cytotherapy *13*, 481–489.

Stachecki, J.J., and Cohen, J. (2004). An overview of oocyte cryopreservation. Reprod. Biomed. Online *9*,

152–163.

Stange, J., Hassanein, T.I., Mehta, R., Mitzner, S.R., and Bartlett, R.H. (2002). The molecular adsorbents recycling system as a liver support system based on albumin dialysis: a summary of preclinical investigations, prospective, randomized, controlled clinical trial, and clinical experience from 19 centers. Artif. Organs *26*, 103–110.

Steponkus, and Wiest (1978). Plasma membrane alterations following cold acclimation. Academic Press, new York. *75*, 75–91.

Stroh, C., Cassens, U., Samraj, A.K., Sibrowski, W., Schulze-Osthoff, K., and Los, M. (2002). The role of caspases in cryoinjury: caspase inhibition strongly improves the recovery of cryopreserved hematopoietic and other cells. FASEB J. *16*, 1651–1653.

Sugimachi, K., Roach, K.L., Rhoads, D.B., Tompkins, R.G., and Toner, M. (2006). Nonmetabolizable glucose compounds impart cryotolerance to primary rat hepatocytes. Tissue Eng. *12*, 579–588.

Sum, A.K., and de Pablo, J.J. (2003). Molecular simulation study on the influence of dimethylsulfoxide on the structure of phospholipid bilayers. Biophys. J. *85*, 3636–3645.

Swan, H., Cowan, M., Tornabene, M., and Owens, L. (1994). Aminosulfonic acid buffer preserves myocardium during prolonged ischemia. Ann. Thorac. Surg. *57*, 1590–1595.

Tacke, F., Luedde, T., and Trautwein, C. (2009). Inflammatory pathways in liver homeostasis and liver injury. Clin. Rev. Allergy Immunol. *36*, 4–12.

Taylor, M.J. (1982). The role of pH and buffer capacity in the recovery of function of smooth muscle cooled to -13 degrees C in unfrozen media. Cryobiology *19*, 585–601.

Terry, C., Dhawan, A., Mitry, R.R., Lehec, S.C., and Hughes, R.D. (2010). Optimization of the cryopreservation and thawing protocol for human hepatocytes for use in cell transplantation. Liver Transplant. Off. Publ. Am. Assoc. Study Liver Dis. Int. Liver Transplant. Soc. *16*, 229–237.

Thuwanut, P., Chatdarong, K., Techakumphu, M., and Axnér, E. (2008). The effect of antioxidants on motility, viability, acrosome integrity and DNA integrity of frozen-thawed epididymal cat spermatozoa. Theriogenology *70*, 233–240.

Tominaga, K., Hamada, Y., Yabuue, T., and Ariyoshi, T. (2000). Effect of linoleic acid-albumin on post-thaw survival of in vitro-produced bovine embryos at the 16-cell stage. J. Vet. Med. Sci. *62*, 465–467.

Toner, M., Cravalho, E.G., and Armant, D.R. (1990). Water transport and estimated transmembrane potential during freezing of mouse oocytes. J. Membr. Biol. *115*, 261–272.

Tristram-Nagle, S., Moore, T., Petrache, H.I., and Nagle, J.F. (1998). DMSO produces a new subgel phase in DPPC: DSC and X-ray diffraction study. Biochim. Biophys. Acta *1369*, 19–33.

Umlas, J., and O'Neill, T.P. (1980). Use of the refractive index to measure the adequacy of glycerol removal from previously frozen erythrocytes. Transfusion *20*, 720–724.

Vairetti, M., Griffini, P., Pietrocola, G., Richelmi, P., and Freitas, I. (2001). Cold-induced apoptosis in isolated rat hepatocytes: protective role of glutathione. Free Radic. Biol. Med. *31*, 954–961.

Valdez, C.A., Abas Mazni, O., Takahashi, Y., Fujikawa, S., and Kanagawa, H. (1992). Successful cryopreservation of mouse blastocysts using a new vitrification solution. J. Reprod. Fertil. *96*, 793–802.

Valeri, F., Boess, F., Wolf, A., Göldlin, C., and Boelsterli, U.A. (1997). Fructose and tagatose protect against oxidative cell injury by iron chelation. Free Radic. Biol. Med. *22*, 257–268.

Vanhulle, V.P., Neyrinck, A.M., Pycke, J.-M., Horsmans, Y., and Delzenne, N.M. (2006). Role of apoptotic signaling pathway in metabolic disturbances occurring in liver tissue after cryopreservation: Study on rat precision-cut liver slices. Life Sci. *78*, 1570–1577.

Walcerz, D.B., Taylor, M.J., and Busza, A.L. (1995). Determination of the kinetics of permeation of dimethyl sulfoxide in isolated corneas. Cell Biophys. *26*, 79–102.

Wang, L., Pegg, D.E., Lorrison, J., Vaughan, D., and Rooney, P. (2007). Further work on the cryopreservation of articular cartilage with particular reference to the liquidus tracking (LT) method. Cryobiology *55*, 138–147.

Wang, X., Al Naib, A., Sun, D.-W., and Lonergan, P. (2010). Membrane permeability characteristics of bovine oocytes and development of a step-wise cryoprotectant adding and diluting protocol. Cryobiology *61*, 58–65.

Wassenaar, C., Bax, W.A., van Suylen, R.J., Vuzevski, V.D., and Bos, E. (1997). Effects of cryopreservation on contractile properties of porcine isolated aortic valve leaflets and aortic wall. J. Thorac. Cardiovasc. Surg. *113*, 165–172.

Watts, P., and Grant, M.H. (1996). Cryopreservation of rat hepatocyte monolayer cultures. Hum. Exp. Toxicol. *15*, 30–37.

Weihe, W.H. (1973). The effect of temperature on the action of drugs. Annu. Rev. Pharmacol. *13*, 409–425.

Williams, R.J. (1989). Four modes of nucleation in viscous solutions. Cryobiology *26*, 568–568.

Wowk, B., Leitl, E., Rasch, C.M., Mesbah-Karimi, N., Harris, S.B., and Fahy, G.M. (2000). Vitrification enhancement by synthetic ice blocking agents. Cryobiology *40*, 228–236.

Wowk, null, Darwin, null, Harris, null, Russell, null, and Rasch, null (1999). Effects of solute methoxylation on glass-forming ability and stability of vitrification solutions. Cryobiology *39*, 215–227.

Wusteman, M., Rauen, U., Simmonds, J., Hunds, N., and Pegg, D.E. (2008). Reduction of cryoprotectant

toxicity in cells in suspension by use of a sodium-free vehicle solution. Cryobiology *56*, 72–79.

Xu, X., Cowley, S., Flaim, C.J., James, W., Seymour, L., and Cui, Z. (2010). The roles of apoptotic pathways in the low recovery rate after cryopreservation of dissociated human embryonic stem cells. Biotechnol. Prog. *26*, 827–837.

Yagi, H., Tafaleng, E., Nagaya, M., Hansel, M.C., Strom, S.C., Fox, I.J., and Soto-Gutierrez, A. (2009). Embryonic and induced pluripotent stem cells as a model for liver disease. Crit. Rev. Biomed. Eng. *37*, 377–398.

Yagi, T., Hardin, J.A., Valenzuela, Y.M., Miyoshi, H., Gores, G.J., and Nyberg, S.L. (2001). Caspase inhibition reduces apoptotic death of cryopreserved porcine hepatocytes. Hepatol. Baltim. Md *33*, 1432–1440.

Yamamoto, K., and Ando, J. (2013). Endothelial cell and model membranes respond to shear stress by rapidly decreasing the order of their lipid phases. J. Cell Sci. *126*, 1227–1234.

Yogev, L., Kleiman, S.E., Shabtai, E., Botchan, A., Paz, G., Hauser, R., Lehavi, O., Yavetz, H., and Gamzu, R. (2010). Long-term cryostorage of sperm in a human sperm bank does not damage progressive motility concentration. Hum. Reprod. *25*, 1097–1103.

Zhang, J.-M., Li, L.-X., Yang, Y.-X., Liu, X.-L., and Wan, X.-P. (2009). Is caspase inhibition a valid therapeutic strategy in cryopreservation of ovarian tissue? J. Assist. Reprod. Genet. *26*, 415–42

Appendices

Appendix to Chapter 3:

Table 3.3 Low FDA threshold

cell number (cells/ml beads)	$10.3*10^6$		$14.88*10^6$		$17.89*10^6$		**$20.22*10^6$**		**$26.31*10^6$**	
sample	1	2	1	2	1	2	1	2	1	2
threshold	23	21	28	27	29	31	44	43	31	44
	21	26	31	30	36	32	45	44	46	41
	18	20	29	28	35	31	46	29	46	41
	26	26	33	28	34	33	43	38	43	42
	26	19	32	31	37	33	45	31	43	44
average	22.8	22.4	30.6	28.8	34.2	32	44.6	37	41.8	42.4
final threshold:							**average = 41 +/-3.2 SD**			

Table 3.4 Low PI threshold

Cell number: **$20.22*10^6$ cells/ml**	Sum intensity FDA	Aim sum Intensity of **31748525*** for PI	Lower threshold PI
sample 1 image 1	35187045	31187355	12
sample 1 image 2	38169857	31797561	29
sample 1 image 3	34900386	31271788	32
sample 1 image 4	35053162	31184015	30
sample 1 image 5	40404321	30165638	20
average			24.6
sample 2 image 1	29079423	31162474	36
sample 2 image 2	41418401	31130723	33
sample 2 image 3	19800704	31775390	20
sample 2 image 4	29055327	31280522	27
sample 2 image 5	14416622	31230720	33
average	**31748525***		28.0
Cell number: **$26.31*10^6$ cell/ml**	Sum intensity FDA	Aim sum intensity of **40262498*** for PI	Lower threshold for PI
sample 1 image 1	21992407	40232118	42
sample 1 image 2	50834677	40564241	44
sample 1 image 3	47952834	40331949	40
sample 1 image 4	35581092	40491603	48
sample 1 image 5	36197089	40450072	65
average			47.8
sample 2 image 1	46908396	40249895	65
sample 2 image 2	40175423	40094759	52
sample 2 image 3	39859186	40518308	68
sample 2 image 4	42406002	40969637	67
sample 2 image 5	40717872	40202528	51
average	**40262498***		58.4
Final threshold average +/- SD			**41 +/-16.1**

*sum intensity for PI had to be approximately the same as or FDA. This was achieved by adjusting the PI threshold.

Table 3.6 FDA and PI threshold setting (AELC one day after encapsulation, FDA exposure time: 150ms, PI exposure time: 1s)

encapsulation 1-4 day 1	Low threshold FDA	Sum intensity FDA	Sum Intensity PI	Low threshold PI
encapsulation 1 image 1	16	3094206	4559859	21
encapsulation 1 image 2	19	3609000	4470615	21
encapsulation 1 image 3	23	5070708	4524616	19
encapsulation 1 image 4	22	5755816	4452720	18
encapsulation 1 image 5	23	5111211	4706646	20
average	21	4528188	4542891	20
encapsulation 2 image 1	18	4095644	5174288	22
encapsulation 2 image 2	19	4858627	5242796	24
encapsulation 2 image 3	27	5740505	5104872	24
encapsulation 2 image 4	23	5236164	5170000	22
encapsulation 2 image 5	21	5133087	5183549	11
average	22	5012805	5175101	21
encapsulation 3 image 1	15	3814405	5624252	19
encapsulation 3 image 2	15	3847213	5684750	20
encapsulation 3 image 3	26	7905982	5694455	18
encapsulation 3 image 4	25	7032799	5582154	16
encapsulation 3 image 5	N/A	N/A	5629549	21
average	20	5650100	5643032	19
encapsulation 4 image 1	22	9023726	9635147	17
encapsulation 4 image 2	24	11006639	9635779	17
encapsulation 4 image 3	24	9278548	9694020	23
encapsulation 4 image 4	21	8058352	9669975	21
encapsulation 4 image 5	25	10985479	9590066	18
average	23	9670549	9644997	19
average +/- SD	**21 +/- 1.3**			**20 +/- 1.0**

Table 3.9 Gain and equalization factor evaluation: Viability data of samples listed in Figure 3.11

day 1			day 5			day 10			day 16		
600/ 300	**900/ 300**	**1200/ 300**	**600/ 300**	**900/ 300**	**1200/ 300**	**600/ 300**	**900/ 300**	**1200/ 300**	**600/ 300**	**900/ 300**	**1200/ 300**
90.03	88.26	87.73	87.09	86.23	86.22	88.47	87.05	87.24	86.26	84.42	84.97
91.36	89.45	88.89	88.77	87.60	87.50	89.98	88.35	88.44	88.03	85.94	86.35
81.86	81.53	80.41	77.13	78.63	78.22	79.31	79.80	79.70	75.84	76.10	76.45
46.61	44.44	42.95	39.49	40.00	39.71	42.59	41.71	41.86	37.79	36.58	37.32
600/ 600	**900/ 600**	**1200/ 600**	**600/ 600**	**900/ 600**	**1200/ 600**	**600/ 600**	**900/ 600**	**1200/ 600**	**600/ 600**	**900/ 600**	**1200/ 600**
90.57	88.79	88.77	89.63	87.91	88.08	89.84	88.57	88.74	88.98	86.98	86.98
90.57	88.40	88.30	88.76	87.50	87.58	89.83	88.18	88.28	88.12	86.54	86.45
80.33	79.82	79.42	77.05	78.42	78.30	78.98	79.48	79.38	75.93	76.95	76.54
44.15	41.75	41.45	39.40	39.71	39.82	42.12	41.24	41.39	37.92	37.69	37.43
600/ 900	**900/ 900**	**1200/ 900**	**600/ 900**	**900/ 900**	**1200/ 900**	**600/ 900**	**900/ 900**	**1200/ 900**	**600/ 900**	**900/ 900**	**1200/ 900**
86.87	84.50	84.47	84.25	83.13	83.32	85.01	83.37	83.59	81.71	80.09	80.09
86.96	84.12	83.98	84.36	82.71	82.79	85.12	82.96	83.07	81.84	79.62	79.49
74.39	73.78	73.29	70.14	71.77	71.58	71.35	72.11	71.98	66.24	67.49	66.98
44.18	41.79	41.48	39.03	39.34	39.42	40.43	39.75	39.88	34.84	34.63	34.38

Values in **bold** represent the PI/FDA combination. Viability was calculated with the corresponding equalization factor listed in Table 3.5. Sample 1 (positive control), sample 2 (AELC incubated in 40% Me_2SO), sample 3 (AELC incubated in 50% Me_2SO), sample 4 (AELC incubated in 80% Me_2SO), listed from top to bottom.

Appendix to Chapter 6:

6.3.3.2 Combined manual/automatic LT

Delta T program:

Start temperature was set to -20˚C (on hold)

Manual inlet (inlet speed: 60 ml/minute):

- Waited until sample temperature was at 12˚C, then inlet of 31ml of 50% (w/v) CPA.
- Waited until sample temperature was at 4˚C, then inlet of 89ml of 50% (w/v) CPA.
- Waited until sample temperature was at 0.5˚C, then inlet of 67ml of 50% (w/v) CPA.
- 252ml of sample were extracted and outlet re-primed with 35ml of 50% (w/v) CPA.
- Waited until sample temperature was at -4˚C, then inlet of 50ml of 50% (w/v) CPA.
- Waited until sample temperature was at -5˚C, then inlet of 75ml of 50% (w/v) CPA.
- Waited until sample temperature was at -7˚C, then inlet of 125ml of 50% (w/v) CPA.
- 135ml sample solution was extracted and outlet was primed with 50% (w/v) CPA.

Automatic Planer CfgPid profile started at -12˚C

Delta Program:

cooling rate: -0.5˚C/minute to -56˚C hold for 10 minute

cooling rate -10˚C/minute to -160˚C hold for 20 minute

Table 6.2 CfgPid profile for automatic LT

CfgPid profile		measured T/C curve (approximate)	
Freezer temperature (C˚)	sample CPA concentration (w/v)	Sample temperature (C˚)	sample CPA concentration (w/v)
-22.15	32.10	-14	41
-27.65	37.50	-15	45
-32.65	42.50	-19	51
-36.65	46.49	-21	52
-40.65	50.49	-26	57
-44.65	54.48	-27	59
-47.65	57.47	-32	62
-50.65	60.47	-35	65
-53.25	63.07	-38	
-55.85	65.66	-40	

The stirrer was stopped at -40˚C (Me_2SO) or -35˚C (CPA No.18) and aliquots of 2.5ml of LT-processed AELC were added into a 15ml centrifuge tube held in a bucket of liquid nitrogen. Samples were stored at liquid nitrogen tempertures until warming.

Appendix to Chapter 7:

7.3.1 The 50-60-66% inlet:

Manual inlet with 50% (w/v) CPA

- Waited until sample temperature was at 12˚C, then influx of 190ml of 50% (w/v) CPA at 12.5ml/minute.
- Waited until sample temperature was at 7˚C, then freezer was set to -20˚C (on hold).
- Waited until sample temperature was 2˚C, then 252ml were extracted at 25ml/minute and outlet was re-primed with 35ml 50% (w/v) CPA.
- Waited until sample temperature was at -1.5˚C, then inlet of 250ml of 50% (w/v) CPA at 20ml/minute (temperature after inlet was -10˚C).
- Waited until sample temperature was at -12˚C, then freezer was set to -25˚C (on hold) and inlet of 150ml (tube volume) of 50% (w/v) CPA at 20ml/minute while 60% (w/v) CPA was primed in. Simultaneously 150ml were extracted (at 20ml/minute).
- Waited until sample temperature was at -16˚C, then freezer was set to -30˚C and samples were taken at -16˚C at a concentration of 40% (w/v) CPA.
- Inlet of 60% (w/v) CPA at 20ml/minute until a sample CPA concentration of 50% (w/v) was reached.
- Inlet of 150ml (tube volume) of 60% (w/v) CPA at 20ml/minute while 66% (w/v) CPA was primed in. Simultaneously 150ml were extracted (at 20ml/minute).
- Inlet of 66% (w/v) CPA until a sample CPA concentration of 65% (w/v) was reached, then freezer temperature was set to -60˚C.
- The stirrer was stopped at a sample temperature of -40˚C (Me_2SO) or -35˚C (CPA No.18) and aliquots of 2.5ml were added into a 15ml centrifuge tube hold in a bucket of liquid nitrogen. Samples were stored at liquid nitrogen until warming.
- Freezer setting for vitrification: at -10˚C/minute to-160˚C until the sample reaches a temperature of -125˚C.

7.3.4 The manual two-step LT approach

Method:

To obtain sufficient material for five repetitions the following pre-mix (all solutions at 0.5˚C - on ice water) was prepared: 6ml of 50% (w/v) CPA No.18 was added to 1.5ml of settled beads contained in a total volume of 3ml of PBS. After mixing, an additional amount of 6ml of 50% (w/v) CPA No.18 was added to increase the concentration to 40% (w/v) CPA. After 3 minutes on ice while the beads settled to the bottom, the volume was reduced to 3.6ml by extracting the supernatant. The solution was mixed and 0.6ml of bead solution (0.25ml of settled beads) was added to a new 15ml centrifuge tube which was held in a 50ml centrifuge tube containing 70% (v/v) ethanol for insolation as described in Chapter 4. Samples were placed into the controlled rate freezer and were cooled to -20˚C at -0.5˚C/minute. The sample concentration was increased to 65% CPA by adding 1ml of 80% CPA solution (at -20˚C). Volumes were chosen to be equal or below 1ml to be able to use a 1ml pipette to perform pipetting in one step.

The two-step warming process was as following: vitrified samples were taken from liquid nitrogen and placed inside the controlled rate freezer (at -20˚C). Samples were kept for 15 minutes until they were completely liquid. Then 8ml of 40% (w/v) CPA No.18 (at -20˚C) were added which decreased the sample CPA concentration to 44% (w/v). Samples were mixed by inversion and left in the freezer for 15 minutes. Samples were poured through cell strainers which were then placed in 8ml of ice cold 20% (w/v) glucose solution for 10 minutes. The solution was exchanged three times with fresh PBS (ice-cold) to remove all CPA. Finally AELC were incubated in 8ml of complete media at 37˚C until measurement. This approach was used to test different variations of CPA No.18, for example replacing half of the glucose concentration with sucrose, raffinose or trehalose, pre-testing different sample carrier solutions such as HEPES, Viaspan or HTK and to test AELC that were incubated for 24 hours in complete media containing Proline, trehalose or an increased concentration of linoleic acid